DALIBOR MILIĆ

STRUCTURAL BASIS FOR THE ENZYMATIC ACTIVITY OF TYROSINE PHENOL-LYASE

Doctoral Thesis

submitted to the Department of Chemistry,
Faculty of Science, University of Zagreb,
for the academic degree of
Doctor of Natural Sciences (Chemistry)

Zagreb
2010

This Doctoral Thesis was done in the Laboratory of General and Inorganic Chemistry, Department of Chemistry, Faculty of Science, University of Zagreb, Croatia and in the York Structural Biology Laboratory, Department of Chemistry, University of York, UK under the supervision of Prof. Dubravka Matković-Čalogović and Dr. Alfred A. Antson.

To my family

Acknowledgments

This thesis could not have been written without people which provided me with their assistance, support and guidance – it is my pleasure to thank them.

First of all, I wish to express my sincere gratitude to my supervisor Prof. Dubravka Matković-Čalogović for her kindness, support and expertise. Her guidance during my Dr. Sc. study is invaluable.

I am particularly indebted and grateful to my co-supervisor Dr. Alfred A. Antson. Research described in this thesis is a continuation of his previous studies on the structure and enzymatic mechanism of tyrosine phenol-lyase. His patience and profound knowledge make him an excellent teacher. I also thank him and his family for generosity and hospitality during my visits to York.

My acknowledgments also go to members of the evaluation committees: Prof. Ivana Weygand-Đurašević, Dr. Marija Luić, Dr. Ines Primožič and Dr. Ita Gruić-Sovulj. Their comments and suggestions were very constructive for improving the thesis.

Dr. Tatyana V. Demidkina and Dr. Nicolai G. Faleev are gratefully acknowledged for their previous research on tyrosine phenol-lyase and the related fruitful discussions which I had with them.

I thank Dr. Martin Walsh (beamline BM14) and Dr. Richard Kahn (beamline BM30A) for help during data collection at the European Synchrotron Radiation Facility (Grenoble).

I greatly appreciate informatics support provided by Zoran Bojanić and Alen Kovač.

I thank Prof. Eleanor J. Dodson and her family for their hospitality during one of my visits to York.

I am very grateful to my colleagues from the Department of Chemistry, and especially those from the Laboratory of General and Inorganic Chemistry, for giving me support and creating a pleasant working environment. I am also grateful to the staff of the York Structural Biology Laboratory for help and advice.

Most importantly, I thank members of my family for their support and encouragement throughout my life. This thesis is dedicated to them.

Dalibor Milić

Contents

University of Zagreb
Faculty of Science
Department of Chemistry

Doctoral Thesis

STRUCTURAL BASIS FOR THE ENZYMATIC ACTIVITY OF TYROSINE PHENOL-LYASE

DALIBOR MILIĆ

Laboratory of General and Inorganic Chemistry, Department of Chemistry,
Faculty of Science, University of Zagreb
Horvatovac 102a, HR-10000 Zagreb, Croatia

Tyrosine phenol-lyase (TPL) is a pyridoxal 5′-phosphate dependent enzyme which catalyzes the hydrolytic cleavage (β-elimination) of L-tyrosine to phenol and ammonium pyruvate, and also many other chemical reactions with different natural and synthetic substrates. The β-elimination reaction of L-tyrosine proceeds through several intermediate steps. In this work, the three-dimensional structures of several different forms of *Citrobacter freundii* TPL, including mutant proteins and complexes with ligands, were studied by the single-crystal X-ray diffraction analysis in a resolution range of 1.80–2.25 Å. The refined structures mimic the key intermediate steps in the reaction mechanism and provide a detailed view at the structural events during the enzymatic catalysis. The data indicate that a significant conformational change of the protein subunit is crucial for the β-elimination reaction. The catalytically important residues arginine-381 and threonine-124 interact with the bound substrate only in the closed conformation of the active site. Structural data also show that phenylalanine-448 destabilizes the quinonoid intermediate.

(125 + xxxv pages, 51 figures, 29 schemes, 16 tables, 205 references, original in English)

Thesis is deposited in the National and University Library (Zagreb, Croatia) and the Central Chemical Library, Faculty of Science, University of Zagreb (Zagreb, Croatia).

Keywords: β-elimination / enzyme / protein crystallography / pyridoxal 5′-phosphate / quinonoid / reaction mechanism / tyrosine phenol-lyase

Supervisors: Dr. Dubravka Matković-Čalogović, Professor (University of Zagreb)
Dr. Alfred A. Antson, Senior Wellcome Trust Fellow (University of York, UK)

Reviewers: Dr. Ivana Weygand-Đurašević, Professor (University of Zagreb)
Dr. Dubravka Matković-Čalogović, Professor (University of Zagreb)
Dr. Marija Luić, Senior Scientist (Ruđer Bošković Institute, Zagreb)

Thesis accepted: May 26, 2010

Sveučilište u Zagrebu
Prirodoslovno-matematički fakultet
Kemijski odsjek

Doktorska disertacija

STRUKTURNA OSNOVA ENZIMSKE AKTIVNOSTI TIROZIN–FENOL-LIAZE

DALIBOR MILIĆ

Zavod za opću i anorgansku kemiju, Kemijski odsjek,
Prirodoslovno-matematički fakultet, Sveučilište u Zagrebu
Horvatovac 102a, HR-10000 Zagreb, Hrvatska

Tirozin–fenol-liaza (TPL) je enzim ovisan o piridoksal-5′-fosfatu. Katalizira hidrolitičko cijepanje (β-eliminaciju) L-tirozina na fenol i amonijev piruvat, no također i mnoge druge kemijske reakcije s različitim prirodnim i sintetskim supstratima. β-Eliminacija L-tirozina napreduje kroz nekoliko međukoraka. U ovome su radu istražene trodimenzijske strukture nekoliko različitih oblika TPL-a iz *Citrobacter freundii*, uključujući mutirane proteine i komplekse s ligandima. Korištena je rentgenska difrakcijska analiza na jediničnom kristalu u rasponu rezolucija 1,80–2,25 Å. Utočnjene strukture modeliraju ključne međukorake reakcijskog mehanizma i daju detaljni uvid u strukturne događaje tijekom enzimske katalize. Podaci ukazuju da je za reakciju β-eliminacije od velike važnosti znatna konformacijska promjena proteinske podjedinice. Katalitički važni ostaci arginin-381 i treonin-124 međudjeluju s vezanim supstratom samo u zatvorenoj konformaciji aktivnog mjesta. Strukturni podaci također pokazuju da fenilalanin-448 destabilizira kinonoidni međuprodukt.

(125 + xxxv stranica, 51 slika, 29 shema, 16 tablica, 205 literaturnih navoda, jezik izvornika: engleski)

Rad je pohranjen u Nacionalnoj i sveučilišnoj knjižnici (Zagreb, Hrvatska) i u Središnjoj kemijskoj knjižnici Prirodoslovno-matematičkog fakulteta Sveučilišta u Zagrebu (Zagreb, Hrvatska).

Ključne riječi: β-eliminacija / enzim / kinonoid / piridoksal-5′-fosfat / proteinska kristalografija / reakcijski mehanizam / tirozin–fenol-liaza

Mentori: Dr. sc. Dubravka Matković-Čalogović, red. prof. (Sveučilište u Zagrebu)
Dr. sc. Alfred A. Antson (Sveučilište u Yorku, UK)

Ocjenitelji: Dr. sc. Ivana Weygand-Đurašević, red. prof. (Sveučilište u Zagrebu)
Dr. sc. Dubravka Matković-Čalogović, red. prof. (Sveučilište u Zagrebu)
Dr. sc. Marija Luić, zn. savj. (Institut "Ruđer Bošković", Zagreb)

Rad prihvaćen: 26. svibnja 2010.

Prošireni sažetak

Enzimi čija aktivnost ovisi o kofaktoru piridoksal-5′-fosfatu (PLP), jednom od derivata vitamina B6, kataliziraju razne kemijske reakcije u metabolizmu aminokiselina i drugih kemijskih spojeva koji sadrže amino-skupinu. Među kemijskim reakcijama kataliziranima enzimima ovisnim o PLP-u nalaze se reakcije kao što su transaminacija, racemizacija, dekarboksilacija, α-eliminacija, α-supstitucija, β-eliminacija, β-supstitucija, γ-eliminacija, γ-supstitucija, retro-aldolno cijepanje i druge [M. D. Toney, *Arch. Biochem. Biophys.* **433** (2005) 279–287]. Svim tim reakcijama zajedničko je to da napreduju kroz nekoliko koraka, od kojih je prvi korak nastanak vanjskog aldimina iz PLP-a i molekule supstrata. Za aminokiselinske supstrate sljedeći korak u mehanizmu je nastanak kinonoidnog međuprodukta, a kojim će mehanizmom reakcija dalje napredovati ovisi isključivo o enzimu i supstratu, tj. o vrsti reakcije koju enzim katalizira.

Tirozin–fenol-liaza (TPL) je jedan od enzima ovisnih o piridoksal-5′-fosfatu [H. Kumagai, H. Yamada, H. Matsui, H. Ohkishi, K. Ogata, *J. Biol. Chem.* **245** (1970) 1767–1772]. Ovaj je enzim prvenstveno pronađen u organizmima iz porodice *Enterobacteriaceae*, no nalazi se i u drugim porodicama bakterija i u nekim člankonošcima. U fiziološkim uvjetima TPL katalizira reverzibilnu β-eliminaciju molekule L-tirozina pri čemu nastaje molekula fenola, amonijev kation i piruvatni anion. β-Eliminacija u ovome kontekstu predstavlja reverzibilno hidrolitičko cijepanje veze Cβ–Cγ u molekuli L-tirozina. *In vitro*, TPL može katalizirati cijeli niz drugih reakcija. Osim β-eliminacije nekih β-supstituiranih L- i D-aminokiselina, njihovih derivata, kao i spojeva strukturno analognih L-tirozinu, TPL također katalizira reakciju suprotnu β-eliminaciji, zatim β-supstituciju derivatima fenola, racemizaciju L- i D-alanina, te ireverzibilnu polu-transaminaciju (pretvorbu u α-ketokiselinu) nekih aminokiselina. Veliki broj reakcija koje TPL može katalizirati čini ovaj enzim pogodnim za uporabu u organskoj sintezi i biotehnologiji, pa je stoga korišten za sintezu 3,4-dihidroksi-L-fenilalanina (L-DOPA) [S.-G. Lee, H.-S. Ro, S.-P. Hong, E.-H. Kim, M.-H. Sung, *J. Microbiol. Biotechnol.* **6** (1996) 98–102] i antitumorskog lijeka 2-aza-L-tirozina [E. B. Watkins, R. S. Phillips, *Bioorg. Med. Chem. Lett.* **11** (2001) 2099–2100].

Cilj istraživanja opisanog ovom disertacijom jest sa strukturnog stajališta okarakterizirati mehanizme reakcija kataliziranih tirozin–fenol-liazom, tj. odrediti trodimenzijske strukture najvažnijih međuprodukata u tim reakcijskim mehanizmima. Poznavanje ovih strukturnih detalja pridonosi razumijevanju dotičnih reakcijskih mehanizama kao i ulogâ pojedinih aminokiselinskih ostataka u tim mehanizmima. Pretpostavka je da je mehanizam β-eliminacije (a možda i mehanizmi nekih drugih reakcija kataliziranih TPL-om)

popraćen znatnijom promjenom u konformaciji proteinske molekule i da upravo o toj konformacijskoj promjeni ovisi enzimska učinkovitost i specifičnost TPL-a.

Molekula tirozin–fenol-liaze je homotetramerna, tj. sastoji se od četiri identične proteinske podjedinice molekulske mase 51,4 kDa – kako u otopini, tako i u istraživanim kristalnim strukturama TPL-a iz *Citrobacter freundii* [A. A. Antson, T. V. Demidkina, P. Gollnick, Z. Dauter, R. L. Von Tersch, J. Long, S. N. Berezhnoy, R. S. Phillips, E. H. Harutyunyan, K. S. Wilson, *Biochemistry* **32** (1993) 4195–4206; B. Sundararaju, A. A. Antson, R. S. Phillips, T. V. Demidkina, M. V. Barbolina, P. Gollnick, G. G. Dodson, K. S. Wilson, *Biochemistry* **36** (1997) 6502–6510] i *Erwinia herbicola* [S. V. Pletnev, A. A. Antson, N. I. Sinitsyna, Z. Dauter, M. N. Isupov, E. N. Hurs, N. G. Faleev, K. S. Wilson, G. Dodson, T. V. Demidkina, E. G. Arutyunyan, *Crystallogr. Rep.* **42** (1997) 809–819]. Jedan tetramer može vezati četiri molekule PLP-a, a sastoji se od dva katalitička dimera povezana isprepletenim "N-terminalnim rukama" iz susjednih podjedinica i hidrofobnim klusterom u središtu tetramera. Način smatanja polipeptidnog lanca podjedinice TPL-a pripada "tipu smatanja I" enzima ovisnih o PLP-u (porodica aspartat-aminotransferaze). Svaku podjedinicu možemo podijeliti na dvije proteinske domene – malu i veliku domenu. Aktivno mjesto grade aminokiselinski ostatci iz obje domene jedne podjedinice i male domene druge podjedinice koja pripada istom katalitičkom dimeru. Za katalitičku aktivnost važan je i kalijev ili neki drugi jednovalentni kation [B. Sundararaju, H. Chen, S. Shilcutt, R. S. Phillips, *Biochemistry* **39** (2000) 8546–8555] za kojeg je utvrđeno da se veže u blizini aktivnog mjesta između dvije proteinske podjedinice.

Na osnovi kristalnih struktura TPL-a iz *C. freundii* (strukture apo-oblika [A. A. Antson, T. V. Demidkina, P. Gollnick, Z. Dauter, R. L. Von Tersch, J. Long, S. N. Berezhnoy, R. S. Phillips, E. H. Harutyunyan, K. S. Wilson, *Biochemistry* **32** (1993) 4195–4206] i holo-oblika u kompleksu s analogom supstrata 3-(4′-hidroksifenil)propanskom kiselinom, HPPA [B. Sundararaju, A. A. Antson, R. S. Phillips, T. V. Demidkina, M. V. Barbolina, P. Gollnick, G. G. Dodson, K. S. Wilson, *Biochemistry* **36** (1997) 6502–6510]), te kristalnih struktura TPL-a iz *E. herbicola* (strukture apo- i holo-oblika, te kompleksa s kvazi-supstratom *N*-(5′-fosfopiridoksil)-L-tirozinom, PPT [S. V. Pletnev, A. A. Antson, N. I. Sinitsyna, Z. Dauter, M. N. Isupov, E. N. Hurs, N. G. Faleev, K. S. Wilson, G. Dodson, T. V. Demidkina, E. G. Arutyunyan, *Crystallogr. Rep.* **42** (1997) 809–819]) određena je struktura aktivnog mjesta i pretpostavljena je uloga pojedinih aminokiselinskih ostataka u mehanizmima reakcija kataliziranih TPL-om [R. S. Phillips, T. V. Demidkina, N. G. Faleev, *Biochim. Biophys. Acta* **1647** (2003) 167–172]. Kompleks s HPPA modelira strukturu Michaelisovog kompleksa, dok kompleks s PPT-om modelira strukturu vanjskog aldimina.

Smatra se da reakcija β-eliminacije L-tirozina katalizirana TPL-om napreduje kroz nekoliko glavnih koraka. U holo-obliku enzima kofaktor PLP je kovalentno vezan na bočni ogranak lizina-257 tvoreći unutrašnji aldimin. Reakcijom unutrašnjeg aldimina i molekule L-tirozina nastaje vanjski aldimin u kojemu je L-tirozin kovalentno vezan na PLP. Nadalje

se pretpostavlja da amino-skupina iz bočnog ogranka lizina-257 oduzima hidron (jezgru atoma vodika) s atoma Cα molekule supstrata pri čemu nastaje kinonoidni međuprodukt. Hidroksilna skupina tirozina-71 iz druge proteinske podjedinice donira hidron atomu Cγ kinonoidnog međuprodukta što dovodi do nastanka keto-kinonoidnog međuprodukta (ili prijelazne strukture). U razmjerno "napetoj" keto-kinonoidnoj strukturi dolazi do cijepanja veze Cβ–Cγ te nastanka molekule fenola i α-aminoakrilatnog međuprodukta. U posljednjem koraku reakcijskog mehanizma iz aminoakrilatnog međuprodukta ponovno nastaje unutrašnji aldimin i iminopiruvat koji se konačno hidrolizira u amonijev piruvat. Ciljanim mutacijama pokušalo se otkriti uloge u katalizi i nekih drugih aminokiselinskih ostataka u aktivnom mjestu TPL-a. Otkriveno je da su za enzimsku aktivnost pri β-eliminaciji L-tirozina, među ostalima, važni i treonin-124, arginin-381 i fenilalanin-448, no njihove uloge u katalizi nisu još sasvim razjašnjene.

Predmet ovog rada je tirozin–fenol-liaza iz *Citrobacter freundii*. Glavna metoda istraživanja je rentgenska strukturna analiza kristala različitih formi TPL-a. Pročišćeni uzorak TPL-a korišten je za kristalizaciju raznih oblika TPL-a i za pripravu kristalnih kompleksa TPL-a s odabranim molekulama – ligandima. Kristali kompleksa pripravljeni su namakanjem proteinskog kristala u odgovarajućoj stabilizacijskoj otopini koja sadrži željeni ligand. Pripravljeni jedinični kristali okarakterizirani su rentgenskom strukturnom analizom u rasponu razlučivanja 1,80–2,25 Å. Strukture su riješene metodom molekulske zamjene koristeći otprije poznate strukture TPL-a kao ishodne modele.

Struktura holo-oblika TPL-a riješena je pri razlučivanju 1,90 Å. Ova struktura otkriva strukturnu ulogu kalijevih kationa, a daje i detaljni uvid u međudjelovanja između PLP-a i aminokiselinskih ostataka u aktivnom mjestu enzima. Struktura holo-oblika mutanta D214A TPL riješena pri razlučivanju 1,90 Å pokazuje kako dotična mutacija mijenja konformaciju aktivnog mjesta što posljedično mijenja i međudjelovanja proteina s molekulom kofaktora. Time je sa strukturnog aspekta detaljno objašnjena smanjena aktivnost D214A TPL-a.

Struktura apoenzima pri pH 8,0 (što je blisko pH vrijednosti pri kojoj je enzimska aktivnost najveća) riješena je pri razlučivanju 1,85 Å. Jedna od dvije kristalografski neovisne proteinske podjedinice u strukturi apoenzima nalazi se u zatvorenoj konformaciji. Zatvorena konformacija nastaje zakretanjem male proteinske domene za oko 16° oko spone koja povezuje veliku i malu domenu što uzrokuje i zatvaranje aktivnog mjesta. S obzirom na ovu konformacijsku promjenu, molekulu TPL-a možemo podijeliti na: veliku krutu regiju (aminokiselinski ostatci 1–13, 45–345 i 405–422), malu krutu regiju (ostatci 19–44, 346–404 i 434–456), te na fleksibilne dijelove (ostatci 14–18 i 423–433) koji povezuju dvije krute regije. Zatvaranjem aktivnog mjesta smanjuje se njegova površina dostupna otapalu. U stukturama holoenzima namakanog fenolom (razlučivanje 1,85 Å), te amonijevim piruvatom (razlučivanje 1,80 Å) zamijećen je diskretni nered čitave male krute regije i fleksibilnih dijelova jedne od kristalografski neovisnih proteinskih podjedinica. Neuređeni su dijelovi uspješno modelirani i u otvorenoj i u zatvorenoj konformaciji s populacijskim

parametrom od oko 50 % za svaku konformaciju. Analiza kontakata u kristalu objašnjava zašto su obje konformacije podjednako povoljne u kristalima TPL-a, te sugerira da je konformacijska promjena iz otvorene u zatvorenu konformaciju podjednako povoljna i u otopini TPL-a.

Namakanjem kristala holo-forme u otopinama inhibitorâ L-alanina i L-metionina priređeni su kinonoidni međuprodukti dotičnih aminokiselina (pri razlučivanjima, redom, 1,90 Å i 1,95 Å). Njihovim strukturama razjašnjen je mehanizam racemizacije L-alanina, kao i unutarnji povrat Cα-hidrona u reakcijama kataliziranim TPL-om, te su otkrivene uloge pojedinih aminokiselinskih ostataka koji sudjeluju u tim procesima.

Kompleks mutanta Y71F s analogom supstrata 3-fluor-L-tirozinom (razlučivanje 2,05 Å) u otvorenom aktivnom mjestu sadrži kinonoidni međuprodukt (zbog mutacije reakcija β-eliminacije ne može napredovati dalje od nastanka kinonoidnog međuprodukta), dok je u zatvorenom aktivnom mjestu najvjerojatnije vezan vanjski aldimin. Vodikove veze bočnih ogranaka treonina-124 i arginina-381 s hidroksilnom skupinom supstrata postoje samo u zatvorenoj konformaciji aktivnog mjesta. Pretpostavlja se da ove vodikove veze olakšavaju eliminaciju fenola, tj. cijepanje veze Cβ–Cγ u molekuli tirozina i njegovih derivata, stoga je zatvaranje aktivnog mjesta neophodna strukturna promjena tijekom enzimske reakcije. Osim toga, na temelju kinetičkih studija razumno je pretpostaviti da dehidronirana gvanidinska skupina arginina-381 djeluje kao opća baza u enzimskoj reakciji. Molekula liganda ostvaruje van der Waalsov kontakt s bočnim ogrankom fenilalanina-448.

U strukturi kompleksa mutanta F448H s 3-fluor-L-tirozinom (razlučivanje 2,00 Å) sva se aktivna mjesta nalaze u zatvorenoj konformaciji. U aktivnim je mjestima vezan ligand čiji je identitet nemoguće sa sigurnošću utvrditi na temelju dostupnih kristalografskih podataka. Vjerojatno se radi o smjesi vanjskog aldimina i kinonoidnog međuprodukta, ali s "napetom" geometrijom zbog prostornih ograničenja unutar zatvorenog aktivnog mjesta. Bez obzira na pravi identitet vezanog liganda, fenolna skupina supstrata tvori vodikove veze s bočnim ograncima treonina-124 i arginina-381, te s imidazolnim prstenom histidina-448 koji se na tom položaju nalazi umjesto fenilalanina u divljem tipu proteina. Ovo posljednje međudjelovanje stabilizira zatvorenu konformaciju, te tako čini mutant F448H neaktivnim za reakciju β-eliminacije derivata L-tirozina.

Struktura kompleksa alaninskog kinonoidnog međuprodukta s piridin-*N*-oksidom (razlučivanje 2,25 Å) modelira strukturu neposredno nakon cijepanja veze Cβ–Cγ. U zatvorenom aktivnom mjestu nalazi se alaninsko-kinonoidna molekula (modelira α-aminoakrilatnu molekulu), te molekula piridin-*N*-oksida (modelira molekulu fenola neposredna nakon njenog nastanka). I dalje su sačuvana međudjelovanja liganda (u ovom slučaju piridin-*N*-oksida) s bočnim ograncima treonina-124 i arginina-381 opažene u zatvorenom aktivnom mjestu kompleksa Y71F TPL-a s 3-fluor-L-tirozinom.

Postojanje diskretnog nereda čitave proteinske domene u nekim ovdje opisanim kristalnim strukturama TPL-a upućuje na zaključak da je slična konformacijska promjena moguća i u fiziološkim uvjetima u otopini. Do zatvaranja aktivnog mjesta može doći

odmah nakon nastanka vanjskog aldimina. Zatvorena konformacija aktivnog mjesta nije ključna za nastanak kinonoidnog međuprodukta, no za nastavak enzimske reakcije, tj. nastanak keto-kinonoidnog međuprodukta (ili prijelaznog stanja), presudno je da konformacija aktivnog mjesta bude zatvorena. Zatvaranjem aktivnog mjesta katalitički važni aminokiselinski ostatci treonin-124 i arginin-381 dolaze u položaje na kojima mogu katalizirati reakciju β-eliminacije derivata L-tirozina. Osim toga, postojanje van der Waalsovih kontakata između fenolnog prstena supstrata i bočnog ogranka fenilalanina-448 dodatno olakšava eliminaciju fenola, i to tako da destabilizira prijelazno stanje na reakcijskom putu između kinonoidnog i α-aminoakrilatnog međuprodukta.

1 Introduction

1.1 Background: tyrosine phenol-lyase in brief

Tyrosine phenol-lyase (TPL) is an enzyme with activity dependent on pyridoxal 5′-phosphate (PLP),[1] one of the derivatives of vitamin B6. It is primarily found in bacteria.[2] At physiological conditions TPL catalyzes the reversible hydrolytic cleavage (β-elimination) of L-tyrosine to produce phenol and ammonium pyruvate.[1] *In vitro*, TPL can also catalyze many other reactions with a variety of different substrates, so it is applied as a biocatalyst in organic synthesis and biotechnology.

A molecule of TPL is homotetrameric, both in solution and in the investigated crystal structures of TPL from *Citrobacter intermedius* and *Erwinia herbicola*.[3–5] A TPL tetramer is composed of four identical protein subunits, each with the molecular mass of 51.4 kDa. One tetramer binds 4 PLP molecules. TPL belongs to the Fold Type I group of PLP-dependent enzymes (aspartate-aminotransferase family). TPL subunit is constructed of two protein domains: a large and a small one. The active site is built of the residues from both domains of one subunit and the small domain of the neighboring subunit. The two subunits forming the active sites are referred to as the catalytic dimer.

The postulated mechanism of the physiological β-elimination reaction of *Citrobacter freundii* TPL includes several key steps:[6,7] (a) formation of the external aldimine in the reaction of the internal aldimine with the substrate; (b) Cα hydron abstraction performed by the cofactor-binding residue Lys257 resulting in formation of the quinonoid intermediate; (c) Cγ hydronation by Tyr71 assisted by Arg381; and, finally, (d) cleavage of the Cβ–Cγ bond to form phenol and the α-aminoacrylate intermediate which is decomposed to ammonium pyruvate. The formation of the quinonoid intermediate with an amino acid is an essential step in the reaction mechanism of almost all PLP-dependent enzymes.[8]

1.2 Topic and objectives

Although previous biochemical and structural data pinpointed the role of individual residues in the catalysis by TPL, the details of their interactions with different substrates and molecular interactions stabilizing their active conformation during the intermediates' formation remained obscure. This is not surprising if we take into account that the reaction intermediates are often unstable, so their analysis by crystallographic methods

is not straightforward. For example, before the work presented in this thesis, the crucial quinonoid intermediates were only available for serine hydroxymethyltransferase[9] and tryptophan synthase.[10]

Domain closure was identified in a number of PLP-dependent enzymes.[11] Aspartate aminotransferase (AspAT) is an archetype for such conformational change during the enzymatic reaction.[12] The small domain of AspAT rotates during the substrate binding by 13° relative to the large domain. This closure buries the substrate in the active site and reorients the two Arg side chains in order to form salt bridges with the substrate carboxylate groups, thus moving the substrate into the optimal position for the transamination reaction. All domain movements are a consequence of coordinated small structural changes, and only a few side chains change their conformations. The domain closure was also identified in the structure of tryptophan indole-lyase (tryptophanase; Trpase).[13] Trpase and TPL are two paralogs with more than 40 % of sequence identity, with very similar structures[5,13,14] and analogous reaction mechanisms.[6,7] Nevertheless, it has been unknown whether a TPL molecule undergoes any significant conformational change during the enzymatic reactions.

The aim of this work is to understand/establish the structural basis for the enzymatic activity of TPL. The starting hypothesis was that the β-elimination reaction mechanism, and probably the mechanisms of some other reactions catalyzed by TPL, involved significant conformational change affecting the active site. Also, it was assumed, based on the results of site-directed mutagenesis and kinetic studies,[4,15] that enzymatic efficiency and substrate specificity depended on this conformational change.

The object of the research described in this thesis was TPL from *C. freundii*. The three-dimensional structures of different TPL forms (mutants and protein–ligand complexes) were studied by single-crystal X-ray structural analysis. These include the holo- and apo-form at pH 8.0, D214A mutant TPL, the holoenzyme soaked with phenol and ammonium pyruvate, the complexes of the wild-type holoenzyme with L-alanine and L-methionine, the complexes of TPL mutants Y71F and F448H with a substrate analog 3-fluoro-L-tyrosine, and the wild-type holoenzyme complexed with both piridine *N*-oxide and L-alanine. These structures represent "snapshots" of the reaction mechanisms. They mimic the key intermediates of the β-elimination, β-substitution, and alanine racemization reaction catalyzed by TPL. Also, they clarify the roles of catalytically important residues in the TPL active site, including Lys257, Tyr71, Thr124, Arg381, Phe448, and Asp214. The results presented here are very important for understanding the TPL reaction mechanisms, so they can serve as a basis for rational design of modified TPL molecules with optimal performance in specific catalytic tasks (different from the physiological reaction).

2 Literature Review

2.1 Pyridoxal 5′-phosphate-dependent enzymes: an abridged overview

Pyridoxal 5′-phosphate (PLP) is the most active form (vitamer) of vitamin B6 (Scheme 2.1).[16] It serves as a cofactor for a large family of PLP-dependent enzymes. This broad

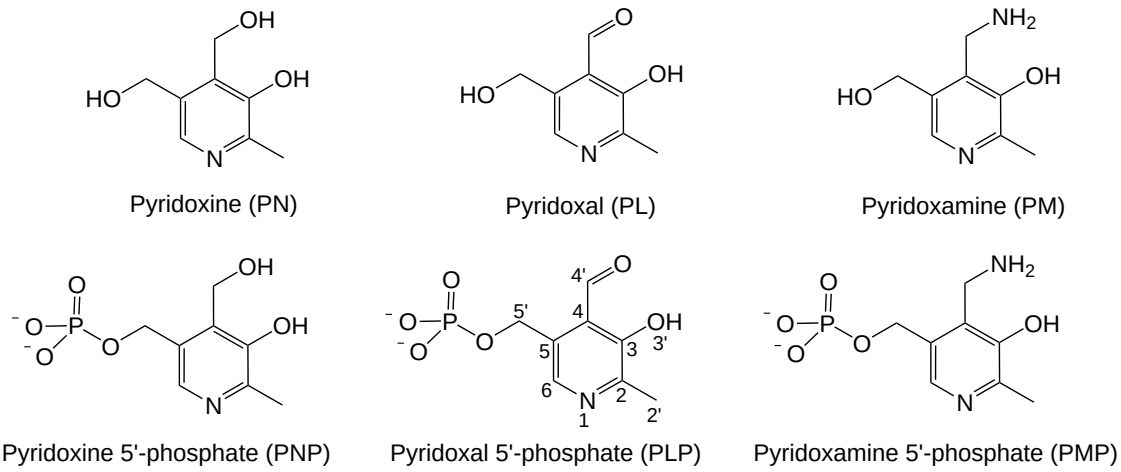

Scheme 2.1. Chemical forms (vitamers) of vitamin B6. Atom-numbering scheme is given for pyridoxal 5′-phosphate.

enzyme family comprises more than 140 different enzymes which belong to five (out of the six) enzyme classes defined by the Enzyme Nomenclature Committee of the International Union of Biochemistry and Molecular Biology. Namely, PLP-dependent enzymes are found among oxidoreductases (EC 1), transferases (EC 2), hydrolases (EC 3), lyases (EC 4) and isomerases (EC 5). Several PLP-dependent enzymes are already drug targets for approved drugs, whereas about twenty additional PLP-dependent enzymes are proposed as drug targets.[17]

Most PLP-dependent enzymes are involved in the metabolism of amino acids and amine-containing compounds (including amino sugars).[11] Some of the PLP-dependent enzymes participate in the metabolism of fatty acids: *e.g.* δ-6-desaturase (linoleoyl-CoA desaturase; EC 1.14.19.3) catalyzes the synthesis of vital polyunsaturated fatty acids by the desaturation of linolic and γ-linolenic acid.[18] PLP is also a cofactor entailed in the decomposition of storage carbohydrate: *e.g.* PLP-dependent glycogen phosphorylase (EC 2.4.1.1) is involved in glycogen degradation to glucose.[19] The formation

of δ-aminolevulinic acid is the rate-limiting step in the biosynthesis of hemoglobin and chlorophyll. This process is catalyzed by the two PLP-dependent enzymes: glutamate-1-semialdehyde 2,1-aminomutase (EC 5.4.3.8) in algae and plants, and δ-aminolevulinic acid synthase (EC 2.3.1.37) in birds and mammals.[20] Furthermore, PLP-dependent 1-aminocyclopropane-1-carboxylate synthase (EC 4.4.1.14) catalyzes the synthesis of 1-aminocyclopropane-1-carboxylate, a precursor for the biosynthesis of the phytohormone ethene, by cleaving the Cγ–Sδ bond in *S*-adenosyl-L-methionine.[21]

The most common reaction types catalyzed by PLP-dependent enzymes, and involving α-amino acids, can be divided according to the position in the substrate molecule at which the total reaction occurs. Reactions at the α position include transamination, decarboxylation, racemization, α-elimination and α-substitution (α-replacement) of an electrophilic R group. β-elimination and β-substitution (β-replacement) reactions occur at the β position, while γ-elimination and γ-substitution (γ-replacement) involve the change at γ position. Since many of these reaction pathways have common intermediates, the combinations of basic reaction types catalyzed by PLP-dependent enzymes are also known (*e.g.* decarboxylation-dependent transamination, or the coupled γ-elimination and β-substitution). Mechanisms of all these reactions have some common features. In the active form of an enzyme, PLP is covalently linked by an aldimine bond to the ε-amino group of a lysine residue in the active site, forming the internal aldimine (Scheme 2.2). When the aldimine bond is formed between a substrate molecule and PLP, the resulting Schiff base is termed the external aldimine. The first step of the reaction with an amino acid substrate is transaldimination, *i.e.* conversion from the internal to external aldimine. The next step is heterolytic cleavage of a σ-bond, *i.e.* the formation of a carbanionic structure referred as the quinonoid intermediate (Scheme 2.2). The role of PLP is stabilization of the carbanionic structure by delocalization of its negative charge through the extensive conjugation of the π-electrons in the aldimine bond, pyridine ring and phenolate group (dehydronated O3′ atom) of PLP. In a few cases the reaction proceeds by a concerted mechanism and the quinonoid is just the transition structure.[8] According to H. C. Dunathan's stereochemical hypothesis,[22] the bond to be broken has to be oriented perpendicular to the plane of the π-system (Fig. 2.1), so interactions between the polypeptide chain and the external aldimine are important in directing the catalyzed reaction and defining the reaction specificities of PLP-dependent enzymes.[8] The PLP-dependent enzymes belonging to the glycogen phosphorylase and aminomutase families do not obey the same basic principle of enzymatic catalysis. The enzymes in the aminomutase family catalyze the radical-initiated reaction on the PLP-bound amino acid,[23] while the enzymes in the glycogen phosphorylase family utilize the phosphate group of PLP for catalysis.[24]

The PLP-dependent enzymes compose the superfamily of PLP-dependent enzymes. They are classified into five different fold types (Fig. 2.2).[25] Each fold type contains representatives of at least two reaction types. The majority of known structures of PLP-dependent ezymes belong to the Fold Type I (aspartate aminotransferase) family. They

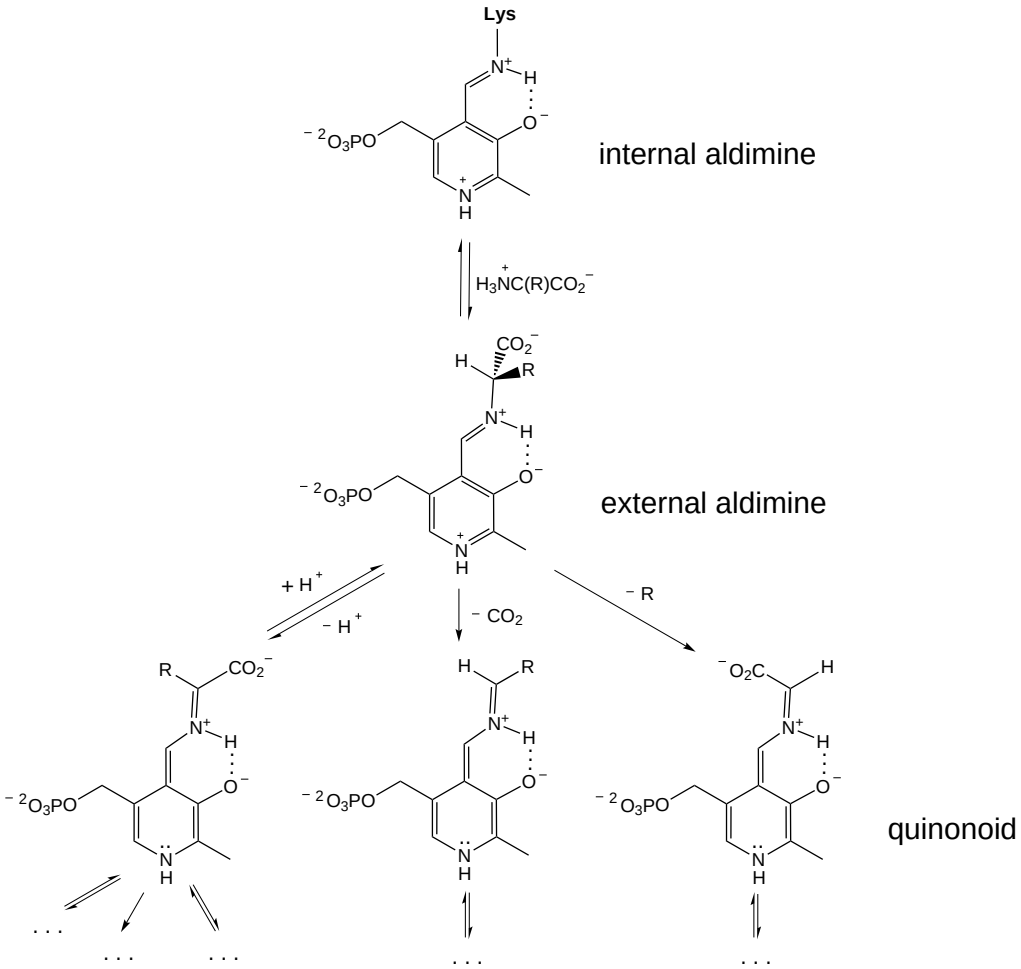

Scheme 2.2. Key intermediates common to almost all PLP-dependent enzymes.

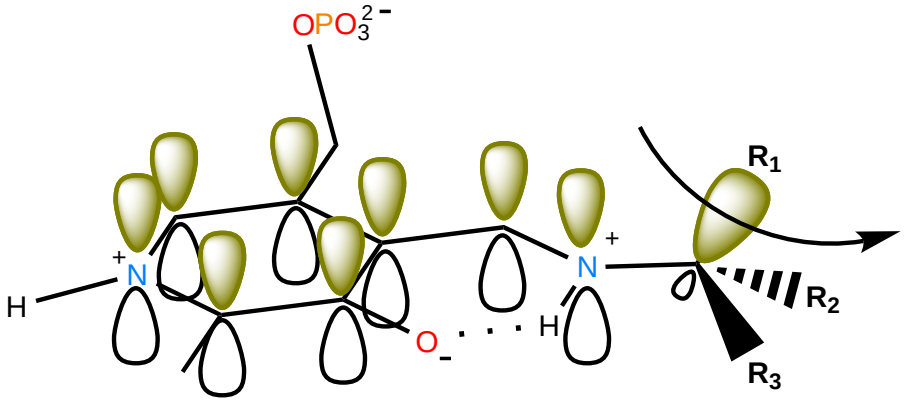

Figure 2.1. Illustration of Dunathan's hypothesis. The chemical bond to be broken (denoted by a *curved arrow*) must be aligned parallel with the π-molecular-orbital system in the external aldimine in order for the necesary orbital overlap to occur. The leaving group R_1 can be H, CO_2^-, or an electrophilic R group (*cf.* Scheme 2.2).

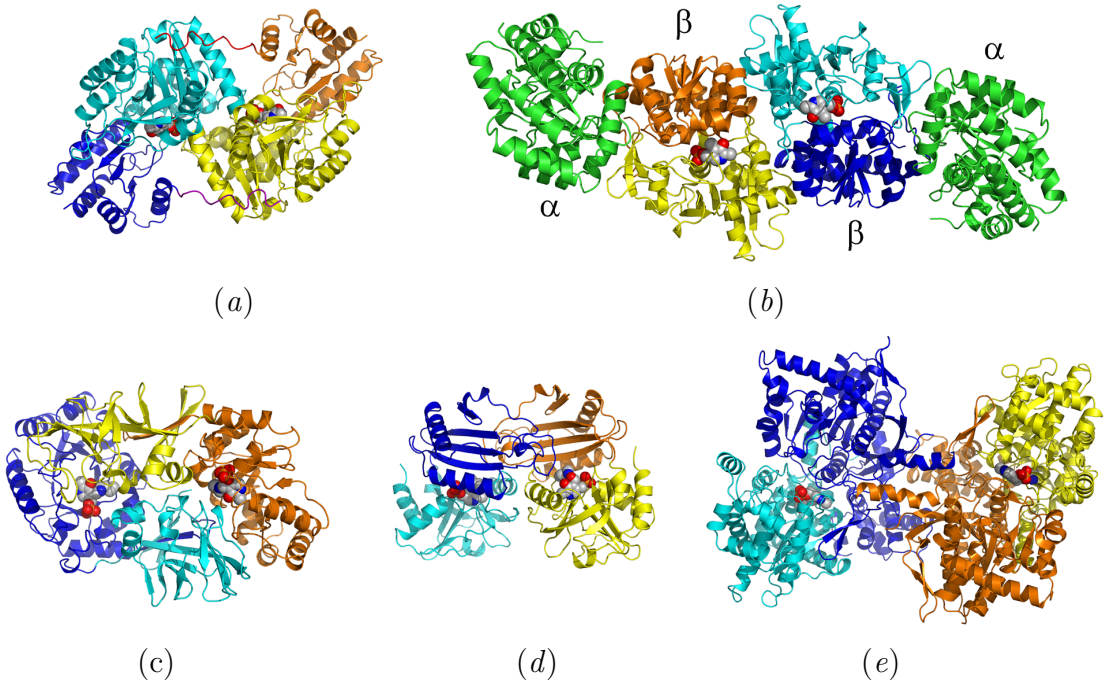

Figure 2.2. Representatives of the five fold types found for PLP-dependent enzymes. The PLP–lysine aldimines are shown as *spheres*. (*a*) Aspartate aminotransferase (PDB code: 7AAT).[12] Color code: *orange*, small domain of subunit 1; *yellow*, large domain of subunit 1; *red*, N-terminal arm of subunit 1; *blue*, small domain of subunit 2; *cyan*, large domain of subunit 2; and *purple*, N-terminal arm of subunit 2. (*b*) Tryptophan synthase $\alpha_2\beta_2$ complex (PDB code: 1TTQ).[26,27] Color code: *green*, α subunits; *orange*, N-terminal domain of β subunit 1; *yellow*, C-terminal domain of β subunit 1; *blue*, N-terminal domain of β subunit 2; *cyan*, C-terminal domain of β subunit 2. (*c*) Alanine racemase (PDB code: 1SFT).[28] (*d*) D-amino acid aminotransferase (PDB code: 1DAA).[29] Instead of PLP–lysine aldimine, non-covalently bonded PLP is bound in the active site. (*e*) Glycogen phosphorylase (PDB code: 1A8I).[19] Color code for (*c*)–(*e*): *orange*, N-terminal domain of subunit 1; *yellow*, C-terminal domain of subunit 1; *blue*, N-terminal domain of subunit 2; *cyan*, C-terminal domain of subunit 2.

are dimers, or higher-order oligomers, with two active sites per dimer on the interface between monomers. Each monomer contributes the catalytically essential residues to both active sites. In general, the active sites are independent, but in a few cases the cooperativity in enzyme action was observed.[11] Each protein monomer has a large and a small domain. In many enzymes significant movement of these domains was observed upon substrate binding, resulting in formation of a closed conformation of the active site.

Structures of the enzymes belonging to the Fold Type II (tryptophan synthase β subunit) family are similar to those of Fold Type I, but the proteins are evolutionary distinct. The active sites are composed entirely of residues from one monomer. Nevertheless, the functional form is a dimer or a higher-order oligomer. Enzymes from the Fold Type II often contain additional regulatory domains which bind allosteric regulators like *S*-adenosyl-L-methionine, valine, or isoleucine.

The enzymes in Fold Type III (alanine racemase) family are notably different from

the other PLP-dependent enzymes. A protein monomer consists of a classical α/β barrel and a second β-strand domain. In spite of the significant differences in the structural organization, the mode of PLP binding is similar to other fold types. The active enzymatic forms are homodimers, and each monomer contributes residues to both active sites.

The Fold Type IV (D-amino acid aminotransferase) family is similar to Fold Types I and II. The functional enzymatic forms are homodimers, with the catalytic portion of each monomer composed of a small and a large domain. A catalytic site is a near mirror image of those found in Fold Types I and II, with *re* face of PLP exposed to solvent.

Enzymes belonging to the Fold Type V (glycogen phosphorylase) family are structurally and mechanistically totally different from the other PLP-dependent enzymes. They utilize the phosphate group of PLP in hydron transfer. Glycon phosphorylase is a dimeric protein. Each subunits consists of three domains: N-terminal domain, glycogen-binding domain, and C-terminal domain. The C-terminal domain has a dinucleotide-binding fold and binds PLP.[24]

2.2 Tyrosine phenol-lyase

Tyrosine phenol-lyase* [TPL, EC 4.1.99.2; systematic name: L-tyrosine phenol-lyase (deaminating; pyruvate-forming); other names: β-tyrosinase, L-tyrosine phenol-lyase (deaminating)] is a pyridoxal 5′-phosphate (PLP) dependent enzyme.[1] The first report of TPL activity was published in 1953 by Y. Kakihara and K. Ichihara.[30] They observed that phenol in bacterial cultures of *Escherichia coli* (at that time called "*Bacterium coli phenologenes*") isolated from human feces is produced by direct cleavage of L-tyrosine and its derivatives, and not by stepwise degradation. M. Uchida *et al.* partially isolated the enzyme responsible for L-tyrosine cleavage from the cell extract of *E. coli*, grown in a medium containing L-tyrosine, and named it "β-tyrosinase".[31] Soon afterwards H. Yoshimatsu demonstrated that β-tyrosinase is a PLP-dependent enzyme which catalyzes the stoichiometric conversion of L-tyrosine to phenol and ammonium pyruvate (Scheme 2.3).[32] This observation was confirmed by Brot *et al.* who used a partially purified enzyme from another bacterial species – *Clostridium tetanomorphum*.[33]

TPL was primarily found in enterobacteria (*Enterobacteriaceae* family),[2] but it also occurs in other bacteria and presumably in some arthropods, as indicated for insect *Leptoglossus phyllopus*[34] and polydesmid millipedes *Oxidus gracilis*, *Pseudopolydesmus erasus*, and *Euryurus maculatus*.[35] Before the first complete bacterial genome (also the first genome of a living organism) was published in 1995,[36] several TPL genes from different bacterial species, including *Citrobacter intermedius* (formely *Escherichia intermedia*),[37] *Citrobacter freundii*,[3,38] *Enterobacter agglomerans* (also known as *Pantoea agglomerans* or

*A similar name "tyrosinase" has been used for a group of copper proteins that catalyze the reaction of monophenol monooxygenase (EC 1.14.18.1) and/or catechol oxidase (EC 1.10.3.1). These enzymes should not be confused with β-tyrosinase (TPL).

Erwinia herbicola),[39,40] and *Symbiobacterium thermophilum*,[41] were cloned and the primary structures were deduced from the DNA sequences. Now, TPL sequences from more than 50 bacterial species are known, mainly through genome sequencing projects. All of the known polypeptide sequences are highly similar with identities no less than 43 %, as found by BLAST alignment.[42]

TPL was located in cytoplasmic space of a bacterial cell.[39,43] Its synthesis is induced by L-tyrosine[39,44] and regulated through the TyrR protein and the cyclic AMP receptor protein.[45,46]

2.2.1 Tyrosine phenol-lyase catalyzes a wide variety of chemical reactions

TPL catalyzes at physiological conditions the reversible hydrolytical cleavage (α,β-elimination or β-elimination reaction) of L-tyrosine to produce phenol and ammonium pyruvate (Scheme 2.3).[47]

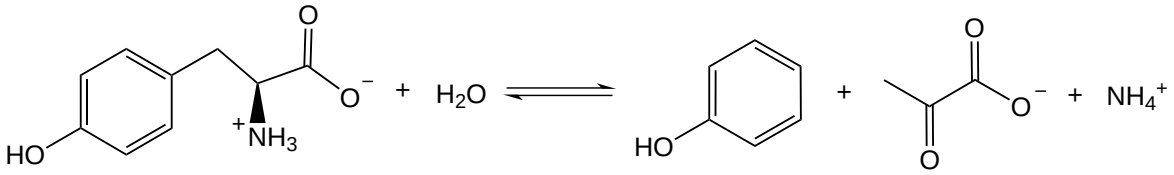

Scheme 2.3. Reversible β-elimination reaction of L-tyrosine catalyzed by TPL.

In vitro, this protein can catalyze a variety of other chemical reactions involving many different substrates.

2.2.1.1 β-Elimination reactions

In addition to β-elimination of its physiological substrate, TPL also catalyzes the β-elimination reaction of several β-substituted L-amino acids and even some D-amino acids with good leaving groups (Table 2.1). Amino acids and their analogs without good leaving groups, including L-alanine, L-phenylalanine,[48] L-methionine,[49] and dicarboxylic amino acids,[50] act like competitive inhibitors of the wild-type TPL. β-Elimination reaction is observed for 3-chloro-L-alanine (β-chloro-L-alanine; Scheme 2.4).[51,52] L-serine, L-cysteine,

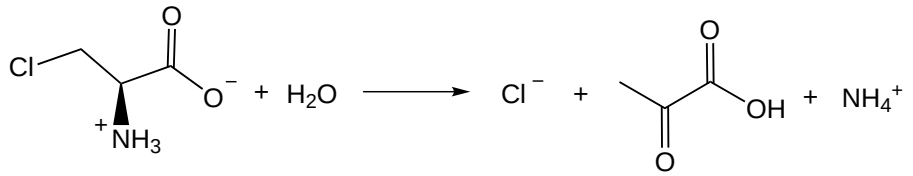

Scheme 2.4. β-Elimination reaction of β-chloro-L-alanine catalyzed by TPL.

and their alkyl and aryl derivatives undergo practically irreversible decomposition catalyzed by TPL[47,49,53] (Scheme 2.5). The relative rates of these reactions are significantly lower than that for the L-tyrosine.

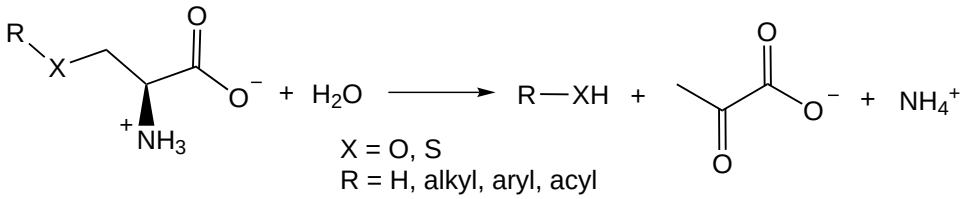

Scheme 2.5. Irreversible β-elimination reaction of L-serine and L-cysteine derivatives catalyzed by TPL.

Table 2.1. Steady-state kinetic parameters for the β-elimination reactions of *C. freundii* TPL with the selected substrates[49]

Substrate	$\frac{K_m}{\text{mmol dm}^{-3}}$	$\frac{k_{cat}}{\text{s}^{-1}}$	$\frac{k_{cat}/K_m}{\text{dm}^3\,\text{mol}^{-1}\,\text{s}^{-1}}$
L-tyrosine	0.20	3.5	$1.8 \cdot 10^4$
3-fluoro-L-tyrosine	0.10	1.4	$1.4 \cdot 10^4$
SOPC	0.10	5.1	$4.6 \cdot 10^4$
S-ethyl-L-cysteine	6.6	3.9	$5.9 \cdot 10^2$
S-methyl-L-cysteine	3.4	0.9	$2.8 \cdot 10^2$
S-benzyl-L-cysteine	0.2	0.5	$2.7 \cdot 10^3$
β-chloro-L-alanine	2.0	0.7	$3.5 \cdot 10^2$
L-serine	18	0.17	9.5
O-benzoyl-L-serine	2.9	8.3	$2.9 \cdot 10^3$

S-(*o*-nitrophenyl)-L-cysteine (SOPC) is an excellent substrate for the β-elimination reaction (Table 2.1), so it is routinely used for spectroscopic measurement of TPL enzymatic activity: one unit of TPL enzymic acitivity is defined as the amount of enzyme catalyzing transformation of 1 μmol of SOPC per one minute under standard conditions.[53] The irreversible β-elimination reaction was also detected for *O*-acyl-L-serine derivatives: while *O*-benzoyl-L-serine is a relatively good substrate for β-elimination, *O*-acetyl-L-serine is a very poor substrate.[53] It was also found that D-serine[47] and both enantiomers of threonine[54] are substrates for the β-elimination catalyzed by TPL. In the case of L- and D-threonine, α-ketobutyrate is formed (Scheme 2.6), but the same was not observed for two *allo*-threonine enantiomers.[54]

L-Tyrosine-related amino acids are also substrates for the β-elimination reaction catalyzed by TPL. It was observed that hydroxyl group at the *para*-position is essential for the substrate molecule to interact with the enzyme and to progress to the β-elimination – thus *e.g.* L-phenylalanine, *o*-L-tyrosine, *m*-L-tyrosine, 4-fluoro-L-phenylalanine, and 4-chloro-L-phenylalanine are not substrates for TPL.[55] Molecules that possess the hydroxyl group at the *para*-position and hydroxyl, halogen, methyl, or methoxy group at *ortho*- or

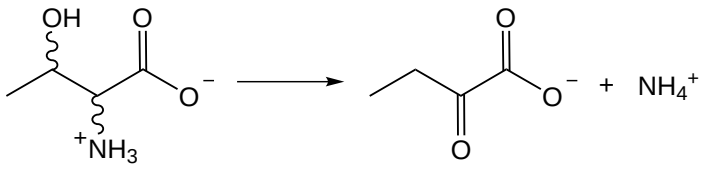

only (2*S*, 3*R*) and (2*R*, 3*S*)

Scheme 2.6. Overall β-elimination reaction of L-threonine (2*S*, 3*R*) and D-threonine (2*R*, 3*S*) catalyzed by TPL.

meta-position could be degraded by TPL, but at a lower rate than L-tyrosine. Exceptions are substrates with bulkier groups: 3-iodo-L-tyrosine and 3,5-diiodo-L-tyrosine.[55]

TPL also catalyzes the β-elimination reaction of other compounds structurally analogous to L-tyrosine. One example is an amino-acid alkaloid mimosine [IUPAC name: (2*S*)-3-amino-3-(3-hydroxy-4-oxopyridin-1-yl)propionic acid; Scheme 2.7].[55] Other exam-

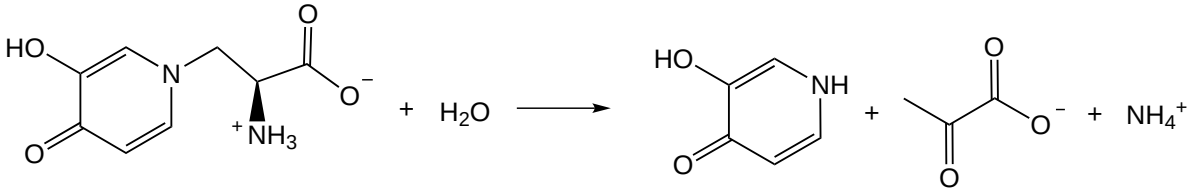

Scheme 2.7. β-Elimination reaction of mimosine catalyzed by TPL.

ples include some non-amino-acid derivatives, like organophosphorous compounds: 1-amino-2-(4-hydroxyphenyl)ethyl phosphinic acid and 1-amino-2-phenylethyl phosphinic acid (Scheme 2.8).[56] Substitution of a planar carboxylic group (in an amino acid) by a tetrahedral phosphinic group in these phosphinic substrates slightly affected their affinities for TPL, but considerably diminished the reaction rates. It is interesting to note that the corresponding reactions of phosphonic analogs were not observed.[56]

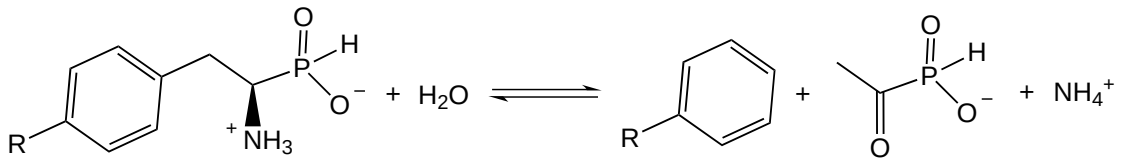

R = H, OH

Scheme 2.8. β-Elimination reaction of phosphinic acid derivatives catalyzed by TPL.

2.2.1.2 Reversals of the β-elimination reaction

The β-elimination reaction becomes reversible (Scheme 2.9) in conditions with high concentration of ammonium pyruvate and with an adequate concentration of phenol or its suitable derivative.[55,57,58] In addition to phenol,[57,58] relatively good substrates for the re-

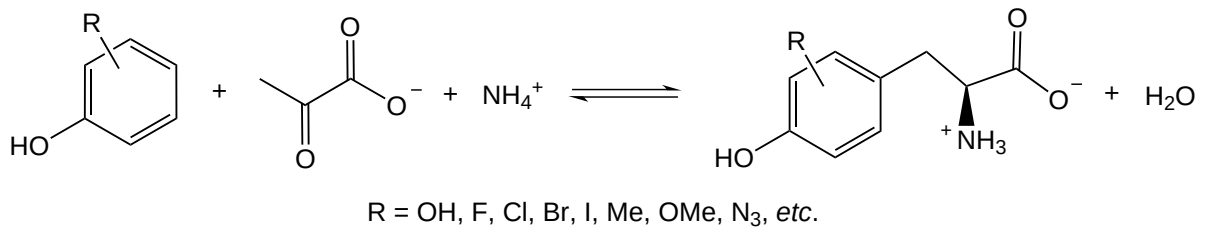

Scheme 2.9. Reversal of β-elimination reaction catalyzed by TPL.

versal of β-elimination are catechol (benzene-1,2-diol),[57] *o*-fluorophenol, *m*-fluorophenol, *m*-chlorophenol, and *m*-methoxyphenol.[55]

Reversal of the β-elimination reaction catalyzed by TPL is also known as "synthethic reaction", because it has been used for the one-step synthesis of L-tyrosine, several L-tyrosine derivatives and heterocyclic analogs. The most prominent is the synthesis of 3,4-dihydroxyphenyl-L-alanine (L-DOPA),[51,57,59] a psychoactive drug used in the clinical treatment of Parkinson's disease and dopamine-responsive dystonia.

TPL from *C. freundii* was used to synthesizes 2-aza-L-tyrosine and 3-aza-L-tyrosine from 3-hydroxypyridine and 2-hydroxypyridine, respectively, and ammonium pyruvate (Scheme 2.10).[60] 2-Aza-L-tyrosine is a natural product, originally isolated from a *Streptomyces* sp., for which the antitumor activity was shown.[61] 3-Aza-L-tyrosine is also a natural product isolated from the poisonous mushroom *Clitocybe acromelalga*.[62] Athough the yields of these two syntheses are relatively low, chiral products are obtained from readily available achiral starting materials. Both azatyrosines were shown to be antimetabolites of L-tyrosine and inhibitors of enzymes which react with free L-tyrosine in solution or tyrosyl residues in polypeptides. Moreover, 2-aza-L-tyrosine was found to be the most potent competitive inhibitor of TPL.[63]

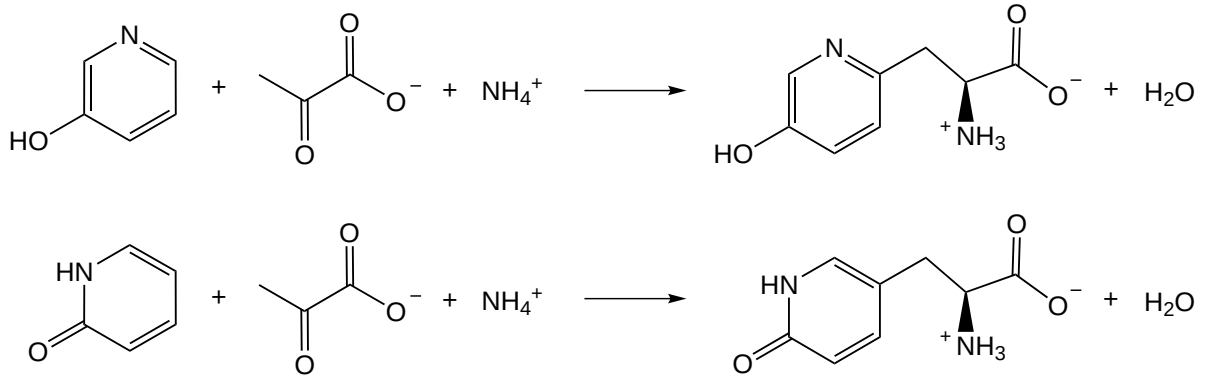

Scheme 2.10. Syntheses of 2-aza-L-tyrosine (*top*) and 3-aza-L-tyrosine (*bottom*) catalyzed by TPL.

Syntheses by the reversal of β-elimination reaction of all di- and trifluoro-L-tyrosines,[64] 3-chloro-L-tyrosine, both monobromo-L-tyrosines, 2-iodo-L-tyrosine, both monomethyl-L-tyrosines, 2-ethyl-L-tyrosine, 3-methoxy-L-tyrosine,[43] and 2-azido-L-tyrosine[65] were also reported. In addition, TPL was used for syntheses of 6-[^{18}F]fluoro-3,4-dihydroxyphenyl-

L-alanine[66] and some ^{11}C-labeled analogs of L-tyrosine.[67] These radioactive tracers were used to evaluate presynaptic dopaminergic function *in vivo* by positron emission tomography.[68] Another interesting example of reversal of the β-elimination reaction is a single-step stereospecific synthesis of (2*S*,3*R*)-β-methyltyrosine from achiral reactants ammonium α-ketobutyrate and phenol (Scheme 2.11).[69] This reaction is not feasible under standard conditions of TPL catalysis, but a significant amount of product was detected at pH 9 by using increased concentrations of PLP and TPL, and omitting 2-mercaptoethanol. In comparison, the most efficient non-enzymatic stereospecific synthesis of (2*S*,3*R*)-β-methyltyrosine requires nine steps.[70]

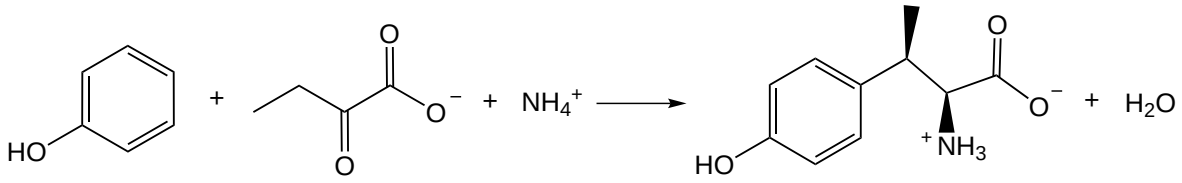

Scheme 2.11. Synthesis of (2*S*,3*R*)-β-methyltyrosine in a single, environmentally friendly step from achiral starting materials. The reaction is catalyzed by TPL.

2.2.1.3 β-Substitution reactions

TPL catalyzes the β-substitution (β-replacement) reactions mainly between the substrates for β-elimination and phenol derivatives (Scheme 2.12). One of the first ob-

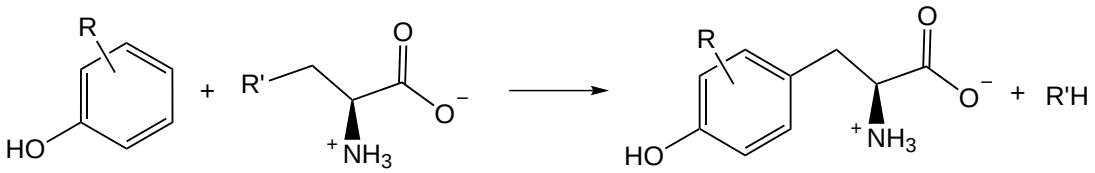

Scheme 2.12. β-Substitution reactions catalyzed by TPL.

served β-substitution reactions catalyzed by crystalline TPL was between catechol and L-tyrosine, with L-DOPA as a product.[71] Except for L-tyrosine, other amino acid derivatives were also used as substrates for β-substitution. Reaction of L-serine, L-cysteine and *S*-methyl-L-cysteine with catechol or phenol gave L-tyrosine or L-DOPA, respectively.[71,72] When resorcinol (benzene-1,3-diol) reacts with *S*-methyl-L-cysteine, the final product is (3*S*)-3,4-dihydro-3-amino-7-hydroxycoumarin, formed through the intramolecular esterification (Scheme 2.13).[73] Pyrogallol (benzene-1,2,3-triol) and *S*-methyl-L-cysteine gave 2,3,4-trihydroxyphenyl-L-alanine as a product in the β-substitution reaction catalyzed by TPL.[74]

Similar as for the β-elimination reaction, *O*-benzoyl-L-serine is a good substrate, while *O*-acetyl-L-serine is a very poor substrate for the β-substitution reaction.[53] Reaction of

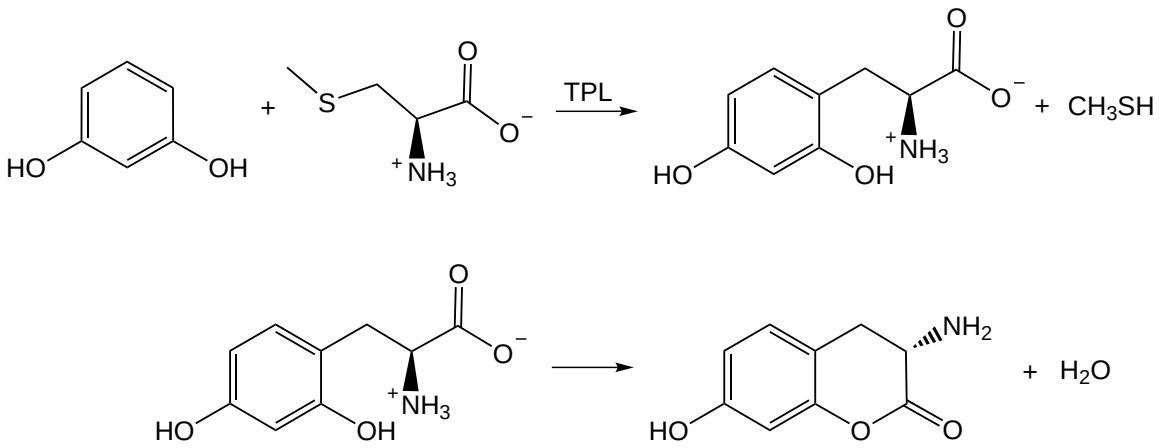

Scheme 2.13. Synthesis of (3*S*)-3,4-dihydro-3-amino-7-hydroxycoumarin.

S-(*o*-nitrophenyl)-L-cysteine (SOPC) with phenol or monofluorinated phenols catalyzed by TPL from *C. freundii* is a very efficient (approximately 70 % of conversion) and relatively fast route to produce L-tyrosine and its monofluorinated derivatives.[75] This is not surprising for SOPC, which is a substrate with relatively low K_m and high V_{max} of the β-elimination reaction.[53]

All mono-, di- and trifluoro-L-tyrosines were synthesized by β-substitution TPL catalyzed reaction from L-serine or 3-chloro-L-alanine, and the appropriate fluorinated phenols.[64,76] The analogous TPL catalyzed reactions from β,β,β-trifluoro-L-alanine with fluorophenols result in the ring fluorinated β,β-difluoro-L-tyrosines, but these products are unstable and undergo a rapid elimination of fluoride ions which results in the β-keto compound (Scheme 2.14). The lifetime of β,β-difluoro-L-tyrosines depends on the presence and position of fluoro substituents on the ring: when multiple fluoro substituents are present, the stability of β,β-difluoro-L-tyrosines is considerably increased.[64]

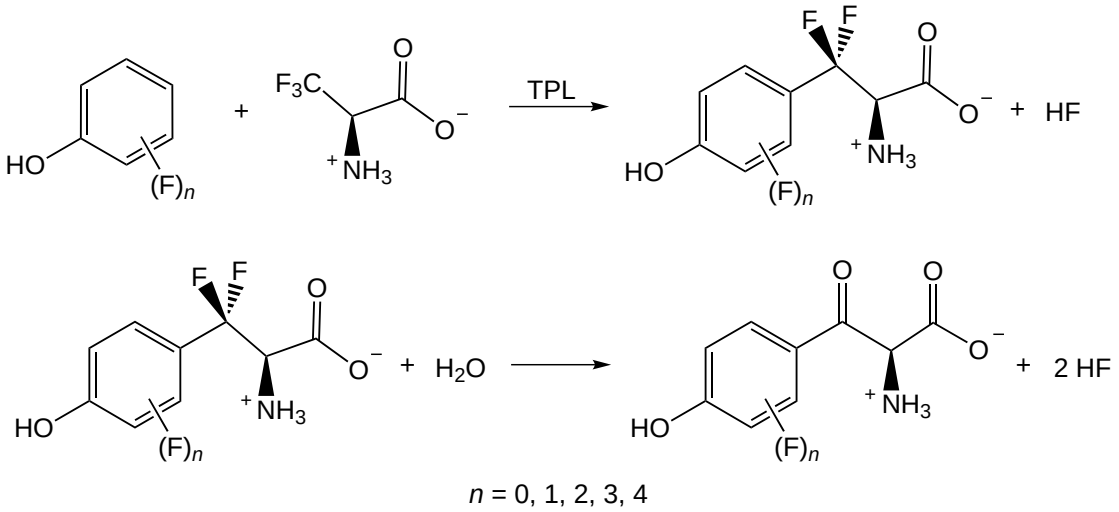

Scheme 2.14. Synthesis of β,β-difluoro-L-tyrosines catalyzed by TPL and their degradation to α-amino-β-keto acids.

2.2.1.4 Racemization of alanine

The alanine molecule does not have a suitable leaving group at the Cβ atom, so it cannot be a substrate for the β-elimination nor β-substitution reactions catalyzed by TPL. Instead, TPL catalyzes the racemization of L- and D-alanine, *i.e.* their conversion into the racemic mixture (Scheme 2.15). This slow non-physiological side reaction was first observed for

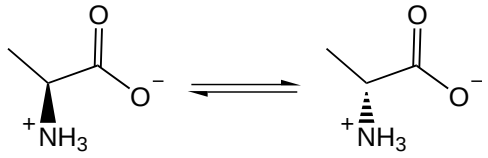

Scheme 2.15. Racemization of alanine catalyzed by TPL.

crystalline TPL prepared from cells of *C. intermedius* (formely *E. intermedia*),[71,77] and later it was studied in more detail.[48,78,79] The steady-state kinetic parameters for alanine racemization by TPL from *C. freundii*, K_m and k_{cat}, are 11 mmol dm^{-3} and 0.03 s^{-1}, and 32 mmol dm^{-3} and 0.008 s^{-1} for L- and D-alanine, respectively.[48]

2.2.1.5 Transamination reactions

Many PLP-dependent enzymes, aside from their physiological reactions, catalyze the transfer of the amino group of a substrate (usually an amino acid) to the cofactor (PLP) with the formation of pyridoxamine 5′-phosphate (PMP) and a keto acid (the half-transamination reaction; Scheme 2.16). It was demonstrated that TPL catalyzes, as the side reaction, the half-transamination of its substrates L-tyrosine and L-serine, and the competitive inhibitors L-alanine, L-phenylalanine, L-*m*-tyrosine,[80] L-aspartate, and L-glutamate.[81] In all cases, the half-transamination reactions were irreversible. Due to the limited solubility of L-tyrosine and the low rate of its transamination, it was not possible to determine the kinetic parameters of half-transamination with this amino acid as a substrate. Kinetic parameters of half-transaminations for other investigated substrates are given in Table 2.2.

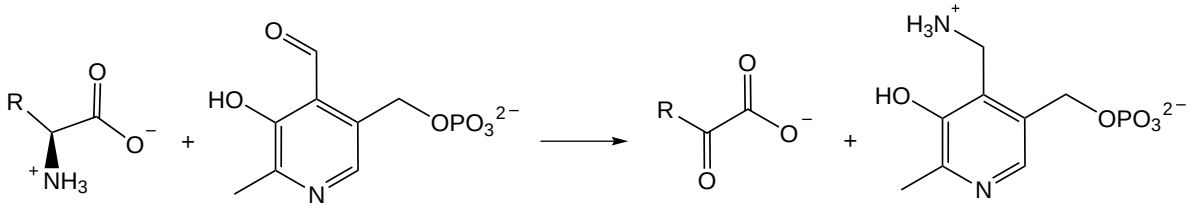

Scheme 2.16. Irreversible half-transamination catalyzed by TPL.

Table 2.2. Kinetic parameters for the half-transamination reactions of TPL

Substrate	$\frac{K_m}{\text{mmol dm}^{-3}}$	$\frac{k_{cat}}{\text{s}^{-1}}$	$\frac{k_{cat}/K_m}{\text{dm}^3\,\text{mol}^{-1}\,\text{s}^{-1}}$
L-serine[a]	51	$1.0 \cdot 10^{-3}$	$2 \cdot 10^{-2}$
L-*m*-tyrosine[a]	0.94	$2.69 \cdot 10^{-3}$	2.86
L-phenylalanine[a]	4.15	$0.8 \cdot 10^{-3}$	1.93
L-alanine[a]	6.1	$1.53 \cdot 10^{-3}$	2.5
L-aspartate[b]	not reported	$1.1 \cdot 10^{-4}$	not reported
L-glutamate[b]	not reported	$1.3 \cdot 10^{-4}$	not reported

[a] From (Demidkina *et al.*, 1987).[80]
[b] From (Mouratou *et al.*, 1999).[81]

2.2.2 Structural studies of tyrosine phenol-lyase

Already in the early days of research on TPL, crystallization with ammonium sulfate as precipitant was used in TPL purification.[47,82] TPL crystallized in the habitus of rods[47] and the obtained crystalline enzyme preparation was shown to catalyze the enzymatic reactions.[47,58,71,73,74,77] But, regardless of the crystal availability, at that time it was a very demanding task to solve TPL structure by X-ray diffraction. The first crystallographic investigation of TPL from *C. intermedius* was reported by Demidkina *et al.* in 1988.[83] Crystallization was carried out using the hanging-drop and sitting-drop vapor diffusion techniques at 4 °C in 50 mmol dm^{-3} potassium phosphate buffer (pH 6.5–8.0) and with ammonium sulfate or poly(ethylene glycol) (PEG) (6000 or 4000) as precipitants. The enzyme concentration was between 10 and 30 mg cm^{-3}. The best (largest) crystals were obtained when the protein solution (25–30 mg cm^{-3}) in 50 mmol dm^{-3} potassium phosphate buffer (pH 7.0), 20 %-saturated (1.1 mol dm^{-3}) $(NH_4)_2SO_4$ and 0.2 mmol dm^{-3} dithiotreitol (DTT) was equlibrated with 30 %-saturated (1.6 mol dm^{-3}) $(NH_4)_2SO_4$ solution in the sitting-drop experimental setting. In concentrated $(NH_4)_2SO_4$ solutions the holoenzyme is separated into the apoenzyme and a cofactor PLP, so the resulting prismatic crystals were crystals of the apoenzyme. The crystals had the orthorhombic $P2_12_12$ space-group symmetry with the unit-cell dimensions of $a = 75.5$ Å, $b = 138.4$ Å, $c = 94.1$ Å and diffracted X-rays up to 2.7 Å resolution. Also, isomorphous heavy-atom derivatives were prepared by soaking the apoenzyme crystals in solutions of heavy-atom compounds (K_2PtCl_4 and *p*-chloromercuriphenylsulfonic acid). Because NH_3 can coordinate metal ions, the stabilization solution for soaking was composed of 1 mol dm^{-3} $MgSO_4$ in 50 mmol dm^{-3} HEPES-KOH buffer (pH 7.0).[83]

Two years later, a three-dimensional structural model at very low resolution (25 Å) became available through an electron microscopy study of tubular TPL crystals.[84] Not long afterwards, a preliminary, incomplete model of *C. intermedius* TPL at 2.7 Å-resolution was published.[85] The crystals of apo-TPL were produced by vapor diffusion in slightly modified conditions using a pH gradient: drop of the protein solution, containing 20 mg cm^{-3} apo-TPL, 0.1 mol dm^{-3} potassium phosphate buffer (pH 7.0), and 1 mol dm^{-3} $(NH_4)_2SO_4$,

was equilibrated against a reservoir solution with 0.1 mol dm^{-3} potassium phosphate buffer (pH 6.0), and 1 mol dm^{-3} $(NH_4)_2SO_4$. The structure was solved by multiple isomorphous replacement using the uranium (UO_2SO_4) and mercury ($C_2H_5HgH_2PO_4$) derivatives. The resulting model of apo-TPL contained 85 % of protein atoms and gave insight into the overall architecture and topology of a TPL molecule.

Table 2.3. Basic crystallographic data for the published TPL crystal structures

Structure[a]	**1**	**2**	**3**	**4**	**5**	**6**
PDB code	1TPL	2TPL	–	–	–	1C7G
Crystal space group	$P2_12_12$	$P2_12_12$	$P6_222$	$P6_222$	$P2_12_12_1$	$P2_12_12$
Unit cell parameters						
a / Å	76.0	135.07	145.5	144.6	111.8	163.49
b / Å	138.3	143.91	145.5	144.6	158.3	113.04
c / Å	93.5	59.80	171.5	176.0	202.4	101.09
α	90°	90°	90°	90°	90°	90°
β	90°	90°	90°	90°	90°	90°
γ	90°	90°	120°	120°	90°	90°
No. of TPL subunits in the asymmetric unit	2	2	1	1	8	4
Ligands in the model	4 SO_4^{2-}	2 Cs^+ 2 PLP HPPA	K^+	NH_4^+ PLP	8 K^+ 8 PLP 8 PPT	4 PLP
T / K	RT[b]	RT	120	293	120	?
d_{min}[c] / Å	2.3	2.5	2.4	2.7	2.0	2.0
R_{cryst}	0.162	0.183	0.202	0.169	0.206	0.186
R_{free}	–	0.263	0.235	0.207	0.272	0.242

[a] Structure codes and references: **1** – apo-TPL from *C. intermedius*;[3] **2** – holo-TPL from *C. intermedius* complexed with 3-(4′-hydroxyphenyl)propanoic acid (HPPA);[4] **3** – apo-TPL from *E. herbicola* (*P. agglomerans pv. gypsophilae*);[5] **4** – holo-TPL from *E. herbicola*;[5] **5** – apo-TPL from *E. herbicola* complexed with *N*-(5′-phosphopyridoxyl)-L-tyrosine (PPT);[5] **6** – holo-TPL from *E. herbicola*.[86]
[b] Room temperature.
[c] Resolution.

Finally, in 1993 Antson *et al.* published the first (almost) complete crystal structure of *C. intermedius* apo-TPL at 2.3 Å-resolution (PDB code: 1TPL; **1**).[3] In 1997, the structure of *C. intermedius** holo-TPL complexed with a substrate analog 3-(4′-hydroxyphenyl)propanoic acid, HPPA (PDB code: 2TPL; **2**) was published.[4] Crystals of **2** were obtained in different crystallization conditions using monomethyl ether poly(ethylene glycol) 5000 as the precipitant in the hanging drop vapor diffusion method.

*In the original publication the crystal structure was referred as that of *C. freundii* TPL,[4] while the title of the PDB entry (2TPL) and the corresponding sequence indicate that the source organism was *C. intermedius*. Primary structures of TPL from *C. intermedius* and *C. freundii* differ only in an amino acid residue 205, which is Ala in *C. intermedius* and Glu in *C. freundii* protein. In spite of only minor sequence difference between these two orthologs, several differences were observed in their reaction kinetics.[3]

The protein solution (20 mg cm^{-3} TPL, 50 mmol dm^{-3} HPPA, 1 mmol dm^{-3} DTT, and 0.2 mmol dm^{-3} PLP in 50 mmol dm^{-3} triethanolamine buffer) was half diluted with a reservoir solution containing 0.30–0.45 g cm^{-3} monomethyl ether poly(ethylene glycol) 5000 and monovalent cation salts KCl or CsCl (0.15–0.6 mol dm^{-3}). The structures of TPL from *Erwinia herbicola* (scientific name: *Pantoea agglomerans pv. gypsophilae*; *Enterobacter agglomerans*) are also known. These include structures of the apoenzyme (**3**), holoenzyme (**4**), and the complex with the quasi-substrate *N*-(5′-phosphopyridoxyl)-L-tyrosine (PPT; **5**).[5] The crystals used for X-ray structural analyses were prepared by the hanging drop method using 3.6 mol dm^{-3} KCl, 1.8 mol dm^{-3} $(NH_4)_2SO_4$, and 0.20 g cm^{-3} monomethyl ether poly(ethylene glycol) 5000 solutions as precipitants for **3**, **4**, and **5**, respectively. Crystallization with 0.30 g cm^{-3} PEG 6000 in 0.2 mol dm^{-3} ammonium acetate and 0.1 mol dm^{-3} sodium citrate (pH 6.2) resulted in other crystal form of *E. herbicola* holo-TPL (PDB code: 1C7G; **6**).[86] The published TPL structures are summarized in Table 2.3.

2.2.2.1 Overall organization of a TPL molecule – a quaternary structure

A molecule of tyrosine phenol-lyase is homotetrameric, both in solution[87] and in all known crystal structures (Fig. 2.3).[3–5,86,88] It is composed of four identical protein subunits (α_4), each with the molecular mass of about 51 kDa.[87] The protein subunits are arranged in corners of a flattened (orthorhombic) tetrahedron thus forming the homotetramer with an approximate point group symmetry of D_2 ($\equiv$ 222). Dimensions of the tetramer are approximately $80 \times 60 \times 105$ Å^3.

One TPL monomer (subunit) binds one PLP molecule.[1] It was shown that the PLP binding residue is Lys257.[3] The enzymatic active site is situated between two protein subunits that are related by a 2-fold molecular axis (denoted by Q in Fig. 2.3a). These two subunits are mutually firmly connected forming the catalytic dimer. The architecture of the TPL catalytic dimer is very similar to that of a dimeric molecule of aspartate aminotransferase[89] (Fig. 2.2a). Two catalytic dimers in a tetrameric TPL molecule are related by molecular 2-fold axis denoted by P and R in Fig. 2.3a, thus forming a dimer of dimers.

Number of protein subunits (monomers) in the crystallographic asymmetric units differ between the solved crystal structures (Table 2.3). In **2**, the asymmetric unit comprises the catalytic dimer, with the P axis being the crystallographic 2-fold axis.[4] The asymmetric unit in **1** is composed of a non-catalytic dimer where the Q axis is the crystallographic 2-fold axis.[3] The asymmetric unit of structures **3** and **4** is made of a TPL monomer, whereas two tetramers are crystallographically independent in **5**.[5] The unit cell volume of **6** is approximately two times smaller then that of **5**, so there is only one TPL tetramer in the asymmetric unit of **6**.[86]

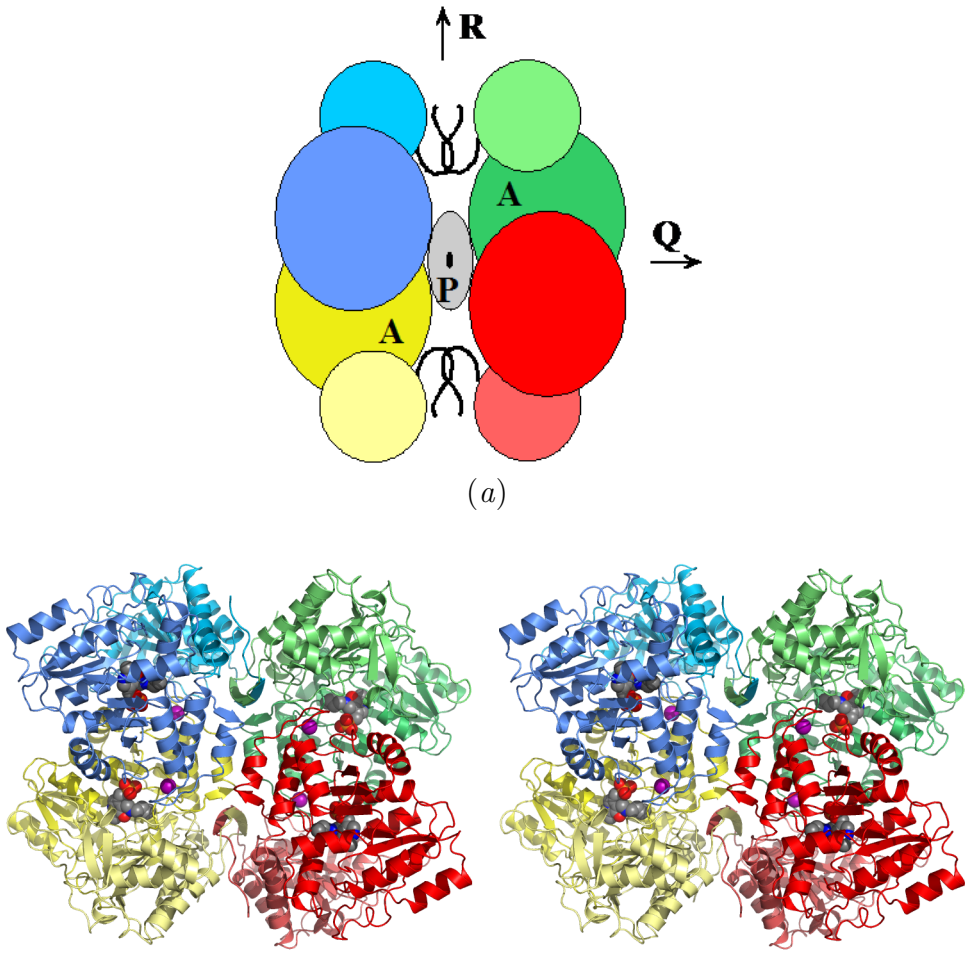

(*a*)

(*b*)

Figure 2.3. Quaternary structure of TPL molecule. (*a*) Schematic representation of overall organization of the TPL homotetramer. The 2-fold molecular axis are denoted as P, Q, and R, as defined by Antson *et al.* in 1993.[3] Different subunits are shown in *different colors*, and the two domains of each subunit are shown in *different color tones*. One catalytic dimer consists of the subunits shown in *blue* and *yellow*, while the other is formed from the subunits shown in *green* and *red*. Positions of the active site clefts (at the front side of the tetramer) are indicated by A. The hydrophobic core is depicted as a *grey ellipse*. The N-terminal arms are shown as *bold black lines*. (*b*) Stereo view of *ribbon diagram* of the TPL molecule (**2**; PDB code: 2TPL). The coloring scheme is the same as in (*a*). Cofactor PLP, the side chains of the PLP-binding Lys257 residues, and monovalent cations (Cs^+) are represented by *spheres*. The view is along the molecular 2-fold axis P.

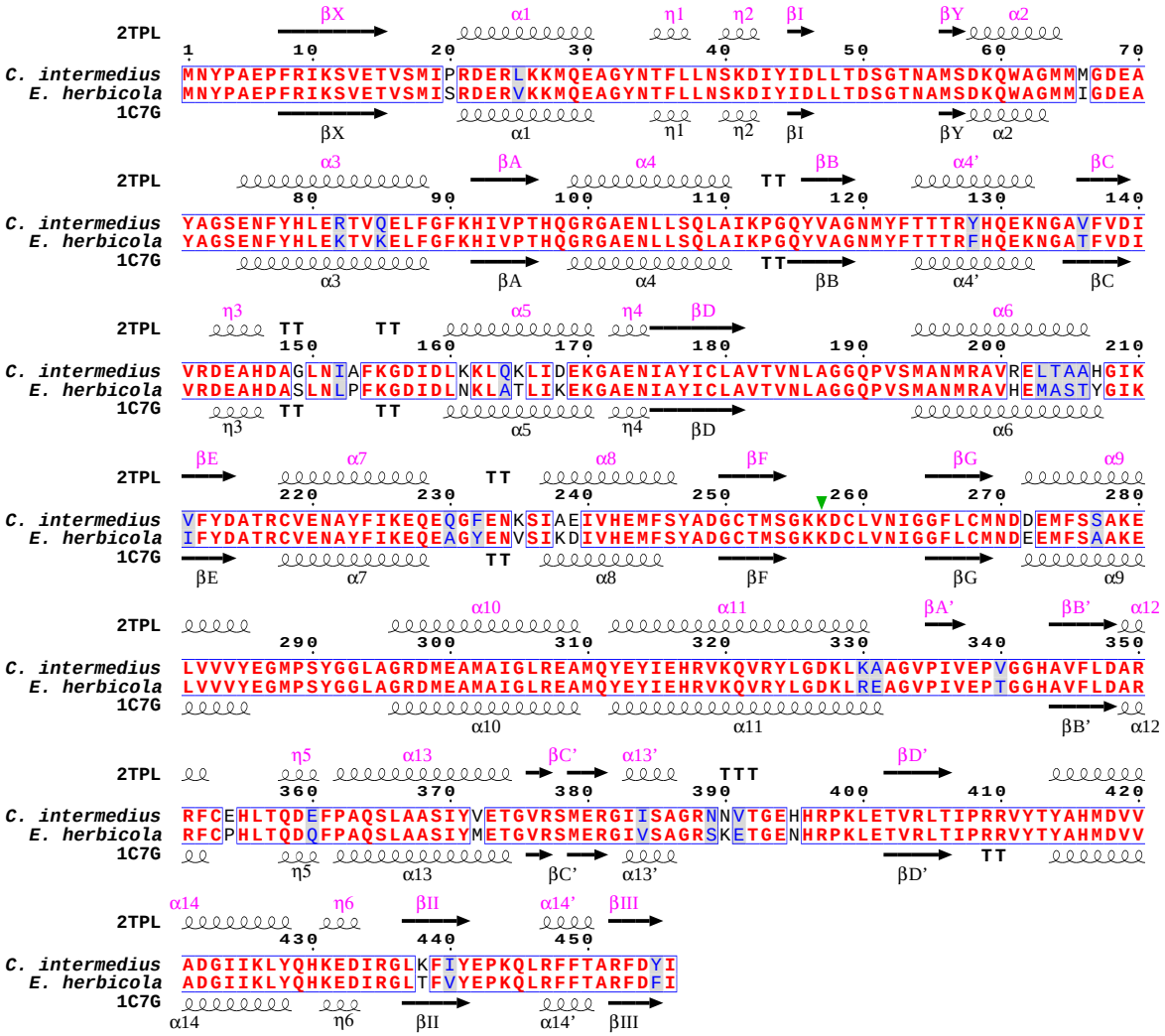

Figure 2.4. Sequence alignment of *C. intermedius* and *E. herbicola* TPL. The secondary-structural elements (assigned by the DSSP algorithm)[92] correspond to the structures of *C. intermedius* holo-TPL complexed with HPPA (**2**; PDB code: 2TPL) and *E. herbicola* holo-TPL (**6**; PDB code: 1C7G). α-Helices are represented with *squiggles*, β-strands with *arrows*, 3_{10}-helices with *curly lines* denoted by η, and β-turns by TT letters. Conserved residues are written in *red*, while chemically similar residues are written in *blue* and framed in a *grey box*. The PLP-binding residue Lys257 is labeled with a *green triangle*. The figure was prepared using ESPript.[93]

2.2.2.2 Structure of the TPL subunit

TPL is a typical α/β protein which belongs to the Fold Type I (aspartate aminotransferase type) class of the PLP-dependent enzymes.[3,90,91] Each subunit of both *C. intermedius* and *E. herbicola* TPL is composed of 456 amino acid residues. The amino acid sequences of TPL from *E. herbicola* and *C. intermedius* are 90.6 % identical (Fig. 2.4).[39] Accordingly, the polypeptide folds of TPL from *C. intermedius* and *E. herbicola* differ only in some minor details, and only the spatial organization of *C. intermedius* protein subunit is described here. In the structural model of *C. intermedius* apo-TPL (**1**), about 6 % of amino-acid residues had poor electron density and could not have been modeled.[3] These

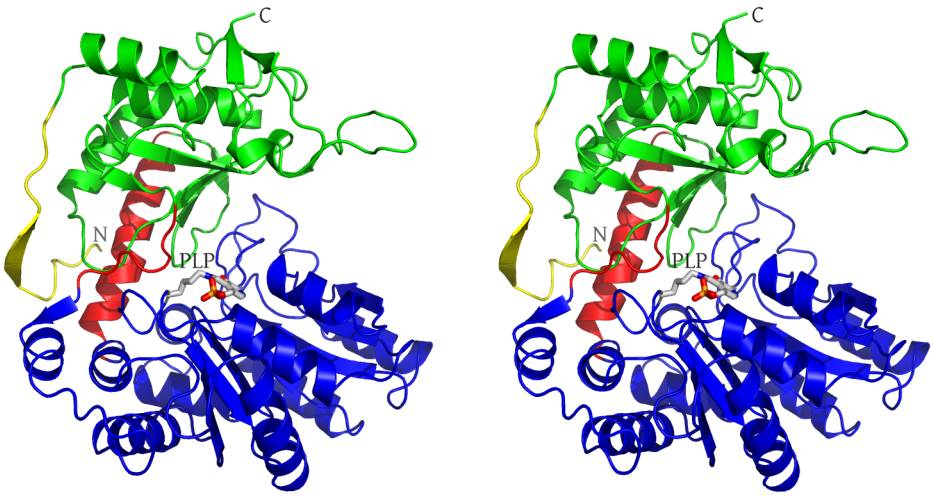

Figure 2.5. Structural and functional parts of the TPL subunit (a stereo view): the N-terminal arms (*yellow*), the small domain (*green*), the large domain (*blue*) and the connecting regions between domains (*red*). PLP and the PLP-binding side chain of Lys257 are depicted as *sticks*.

include residues 123–131, 384–398, and 442–447 in one subunit and residues 123–133, 384–398, and 442–445 in the other crystallographically independent subunit. The structural model of *C. intermedius* holo-TPL complexed with the substrate analog HPPA (**2**)[4] is more complete, so it will be used to describe the structure of a TPL subunit.*

Each protein subunit can be divided into four structural and functional parts (Fig. 2.5):

- the N-terminal arms,
- the small domain,
- the large domain, and
- the connecting regions between domains.

The **small domain** comprises amino acid residues from N-terminal (19–48) and C-terminal (333–456) parts (34 % of the total residues). According to CATH structural classification,[94,95] it possesses an architecture of an alpha-beta complex. The core of the domain is a four-stranded antiparallel β-sheet (β-strands βA′, βB′, βC′, and βD′; Fig. 2.6) which is situated in the C-terminal part of the small domain. The topology of this β-sheet is $+1, +2x, -1$ in Richardson's notation,[96] with the right-handed crossover. All six α-helices of the small domain are on the solvent-accessible side of the β-sheet. A parallel β-bridge (βI, residues 45–47) is formed with strands βC′and βD′ and thus connects the N- and C-terminal parts of the small domain. Two C-terminal parts of the polypeptide chain make an antiparallel two-stranded β-hairpin (strand βII, residues 437–441, and strand βIII, residues 452–455).

The **large domain** includes residues 56–310 (which accounts for 56 % of the total). In CATH structural classification, the architecture of the large domain is a 3-layer (αβα)

*Wherever possible, nomenclature from the original paper[3] is used. The structural model **1** lacks helices α4′, α13′, and α14′, so their symbols are introduced here (*cf.* Fig. 2.4).

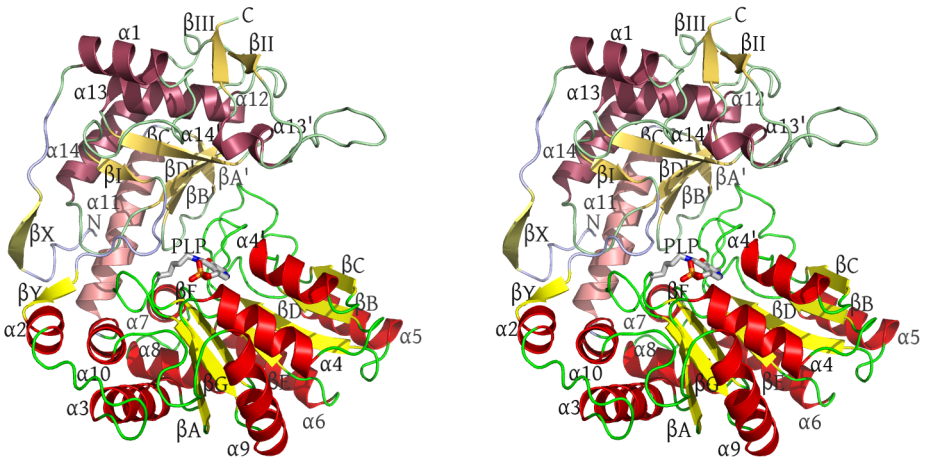

Figure 2.6. Folding of the TPL subunit (a stereo view). Secondary structure elements in different parts of the monomer are shown in *different colors* and all α-helices and β-strands are labeled. The cofactor molecule (PLP) covalently bound to Lys257 is represented by *sticks*.

sandwich with a characteristic PLP-binding fold, at first identified in aspartate aminotransferase.[97,98] It is composed of a seven-stranded β-sheet and ten α-helices. The topology of the seven-stranded β-sheet (β-strands βA, βG, βF, βE, βD, βB, and βC) is typical for Fold Type I PLP-dependent enzymes and can be described by Richardson's notation as $+5x, +1x, -2x, -1x, -1x, -1$ (Fig. 2.6). The directions of β-strands are $(+, -, +, +, +, +, +)$, respectively, and all crossovers are right-handed. Helices α2, α3, α5, α6, α7, α8, and α10 are located at the solvent side of the β-sheet, while helices α4, α4′, and α9 are at the opposite side, facing the small domain (Fig. 2.6).

The **connecting regions** between the domains are made of residues 49–56 and 311–332. The first connecting piece lies in the cavity between the two domains. The second piece includes helix α11 (residues 312–330) on the surface of the subunit. It is the longest helix in the structure (approximately 35 Å long), slightly curved, but with no obvious kink. Ends of helix α11 are at an angle of approximately 25°.

2.2.2.3 Intersubunit contacts in TPL

The catalytic dimer (Fig. 2.7) is stabilized by hydrogen bonds and ionic interactions at the interface of the two subunits. Binding of PLP molecules in the active sites, as well as monovalent cations in their proximity, causes formation of new interactions between monomers (*qq.v.* in Subsections 2.2.2.4 and 2.2.2.5) and additionaly stabilizes the dimeric structure.

TPL homotetramer is stabilized by a hydrophobic cluster in the center of the molecule formed by the side chains of Met56, Trp61, Met64 and Met65, each from a different protein subunit. Sulfur atoms of Met65 and indole rings of Trp61 are in the core of the hydrophobic cluster.

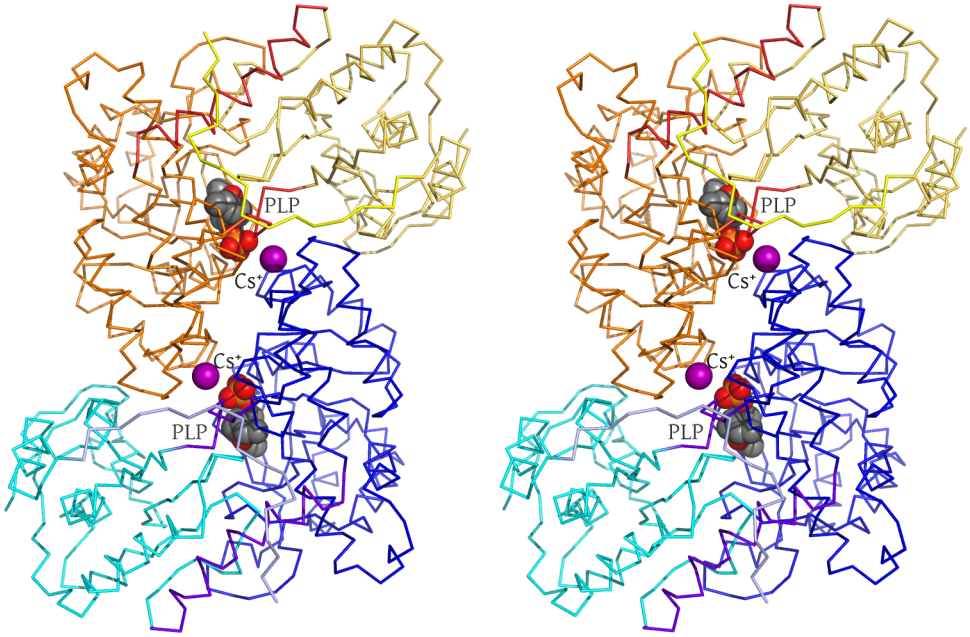

Figure 2.7. TPL catalytic dimer. A stereo view is approximately along the molecular Q axis (Fig. 2.3*a*). Parts of each subunit are highlighted by *different colors*: the large domains – *blue* and *orange*; the small domains – *cyan* and *yellow-orange*; the connecting parts – *purple-blue* and *red*; the N-terminal arms – *light blue* and *yellow*. Monovalent cations (Cs^+ in this case) and non-hydrogen atoms in PLP molecules are shown as *spheres*.

Quaternary structure is additionally stabilized by hydrogen bonds between intertwined N-terminal arms (residues 1–18) of the two subunits related by the R axis. Residues 9–14 (β-strand βX) participate in formation of the "inter-subunit" antiparallel β-structure. In addition, these residues make parallel β-structure with residues 56–58 (β-strand βY) from the other monomer. In summary, N-terminal arms build a four-stranded β-sheet with two pairs of adjacent and parallel chains, while the pairs being antiparallel to each other (Fig. 2.3). Although Lys11 is part of the β-strand βX, values of its main-chain conformational angles are typical for an α-helix. This makes a kink in the β-strand and allows intertwining of two β-strands from neighboring subunits. A hydrogen bond is created between the hydroxyl group of Tyr3 and the carboxyl group of Asp327 – both residues being from the same subunit. This interaction fixes the N-termini on the α11 helix.

2.2.2.4 Monovalent cation binding site in TPL

It was shown that K^+, Rb^+, Cs^+, and NH_4^+ are non-competitive activators for β-elimination of L-tyrosine, Li^+ exerts no effect on the enzymatic activity, but Na^+ is a non-competitive inhibitor of this reaction.[99,100] The K^+ concentration in the cell is approximately 150–200 mmol dm^{-3}. The enzyme present in the bacterial cells is mainly in the K^+-bound

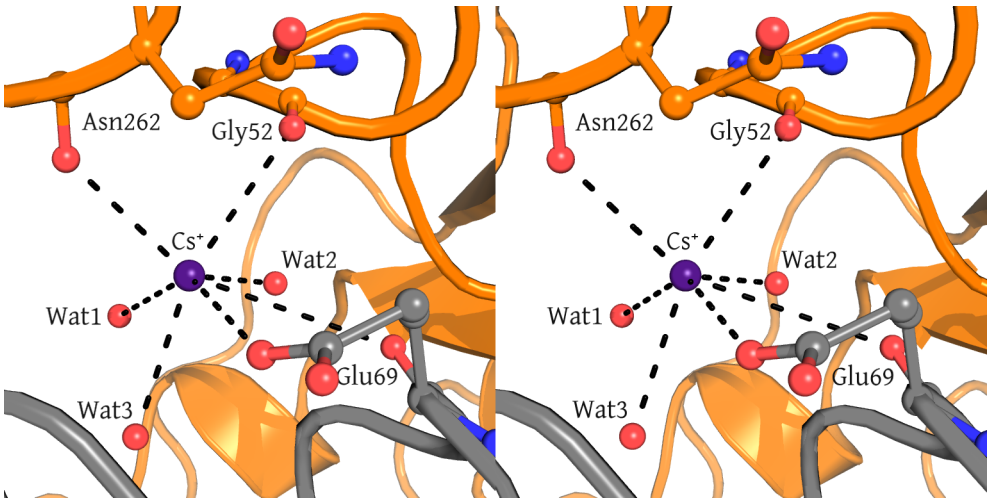

Figure 2.8. Monovalent cation binding site in TPL (a stereo view). Each cation is coordinated by seven oxygen atoms. Different subunits are shown in *different colors*.

form, so the complex of TPL with K^+ is considered to be an active form.[5] Crystals of *C. intermedius* holoenzyme containing K^+ or Cs^+ were made by soaking the apoenzyme crystals with PLP in the presence of KCl or CsCl, respectively.[88] Cation binding sites were determined from a difference Fourier synthesis calculated with coefficients $(|F_{Cs}| - |F_K|)\exp(i\alpha_K)$, where $|F_{Cs}|$ and $|F_K|$ are structural amplitudes for the complexes with PLP in solutions containing KCl and CsCl; α_K are relative phases calculated from the model of the holoenzyme in KCl.* Monovalent cations are bound between two subunits in the catalytic dimer: one cation per each TPL monomer (Fig. 2.7).[88] Each cation is coordinated by seven oxygen atoms: two main chain carbonyl atoms of Gly52 and Asn262 from one protein subunit, one main chain and one of the side chain oxygen atoms of Gly69 from the other subunit in the catalytic dimer, and three atoms from water molecules (Fig. 2.8). The monovalent cation binding site is the same in all published TPL structures for which the cation was modeled (Table 2.3). In the structural models **2** and **4**, Cs^+ and NH_4^+ are bound instead of K^+, while there is no modeled cation in the structural model **1**.

2.2.2.5 Active site of TPL

TPL active site is located about 6 Å from the monovalent cation binding site. Each active site of TPL is situated in a crevice built up of residues belonging to the large and small domain of one subunit, and the large domain of the other subunit in the same catalytic dimer (Fig. 2.7). It is constructed of the following residues (as found in *C. intermedius* TPL):

*This *C. intermedius* holoenzyme structure at 2.7 Å resolution has never been published on the whole. Instead, a very brief description of the active site with bound PLP is provided in the proceedings of the International Meeting on Vitamin B6 and Carbonyl Catalysis, held on 22–27 May, 1994 at Capri, Italy.[88]

- Thr49 and Ser51 from the connecting regions between the domains;
- Gln98, Gly99, Arg100, Phe123, Thr124, Asn185, Asp214, Arg217, Ser254, Lys256, and Lys257 from the large domain;
- Phe36, Met379, Arg381, Arg404, Phe448, and Phe449 from the small domain;
- Tyr71, Met288, and Tysr291 from the large domain of the adjacent subunit.

When bound to the enzyme, PLP forms an aldimine bond with the ε-amino group of Lys257 (the **internal aldimine**). The phosphate group of PLP is hydrogen bonded to the main-chain NH group of Gly99 and Arg100, and also to the side chains of Gln98 (Asp98 in *E. herbicola* TPL), Arg100, and Ser254. In the active sites of *C. intermedius* apo-TPL (**1**), the sulfate anions are bound in the same site as the phosphate group of PLP. The nitrogen atom of the PLP pyridine ring is hydrogen bonded to side chain of Asp214, whereas the PLP O3′atom is hydrogen bonded to the side chain of Arg217. The pyridine ring is stacked with the nearly parallel phenyl group of Phe123. These interactions presumably stabilize the protein structure as a whole. In addition, the structures of *E. herbicola* apo- (**3**) and holo-TPL (**4**) revealed a displacement of the small domain towards the large one (by 1.5 Å on the average) and the narrowing of the active site cleft upon the cofactor (PLP) binding.[5] As shown by the pH dependence of the absorption and circular dichroism spectra and their lognormal decomposition, at pH range 6.0–8.7 and in the presence of activating K^+ cations the internal aldimine of *C. freundii* TPL occurs in a cationic tautomeric form.[101] The predominant form (70 %) is ketoenamine (absorption maximum at ≈ 417 nm) with hydronated nitrogen atoms (NZ and N1) and dehydronated O3′ atom (Scheme 2.17). Ketoenamine is in the tautomeric equilibrium with enolimine (absorption maximum at ≈ 336 nm) which has a dehydronated nitrogen atom of the aldimine bond and a dehydronated O3′ atom.[101]

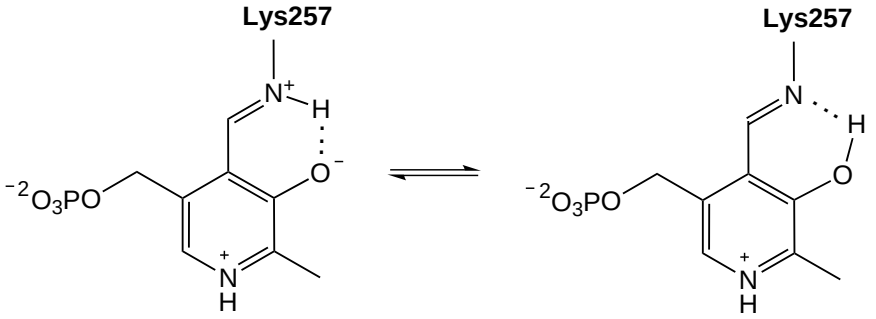

Scheme 2.17. Tautomeric equilibria between cationic ketoenamine (*left*) and enolimino (*right*) tautomers of the internal aldimine.

C. intermedius holo-TPL complex with HPPA (**2**) mimicks the **Michaelis complex**.[4] Although HPPA molecule has all features of the natural substrate L-tyrosine, except for the α-amino group, this substrate analog is bound in only one of the two crystallographically independent active sites in the asymmetric unit. This is probably due to the different crystallographic environments around the two protein subunits. The carboxyl group of

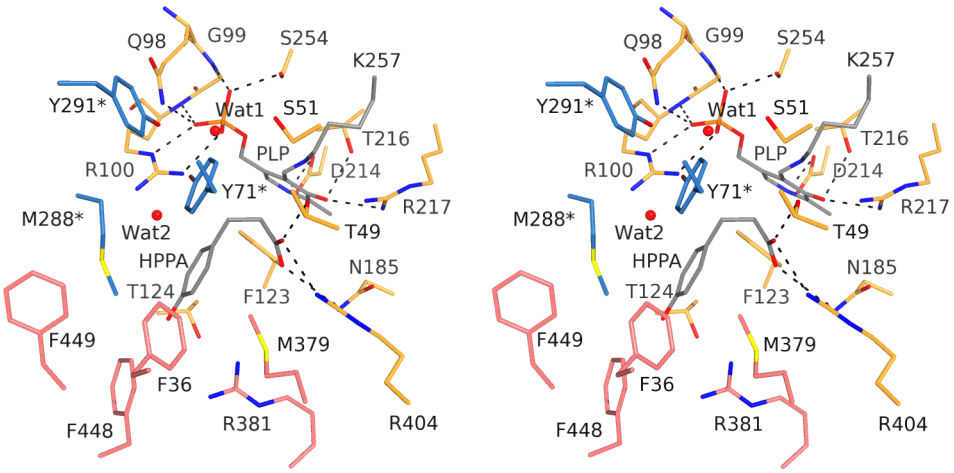

Figure 2.9. A molecule of the substrate analog 3-(4′-hydroxyphenyl)propanoic acid (HPPA) bound in the active site of TPL (a stereo view). Residues from the large domain of the adjacent subunit are shown in *blue* and denoted by an *asterisk*. Hydrogen bonds are represented as *dashed lines*.

HPPA is hydrogen bonded by the guanidinium group of Arg404 and by the hydroxyl group of Thr49 (Fig. 2.9). C4′ atom of PLP is 4.3 Å from the HPPA Cα atom, in the position which would allow interaction of the amino group of L-tyrosine (the real substrate) with the PLP molecule.

The complex of TPL with the quasi-substrate PPT (**5**)[5] models the **external aldimine** intermediate. The plane of the PLP pyridine ring is twisted about the C5–C5′ bond by 22.5° towards the solvent in respect to its orientation in the holoenzyme structure **4**.[5] This orientation allows the formation of additional hydrogen bond (absent in holoenzyme) between the PLP atom O3′ and the side chain of Asn185. The mutual arrangement of the large and small domains in one of four subunits (denoted B and H) in each crystallographically independent tetramer significantly differs from that observed in the remaining three subunits (A, C, and D and E, F, and G). While the three subunits of each tetramer have the same conformation as observed in the holoenzyme structure **4** (Fig. 2.10a), the conformation of the subunits B and H is more closed and the active site is isolated from the solvent to a greater extent (Fig. 2.10b). If the Cα atoms of the large domains are superimposed (the r.m.s. deviation of 0.5 Å), one observes a 3 Å r.m.s. deviation for the Cα atoms of the small domain of subunits B and H in comparison to the other subunits. In addition, the conformations of the quasi-substrate molecules are different (Fig. 2.11): in subunits B and H the phenyl and pyridine rings are mutually perpendicular (conformation I), whereas in the other subunits the angle between the rings is 23.2° (conformation II). For conformation I, the quasi-substrate carboxyl group makes hydrogen bonds with the side chains of Arg404 and Thr49, and the phenol moiety forms many van der Waals contacts with Tyr71. On the contrary, the van der Waals contacts between the phenol moiety and Tyr71 is absent in conformation II, as well as a hydrogen bond between the carboxyl group and Arg404, but a new hydrogen bond is created between the PPT hydroxyl group

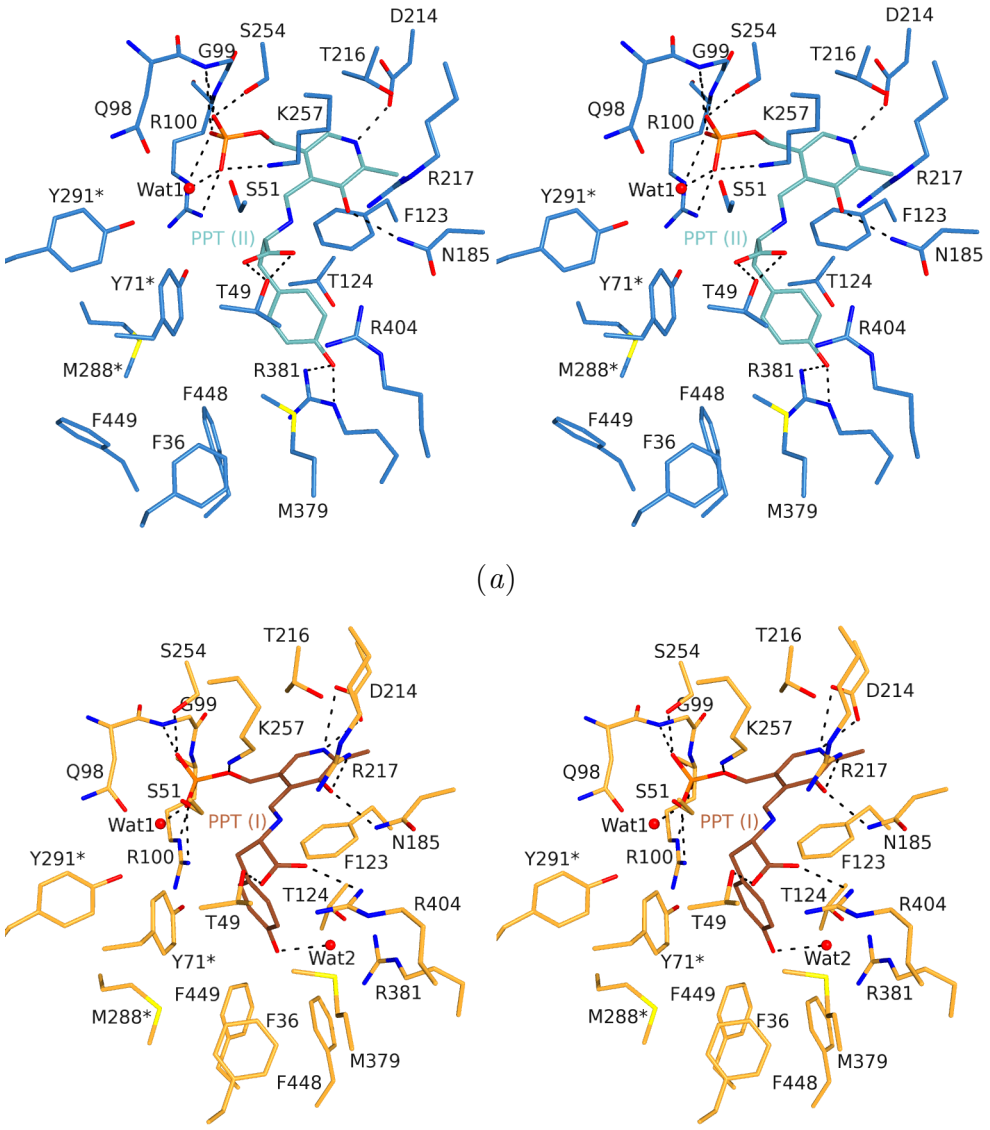

Figure 2.10. Active sites of the TPL complex with the quasi-substrate *N*-(5′-phosphopyridoxyl)-L-tyrosine (PPT). Stereo views of the active sites (*a*) A and (*b*) B. The active site B is more solvent protected and contains a PPT molecule in a different conformation then that observed in the active site A. Hydrogen bonds between the quasi-substrate molecule and the active site residues are denoted by *dashed lines*. The residues from the neighboring subunits are labeled with an *asterisk*.

and the side chain of Arg381. The oberved differences in the conformations of protein subunits and the quasi-substrate molecule in the TPL–PPT complex are attributed to the different environments of the protein subunits in the crystal.

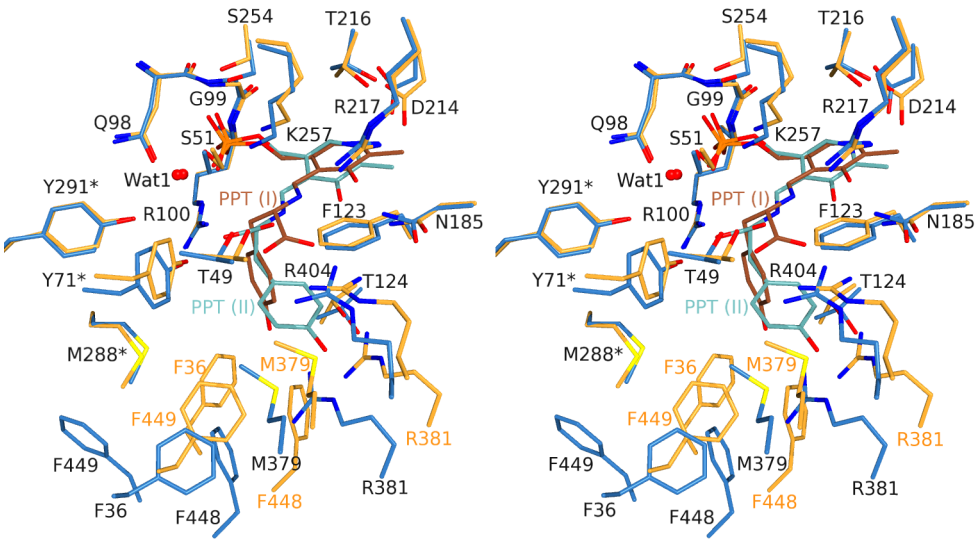

Figure 2.11. Comparison of the two different active site conformations in the TPL complex with the quasi-substrate *N*-(5′-phosphopyridoxyl)-L-tyrosine (PPT). Stereo view of the active sites A (*blue*) and B (*orange*) superimposed by Cα atoms of the corresponding large domains. Ligand denoted as PPT(I) (shown in *brown*) belongs to the active site B, while that denoted as PPT(II) (shown in *cyan*) is bound in the active site A. Hydrogen bonds between the quasi-substrate molecule and the active site residues are denoted by *dashed lines*. The residues from the neighboring subunits are labeled with an *asterisk*.

2.2.3 β-Elimination reaction mechanism of tyrosine phenol-lyase

The proposed reaction mechanism for the β-elimination of L-tyrosine catalyzed by TPL proceeds via several main steps (Scheme 2.18):[6] (1) formation of the external aldimine with the substrate molecule as a result of a nucleophilic attack of the amino group of the substrate (the transaldimination reaction), (2) abstraction of the Cα hydron of the substrate yielding the quinonoid intermediate, (3) hydronation of Cγ and cleavage of the Cβ–Cγ bond, resulting in the removal of phenol and formation of the α-aminoacrylate intermediate. The later is attacked further by the ε-amino group of the active site lysine residue that binds the coenzyme (Lys257), resulting in regeneration of the holoenzyme and a release of iminopyruvate. Finally, iminopyruvate is non-enzymatically hydrolyzed to give ammonium pyruvate. Some investigations of kinetic isotope effects in the reaction catalyzed by TPL[102–104] indicate that the Cβ–Cγ bond cleavage might proceed by the concerted S_E2 reaction mechanism instead of the more usual Friedel–Crafts electrophilic aromatic substitution. In that case ketoquinonoid would be a transition structure, and not the reaction intermediate.

From the pH dependence of k_{cat}/K_m it was concluded that the β-elimination mechanism requires two bases, one of which ($pK_a \approx 7.6$–7.8) abstracts the Cα hydron to form a quinonoid intermediate, and the second of which ($pK_a \approx 8.0$–8.2) abstracts a hydron from the substrate's hydroxyl group to facilitate elimination of phenol.[50,105] Based on

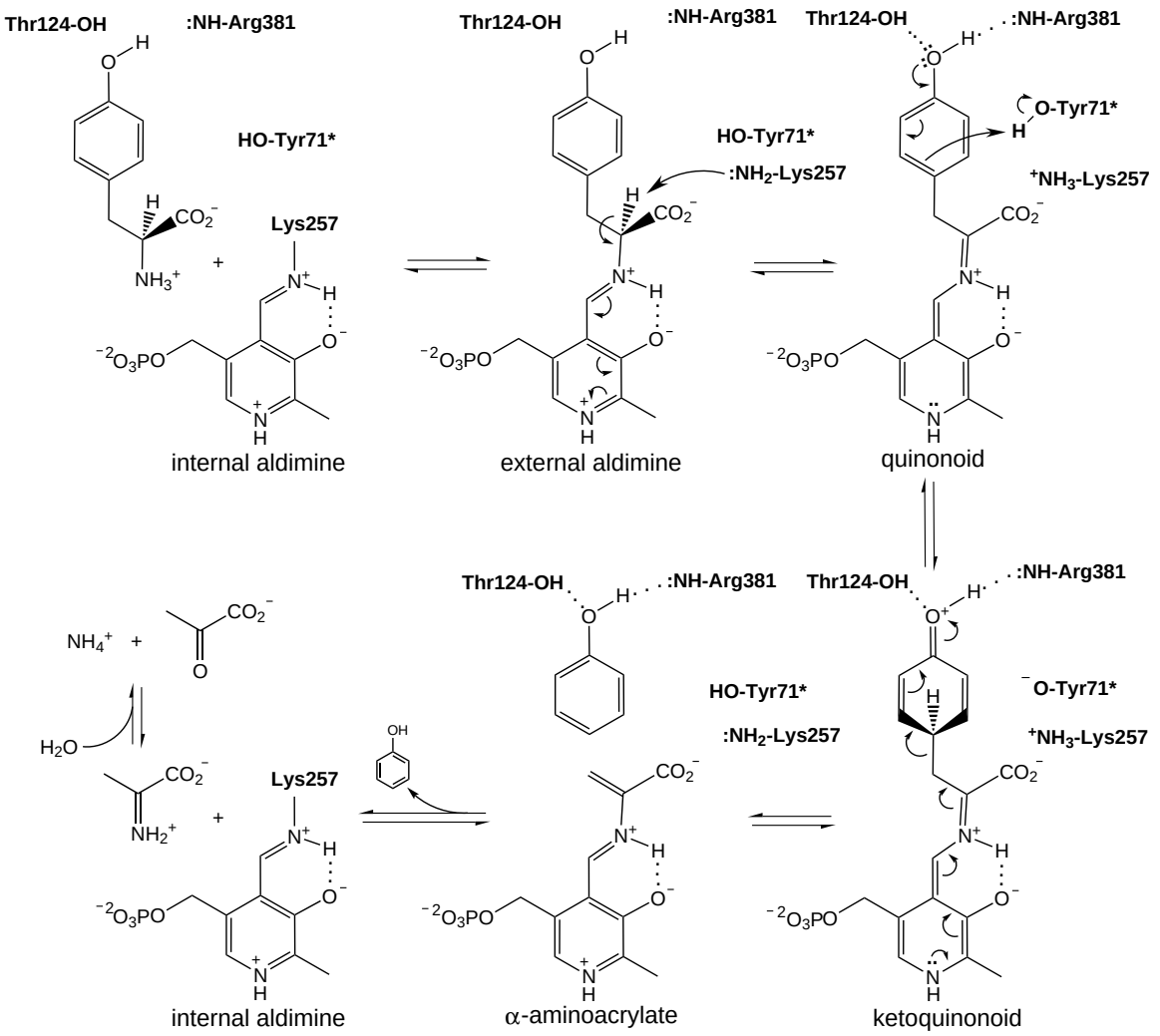

Scheme 2.18. Postulated reaction mechanism of the β-elimination reaction of L-tyrosine catalyzed by TPL.

the structural investigations,[4,5] it has been assumed that the ε-amino group of Lys257 is the most probable base which abstracts the Cα hydron of the substrate. The role of several other amino acids in the catalysis were studied by site-directed mutagenesis. It was demonstrated that Asn185 takes part in substrate binding as well as in the catalysis through stabilization of the quinonoid intermediate and possibly also the ketoquinonoid intermediate.[106] It was also shown that Tyr71 (from the adjacent subunit) is important for the removal of phenol.[52] The Tyr71 hydroxyl group plays the role of the general acid catalyst during the formation of the key transition structure – the ketoquinonoid intermediate. Investigations of β-elimination activities of mutant enzymes performed with the physiological substrate indicated that Arg381 assists in abstraction of a hydron from the phenol hydroxyl group, so it is possibly the second catalytic base observed in the pH dependence of $k_{\mathrm{cat}}/K_{\mathrm{m}}$.[4] The expected p$K_{\mathrm{a}}$ value for the guanidinium moiety of arginine is about 12.5, and the pK_{a} of about 8 appears to be too low for Arg381 to act as the second catalytic base. Nevertheless, the hydrophobic environment around the side chain of Arg381 could significantly decrease the pK_{a} of its guanidinium group. The small residual

activity of R381A TPL suggests that removal of the substrate's phenolic hydron is not absolutely necessary for catalysis: the main function of Arg381 may thus be to serve as a hydrogen bond acceptor. In this case, Arg381 is required for the substrate specificity of TPL.[4] In addition, Thr124 and Phe448 were also shown to be the residues providing substrate specificity of the enzyme.[15] Thr124 could make a hydrogen bond with the substrate phenolic group and thus properly orient the substrate ring for the β-elimination to occur, while the more exact role of Phe448 has been unclear.

2.2.4 Applications of tyrosine phenol-lyase

The ability of TPL to catalyze a broad range of reactions makes this enzyme useful in organic synthesis and biotechnology for the production of L-tyrosine and its derivatives. L-Tyrosine is a precursor of several neurotransmitters, such as L-DOPA, dopamine, epinephrine, and norepinephrine. Some of its derivatives have regulatory roles in the function of the hormonal systems in the adrenal, thyroid, and pituitary glands. L-Tyrosine is utilized as a common dietary supplement and a starting compound for synthesis of other high-value materials.[107] L-DOPA is used as a drug for the treatment of Parkinson's disease. About half of the 250 tons of L-DOPA supplied each year is produced by an enzymatic method involving TPL.[108] Several other tyrosine derivatives are used as part of pharmaceuticals or as precursors in syntheses of a few drugs.[109]

The application of the wild-type TPL as a catalyst in organic syntheses is discussed in detail in Subsection 2.2.1 (pages 8–14). A few attempts were made to optimize TPL catalytic activity towards various substrates. These efforts were driven by the structure-based rational design of the enzymatic active site. The first such example is a creation of the mutated TPL with dicarboxylic amino acid β-lyase activity.[81] Dicarboxylic amino acids are competitive inhibitors of the wild-type TPL.[50] The substrate specificity to dicarboxylic amino acids was redesigned by mutagenesis based on a homology modeling that used the structure of AspAT as a template. Therefore, R100T and R100T/V283R mutants of TPL from *C. freundii* catalyze the β-elimination reaction of L-aspartate, L-2-aminoadipate, and L-glutamate to yield ammonium pyruvate together with formate, acetate, and propionate, respectively.[81] Such dicarboxylic amino acid β-lyase activity has no counterpart among natural enzymes. Recently, several mutants of *C. freundii* TPL were designed for "green" single-step synthesis of 3-substituted L-tyrosine derivatives.[109] The most efficient variant was M379V mutant which showed very high conversion rates for syntheses of 3-methyl-, 3-methoxy-, and 3-chloro-L-tyrosine, from ammonium pyruvate and *o*-methylphenol (*o*-cresol), *o*-methoxyphenol (guaiacol), and *o*-chlorophenol, respectively. All these three phenol derivatives are poor substrates in the reversal β-elimination reaction catalyzed by the wild-type TPL.[55] The synthesized 3-substituted L-tyrosine derivatives are used as building blocks for some anticancer drugs. The previously used methods for their syntheses required several cumbersome steps with very low final yields.[109]

Biotechnological potential of TPL was investigated already in the 1970's. The first such studies concentrated on TPLs from enterobacteria *E. herbicola*, *C. intermedius* (formerly *E. intermedia*), and *C. freundii*, because of their high enzymatic activities. Production of L-tyrosine, L-DOPA, and other derivatives of L-tyrosine were tested in various conditions and setups, but in all cases the β-elimination reaction was reversed in the synthetic direction by using an excess supply of ammonium pyruvate. Concentration of phenol or its derivatives was often maintained at a minimum due to their negative influence on bacterial cell walls (if whole cells were used) and protein (TPL) stability and activity. Solubilized intact cells of *E. herbicola*, *C. freundii*, and *E. coli* with *tpl* gene cloned from *E. herbicola* were used for production of L-tyrosine and L-DOPA.[2,40,108,110–112] Considerable increase in enzyme stability during the biotechnological production of L-tyrosine and L-DOPA was observed for *C. intermedius* cells entrapped in a polyacrylamide gel,[113,114] and *E. herbicola* cells encapsulated within alginate–polylysine–alginate microcapsules.[115] Crystalline preparations of TPL also proved to be efficient in the synthesis of L-tyrosine and its derivatives from ammonium pyruvate and the corresponding phenol derivative.[47,55,58] Easier separation of the catalyst and the reaction products at the end of the production process as well as greater enzyme stability were obtained by direct immobilization of *C. intermedius* TPL to Sepharose beads.[116,117] Disadvantages of using pure enzyme as a biocatalyst are costly preparation steps and a requirement for continuous supply of PLP.

Intact *E. herbicola* cells were used for production of L-tyrosine or L-DOPA from DL-serine and phenol or pyrocathechol.[72] Later, this reaction was coupled with the synthesis of L-serine from glycine and formaldehyde catalyzed by the enzyme glycine hydroxymethyltransferase (EC 2.1.2.1). The two reactions were combined by coincubating *Klebsiella aerogenes* and *E. herbicola* cells to express glycine hydroxymethyltransferase and TPL, respectively.[118] Very efficient and economically competitive is the synthesis of L-tyrosine from SOPC and phenol.[75] SOPC is readily available by the high-yield reaction of L-cysteine and *o*-fluoronitrobenzene in a dimethylformamide solution. Also, a hybrid pathway for the production of L-DOPA from benzene in *E. coli* and *Pseudomonas aeruginosa* cells was constructed.[119] This system consisted of three key enzymes: toluene dioxygenase (EC 1.14.12.11), toluene *cis*-glycol dehydrogenase, and TPL.

More recently, thermo- and chemostable TPL from obligatory symbiotic thermophile, *S. toebii*, overexpressed in recombinant *E. coli* was employed for production of L-tyrosine and its derivatives.[59,120] TPLs from *S. toebii* and *S. thermophilum* proved to be more stable against phenolic substrates than TPL from *C. freundii* or other mesophilic bacteria. Also, the reactions biocatalyzed by *S. toebii* TPL can be conducted at a higher temperature. In order to additionaly improve catalytic activity, thermal stability and denaturant tolerance of *S. toebii* and *C. freundii* TPLs, random mutagenesis techniques were applied to reveal the protein mutant with the enhanced properties.[121–123] The A13V mutation of *S. toebii* TPL raised the temperature and denaturant stability.[121] Also, in the random mutagenesis by directed evolution A13V, E83K and T407A mutations im-

proved the stability, whereas T129I and T451A mutations improved the catalytic activity of the *S. toebii* TPL.[123] Combination of the several mutations improved both stability and activity. As shown by homology modeling, most of the stability-improving mutations in the multiple mutants were located at the dimer–dimer interface, including the N-terminal arm, while the activity-improving mutations were located farther away and not interfering with the stability-improving mutations.[123] The T15A mutation in *C. freundii* TPL improved PLP-binding affinity at high temperatures and significantly increased activity towards L-DOPA.[122] Again, Thr15 is situated in the N-terminal arm, so the effect of the T15A mutation was presumably related to changes in the intersubunit architecture of the catalytic dimer.

Application of a thermostable TPL for removal and bioconversion of phenol in wastewater created during the manufacture of phenolic resin was also examined.[124] TPL form *Symbiobacterium* sp., in tandem with tyrosine decarboxylase (EC 4.1.1.25) from *Streptococcus faecalis*, was used as a biocatalyst in an enzymatic system for the production of dopamine from pyrocatechol, pyruvate and ammonia.[125] TPL also played an important role in the "green" production of phenol from glucose by the solvent-tolerant strain *Pseudomonas putida* S12 with *tpl* gene introduced from *P. agglomerans*.[126]

There were also several studies on utilizing TPL as a chemotherapeutic agent.[127–129] Namely, some neoplastic cells have enhanced requirements for the essential amino acids, phenylalanine and tyrosine. Depletion of tyrosine in plasma by administered *E. herbicola* TPL had antineoplastic activity against B-16 melanoma in mice.[127] The stability of TPL in plasma remained an unresolved problem,[128,129] so this enzyme has never become a chemotherapeutic drug.

2.3 Tryptophan indole-lyase – a paralog of tyrosine phenol-lyase

Tryptophan indole-lyase or tryptophanase* [Trpase, EC 4.1.99.1; systematic name: L-tryptophan indole-lyase (deaminating; pyruvate-forming); other names: L-tryptophanase, L-tryptophan indole-lyase (deaminating)] is a PLP-dependent enzyme which catalyzes *in vivo* β-elimination of L-tryptophan to produce indole and ammonium pyruvate (Scheme 2.19).[130] In excess of ammonium pyruvate and a moderate quantity of indole Trpase catalyzes the reversal of the β-elimination reaction.[131] Except for the physiological reaction, Trpase also catalyzes β-elimination and β-substitution reactions of L-tryptophan and many other β-substituted L-amino acids and their analogs,[132–135] including SOPC which is used for spectrophotometric assays of Trpase.[136] Surprisingly, in the highly concentrated

*Name "tryptophanase" was also used for an enzyme tryptophan 2,3-dioxygenase (EC 1.13.11.11) which catalyzes the oxidation of L-tryptophan by molecular dioxygen to give *N*-formyl-L-kynurenine, the first product in the kynurenine pathway. This enzyme should not be confused with tryptophan indole-lyase (Trpase).

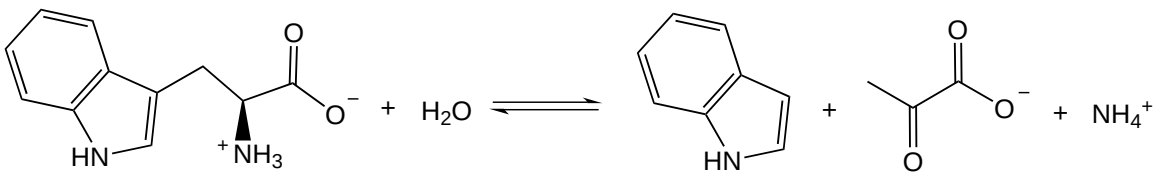

Scheme 2.19. Reversible β-elimination reaction of L-tryptophan catalyzed by Trpase.

solutions of $(NH_4)_2HPO_4$ Trpase changes its stereospecificity and catalyzes β-elimination of D-tryptophan[137,138] and β-substitution of D-serine with indole to yield L-tryptophan.[139] The broad substrate promiscuity of Trpase can be used industrially for economical syntheses of L-tryptophan and related amino acids, as well as for biodegradation of pollutans.

Trpase is a widely distributed bacterial protein which is overexpressed when the bacterial cells experience environmental stress, like drastic change in the pH value of media.[140] As a consequence, substantial amount of indole is produced. Indole serves as a cell-to-cell signaling compound which faciliates quorum sensing and regulates biofilm formation in various bacterial species.[141–143] In addition, indole signaling has a considerable role in the stable maintance of multicopy plasmids which is important in cell division.[144] Trpase can bind Rcd, a short RNA molecule involved in the resolution of plasmid multimers. Binding of Rcd increases the affinity of Trpase for L-tryptophan, so Trpase might act as a multifunctional enzyme.[144] All these functions related to Trpase, and its non-existance in eukaryotes, make this enzyme an interesting target for new potential antibiotics.[145]

2.3.1 Structure of tryptophan indole-lyase

Several structures of Trpase are known from X-ray structural analyses (Table 2.4). The first reported structure is that of *Proteus vulgaris* Trpase holoenzyme (holo-Trpase) solved at 2.1 Å resolution.[146] Later, the structures of two different apo forms of *E. coli* Trpase (apo-Trpase-I[13] and apo-Trpase-II)[14] were determined. Recently, the crystal structures of *E. coli* Trpase Y74F and C298S mutants in their apo form were also reported.[147] *P. vulgaris* and *E. coli* Trpase have 51 % sequence identity and greater than 60 % similarity.[14]

The active form of Trpase is a homotetramer with the molecular mass of about 210 kDa. Each protein subunit binds one PLP molecule.[134] In all published structures Trpase molecule is also in the tetrameric form, analogous to the structure of TPL. Trpase and TPL from various bacteria show more than 40 % overall amino acid sequence identity with relatively few insertions and deletions.[146] As might be expected, structures of these two enzymes are very similar. Trpase also belongs to the tyrosine phenol-lyase subclass in the structural type I of PLP-dependent enzymes[90,91] and, according to the SCOP classification,[148] Trpase and TPL make the family of β-eliminating lyases.

Table 2.4. Basic crystallographic data for the published Trpase crystal structures

PDB code[a]	1AX4	2C44	2OQX	2V1P	2V0Y
Crystal space group	$P2_12_12_1$	$P4_12_12$	$F222$	$F222$	$F222$
Unit cell parameters					
a / Å	115.0	215.5	118.4	118.7	120.5
b / Å	118.2	215.5	120.1	120.2	118.8
c / Å	153.7	107.5	171.2	171.7	171.5
No. of Trpase subunits in the asymmetric unit	4	4	1	1	1
Ligands in the model	$4\,K^+$ 4 PLP	$6\,K^+$ $8\,SO_4^{2-}$	Mg^{2+} Cl^- HEPES	Mg^{2+} Cl^-	Mg^{2+} Cl^-
T / K	281	110	100	100	100
d_{min}[b] / Å	2.1	2.8	1.9	1.9	2.0
R_{cryst}	0.187	0.195	0.203	0.191	0.215
R_{free}	0.228	0.218	0.232	0.227	0.221

[a] Structure codes and references: 1AX4 – holo-Trpase from *P. vulgaris*;[146] 2C44 – apo-Trpase-I from *E. coli*;[13] 2OQX – apo-Trpase-II from *E. coli*;[14] 2V1P – Y74F apo-Trpase from *E. coli*;[147] 2V0Y – C298S apo-Trpase from *E. coli*.[147]
[b] Resolution.

2.3.1.1 Structure of the Trpase subunit

As for TPL, the Trpase monomer (Fig. 2.12) is composed of an N-terminal arm (residues 1–19 in the *P. vulgaris* protein, and 1–21 in the *E. coli* protein) and two α/β domains: the small (residues 20–51 and 323–467 in the *P. vulgaris* protein, and 22–50 and 329–471 in the *E. coli* protein) and the large one (residues 60–319 in the *P. vulgaris* protein, and 60–328 in the *E. coli* protein). The organization of each domain is equivalent as for TPL (Fig. 2.6), with some minor differences arising from the differences in the protein sequences. Conformations of the subunits differ in the published Trpase structures (Fig. 2.13). *E. coli* apo-Trpase is found in the most closed (in apo-Trpase-I structure)[13] and the wide-open* (in apo-Trpase-II structure)[14] conformations, while *P. vulgaris* holo-Trpase[146] is observed in an intermediate state. Conformations of the monomers in the structures of two *E. coli* Trpase mutants[147] are basically the same as in the apo-Trpase-II structure. The conformational change arises from bending of the loops between strands βI and βY, and helices α11 and α12 (Fig. 2.12). The large and small domains presumably behave like rigid bodies during closure/opening movement. When large domains of two *E. coli* apo-Trpase structures are superimposed, the maximal distance between the corresponding Cα atoms of the small domains is 14.5 Å. The maximal distance between the small domains of superimposed subunits of *P. vulgaris* holo-Trpase and apo-Trpase-I equals 7.0 Å. The observed conformational variety most probably reflects the intrinsic flexibility of Trpase molecule. Different conformations are obtained from different crystallization conditions

*The term "wide-open" is adopted from the original publication.[14]

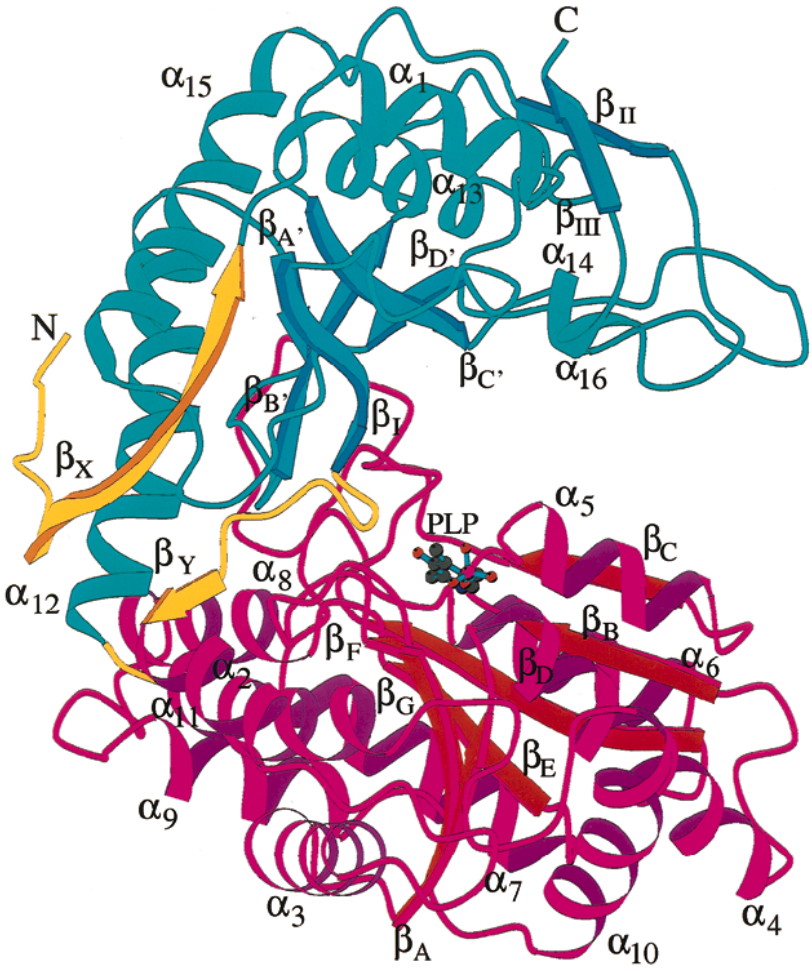

Figure 2.12. Protein subunit of Trpase from *P. vulgaris*. Small domain is shown in *blue*, large domain in *red*, N-terminal arm and interdomain regions in *yellow*. The figure was adapted from (Isupov *et al.*, 1998).[146]

and stabilized in different packing environments. The subunit conformations observed in *C. intermedius* TPL structures[3,4] are very close to the wide-open conformation of apo-Trpase-II, while the more open conformation of *E. herbicola* TPL[5,86] is more similar to the conformation observed for the structure of *P. vulgaris* holo-Trpase.[146]

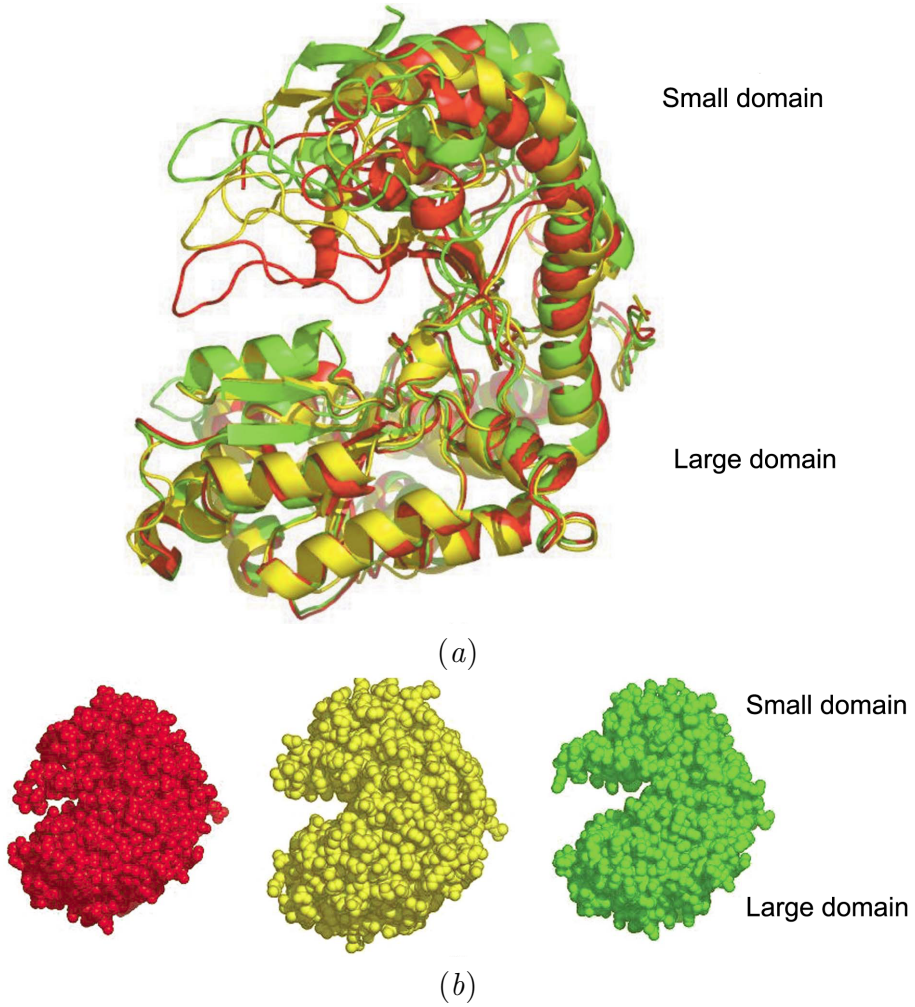

Figure 2.13. Comparison of Trpase monomers from *P. vulgaris* and *E. coli*. (*a*) Superposition of protein monomers from *P. vulgaris* holo-trpase (*yellow*), *E. coli* apo-Trpase-I (*red*) and apo-Trpase-II (*green*). (*b*) *Space-filling models* of the three structures. Coloring code is the same as in (*a*). The figure was adapted from (Tsesin *et al.*, 2007).[14]

2.3.1.2 Cation binding sites of Trpase

As in TPL, two monomers of Trpase create the catalytic dimer. The tetramer is composed of two catalytic dimers which are associated by their intertwined N-terminal arms and a four helix bundle in the middle of the tetramer (Fig. 2.14). In *P. vulgaris* holo-Trpase the catalytic dimer is additionaly stablized by K^+ cations bound in the monovalent cation binding sites at the interface of the two subunits. Each K^+ is hepta-coordinated by three water molecules, Gly53 O and Asn271 O from one subunit, and Glu70 OE1 and Glu70 O from the second subunit in the catalytic dimer. The atoms coordinating this K^+ cation are analogous to those in the structures of TPL.[88] In the structure of *E. coli* apo-Trpase-I two additional cation binding sites are found at the interface between two subunits of the catalytic dimer: K^+ is coordinated by Gln107 OE1, Gln301 O, and Glu302 OE1 from one subunit, and by the equivalent atoms of the second subunit of the catalytic dimer (Fig. 2.14). Surprisingly, a solvated magnesium cation, $[Mg(H_2O)_6]^{2+}$, was found in the

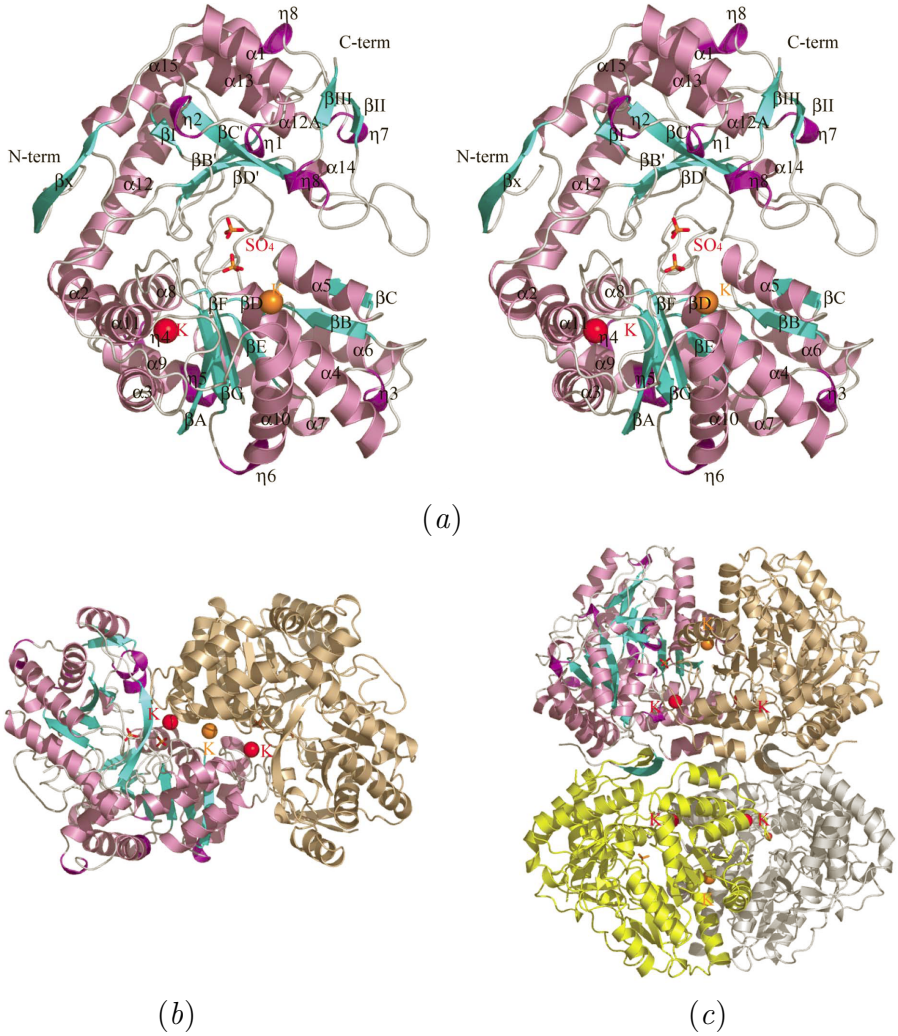

Figure 2.14. The structure of *E. coli* apo-Trpase-I. (*a*) Stereo view of the protein subunit with α-helices shown in *violet*, 3_{10}-helices in *purple*, β-strands in *cyan* and loops in *gray*. Two SO_4^{2-} ions bound in the active site are shown in *stick* representation. K^+ ions in the first binding site, common to all Trpase and TPL structures, are shown as *red spheres*. K^+ ions in the second binding site, specific to *E. coli* apo-Trpase-I, are depicted as *orange spheres*. (*b*) The structure of the catalytic dimer. One subunit is depicted using the same color scheme as in (*a*) and the other subunit is shown in *brown*. (*c*) The structure of the tetramer. Subunits in one catalytic dimer are shown using the same color scheme as in (*b*), while the other two subunits are shown in *yellow* and *gray*. The figure was adapted from (Ku *et al.*, 2006).[13]

being

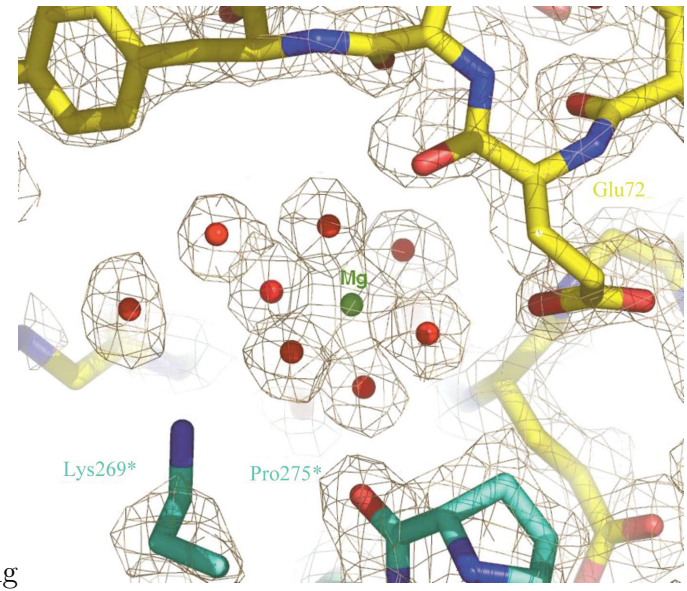

Figure 2.15. Cation-binding site in *E. coli* apo-Trpase-II containing $[Mg(H_2O)_6]^{2+}$. Two subunits are depicted in *different colors*. The corresponding electron density map is shown as *gray mesh*. The figure was adapted from (Tsesin *et al.*, 2007).[14]

cation binding site of *E. coli* apo-Trpase-II (Fig. 2.15). The coordination around Mg^{2+} is octahedral. The second coordination sphere around Mg^{2+} comprises the protein residues of the cation-binding site and the three water molecules. From this observation it was postulated that small cations (Li^+, Na^+ and Mg^{2+}) bind to Trpase in the solvated form, while larger cations (K^+, NH_4^+, Tl^+ and Rb^+) bind without their solvation shell and thus activate Trpase.[14] Namely, Li^+ and Na^+ inhibit the Trpase enzymatic reaction, while K^+, NH_4^+, Tl^+ and Rb^+ were shown to be activators of Trpase.[134]

2.3.1.3 Active site of Trpase

Active site of Trpase is situated at the interface between the large and small domain from one subunit, and a large domain from the second subunit of a catalytic dimer (Fig. 2.14). Conformations of the active sites in different Trpase structures correspond to the conformations of the associated protein subunits (Fig. 2.13). The active sites of *P. vulgaris* holo-Trpase[146] are found in the intermediate open conformation with PLP molecules covalently bonded to Lys266 (Fig. 2.16). The phospate group of PLP makes a salt bridge with the guanidiniom group of Arg101. It is also hydrogen bonded to Gly100 N, Arg101 N, Gln NE2, Ser263 OG, and two water molecules. PLP O3′ atom is hydrogen bonded to the side chain of Arg226, while Asp223 makes a hydrogen bond/salt bridge with the hydronated N1 atom of the PLP pyridine ring. The PLP pyridine ring is sandwiched between the side chains of Ala225 and Phe132. Tyr72 and Tyr301, which form hydrogen bonds with one of the water molecules bound to the PLP phosphate moiety, are residues from the neighboring subunit in the catalytic dimer (Fig. 2.16). The mode of PLP binding in the active site of Trpase is analogous to that observed in TPL structures.[4,5]

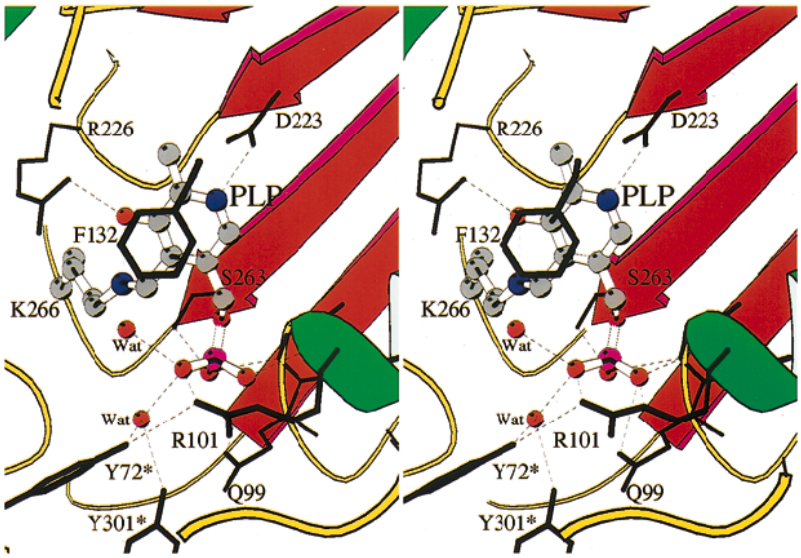

Figure 2.16. Interactions between PLP and active-site residues in Trpase from *P. vulgaris*. Helix α5 is not shown. PLP makes covalent aldimine bond with Lys266. Hydrogen bonds are denoted as *dashed lines*. Residues from the neighboring subunit are marked with a *star*. The figure was adapted from (Isupov *et al.*, 1998).[146]

Two SO_4^{2-} anions, originating from the crystallization solution, are bound in a closed active site of *E. coli* apo-Trpase-I structure (Fig. 2.17).[13] The first sulfate binding site corresponds to the binding site of PLP phosphate moiety in *P. vulgaris* holo-Trpase structure[146] and to the sulfate binding site in the structure of apo-TPL (**1**).[3] The second SO_4^{2-} in the active site is bound between the small and large domains. It forms hydrogen bonds with the side chains of Thr52 and Arg419 from the small domain, and Asn198, Arg203, and Lys270 (equivalent to the PLP-binding Lys266 in *P. vulgaris* protein) from the large domain (Fig. 2.17). Based on the assumption that the second sulfate binding site corresponds to that of the carboxylate group of the substrate, the covalently bound PLP and a L-tryptophan molecule (forming the Michaelis complex) were modeled in the active site of *E. coli* apo-Trpase-I (Fig. 2.17*b*). According to this model, the PLP phosphate group interacts with Arg103 and Lys269. The guanidinium groups of Arg419 and Arg230 form hydrogen bond/salt bridge interactions with α-carboxylate of L-tryptophan. Both Tyr74 and His463, the residues from different subunits, interact with the indole group of L-tryptophan. Asp137 is hydrogen bonded with the indole N atom of the subtrate.

The wide open active site of *E. coli* apo-Trpase-II[14] appears to be occupied by a HEPES molecule from the crystallization solution (Fig. 2.18). Residues Thr52, Tyr74, and Tyr307 interact with the HEPES molecule. Arg419 and His463, which are believed to participate in L-tryptophan binding,[13,149] are significantly shifted from their positions in the other wild-type Trpase structures.[13,146]

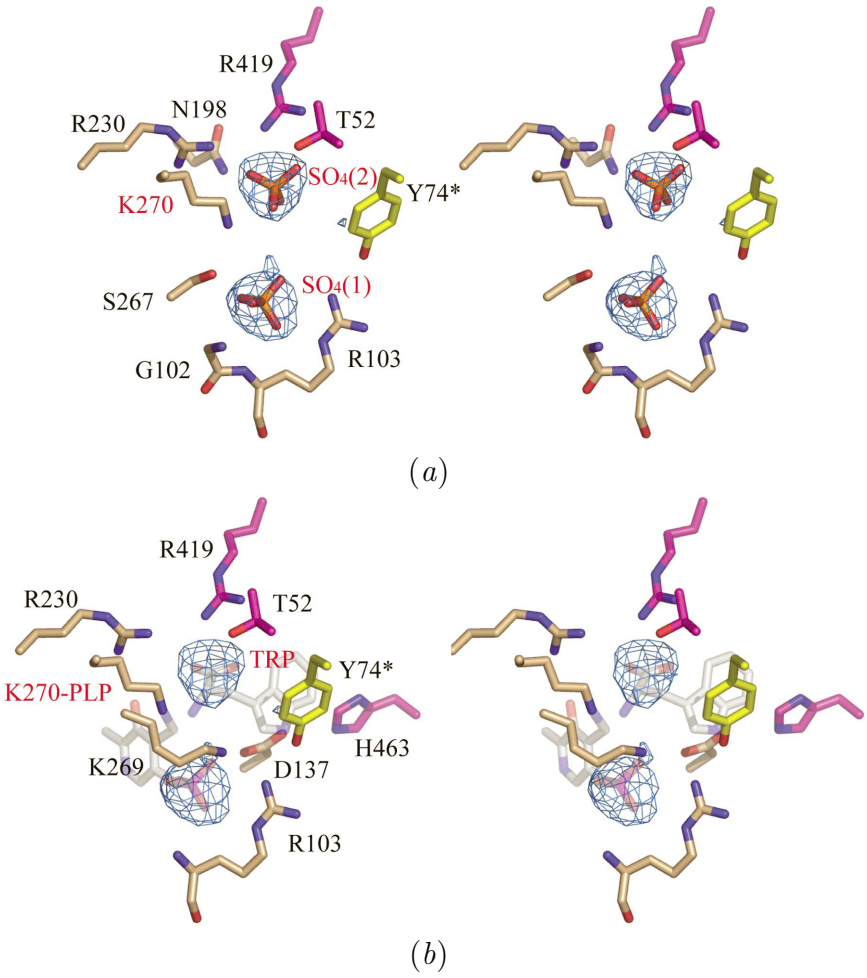

Figure 2.17. Active site of *E. coli* apo-Trpase-I. (*a*) Stereo view of the active site with two bound SO_4^{2-}. The corresponding σ_A-weighted $|F_o| - |F_c|$ electron density omit map (*blue*) is contoured at 3.0σ. The carbon atoms from the large domain are colored in *brown*, those from the small domain are colored in *magenta*, and Tyr74, which is from the second subunit of the catalytic dimer, is depicted in *yellow* and marked with a *star*. (*b*) Stereo view of the calculated model of PLP bound to Lys270 and a L-tryptophan molecule docked with its carboxylate group in the second sulfate-binding site. The coloring scheme is the same as in (*a*). These figures were adapted from (Ku *et al.*, 2006).[13]

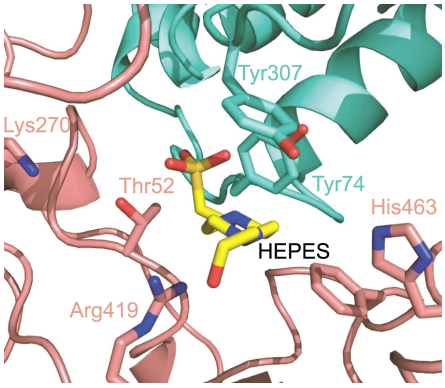

Figure 2.18. HEPES molecule in the active site of *E. coli* apo-Trpase-II. Two different subunits are shown in *different colors*. This figure was adapted from (Tsesin *et al.*, 2007).[14]

2.3.2 Reaction mechanism of tryptophan indole-lyase

The postulated mechanism of the β-elimination reaction of L-tryptophan catalyzed by Trpase (Scheme 2.20) is analogous to the mechanism of β-elimination of L-tyrosine catalyzed by TPL (Scheme 2.18). From the analogy with TPL,[5] it was assumed that the ε-amino

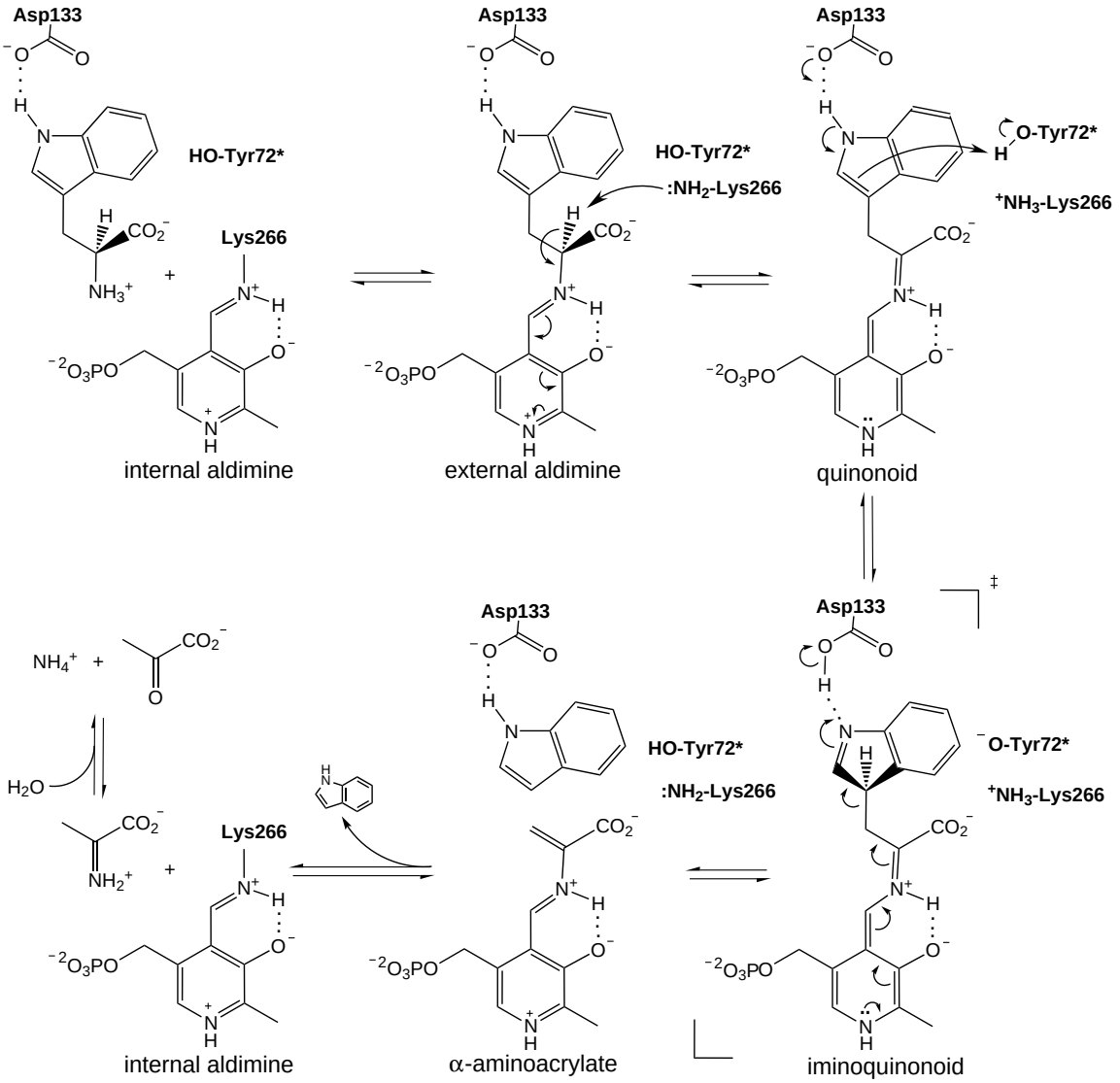

Scheme 2.20. Postulated reaction mechanism of β-elimination of L-tryptophan catalyzed by Trpase. Residue numbering corresponds to *P. vulgaris* Trpase.

group of the PLP-binding lysine (Lys266 in *P. vulgaris*, and Lys270 in *E. coli* enzyme) abstracts the hydron to produce the quinonoid intermediate. Before its elimination the leaving group has to be activated by hydronation of the substrate's Cγ atom.[150] The evidence suggested that the predominant general acid catalyst for this task is a hydroxyl group of Tyr72 in *P. vulgaris* Trpase[151] (Tyr74 in *E. coli* Trpase).[152] Surprisingly, it was observed that the hydronation of the Cγ atom (C3 atom of the evolving indole molecule) proceeds simultaneously with the cleavage of the Cβ–Cγ bond by a rare S_E2 mechanism,[153] so the iminoquinonoid species is not an intermediate, but a structure close to a transition structure. The cleavage of the Cβ–Cγ bond is facilitated by the carboxylate group

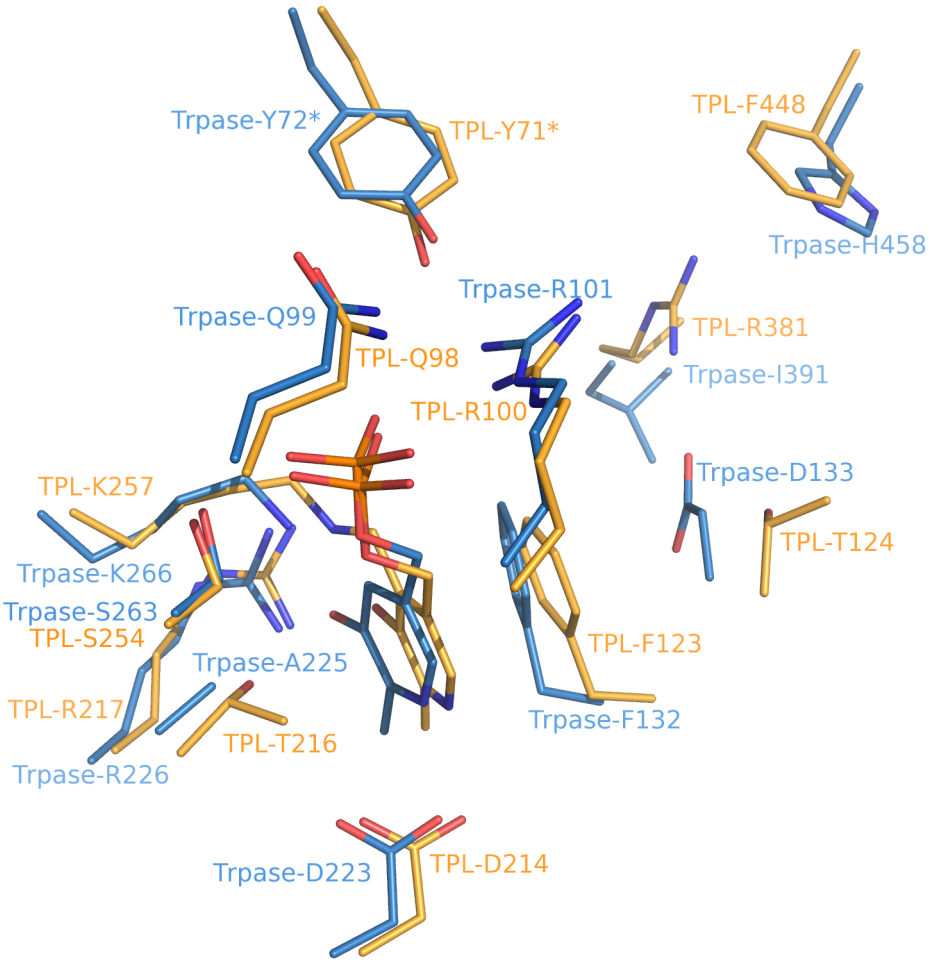

Figure 2.19. Overlay of the active sites of *C. intermedius* TPL (**2**; *orange*) and *P. vulgaris* Trpase (*blue*). Thr124, Arg381, and Phe448 in TPL are replaced by Asp133, Ile391, and His458, respectively, in Trpase.

of Asp133 (Asp137 in *E. coli* enzyme) which acts as a general base catalyst.[149] Asp133 and His458 (His463 in *E. coli* protein) are conserved residues in all known Trpases. As shown by mutatgenesis, His458 plays an accessory role presumably by creating a local environment convenient for β-elimination.[149] Residues Asp133 and His458 in Trpase are replaced by Thr124 and Phe448, respectively, in the TPL active site (Fig. 2.19). In addition, Ile391 in *P. vulgaris* Trpase (Ile396 in *E. coli* Trpase, and Val in some other Trpases) corresponds to Arg381 in TPL. All other residues in the active site are conserved among all known Trpase and TPL, which indicates that Asp133, His458, and Ile391 (or Val) should be responsible for the substrate specificity of Trpase.

3 Materials and Methods

3.1 Crystallization

Wild-type TPL and its D214A, F448H, and Y71F mutants were produced in *E. coli* SVS 370 cells transformed with the plasmid pTZTPL containing the wild-type, D214A, F448H, and Y71F mutant *C. freundii* TPL gene, respectively.[3,15,52,154] Cells were grown, and the enzyme was purified as described previously.[15,52,154]

3.1.1 Crystallization of the wild-type and mutant TPL holoenzyme from *C. freundii*

Before crystallization, the TPL holoenzyme from *C. freundii* was dialyzed against the solution that contained 0.5 mmol dm^{-3} PLP and 2 mmol dm^{-3} DTT in 50 mmol dm^{-3} triethanolamine buffer (pH 8.0). The protein solution was concentrated to 18–20 mg cm^{-3} using a 30K ultrafiltration membrane concentrator (Filtron). Crystals of the wild-type and mutant TPL holoenzymes were grown at both 277 K and 293 K by the hanging drop vapor diffusion technique. The best crystals were obtained by mixing 2 µL of the protein solution with an equal volume of the reservoir solution containing 50 mmol dm^{-3} triethanolamine buffer (pH 8.0), 0.5 mmol dm^{-3} PLP, 2 mmol dm^{-3} DTT, 0.4–0.8 mol dm^{-3} KCl, and 0.35–0.38 g cm^{-3} PEG 5 000 MME.

3.1.2 Crystallization of *C. freundii* TPL apoenzyme

TPL apoenzyme from *C. freundii* was crystallized at both 277 K and 293 K using the hanging drop vapor diffusion method. Prior to crystallization, the purified apoenzyme was dialyzed against the 50 mmol dm^{-3} triethanolamine buffer (pH 8.0) containing 2 mmol dm^{-3} dithiothreitol (DTT) and concentrated using a 30K ultrafiltration membrane concentrator (Filtron) to 18–20 mg cm^{-3}. For crystallization 2 µL aliquots of the protein solution were mixed on siliconized glass cover-slips with an equal volume of the reservoir solution. The reservoir solution contained 50 mmol dm^{-3} potassium phosphate buffer (pH 8.0), 2 mmol dm^{-3} DTT, 0.2 mol dm^{-3} KCl, and 0.325 g cm^{-3} poly(ethylene glycol) 2 000 monomethyl ether (PEG 2 000 MME).[155] Plate-like crystals with the size of 0.1 × 0.5 × 0.5 mm^3 grew within 2 weeks.

3.1.3 Preparation of *C. freundii* TPL holoenzyme complexes

Crystals of the TPL holoenzyme complexes were produced by soaking of the holoenzyme crystals in the stabilization solution containing the appropriate ligand. When phenol and ammonium pyruvate were used as ligands, soaking was done in the stabilization solution which contained 0.2 mol dm^{-3} KCl, 0.35 g cm^{-3} PEG 2 000 MME, 50 mmol dm^{-3} triethanolamine buffer (pH 8.0), 0.2 mmol dm^{-3} PLP, 0.5 mmol dm^{-3} DTT, and either 10 mmol dm^{-3} phenol or 0.3 mol dm^{-3} ammonium pyruvate. Soaking time for both phenol and ammonium pyruvate was 2–3 minutes.

Complexes with alanine and methionine were prepared by soaking the light yellow holo-TPL crystals for 5 min in the stabilization solution containing 0.40 g cm^{-3} PEG 5 000 MME, 50 mmol dm^{-3} triethanolamine buffer (pH 8.0), 0.25 mol dm^{-3} KCl, 0.2 mmol dm^{-3} PLP, 0.5 mmol dm^{-3} dithiothreitol, and either 100 mmol dm^{-3} L-alanine or 70 mmol dm^{-3} L-methionine. Crystals turned dark yellow-red during soaking and were cryo-cooled by dipping into liquid nitrogen directly from the soaking solution. L-Alanine and L-methionine act as competitive inhibitors of TPL[50] and, when added to TPL, they predominantly form relatively stable quinonoid intermediates, both in solution[50] and in the crystal.[156] Despite this, it was not possible to prepare quinonoid complexes by co-crystallization. Soaking times longer than 5 min considerably deteriorated the crystal quality.

Complexes of the mutant TPL molecules were obtained by soaking the Y71F and F448H TPL crystals for 2–3 min, respectively, in a stabilization solution containing 10 mmol dm^{-3} 3-fluoro-L-tyrosine, 0.45 g cm^{-3} PEG 5 000 MME, 50 mmol dm^{-3} triethanolamine buffer (pH 8.0), 0.2 mol dm^{-3} KCl, 0.2 mmol dm^{-3} PLP, and 0.5 mmol dm^{-3} DTT.

The alanine quinonoid complex with pyridine *N*-oxide was prepared by soaking holo-TPL crystals in the stabilization solution which contained 0.40 g cm^{-3} PEG 5 000 MME, 50 mmol dm^{-3} triethanolamine buffer (pH 8.0), 0.25 mol dm^{-3} KCl, 0.2 mmol dm^{-3} PLP, 0.5 mmol dm^{-3} dithiothreitol, 100 mmol dm^{-3} L-alanine and a saturating concentration of pyridine *N*-oxide. Since the crystal's quality deteriorated rapidly by soaking, the soaking time was only about 20 s.

3.2 X-ray data collection, structure determination, refinement and evaluation

The solution containing the combination of KCl and high molecular mass PEG MMEs appeared to be a good cryoprotectant and allowed freezing of TPL crystals directly from the crystallization drops in all cases.

Details on the data collection are given for each structure separately. Data sets were processed with DENZO and SCALEPACK.[157] Most of the other crystallographic calculations were performed using the CCP4 suite of programs.[158] Molecular replacement

calculations were performed by AMoRe[159] or Phaser.[160] Models were built by COOT,[161] water molecules were added using ARP/wARP,[162] and the refinement was carried out by REFMAC[163] using the TLS option.[164] Models of the specific ligands not found in PDB were generated by SKETCHER; the corresponding library files used during the refinement were generated by LIBCHECK.[158] The final models were validated by PROCHECK[165] and MolProbity.[166]

3.2.1 TPL holoenzyme from *C. freundii*

Data collection and refinement statistics for holo-TPL are given in Table 3.1. Diffraction data were collected at a temperature of 120 K at the BW7B beamline (EMBL, Hamburg) using a wavelength of 0.87 Å and the 300 mm MarResearch image-plate detector. Crystals of the TPL holoenzyme belong to the orthorhombic space group $P2_12_12$ with $a = 133.9$ Å, $b = 143.9$ Å, $c = 60.1$ Å. Two subunits of TPL (polypeptide chains A and B) per asymmetric unit of the crystal give a specific volume (V_M)[168] of 2.81 Å^3 Da^{-1} and a solvent content of 55.9 %. The initial molecular replacement (AMoRe)[159] model for the holoenzyme structure was the structure of the TPL apoenzyme previously determined from crystals obtained in different crystallization conditions (PDB ID: 1TPL).[3] The structure was refined to an R-factor of 15.2 % ($R_{free} = 18.5$ %) at 1.9 Å resolution, with the small domain (residues 19–48 and 333–456) and the large domain (residues 57–310) of each subunit as a separate TLS group. The final electron density maps allowed positioning of all residues except for the first N-terminal residues of both subunits (Met1). The final model contains 2 PLP molecules, 2 K^+ cations, and 902 water molecules, giving a total of 8 118 atoms. Forty-five atoms of the final model belong to the totally disordered protein side chains; these were omitted from the refinement and were given an occupancy of zero. The rest of the model is clearly defined in the electron density maps. The side chains of residues Met66(A), Thr124(A), Glu354(A), Thr15(B), Met66(B), Ile93(B), and Thr124(B) were modeled in two conformations with an occupancy of 0.5. None of the non-glycine and non-proline residues lie outside the allowed regions of the Ramachandran plot.[169]

3.2.2 D214A TPL mutant from *C. freundii*

Data collection and refinement statistics for the D214A TPL mutant are given in Table 3.1. Diffraction data were collected at 100 K, at the BM30A beamline (ESRF, Grenoble) using a wavelength of 0.980 Å and a MAR 165 CCD detector (MarResearch). The unit cell parameters for D214A TPL mutant are slightly different than for the native holo-TPL. The structure was refined to an R-factor of 15.6 % ($R_{free} = 17.8$ %) at 1.9 Å resolution, with the small (residues 19–44, 346–404, and 434–456) and the large (residues 1–13, 45–345, and 405–422) rigid regions of each subunit as a separate TLS group. The space group is

Table 3.1. Crystallographic data collection and refinement statistics for holo-TPL and D214A TPL

Structure	holo-TPL	D214A TPL
Space group	$P2_12_12$	$P2_12_12$
Unit cell parameters		
a / Å	133.9	132.6
b / Å	143.8	142.7
c / Å	60.1	59.4
Resolution range / Å	20.0–1.90 (1.95–1.90)[a]	25.0–1.91 (1.97–1.90)
No. of unique reflections	85 710 (4 151)	87 110 (8 589)
R_{merge}[b] / %	7.5 (35.9)	6.9 (5.5)
Average $I/\sigma(I)$	15.4 (3.6)	15.1 (3.1)
Data redundancy[c]	3.2 (2.0)	4.5 (4.2)
Completeness / %	92.1 (90.7)	99.8 (99.4)
Wilson B-factor / Å^2	28.5	24.4
R_{cryst}[d] / %	15.2 (18.5)	15.6 (20.9)
R_{free}[d] / %	18.6 (24.5)	17.8 (26.0)
No. of reflections used for R_{free}	2 508 (174)	1 283
No. of atoms	8 118	8 140
No. of protein residues	910	910
No. of water molecules	902	794
No. of ligands	4 (2 K^+ and 2 PLP)	6 (2 K^+, 2 PLP and 2 PEG fragments)
Average B-factor / Å^2		
Chain A	24.9	33.0
Chain B	24.5	32.9
Water molecules	39.2	31.4
Overall	26.3	32.8
R.m.s. deviations[e]		
Bond length / Å	0.014 (0.022)	0.015 (0.022)
Bond angles	1.3° (2.0°)	1.4° (2.0°)
Estimated coordinate error[f] / Å	0.12	0.11
Ramachandran plot[g]		
Favored / %	98.5	98.3
Allowed / %	100.0	100.0
Outliers / %	0.0	0.0

[a] Values in parentheses are for the outer resolution shell.
[b] The value of the merging R-factor between equivalent measurements of the same reflection, $R_{\mathrm{merge}} = (\sum_{hkl} \sum_i |\langle I_{hkl}\rangle - I_{hkl,i}|) / (\sum_{hkl} \sum_i I_{hkl,i})$.
[c] The average observation of the same reflection.
[d] Crystallographic R-factors, $R = (\sum_{hkl} ||F_{\mathrm{o},hkl}| - |F_{\mathrm{c},hkl}||) / (\sum_{hkl} F_{\mathrm{o},hkl})$.
[e] Target values are given in parentheses.
[f] The diffraction-component precision index (DPI) based on R_{free}.[167]
[g] Analyzed by MolProbity.[166]

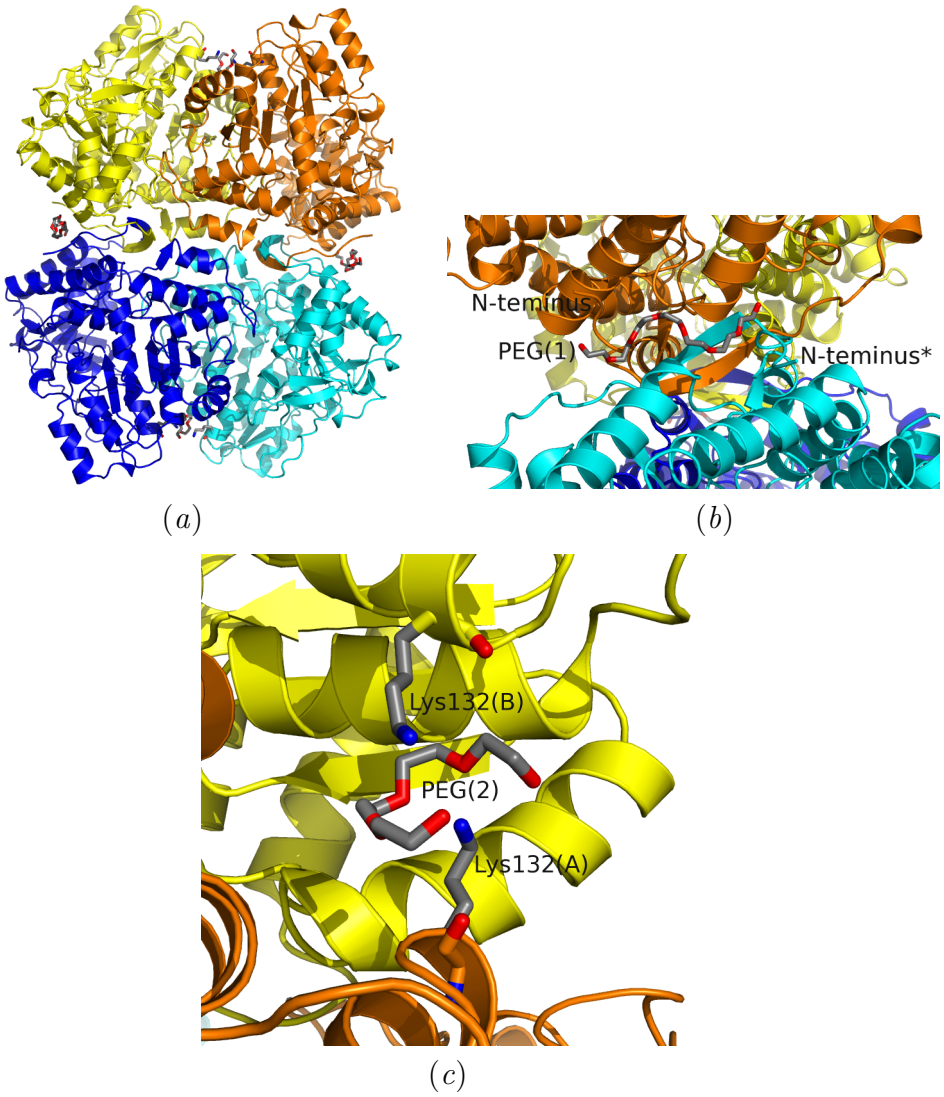

(*a*) (*b*) (*c*)

Figure 3.1. PEG fragments in the structure of D214A TPL.

$P2_12_12$ with two crystallographically independent protein subunits forming the catalytic dimer. All residues, except for the first N-terminal residue of both subunits (Met1), were located in the electron density map. The final model consists of 2 PLP molecules, 2 K^+ cations, 2 PEG fragments, and 794 water molecules, giving a total of 8 140 atoms. The side chains of residues Met66(A), Thr124(A), Arg198(A), Lys210(A), Arg381(A), Asp433(A), Lys41(B), Met66(B), Asn151(B), Arg201(B), Lys210(B), Arg330(B), Ser365(B), and His-430(B) were modeled in two conformations with an occupancy of 0.5. Two patches of electron density at the protein surface were interpreted as fragments of PEG MME used for crystallization.[170] There are two such fragments (Fig. 3.1). A long fragment of the PEG chain (seven –CH_2CH_2O– segments) was fitted into a spiral-shaped electron density between the tips of the N-terminal arms of two neighboring subunits (Fig. 3.1*b*). Another, shorter fragment of the PEG chain (four –CH_2CH_2O– segments) forms a loop situated between residues Lys132(A) and Lys132(B) (Fig. 3.1*c*).

3.2.3 TPL apoenzyme from *C. freundii*

Data collection and refinement statistics for apo-TPL are given in Table 3.2. Diffraction data were collected at 120 K, at the BM14 beamline (ESRF, Grenoble) using a wavelength

Table 3.2. Crystallographic data collection and refinement statistics for apo-TPL

Structure	apo-TPL
Space group	$P2_12_12$
Unit cell parameters	
a / Å	133.6
b / Å	143.7
c / Å	59.9
Resolution range / Å	17.0–1.85 (1.90–1.85)[a]
No. of unique reflections	95 091 (5 902)
R_{merge}[b] / %	5.5 (38.1)
Average $I/\sigma(I)$	19.3 (2.8)
Data redundancy[c]	3.4 (1.4)
Completeness / %	95.5 (85.1)
Wilson B-factor / Å^2	31.0
R_{cryst}[d] / %	17.0 (25.1)
R_{free}[d] / %	20.3 (32.6)
No. of reflections used for R_{free}	939 (64)
No. of atoms	8 304
No. of protein residues	912
No. of water molecules	1 021
No. of ligands	5 (2 K^+ and 2.5 PO_4^{3-})
Average B-factor / Å^2	
Chain A	28.1
Chain B	24.9
Water molecules	27.4
Overall	26.6
R.m.s. deviations[e]	
Bond length / Å	0.015 (0.022)
Bond angles	1.4° (2.0°)
Estimated coordinate error[f] / Å	0.11
Ramachandran plot[g]	
Favored / %	97.9
Allowed / %	100.0
Outliers / %	0.0

[a] Values in parentheses are for the outer resolution shell.
[b] The value of the merging R-factor between equivalent measurements of the same reflection, $R_{\mathrm{merge}} = (\sum_{hkl} \sum_i | \langle I_{hkl} \rangle - I_{hkl,i}|) / (\sum_{hkl} \sum_i I_{hkl,i})$.
[c] The average observation of the same reflection.
[d] Crystallographic R-factors, $R = (\sum_{hkl} ||F_{\mathrm{o},hkl}| - |F_{\mathrm{c},hkl}||) / (\sum_{hkl} F_{\mathrm{o},hkl})$.
[e] Target values are given in parentheses.
[f] The diffraction-component precision index (DPI) based on R_{free}.[167]
[g] Analyzed by MolProbity.[166]

of 1.0 Å and the MarResearch CCD detector. Like holoenzyme, the TPL apoenzyme crystallizes in the space group $P2_12_12$ with one catalytic dimer per asymmetric unit (polypeptide chains A and B). Unit cell parameters $a = 133.6$ Å, $b = 143.7$ Å, $c = 59.9$ Å are almost identical to those of the holoenzyme. The structure of the TPL apoenzyme from *C. freundii* was solved by molecular replacement (AMoRe)[159] using the holoenzyme structure as the initial model. It was refined to an *R*-factor of 17.0 % ($R_{\text{free}} = 20.3$ %) at 1.85 Å resolution, with the small domain (residues 19–48 and 333–456) and the large domain (residues 57–310) of each subunit as a separate TLS group. The final model comprises 8 304 atoms, including 1 021 water molecules, 2 K^+ cations, and 2.5 PO_4^{3-} anions (one of the phosphate anions is modeled with an occupancy of 0.5). Residues Ser17(A), Met66(A), Ser276(A), Val283(A), Lys328(A), Arg9(B), Glu273(B), and His430(B) were modeled with two alternate side-chain conformations with occupancies of 0.5. All non-glycine and non-proline residues, except Met121(A), are in the allowed regions of the Ramachandran plot.[169] Met121(A) has very unfavorable main-chain torsion angles $\varphi = 75°$, $\psi = 144°$), but its average *B*-factor is relatively low (31.7 $Å^2$) and the corresponding electron density unambiguous.

3.2.4 TPL holoenzyme from *C. freundii* soaked with phenol

Data collection and refinement statistics for holo-TPL soaked in the phenol solution [TPL (phenol)] are given in Table 3.3. Diffraction data were collected at 100 K, at the BM30A beamline (ESRF, Grenoble) using a wavelength of 0.980 Å and a MAR 165 CCD detector (MarResearch). The structure was solved by molecular replacement (AMoRe)[159] using the TPL apoenzyme structural model without the small rigid region of both crystallographically independent subunits. The structure of holo-TPL soaked with phenol was refined to an *R*-factor of 15.1 % ($R_{\text{free}} = 17.8$ %) at 1.8 Å resolution, with 3 TLS groups: (1) the small (residues 19–44, 346–404, and 434–456) and (2) the large (residues 2–13, 45–345, and 405–422) rigid regions of subunit B, and (3) the large rigid region (residues 2–13, 45–345, and 405–422) of subunit A. The final model consists of 9 458 atoms, including 947 water molecules, 2 K^+ cations, 2 PLP, 0.52 PO_4^{3-} and 1 PEG fragment (seven $–CH_2CH_2O–$ segments) situated in the groove at the interface between two catalytic dimers of the same tetramer related to each other by non-crystallographic symmetry (similar as in TPL–Ala and TPL–Met; Figs. 3.2 and 3.3). Residue Met1 in both crystallographically independent chains was not modeled due to the poorly defined electron density. Residues 13–45, 121–123, 273, 345–405, and 422–456 in chain A, and residues 9, 78, 79, and 288–291 in chain B were modeled in two alternate positions with occupancies 0.52 and 0.48 for each position. These occupancies were deduced from the refinement in SHELX[171] by the least-squares Konnert-Hendrickson conjugate gradient method. Residues Met66(A), His79(A), Arg82(A), Asn234(A), Val283(A), Met66(B), Lys132(B), Gln230(B), Glu273(B), Arg351(B), Ser365(B), Ser385(B), and Gln429(B) were modeled

in two alternate conformations with a site occupancy factor 0.50.

3.2.5 TPL holoenzyme from *C. freundii* soaked with ammonium pyruvate

Data collection and refinement statistics for holo-TPL soaked in the ammonium pyruvate solution [TPL (AP)] are given in Table 3.3. Diffraction data were collected at 100 K, at the BM30A beamline (ESRF, Grenoble) using a wavelength of 0.980 Å and a MAR 165 CCD detector (MarResearch). The structure was solved by molecular replacement (AMoRe)[159] using the TPL apoenzyme structural model without the small rigid region of both crystallographically independent subunits. The structural model of holo-TPL soaked with ammonium pyruvate was refined to an R-factor of 15.2 % ($R_{\text{free}} =$ 18.0 %) at 1.85 Å resolution, with 3 TLS groups: (1) the small (residues 19–44, 346–404, and 434–456) and (2) the large (residues 2–13, 45–345, and 405–422) rigid regions of subunit B, and (3) the large rigid region (residues 2–13, 45–345, and 405–422) of subunit A. The final model consists of 9 629 atoms, including 1 084 water molecules, 2 K^+ cations, 1.54 PLP, 0.46 aminoacrylate molecule, 0.54 PO_4^{3-} and 1 PEG fragment (seven $-CH_2CH_2O-$ segments) situated in the same location as in the structure of holo-TPL soaked with phenol. Met1(A) and Met1(B) could not be modeled. Residues 13–45, 234, 328, 345–405, and 422–456 in chain A, and residues 9, 78, 79, and 288 in chain B were modeled in two alternate positions with occupancies 0.54 and 0.46 for each position. Residues Met66(A), His79(A), Arg82(A), Glu173(A), Thr216(A), Glu273(A), Val283(A), Lys41(B), Met66(B), Lys132(B), Asn185(B), Arg198(B), Thr216(B), Gln230(B), Glu286(B), Glu354(B), Ser385(B), Gln429(B), and His430(B) were modeled in two alternate conformations with a site occupancy factor 0.50.

Table 3.3. Crystallographic data collection and refinement statistics for holo-TPL soaked with phenol and holo-TPL soaked with ammonium pyruvate (AP)

Structure	holo-TPL soaked with phenol	holo-TPL soaked with AP
Space group	$P2_12_12$	$P2_12_12$
Unit cell parameters		
a / Å	133.0	133.4
b / Å	143.4	143.7
c / Å	59.6	59.8
Resolution range / Å	25.0–1.80 (1.86–1.80)[a]	20.0–1.85 (1.92–1.85)
No. of unique reflections	103 322 (10 016)	98 231 (9 678)
R_{merge}[b] / %	4.5 (53.8)	4.5 (49.2)
Average $I/\sigma(I)$	20.5 (2.3)	20.7 (3.0)
Data redundancy[c]	4.0 (3.6)	3.9 (3.6)
Completeness / %	99.5 (98.1)	99.3 (99.2)
Wilson B-factor / Å^2	27.5	28.9
R_{cryst}[d] / %	15.1 (29.0)	15.2 (24.7)
R_{free}[d] / %	17.8 (32.8)	18.0 (30.1)
No. of reflections used for R_{free}	1 034 (69)	974 (88)
No. of atoms	9 458	9 629
No. of protein residues	910	910
No. of water molecules	947	1 084
No. of ligands	6 (2 K^+, 1 PEG fragment, 2 PLP, 0.52 PO_4^{3-})	6 (2 K^+, 1 PEG fragment, 1.54 PLP, 0.54 PO_4^{3-}, 0.46 aminoacrylate molecule)
Average B-factor / Å^2		
Chain A	24.8	23.9
Chain B	34.9	18.4
Water molecules	29.7	33.6
Overall	29.3	22.9
R.m.s. deviations[e]		
Bond length / Å	0.018 (0.022)	0.015 (0.022)
Bond angles	1.5° (2.0°)	1.4° (2.0°)
Estimated coordinate error[f] / Å	0.10	0.11
Ramachandran plot[g]		
Favored / %	98.3	97.6
Allowed / %	100.0	100.0
Outliers / %	0.0	0.0

[a] Values in parentheses are for the outer resolution shell.
[b] The value of the merging R-factor between equivalent measurements of the same reflection, $R_{\mathrm{merge}} = (\sum_{hkl} \sum_i |\langle I_{hkl}\rangle - I_{hkl,i}|) / (\sum_{hkl} \sum_i I_{hkl,i})$.
[c] The average observation of the same reflection.
[d] Crystallographic R-factors, $R = (\sum_{hkl} ||F_{\mathrm{o},hkl}| - |F_{\mathrm{c},hkl}||) / (\sum_{hkl} F_{\mathrm{o},hkl})$.
[e] Target values are given in parentheses.
[f] The diffraction-component precision index (DPI) based on R_{free}.[167]
[g] Analyzed by MolProbity.[166]

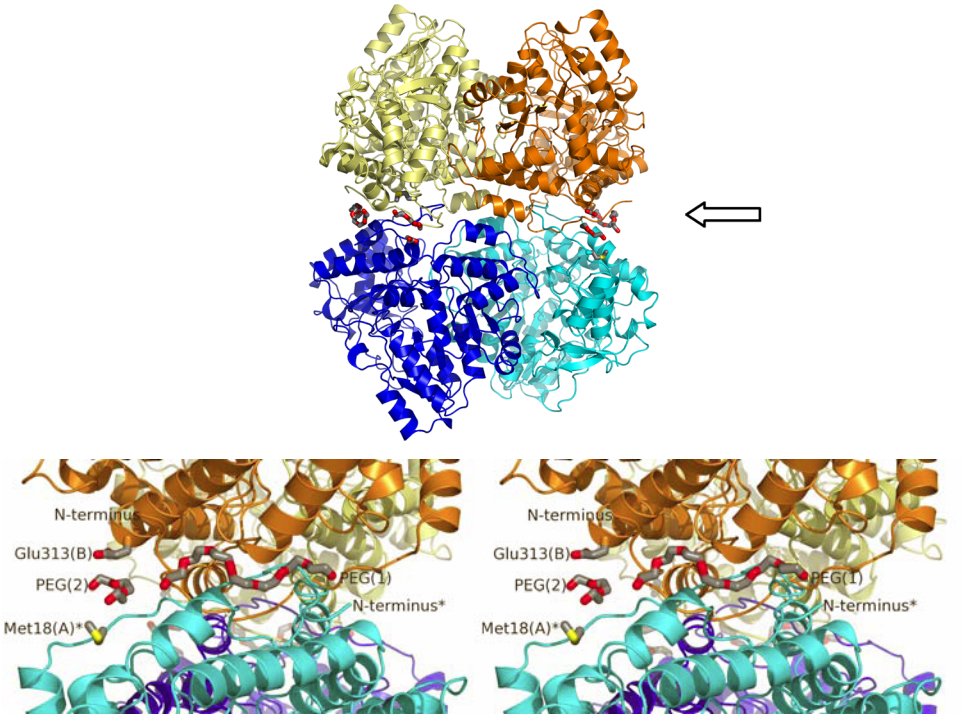

Figure 3.2. The modeled PEG fragments in TPL–Ala. The arrow (*upper* panel) points in the view direction of the enlarged stereo figure (*below*) of the tetramer. Subunits are shown in different colors.

3.2.6 TPL from *C. freundii* complexed with l-alanine

Data collection and refinement statistics for TPL complexed with L-alanine (TPL–Ala) are given in Table 3.4. Diffraction data were collected at the BW7B beamline (EMBL, Hamburg) at 120 K, at a wavelength of 0.862 Å using an image-plate detector (MarResearch). Crystals belong to the space group $P2_12_12$ with one catalytic dimer per asymmetric unit (polypeptide chains A and B) and unit cell parameters very similar to those of holo-TPL. The structure of TPL–Ala was refined to an R-factor of 15.8 % ($R_{\mathrm{free}} = 19.8\,\%$) at 1.9 Å resolution, with the small (residues 19–44, 346–404, and 434–456) and the large (residues 1–13, 45–345, and 405–422) rigid regions of each subunit treated as separate TLS groups. The final model is composed of 8 361 atoms, including 966 water molecules, 2 K^+ cations, 2 alanine quinonoid molecules, and 2 PEG fragments. Namely, several patches of electron density at the protein surface were interpreted as fragments of PEG MME used for crystallization. There are two such fragments and both are situated in the groove at the interface between two catalytic dimers of the same tetramer related to each other by non-crystallographic symmetry (Fig. 3.2). A long fragment of the PEG chain (seven –CH_2CH_2O– segments) was fitted into a spiral-shaped electron density between the tips of the N-terminal arms of two neighboring subunits. Another, shorter fragment of PEG chain (three –CH_2CH_2O– segments) forms a loop situated between Met18(A) and Glu313(B) of the neighboring catalytic dimer. The side chains of residues Met1(A) and Met1(B) were not visible in the electron density map. Residues Met288(A), Ser290(A),

Table 3.4. Crystallographic data collection and refinement statistics for TPL–Ala and TPL–Met

Structure	TPL–Ala	TPL–Met
Space group	$P2_12_12$	$P2_12_12$
Unit cell parameters		
a / Å	132.9	132.9
b / Å	143.7	143.3
c / Å	59.6	59.7
Resolution range / Å	20.0–1.89 (1.93–1.89)[a]	30.0–1.95 (2.02–1.95)
No. of unique reflections	89 055 (4 337)	76 260 (6 854)
R_{merge}[b] / %	7.0 (35.7)	8.2 (42.5)
Average $I/\sigma(I)$	12.2 (1.8)	10.5 (2.3)
Data redundancy[c]	3.7 (2.3)	3.9 (3.6)
Completeness / %	97.3 (87.5)	90.3 (82.3)
Wilson B-factor / Å^2	18.9	27.1
R_{cryst}[d] / %	15.7 (19.8)	15.5 (19.2)
R_{free}[d] / %	19.8 (30.2)	19.2 (22.7)
No. of reflections used for R_{free}	1 065 (52)	1 058 (116)
No. of atoms	8 361	8 244
No. of protein residues	912	912
No. of water molecules	966	887
No. of ligands	6 (2 K^+, 2 PEG fragments, 2 alanine quinonoid molecules)	6 (2 K^+, 2 PEG fragments, 1 methionine quinonoid molecule, 1 PLP)
Average B-factor / Å^2		
Chain A	17.2	32.0
Chain B	14.3	29.5
Water molecules	29.6	41.2
Overall	17.4	32.0
R.m.s. deviations[e]		
Bond length / Å	0.016 (0.022)	0.015 (0.022)
Bond angles	1.4° (2.0°)	1.4° (2.0°)
Estimated coordinate error[f] / Å	0.12	0.13
Ramachandran plot[g]		
Favored / %	98.1	97.9
Allowed / %	100.0	100.0
Outliers / %	0.0	0.0

[a] Values in parentheses are for the outer resolution shell.
[b] The value of the merging R-factor between equivalent measurements of the same reflection, $R_{\mathrm{merge}} = (\sum_{hkl} \sum_i |\langle I_{hkl}\rangle - I_{hkl,i}|) / (\sum_{hkl} \sum_i I_{hkl,i})$.
[c] The average observation of the same reflection.
[d] Crystallographic R-factors, $R = (\sum_{hkl} ||F_{\mathrm{o},hkl}| - |F_{\mathrm{c},hkl}||) / (\sum_{hkl} F_{\mathrm{o},hkl})$.
[e] Target values are given in parentheses.
[f] The diffraction-component precision index (DPI) based on R_{free}.[167]
[g] Analyzed by MolProbity.[166]

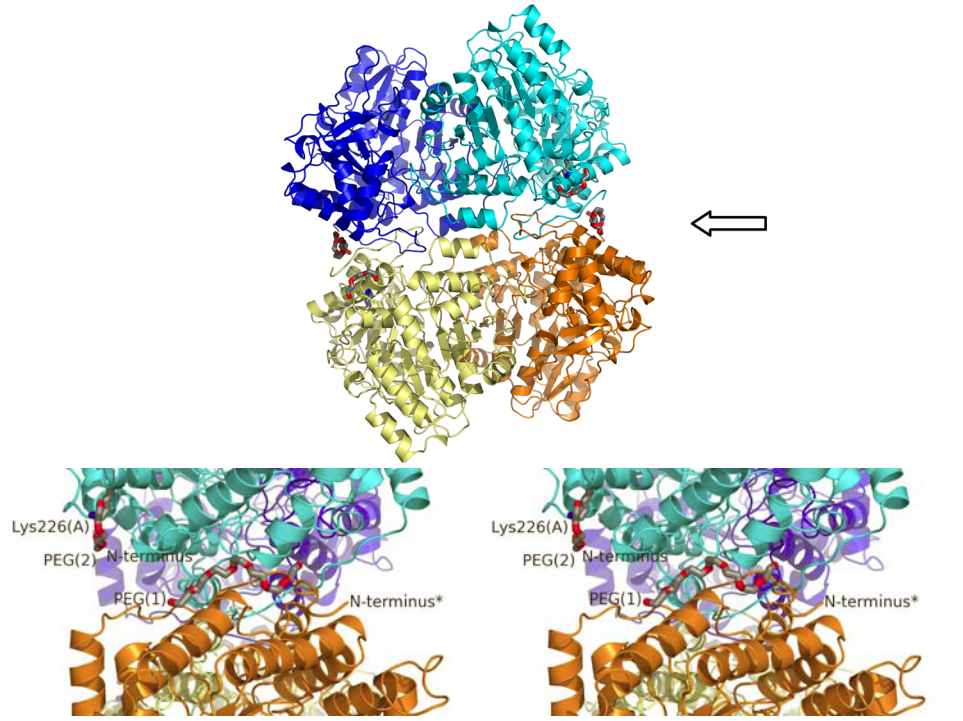

Figure 3.3. The modeled PEG fragments in TPL–Met. The arrow (*upper* panel) points in the view direction of the enlarged stereo figure (*below*) of the tetramer. Subunits are shown in different colors.

and Phe449(B) were modeled with two alternate side-chain conformations with occupancies of 0.7 and 0.3, respectively. Residues Asp422(A), Ile424(A), Met66(B), Thr124(B), Cys179(B), Thr216(B), Gln230(B), Met253(B), Ser276(B), Gln286(B), Ser385(B) and His430(B) were also modeled with two alternate conformations of their side chains, each with occupancy of 0.5.

3.2.7 TPL from *C. freundii* complexed with l-methionine

Data collection and refinement statistics for the complex of holo-TPL and L-methionine (TPL–Met) are given in Table 3.4. Diffraction data were collected at 120 K, at the BM14 beamline (ESRF, Grenoble) at a wavelength of 0.979 Å using a CCD detector (Mar-Research). There is one catalytic dimer in the asymmetric unit (polypeptide chains A and B) of the TPL–Met structure. The structure was refined to an R-factor of 15.5 % ($R_{\mathrm{free}} =$ 19.2 %) at 1.95 Å resolution, with the small (residues 19–44, 346–404, and 434–456) and the large (residues 1–13, 45–345, and 405–422) rigid regions of each subunit treated as separate TLS groups. The final model is composed of 8 244 atoms, including 887 water molecules, 2 K^+ cations, 1 methionine quinonoid molecule, 1 PLP, and 2 PEG fragments. Similarly as for TPL–Ala, several patches of electron density at the protein surface were interpreted as fragments of PEG MME. In the TPL–Met structure the heptameric spiral PEG fragment is found in a similar position as in the TPL–Ala (Fig. 3.3). In addition, there is a trimeric PEG fragment surrounding the side-chain amino group of Lys226(A)

in TPL–Met. Residues Ser17(A), Met66(A), His79(A), Val283(A), Asp422(A), Met66(B), His79(B), Val340(B), and Gln445(B) were modeled with two alternate conformations with 0.5 occupancy.

3.2.8 F448H TPL mutant complexed with 3-fluoro-l-tyrosine

Data collection and refinement statistics for the complex of F448H TPL and 3-fluoro-L-tyrosine (F448H TPL–F-Tyr) are given in Table 3.5. Diffraction data were collected at 100 K at the BM30A beamline (ESRF, Grenoble) using a wavelength of 0.980 Å and a MAR 165 CCD detector (MarResearch). F448H TPL–F-Tyr crystallizes in the orthorhombic space group $P2_12_12_1$ with the unit cell parameter c doubled and with four crystallographically independent protein subunits comprising a whole homotetramer (polypeptide chains A, B, C, and D). The structure was solved by molecular replacement (Phaser)[160] using the whole tetramer of the *C. freundii* TPL apoenzyme as the search model. Structure of F448H TPL–F-Tyr was refined to an R-factor of 13.8 % ($R_{\text{free}} = 17.5$ %) at 2.0 Å resolution, with the small (residues 19–44, 346–404, and 434–456) and the large (residues 1–13, 45–345, and 405–422) rigid regions of each subunit treated as separate TLS groups. Because of significant distortions in electron density corresponding to the 3-fluoro-L-tyrosine quinonoid molecules bound in the closed active sites, planarity restraints for phenyl ring of these ligands were not used. The final model consists of 16 890 atoms, including 1 863 water molecules, 4 K^+ cations, 4 molecules of one of the reaction intermediates formed between PLP and 3-fluoro-L-tyrosine, and 24 PEG fragments. Namely, several fragments of electron density were interpreted as parts of PEG MME chains.[170] There are two heptameric fragments (seven –CH_2CH_2O– mers) found between the two catalytic dimers as in the other TPL structures. All modeled PEG fragments in F448H TPL–3-F-L-Tyr are summarized in Table 3.6. Most of them are bound in the equivalent sites of different protein subunits. Residues Ile43(A), Glu75(A), His79(A), Cys179(A), Arg198(A), Arg397(A), Asp422(A), Arg452(A), Ile43(B), Glu75(B), His79(B), Cys179(B), Arg198(B), Val211(B), Asp422(B), Glu23(C), Ile43(C), Glu75(C), His79(C), Arg82(C), Lys132(C), Cys179(C), Val211(C), Asp422(C), Arg452(C), Ile43(D), His79(D), Cys179(D), Arg198(D), Val211(D), Asp422(D), and Arg452(D) were modeled in two alternate conformations with 0.5 occupancy.

Table 3.5. Crystallographic data collection and refinement statistics for F448H TPL complexed with 3-fluoro-L-tyrosine

Structure	F448H TPL–F-Tyr
Space group	$P2_12_12_1$
Unit cell parameters	
a / Å	136.4
b / Å	143.8
c / Å	118.5
Resolution range / Å	30.0–2.00 (2.07–2.00)[a]
No. of unique reflections	154 478 (13 859)
R_{merge}[b] / %	9.1 (53.1)
Average $I/\sigma(I)$	7.5 (2.5)
Data redundancy[c]	4.7 (4.5)
Completeness / %	99.0 (99.2)
Wilson B-factor / Å^2	22.4
R_{cryst}[d] / %	13.8 (17.7)
R_{free}[d] / %	17.5 (22.9)
No. of reflections used for R_{free}	1 547 (135)
No. of atoms	16 890
No. of protein residues	1 824
No. of water molecules	1 863
No. of ligands	32 (4 K^+, 24 PEG fragments, 4 3-fluoro-L-tyrosine quinonoid molecules)
Average B-factor / Å^2	
Chain A	22.3
Chain B	24.1
Chain C	22.4
Chain D	23.2
Water molecules	23.4
Overall	23.0
R.m.s. deviations[e]	
Bond length / Å	0.016 (0.022)
Bond angles	1.5° (2.0°)
Estimated coordinate error[f] / Å	0.12
Ramachandran plot[g]	
Favored / %	97.8
Allowed / %	99.8
Outliers / %	0.2

[a] Values in parentheses are for the outer resolution shell.
[b] The value of the merging R-factor between equivalent measurements of the same reflection, $R_{\mathrm{merge}} = (\sum_{hkl} \sum_i |\langle I_{hkl}\rangle - I_{hkl,i}|) / (\sum_{hkl} \sum_i I_{hkl,i})$.
[c] The average observation of the same reflection.
[d] Crystallographic R-factors, $R = (\sum_{hkl} ||F_{\mathrm{o},hkl}| - |F_{\mathrm{c},hkl}||) / (\sum_{hkl} F_{\mathrm{o},hkl})$.
[e] Target values are given in parentheses.
[f] The diffraction-component precision index (DPI) based on R_{free}.[167]
[g] Analyzed by MolProbity.[166]

Table 3.6. PEG fragments modeled in the structure of F448H TPL complexed with 3-fluoro-L-tyrosine (F448H TPL–3-F-L-Tyr)

PDB component identifier	No. of $-CH_2CH_2O-$ mers	Location
PGE	3	nearby Lys170(A), Glu169(A), Lys165(A)
PGE	3	around side chain of Lys226(A)
PGE	3	nearby Glu313(A)
PG4	4	around side chain of Lys444(A)
PGE	3	nearby Lys444(A)
P33	7	between the chains A and D (from different catalytic dimers)
PGE	3	around side chain of Lys226(B)
PGE	3	nearby Glu313(B)
PG4	4	around side chain of Lys444(B)
EDO	1	nearby Lys444(B)
PGE	3	next to the hydrophobic core, between Met66(B) and Met66(D)
P33	7	between the chains B and C (from different catalytic dimers)
PG4	4	nearby Lys170(B), Glu169(B), Lys165(B)
PGE	3	nearby Lys170(C), Glu169(C), Lys165(C)
PGE	3	around side chain of Lys226(C)
1PE	5	nearby Glu313(C)
PGE	3	around side chain of Lys444(C)
PEG	2	nearby Lys444(C)
PGE	3	nearby Lys170(D), Glu169(D), Lys165(D)
PGE	3	around side chain of Lys226(D)
PG4	4	nearby Glu313(D)
PGE	3	nearby Lys444(D)
PEG	2	nearby Lys112(D)
PG4	4	around side chain of Lys444(D)

3.2.9 Y71F TPL mutant complexed with 3-fluoro-l-tyrosine

Data collection and refinement statistics for the complex of Y71F TPL and 3-fluoro-L-tyrosine (Y71F TPL–F-Tyr) are given in Table 3.7. Diffraction data were collected at 100 K, at the BM14 beamline (ESRF, Grenoble) using a wavelength of 0.980 Å and a CCD detector (MarResearch). The space group of Y71F TPL–F-Tyr is $P2_12_12$ with the catalytic dimer in the asymmetric unit. The structure was refined to an R-factor of 15.9 % ($R_{\text{free}} = 19.2\,\%$) at 1.95 Å resolution, with the small (residues 19–44, 346–404, and 434–456) and the large (residues 1–13, 45–345, and 405–422) rigid regions of each subunit treated as separate TLS groups. The final model is composed of 8 131 atoms, including 745 water molecules, 2 K^+ cations, 1.33 3-fluoro-L-tyrosine quinonoid molecules, 0.67 3-fluoro-L-tyrosine external aldimine molecule and 2 PEG fragments. In the active site of

Table 3.7. Crystallographic data collection and refinement statistics for Y71F TPL complexed with 3-fluoro-L-tyrosine and wild-type TPL complexed with L-alanine and pyridine *N*-oxide

Structure	Y71F TPL–3-F-L-Tyr	TPL–Ala–PNO
Space group	$P2_12_12$	$P2_12_12$
Unit cell parameters		
a / Å	133.6	134.0
b / Å	144.4	143.8
c / Å	59.7	60.1
Resolution range / Å	17.0–2.05 (2.09–2.05)[a]	20.0–2.25 (2.29–2.25)
No. of unique reflections	71 319 (4 260)	55 230 (2 668)
R_{merge}[b] / %	4.6 (34.6)	4.8 (17.2)
Average $I/\sigma(I)$	13.7 (3.2)	13.8 (4.5)
Data redundancy[c]	3.0 (1.9)	3.4 (2.8)
Completeness / %	96.5 (83.6)	98.8 (94.3)
Wilson B-factor / Å^2	28.2	34.6
R_{cryst}[d] / %	16.0 (19.5)	13.9 (17.0)
R_{free}[d] / %	20.7 (22.9)	18.1 (22.9)
No. of reflections used for R_{free}	1 047 (67)	995 (45)
No. of atoms	8 131	8 174
No. of protein residues	912	910
No. of water molecules	745	792
No. of ligands	6 (2 K^+, 2 PEG fragments, 0.67 3-fluoro-L-tyrosine external aldimine and 1.33 3-fluoro-L-tyrosine quinonoid molecules)	10 (2 K^+, 1.5 PLP, 0.5 PO_4^{3-}, 0.5 alanine quinonoid molecule, 1 PEG fragment, 3 pyridine *N*-oxide molecules)
Average B-factor / Å^2		
Chain A	38.9	29.8
Chain B	34.7	28.4
Water molecules	24.5	25.6
Overall	35.7	28.9
R.m.s. deviations[e]		
Bond length / Å	0.018 (0.022)	0.014 (0.022)
Bond angles	1.5° (2.0°)	1.3° (2.0°)
Estimated coordinate error[f] / Å	0.15	0.16
Ramachandran plot[g]		
Favored / %	97.6	98.1
Allowed / %	100.0	100.0
Outliers / %	0.0	0.0

[a] Values in parentheses are for the outer resolution shell.
[b] The value of the merging R-factor between equivalent measurements of the same reflection, $R_{\mathrm{merge}} = (\sum_{hkl} \sum_i | \langle I_{hkl} \rangle - I_{hkl,i}|) / (\sum_{hkl} \sum_i I_{hkl,i})$.
[c] The average observation of the same reflection.
[d] Crystallographic R-factors, $R = (\sum_{hkl} ||F_{\mathrm{o},hkl}| - |F_{\mathrm{c},hkl}||) / (\sum_{hkl} F_{\mathrm{o},hkl})$.
[e] Target values are given in parentheses.
[f] The diffraction-component precision index (DPI) based on R_{free}.[167]
[g] Analyzed by MolProbity.[166]

chain A the ligand is modeled as two different intermediate species: the quinonoid, with the site occupancy factors of 0.33, and the external aldimine, with occupancy estimated at 0.67. One whole quinonoid species is bound in the active site of chain B. Two PEG fragments (one tetrameric and one dimeric) were modeled in the groove between the two catalytic dimers in the PEG binding site found in most of the *C. freundii* TPL structures. Residues Ser17(A), Asp22(A), His79(A), Arg198(A), Arg351(A), Asp422(A), His79(B), and Cys179(B) were modeled in two alternate conformations with occupancies of 0.5.

3.2.10 TPL complexed with l-alanine and pyridine *N*-oxide

Data collection and refinement statistics for the complex of TPL, L-alanine, and pyridine *N*-oxide (TPL–Ala–PNO) are given in Table 3.7. Diffraction data were collected at 100 K, using Cu-Kα radiation ($\lambda = 1.5418$ Å; Rigaku Ru200 generator with rotating anode) and a Mar345 image plate detector. The asymmetric unit of TPL–Ala–PNO crystal structure is composed of the catalytic dimer. The structure was refined to an *R*-factor of 13.9 % ($R_{\text{free}} = 18.1$ %) at 2.25 Å resolution, with the small (residues 19–44, 346–404, and 434–456) and the large (residues 2–13, 45–345, and 405–422) rigid regions of each subunit treated as separate TLS groups. The final model comprises 8 174 atoms, including 792 water molecules, 2 K^+ cations, 1 PO_4^{3-}, 1.5 PLP, 0.5 alanine quinonoid intermediate, 1 PEG fragment, and 3 pyridine *N*-oxide molecules. The heptameric PEG fragment was found in the cleft between the two catalytic dimers. Met1(B) could not be modeled in the electron density map. Residues Ser17(A), His79(A), Asp147(A), Lys257(A), Glu273(A), Lys328(A), Asp422(A), Met66(B), and His430(B) were modeled in two alternate conformations with occupancies of 0.5.

3.3 Structural analysis and interpretation

Differences in geometrical parameters of the compared structures were determined using LSQMAN[172] and DynDom.[173] Crystal packing contacts were analyzed by PISA.[174] The reaction intermediates were docked in the apo-TPL active sites by using the automatic settings in GOLD.[175,176] All structural figures were made using PyMol.[177]

To describe basic structural changes that produce the domain movements and the closure of the active site, two iterative analyses of error-scaled difference distance matrices of several known TPL structures was done using program ESCET.[178] The initial and preliminary analysis with standard parameters ($n_{\text{hyp}} = 20$, $w_{\text{p}} = 20.0$, $r_{\text{mut}} = 5.0$ %) and lower and upper tolerance levels of $\epsilon_{\text{l}} = 5.0$ and $\epsilon_{\text{h}} = 10.0$ included individual subunits from structures of *C. freundii* TPL apoenzyme at pH 6.0 (PDB ID: 1TPL; **1**),[3] *C. freundii* TPL complexed with 3-(4′-hydroxyphenyl)propanoic acid (HPPA), PLP, and Cs^+ ion at pH 8.0 (PDB ID: 2TPL; **2**),[4] *E. herbicola* TPL holoenzyme at pH 6.2 (PDB ID: 1C7G;

6),[86] and TPL holo- and apoenzyme structures (holo-TPL and apo-TPL) described here. The pairwise comparison for 386 Cα atoms that are present in all models showed high main-chain conformational uniformity for all subunits of 2TPL, 1C7G, and holo-TPL (Table 3.8). Besides being mutually identical, their main-chain conformations are also practically the same as that of the apo-TPL subunit B (open conformation). In order not to overweight redundant conformers, in subsequent ESCET analysis all of these subunits were represented by the apo-TPL subunit B, the conformer with the lowest mean standard uncertainty (0.10 Å). The ESCET analysis for finding the conformationally invariant regions of TPL also included the apo-TPL subunit A (closed conformation), a conformer substantially different from all others. Two subunits of 1TPL with mutually identical main-chain conformations, although different from other subunits, were excluded from the ESCET analysis for finding the conformationally invariant regions of TPL due to two reasons: (a) the main-chain fold in several protein regions was completely different from that found in other TPL structures (see Section 5.2), and (b) about 6 % of amino acid residues had poor electron density and were not modeled.

Table 3.8. The percentage of elements in the error-scaled difference distance matrix, calculated by ESCET for every pair of models, which are smaller than the threshold value of $\epsilon_1 = 5.0$. Values larger than 98.0 % are indicated in bold. The analysis is based on 386 atoms present in all analyzed models

Model and subunit	1TPL A	1TPL B	2TPL A	2TPL B	1C7G A	1C7G B	1C7G C	1C7G D	Holo-TPL A	Holo-TPL B	Apo-TPL A	Apo-TPL B
1TPL A		**100.0**	97.7	97.7	96.4	96.5	96.7	97.1	93.5	92.9	75.5	92.4
1TPL B			97.5	97.5	97.3	97.3	97.3	97.3	96.8	96.7	81.4	96.1
2TPL A				**100.0**	**100.0**	**100.0**	**100.0**	**100.0**	**100.0**	100.0	94.1	**100.0**
2TPL B					**100.0**	**100.0**	**100.0**	**100.0**	**100.0**	**100.0**	93.3	**100.0**
1C7G A						**100.0**	**100.0**	**100.0**	**100.0**	**100.0**	86.7	**99.8**
1C7G B							**100.0**	**100.0**	**100.0**	**100.0**	87.2	**99.8**
1C7G C								**100.0**	**100.0**	**100.0**	86.5	**99.8**
1C7G D									**100.0**	**100.0**	85.5	**100.0**
Holo-TPL A										**100.0**	77.7	**99.7**
Holo-TPL B											77.4	**99.8**
Apo-TPL A												78.5

4 Results

4.1 TPL holoenzyme from *C. freundii*

4.1.1 Overall structure of the TPL holoenzyme from *C. freundii*

Structure of the TPL holoenzyme from *C. freundii* was refined to an *R*-factor of 15.3 % ($R_{\text{free}} = 18.5\,\%$) at 1.9 Å resolution. It comprises two crystallographically independent subunits which constitute the catalytic dimer. A PLP molecule is bound in a deep cleft between the small and large domain of each subunit. It is noted that each subunit contributes to the active site of the neighboring subunit. The structures of the two subunits are essentially identical, with an average r.m.s. deviation between their Cα atoms of only 0.16 Å. Each catalytic dimer contains two K^+ cations, located at the interface between the two subunits. The location of the K^+ cation was confirmed by calculating anomalous difference Fourier maps using phases corresponding to the refined model. As expected for K^+, the coordinating distances are within 2.6–3.8 Å. Two catalytic dimers are related by a crystallographic 2-fold axis (denoted by P in Fig. 2.3*a*) generating the TPL tetramer (as in the structure of the holoenzyme from *C. intermedius* complexed with HPPA; Fig. 2.3*b*).[5]

4.1.2 Protein interactions with PLP and K^+

PLP is attached by its C4′ to the Lys257 side chain Nζ via a covalent linkage (Fig. 4.1; Scheme 4.1). The aldimine bond lies in a plane which is rotated 21.1° relative to

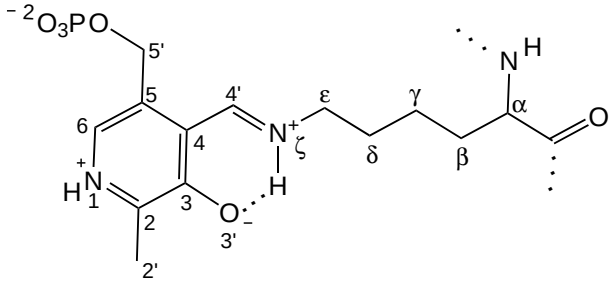

Scheme 4.1. Structural diagram of the internal aldimine with the atom-numbering scheme.

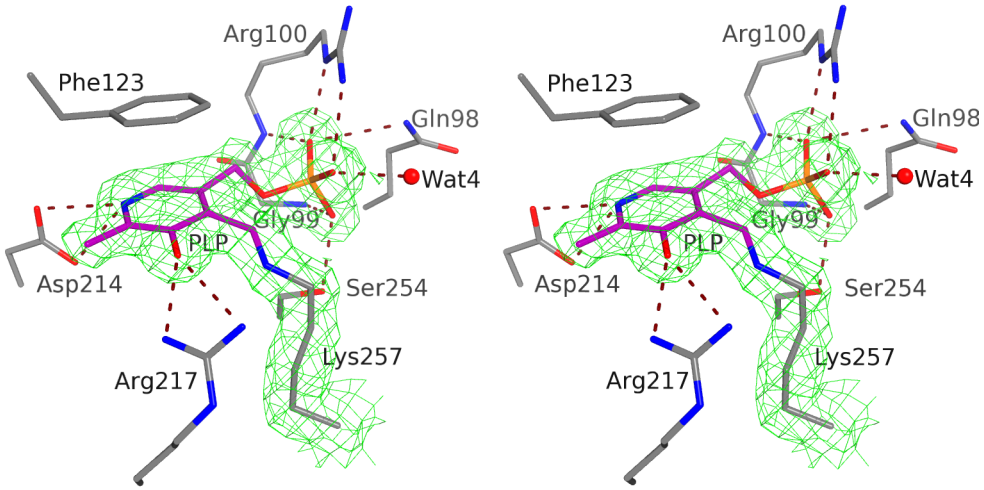

Figure 4.1. Interactions between PLP and the active site residues in the structure of holo-TPL. Hydrogen bonds are denoted by *red dashed lines*. The σ_A-weighted $2|F_o| - |F_c|$ electron density map (*green*) is contoured at the 1.0σ level.

the PLP plane. The Arg217 side chain is positioned with its guanidinium moiety next to the O3′ atom of the pyridine ring stabilizing its dehydronated state. The negative charge at O3′ in turn stabilizes the hydronated form of the imine nitrogen (NH^+) with which it forms a hydrogen-bond/salt-bridge interaction. In agreement with structural observations, spectral studies of the enzyme in the solution suggest that the TPL internal aldimine exists predominantly in the ketoenamine form with both aldimine and pyridinium nitrogen atoms hydrotonated and with the dehydronated hydroxyl group in the pH range 6.5–8.5 (Scheme 2.17).[101] The hydronated N1 nitrogen of the pyridine ring makes a salt bridge with the side-chain carboxyl oxygen of Asp214. The pyridine ring is above the Thr216 side chain, being stacked against Cγ2. From the opposite side, the pyridine ring is stacked with the side chain of Phe123 at an angle of 12° to its phenyl ring. The phosphate moiety of PLP forms hydrogen bonds with side-chain atoms of Ser254 and Gln98, the main-chain NH functions of Gly99 and Arg100, and the water molecule Wat4. In addition, the phosphate of PLP makes a salt-bridge interaction with the guanidinium group of Arg100. Similar protein–PLP interactions are observed in Trpase,[146] except for the PLP pyridine ring. Unlike TPL, where the pyridine ring is positioned between phenylalanine and threonine side chains, in Trpase it lies between the side chains of Phe132 and Ala225.

A molecule of TPL binds four potassium cations, one cation per monomer. Each cation is bound at the interface between two crystallographically related subunits stabilizing the structure of the catalytic dimer. It is coordinated by the carbonyl oxygens of Gly52 and Asn262 from one subunit and by the main-chain carbonyl oxygen and side-chain carboxyl oxygens of Glu69 from the adjacent subunit (Fig. 4.2). All of these residues belong to the large domains of protein subunits. Additionally, there are three water molecules completing the coordination sphere of K^+. One of these water molecules forms a hydrogen bond with the amino group of the active site residue Lys256. The amino group of Lys256

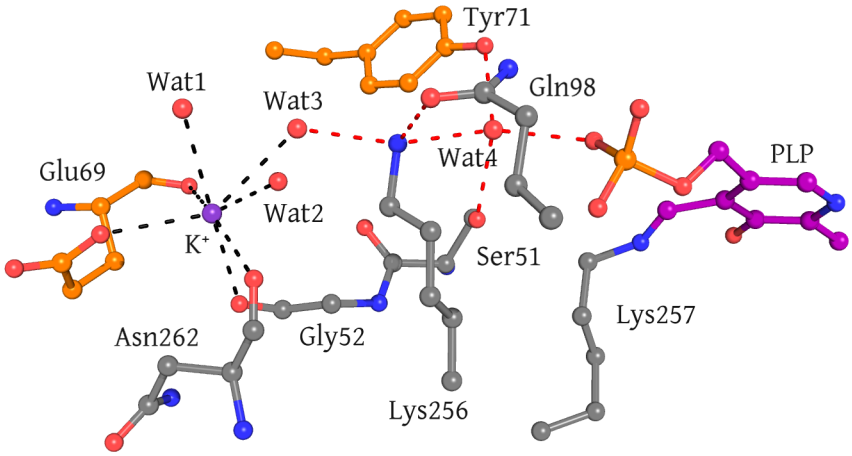

Figure 4.2. The cation-binding site and the active site residues are connected by the hydrogen-bonding interactions. Bonds with K^+ are shown as *black dashed lines*, while hydrogen bonds are indicated by *red dashed lines*. Carbon atoms of residues from the second subunit of the catalytic dimer are shown in *orange*.

makes additional hydrogen bonds with the carboxamido oxygen of Gln98, also a residue from the active site, and with another water molecule. This water molecule lies in the active site, and it is hydrogen-bonded by the PLP phosphate group and hydroxyl groups from side chains of the active site residues Ser51, Tyr71, and Tyr291 (Fig. 4.2).

4.2 D214A TPL holoenzyme from *C. freundii*

The structure of D214A TPL mutant was solved at 1.9 Å resolution. The conformations of the two crystallographically independent subunits (constituing the catalytic dimer) are very similar, with an average r.m.s. deviation between their Cα atoms of 0.30 Å. When the two crystallographically independent subunits are superimposed by the Cα atoms, the largest difference (1.1 Å) is between the positions of Asn390 which is situated in the flexible loop. Differences between the structure of D214A mutant and the wild-type TPL are more pronounced: r.m.s. deviation between their Cα atoms is 0.44 Å (Fig. 4.3). The largest difference is in the conformation of the small domain (the average r.m.s. deviation for residues 333–456 is 0.61 Å and 0.36 Å for A and B subunit, respectively) and a part of the large domain comprising the residues 108–211 (the average r.m.s. deviation is 0.56 Å and 0.44 Å for A and B subunits, respectively). The other parts have the average r.m.s. deviation of only 0.20 Å and 0.18 Å for subunits A and B, respectively.

Mutation of Asp214 to Ala prevents the hydronated N1 nitrogen atom of the PLP pyridine ring from forming a hydrogen-bond/salt-bridge interaction with the side chain of residue 214. This, in turn, changes a position and conformation of the internal aldimine and distorts the geometry of the active site (Fig. 4.4). The PLP pyridine ring is rotated around the C4–C4′ bond by ≈ 10° and moved towards Glu103 by ≈ 0.8 Å. This is accom-

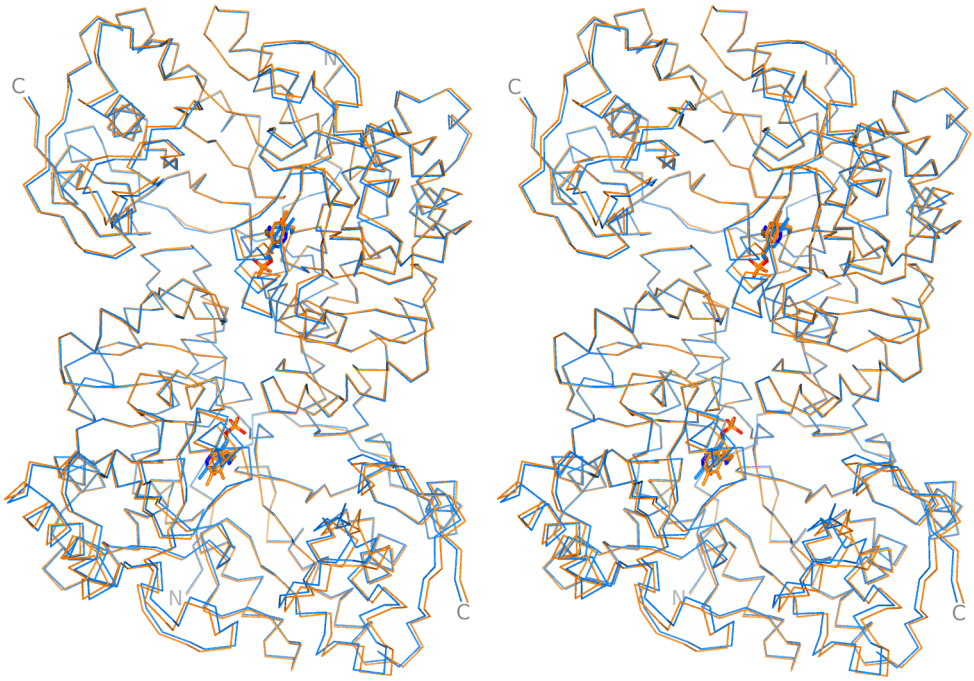

Figure 4.3. Comparison of the D214A mutant (*blue*) and wild-type (*orange*) holo-TPL catalytic dimers. Stereo view of the two structures superimposed using their Cα atoms.

panied by a conformational change in the side chain of Lys257 and formation of the more relaxed internal aldimine geometry which is additionally stabilized by the intramolecular hydrogen bond between the hydronated Lys257 Nζ and dehydronated PLP O3′ atom. New hydrogen bonds, not observed in the structure of the wild-type holoenzyme, are formed between PLP O3′ atom and the side chains of Asn185 and Thr216, and between the PLP N1 atom and the water molecule denoted as Wat2 in Fig. 4.4. Additionally, Wat2 is hydrogen bonded to the side chains of Glu103 and Thr126. The hydrogen bond between PLP O3′ atom and the side chain of Arg217, observed in the wild-type enzyme molecule, is not present in the D214A TPL structure. The most prominent changes in the active site of the D214A mutant are in the conformations of the side chains of Glu103 (χ_2 is changed by $\approx 120°$) and Asn185 (χ_1 is changed by $\approx 111°$). The side chain of Phe123 is stacked to the PLP pyridine ring at an angle of 4° and 7° in the two active sites, respectively, which is a somewhat smaller angle than in the wild-type holo-TPL (12°). Helix α4′, including the active site residues Thr124, Thr125, and Thr126, is moved slightly away from the active site. As a result of this movement, side chains of the three consecutive threonine residues are positioned 1.1–1.5 Å farther away from the PLP molecule. Despite these changes, due to the conformational adjustments of residues 108–211 and 333–456, the active site cleft as a whole is slightly more closed than in the wild-type holoenzyme.

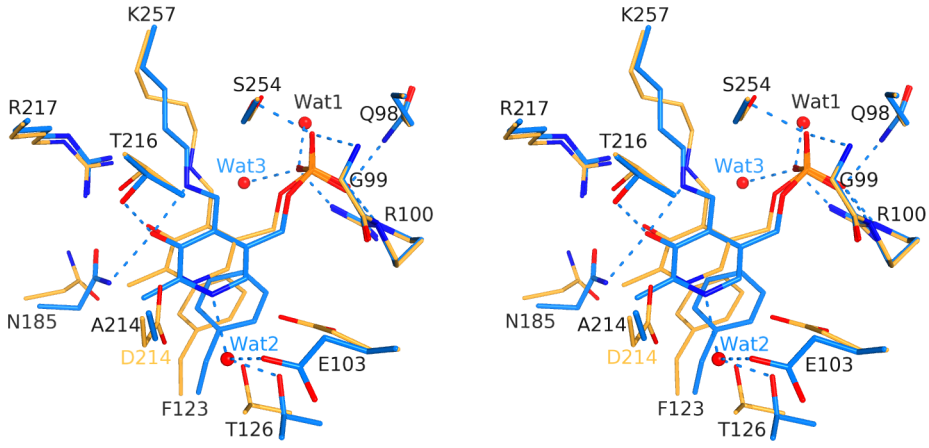

Figure 4.4. Superposition of the active site of D214A mutant (*blue*) and wild-type (*orange*) TPL (a stereo view). Hydrogen bonds in D214A TPL are shown as *dashed lines*.

4.3 TPL apoenzyme from *C. freundii* at pH 8.0

4.3.1 Overall structure of the TPL apoenzyme from *C. freundii* at pH 8.0

In contrast to the holoenzyme structure with two crystallographically independent subunits being essentially identical, two subunits in the asymmetric unit of the apoenzyme have significantly different conformations. One subunit (denoted B) has the same conformation of its main-chain atoms as the holoenzyme, which is characterized by a deep cleft between the two domains of each subunit. In the second subunit (A) protein domains have a different orientation, and the cleft is closed.

4.3.2 Two conformations of apoenzyme subunits in the asymmetric unit

The ESCET analysis[178] of the apoenzyme subunits A and B, using standard parameters and lower and upper tolerance levels of $\epsilon_l = 5.0$ and $\epsilon_h = 10.0$, detected two conformationally invariant (rigid) regions [large (residues 1–13, 45– 345, 405–422) and small (residues 19–44, 346–389, 392–404, 434–456)] and three flexible parts (residues 14–18, 390–391, 423–433) of the apoenzyme TPL subunit (Fig. 4.5). The large rigid region contains almost all of the N-terminal arm (residues 1–13), all of the large domain (residues 57–310), the domain-connecting regions (residues 49–56 and 311–332), and parts of the small domain (residues 45–48, 333–345, and 405–422). The small rigid region is composed exclusively of the residues from the small domain. Two flexible parts (residues 14–18 and 423–433) connect the large and the small rigid regions, while the third flexible part (residues 390 and 391) lies in a loop on the surface of the molecule that comprises residues with high

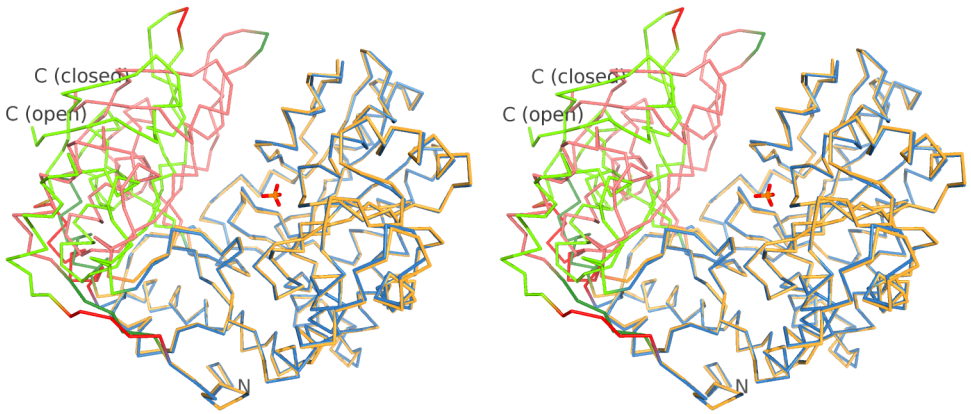

Figure 4.5. Comparison of the open and closed conformations of apo-TPL. The stereo view shows apo-TPL subunits as Cα models superimposed using large rigid regions (residues 1–13, 45–345, 405–422). The large and small rigid regions of the closed subunit are shown in *orange* and *pink*, respectively, and the flexible parts are shown in *dark green*. The large and small rigid regions of the open subunit are shown in *blue* and *pale green*, respectively, while the flexible parts are shown in *red*. The position of the active site is denoted by the phosphate anion which is bound in the same location for both active sites.

B-factors. Comparison of the open and the closed subunits superimposed by their Cα atoms from the large rigid regions (r.m.s. deviation 0.35 Å) reveals structural changes during the active site closure. The closed conformation is achieved by rotation of the small rigid region by about 16° around a hinge connecting the two rigid parts, during which the small rigid region moves toward the large one, with the far end of the small rigid region moving by about 12 Å. The main-chain torsion angles of the residues from the flexible parts, and some of those found to be at the ends of the rigid regions, change considerably upon closure. The extreme examples are Ser17 with $\triangle\varphi$ of $-74°$ and $\triangle\psi$ of $-170°$ and Met18 with $\triangle\varphi$ of $-178°$ and $\triangle\psi$ of 114° ($\triangle\varphi$ and $\triangle\psi$ are differences in the main-chain torsion angles between the closed and open subunit in the apoenzyme structure). The closed conformation of apo-TPL corresponds very well to the most closed conformation of apo-Trpase-I from *E. coli*[13] (Fig. 4.6).

The closed conformation is stabilized by several interactions between the two rigid regions, and the rigid region and the flexible part, which are not observed for the equivalent residues of the open subunit (B) nor for the holo-TPL (Table 4.1; Fig. 4.7). It is interesting to note that interactions Val16(A) O · · · Gln311(B) NE2^{i}, Ile43(A) O · · · Arg9(B) NH2^{i}, Tyr44(A) OH · · · Glu6(B) O^{i}, and Lys59(A) NZ · · · Thr15(B) OG1^{i}, with symmetry code i = $1-x, 1-y, z$, are observed in the holo-TPL (Fig. 4.8). These four interactions between two catalytic dimers of the same TPL tetramer are absent in the apo-TPL structure (Table 4.2).

Although the σ_A-weighted $2\,|F_o| - |F_c|$ electron density map[179] of the apo-TPL structure is very clear and unambiguously defines positions of all protein residues, the average

Table 4.1. Hydrogen bonds and salt bridges (between protein residues) observed in the apo-TPL and absent in the holo-TPL crystal structure

Interaction	Distance / Å	Location[a]
Arg351(A) NH1 · · · Ile336(A) O	3.18	between small and large r. r.
Arg351(A) NH1 · · · Asp348(A) OD2	2.81	in small r. r.
His355(A) NE2 · · · Glu432(A) O	2.92	between small r. r. and flexible p.
Arg404(A) NH1 · · · Asn185(A) OD1	3.19	between small and large r. r.
Tyr441(A) OH · · · Glu280(B) OE2	2.78	between small and large r. r.
Lys444(A) N · · · Glu280(B) OE1	2.78	between small and large r. r.
Gln445(A) NE2 · · · Glu280(B) O	2.97	between small and large r. r.
Phe352(B) O · · · Lys431(B) NZ	3.12	between small and large r. r.
Glu354(B) OE1 · · · Lys431(B) NZ	3.08	between small r. r. and flexible p.

[a] Abbreviations used: r. r. – rigid region(s); p. – part.

Table 4.2. Hydrogen bonds and salt bridges (between protein residues) observed in the holo-TPL and absent in the apo-TPL crystal structure

Interaction	Distance / Å	Location[a]
Val16(A) O · · · Gln311(B) NE2^{i}	3.34	between flexible p. and large r. r.
Ile43(A) O · · · Arg9(B) NH2^{i}	2.91	between small and large r. r.
Tyr44(A) OH · · · Glu6(B) O^{i}	2.66	between small and large r. r.
Lys59(A) NZ · · · Thr15(B) OG1^{i}	3.19	between flexible p. and large r. r.
Arg198(A) NH1 · · · Asp454(A) OD2^{ii}	2.97	between large and small r. r.
Arg198(A) NH2 · · · Asp454(A) OD2^{ii}	3.17	between large and small r. r.
Asn234(A) O · · · Lys26(A) NZ^{ii}	2.83	between large and small r. r.
Glu239(A) OE1 · · · Lys26(A) NZ^{ii}	2.70	between large and small r. r.
Arg351(A) NE · · · Asp359(B) OD1^{iii}	3.52	between small and small r. r.
Glu354(A) OE1 · · · Lys431(A) NZ	3.80	between small r. r. and flexible p.
Glu360(A) OE2 · · · Lys161(B) NZ^{iv}	3.31	between small and large r. r.
Lys399(A) NZ · · · His146(A) O	3.15	between small and large r. r.
Lys399(A) NZ · · · Glu354(B) O^{iii}	2.75	between small and small r. r.
Gln445(A) NE2 · · · Glu280(B) OE2	2.72	between small and large r. r.

[a] Abbreviations used: r. r. – rigid region(s); p. – part.
Symmetry codes: (i) $1-x, 1-y, z$; (ii) $x, y, 1-z$; (iii) $1/2-x, y-1/2, -z$; (iv) $1/2-x, y-1/2, 1-z$.

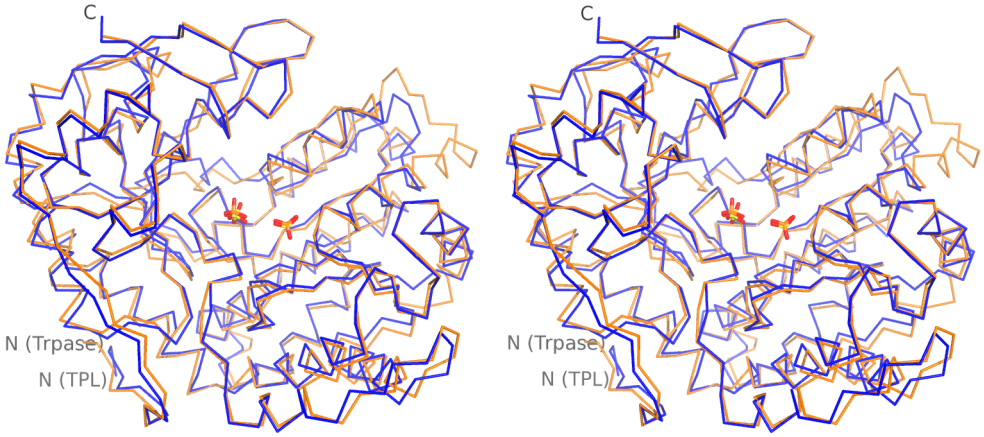

Figure 4.6. Comparison of the closed conformations of apo-TPL (*blue*) and apo-Trpase-I from *E. coli* (*orange*). Stereo view of the superimposed Cα traces. Phosphate and sulfate anions bound in the closed active sites of the two proteins are shown as *sticks*.

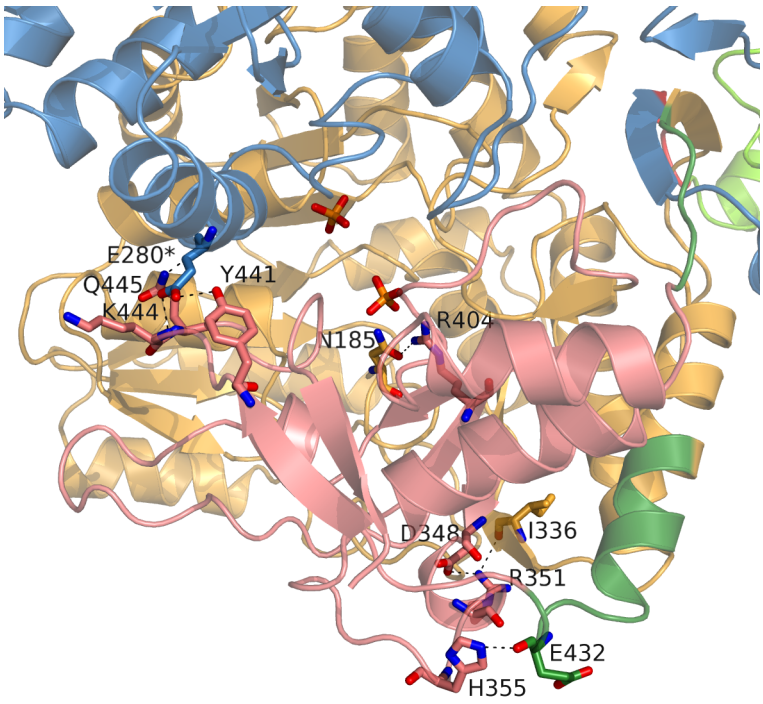

Figure 4.7. Hydrogen bonds and salt bridges in the apo-TPL tetramer that are not observed in the holo-TPL tetramer. The large and small rigid regions of the closed subunit are shown in *orange* and *pink*, respectively, and the flexible parts are shown in *dark green*. The large and small rigid regions of the open subunit are shown in *blue* and *pale green*, respectively, while the flexible parts are shown in *red*. Interactions are denoted by *dashed lines*.

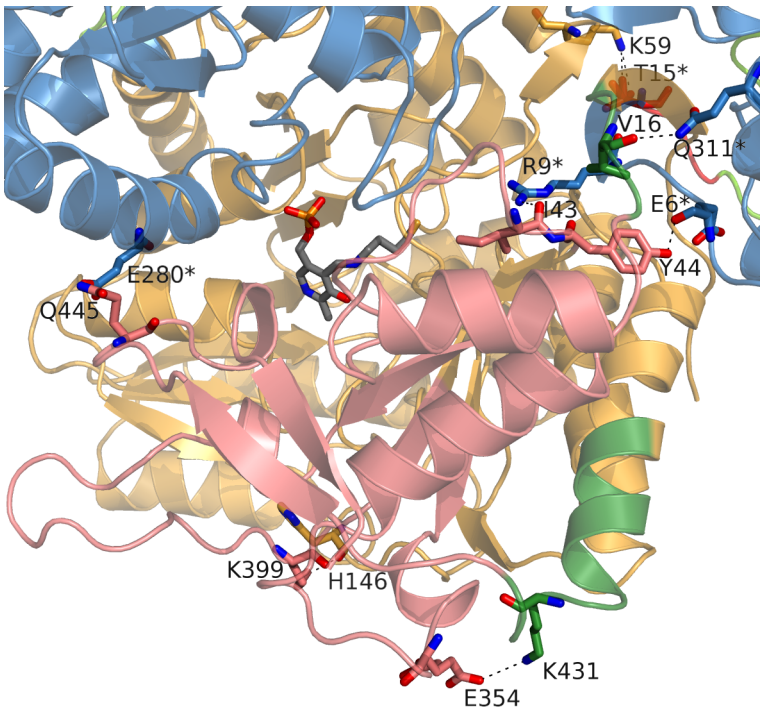

Figure 4.8. Hydrogen bonds and salt bridges in the holo-TPL tetramer that are not observed in the apo-TPL tetramer. The coloring scheme is the analogous to that in Fig. 4.7. Interactions are shown as *dashed lines*.

B-factor of the small rigid region and the flexible parts of subunit A is 39.2 Å^2, significantly higher than the Wilson *B*-factor (31.0 Å^2) and the average *B*-factor of the large rigid region of the same subunit (23.8 Å^2). Moreover, there is some residual electron density near the residues of the small rigid region and the flexible parts of subunit A. This residual electron density appears to correspond to the open conformation of subunit A. Indeed, the highest unassigned peak at 0.45 e Å^{-3} (8.7 σ) level in the σ_A-weighted $|F_o| - |F_c|$ electron density maps, situated next to the carbonyl O atom of Tyr44(A), corresponds to the carbonyl group of Tyr44(A) in the open conformation. Thus the small rigid region and the flexible parts in subunit A appear to be discretely disordered in the crystal of apo-TPL. Electron density maps suggest that the occupancy of the open conformation is low, resulting in separate unconnected peaks and preventing accurate modeling and refinement of this conformation. However, this minor (and not modeled) open conformation should be taken into account when interpreting the results of the structural analysis.

4.3.3 Open *vs* closed active site

The conformation of the open active site in the apoenzyme is almost identical to the conformation of active sites found in the holoenzyme. One phosphate anion is bound in the open active site of the TPL apoenzyme and occupies the same position as the phosphate group of PLP in the active site of the holoenzyme. Thus, all interactions found between the PLP phosphate group and the residues of the holoenzyme active site are also

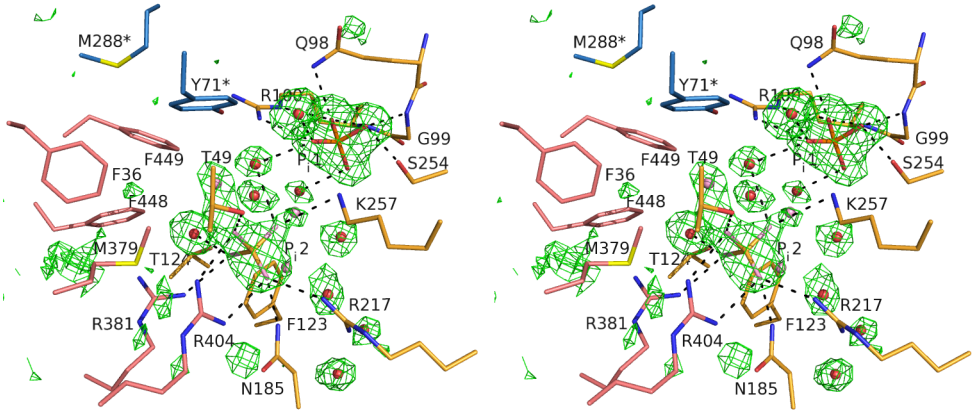

Figure 4.9. The closed active site of apo-TPL (a stereo view). Two phosphate anions (P_i1 and P_i2) and water molecules are superimposed with the corresponding σ_A-weighted $|F_o|-|F_c|$ electron density omit map (*green*) contoured at the 3.0σ level. The phosphate anion P_i2 and the water molecules modeled with the site occupancy factor of 0.5 are shown in *lighter tones*. Hydrogen bonds involving the phosphate anions are indicated by *dashed lines*. Carbon atoms of residues belonging to the large rigid region are shown in *orange*, those from the small rigid region are shown in *pink*, and the residues from the adjacent subunit are shown in *blue* and are labeled with a *star*. The residual electron density near the residues from the small rigid region corresponds to the minor, not modeled portion of the subunit A in the open conformation.

observed in both active sites of the apoenzyme. Additionally, the PO_4^{3-} in the structure of the TPL apoenzyme forms hydrogen bonds with three water molecules and a salt bridge with the side chain of Lys257. As expected, the side-chain conformation of Lys257 changes during cofactor binding and formation of the internal aldimine, as indicated by differences in χ_3 and χ_4 torsion angles of 27° and 91°, respectively. Another significant difference is in the side-chain conformation of Asn185. The carboxamide group of Asn185 in holo-TPL rotates by 90° with concomitant change of χ_1 by 25°. It is also noted that the side chain of Asp214 moves in order to form a salt bridge with the protonated N1 nitrogen of the PLP pyridine ring. Some minor differences are also observed in side-chain conformations of Met288, Phe123, and Thr124. In addition, the side chain of Thr124 in holo-TPL has been found in two alternative conformations related to each other by a rotation around the Cα–Cβ of 120°.

The closure of the active site creates one additional PO_4^{3-} anion binding site, so two PO_4^{3-} anions are modeled in the closed active site of apo-TPL. The first PO_4^{3-} is bound in the same site as in the open active site. The second PO_4^{3-} anion is hydrogen bonded to side chains of residues Thr49, Asn185, Arg217, and Lys257 form the large rigid region, and to the side chains of Arg404 and Arg381 from the small rigid region (Fig. 4.9). Since the disorder observed for the subunit A also affects the closed active site (since it is composed of residues from both the large and the small domains of subunit A), the second PO_4^{3-} anion and few water molecules in the closed active site were modeled with an arbitrary occupancy of 0.5. The two phosphate-binding sites in the closed conformation of apo-TPL

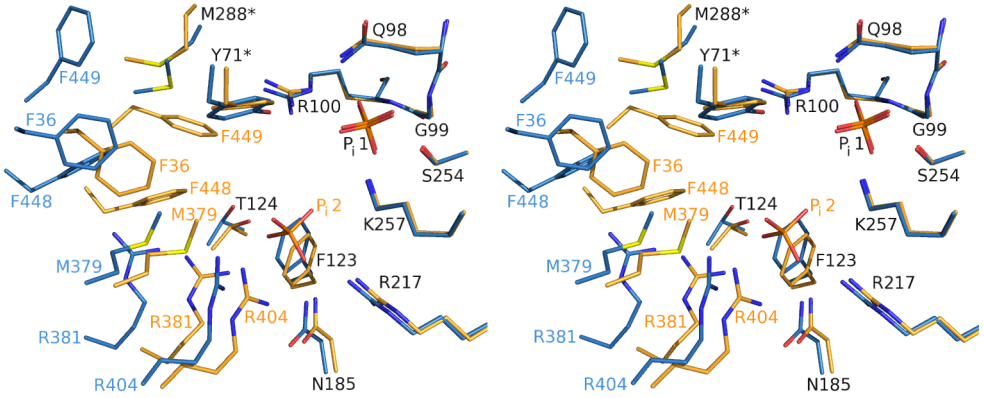

Figure 4.10. Comparison of the open and closed active sites in apo-TPL (a stereo view). Residues of the closed active site are shown in *orange*, and those of the open active site are shown in *blue*. Residues from the neighboring subunit are labeled with an *asterisk*.

are equivalent to the two sulfate-binding sites in apo-Trpase-I from *E. coli*[13] (Fig. 4.6).

The major difference between the closed and the open active sites of the TPL apoenzyme, as expected, is in the position and conformation of the residues from the small rigid region (Phe36, Met391, Arg381, Arg404, Phe448, Phe449; Fig. 4.10). Phe448 and Phe449 make the largest movement during the active site closure. Differences in the positions of their Cα atoms relative to the large rigid region in the closed and the open forms are 4.9 Å. In addition to the movement of the polypeptide chain, some differences in conformation of the side chains are also observed. The largest difference was found for the phenyl moiety of Phe449 for which χ_1 and χ_2 angles changed by 92° and 67°, respectively, so in the closed conformation it points toward the interior of the active site. Because of this, the side-chain conformations of Tyr71 and Met288 from the neighboring subunit, that of Phe36 from the small rigid region, and those of Phe123, Thr124, and Asn185 from the large rigid region have also changed. Other residues from the active site go only through minor conformational changes during the active site closure. The closed active site is not completely buried and remains accessible to the exterior solvent, although the solvent-accessible area of the residues forming the active site cleft is reduced by 240 Å^2 compared to open form (Table 4.3; Fig. 4.11).The conformation of the neighboring monovalent cation-binding site, as being formed only by residues from the large rigid regions, remains the same in both conformations.

Table 4.3. Comparison of solvent accessible surfaces (SAS) of the active-site residues in two active-site conformations in apo-TPL

Active site A (closed)		Active site B (open)		Difference
Residue	$\frac{SAS_{\mathrm{A}}}{\text{Å}^2}$	*Residue*	$\frac{SAS_{\mathrm{B}}}{\text{Å}^2}$	$\frac{SAS_{\mathrm{A}}-SAS_{\mathrm{B}}}{\text{Å}^2}$
Phe36(A)	3.7	Phe36(B)	12.6	−8.9
Thr49(A)	6.1	Thr49(B)	8.0	−1.9
Asp50(A)	0.0	Asp50(B)	0.2	−0.2
Ser51(A)	6.5	Ser51(B)	4.5	2.0
Gly52(A)	0.7	Gly52(B)	0.6	0.1
Tyr71(B)	12.5	Tyr71(A)	22.5	−10.0
Gln98(A)	3.8	Gln98(B)	4.1	−0.3
Gly99(A)	6.7	Gly99(B)	6.2	0.5
Arg100(A)	20.5	Arg100(B)	24.7	−4.2
Phe123(A)	48.1	Phe123(B)	72.4	−24.3
Thr124(A)	8.1	Thr124(B)	88.8	−80.7
Asn185(A)	14.7	Asn185(B)	23.7	−9.0
Asp214(A)	18.2	Asp214(B)	16.5	1.7
Ala215(A)	0.0	Ala215(B)	0.0	0.0
Thr216(A)	13.2	Thr216(B)	13.1	0.1
Arg217(A)	8.2	Arg217(B)	13.4	−5.2
Ser254(A)	7.0	Ser254(B)	6.6	0.4
Lys256(A)	4.9	Lys256(B)	3.8	1.1
Lys257(A)	30.5	Lys257(B)	25.3	5.2
Glu286(B)	2.3	Glu286(A)	3.3	−1.0
Met288(B)	2.8	Met288(A)	11.4	−8.6
Pro289(B)	17.2	Pro289(A)	6.3	10.9
Ser290(B)	11.7	Ser290(A)	5.2	6.5
Tyr291(B)	7.0	Tyr291(A)	7.6	−0.6
Met379(A)	7.7	Met379(B)	6.8	0.9
Glu380(A)	6.5	Glu380(B)	5.3	1.2
Arg381(A)	10.7	Arg381(B)	68.4	−57.7
Arg404(A)	4.2	Arg404(B)	20.0	−15.8
Phe448(A)	4.9	Phe448(B)	35.8	−30.9
Phe449(A)	8.9	Phe449(B)	21.5	−12.6
Total	297.3	Total	538.6	−241.3

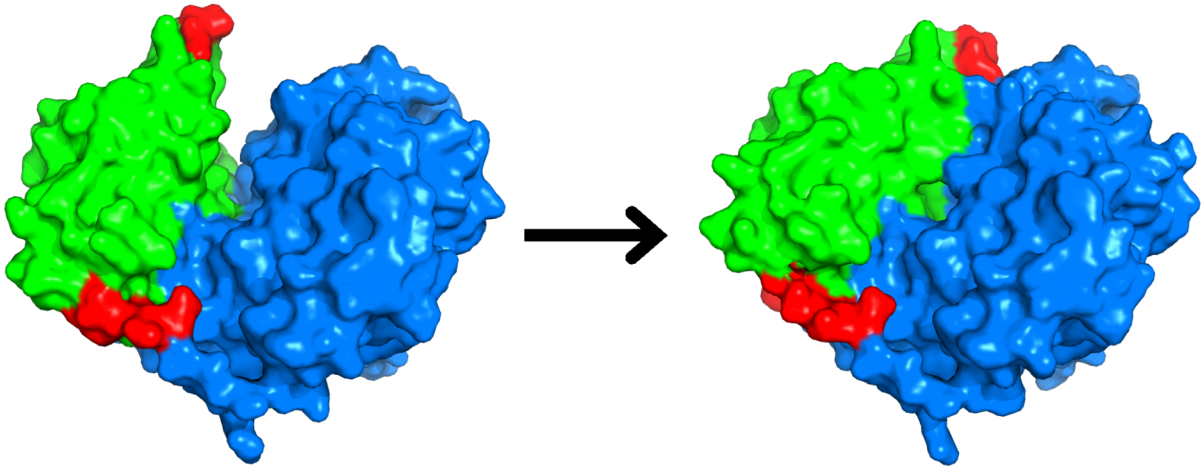

Figure 4.11. Structural transition from the open to the closed state. Molecular surfaces of the apo-TPL subunit are colored as in the open conformation in Fig. 4.5.

4.4 Discrete disorder of the whole protein domain in the TPL crystals

Structures of the TPL holoenzyme soaked with phenol and ammonium pyruvate were solved at 1.8 Å and 1.85 Å resolution, respectively. The asymmetric unit of both structures consists of two protein subunits, which form the catalytic dimer.

In the structure of TPL soaked with ammonium pyruvate there are minima in the difference σ_A-weighted $|F_o| - |F_c|$ electron density map at the putative position of K^+ cations [at $-0.18\,e\,Å^{-3}$ (-4.7σ) level for the site A, and at $-0.20\,e\,Å^{-3}$ (-5.3σ) level for the site B]. Furthermore, the *B*-factors for two K^+ cations are $41.6\,Å^2$ and $42.8\,Å^2$, which is considerably higher than the average *B*-factors of the seven coordinating oxygen atoms, $17.2\,Å^2$ and $16.5\,Å^2$, respectively. These observations suggest that the monovalent cation binding sites in TPL crystals soaked with ammonium pyruvate are partially occupied by NH_4^+ cations from the soaking solution which replaced K^+ cations present in the crystallization solution.

One of the two crystallographically independent subunits (the subunit B) in both structures is found in the open conformation with a clearly defined corresponding electron density map. The other protein subunit (A) shows a discrete disorder of the flexible part and the small rigid region. The disordered regions of subunit A are present in both closed and open conformation as clearly observed in the electron density maps (Fig. 4.12) and modeled with approximately a half occupancy of each conformation. Site occupancy factors for the closed conformation refined in SHELX[171] are 52 % and 54 % for TPL soaked with phenol and ammonium pyruvate, respectively. The remaining 48 % (46 %) of the subunits A in the crystals are in the open conformation. Several residues from subunit B and some water molecules (adjacent to the disordered region of the subunit A) are affected by the whole-domain disorder, so they were also modeled in the two different

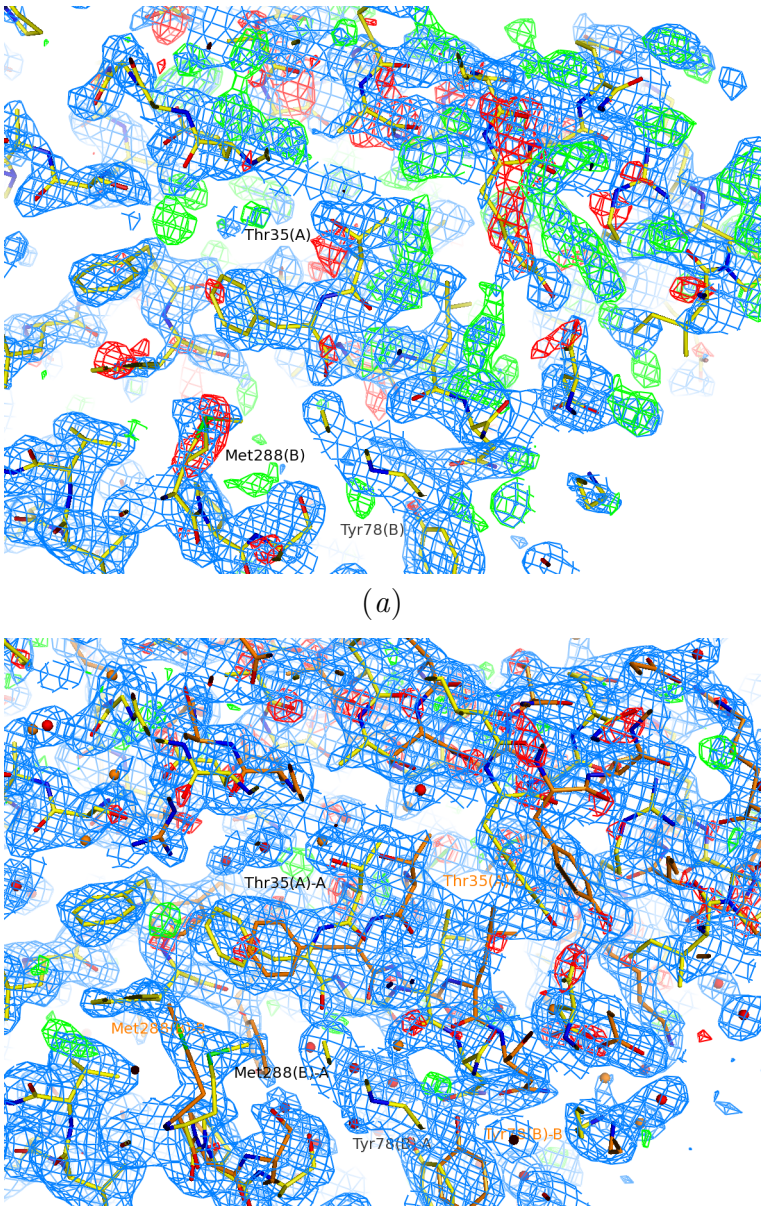

Figure 4.12. Discrete disorder of the whole domain in the crystal of TPL holoenzyme soaked with phenol. (*a*) The structural model with only the closed conformation of the disordered parts and without water molecules ($R_{\mathrm{work}} = 23.9\,\%$; $R_{\mathrm{free}} = 26.5\,\%$). The σ_{A}-weighted $2\,|F_{\mathrm{o}}| - |F_{\mathrm{c}}|$ electron density map (*blue*) is contoured at the 1.0σ level. (*b*) The final structural model ($R_{\mathrm{work}} = 15.1\,\%$; $R_{\mathrm{free}} = 17.8\,\%$) with the disordered parts modeled in two conformations: closed (*yellow*) and open (*orange*). The corresponding σ_{A}-weighted $2\,|F_{\mathrm{o}}| - |F_{\mathrm{c}}|$ electron density map (*blue*) is contoured at the 0.5σ level. The σ_{A}-weighted $|F_{\mathrm{o}}| - |F_{\mathrm{c}}|$ electron density maps in both figures are contoured at the 3.0σ (*green*) and -3.0σ (*red*) levels.

conformations with the corresponding site occupancy factors.

4.4.1 Active sites of the holo-TPL soaked with phenol

An intention of soaking the holo-TPL crystals in a phenol solution was to find specific phenol-binding sites in the TPL molecule. Such phenol-binding sites could not be detected

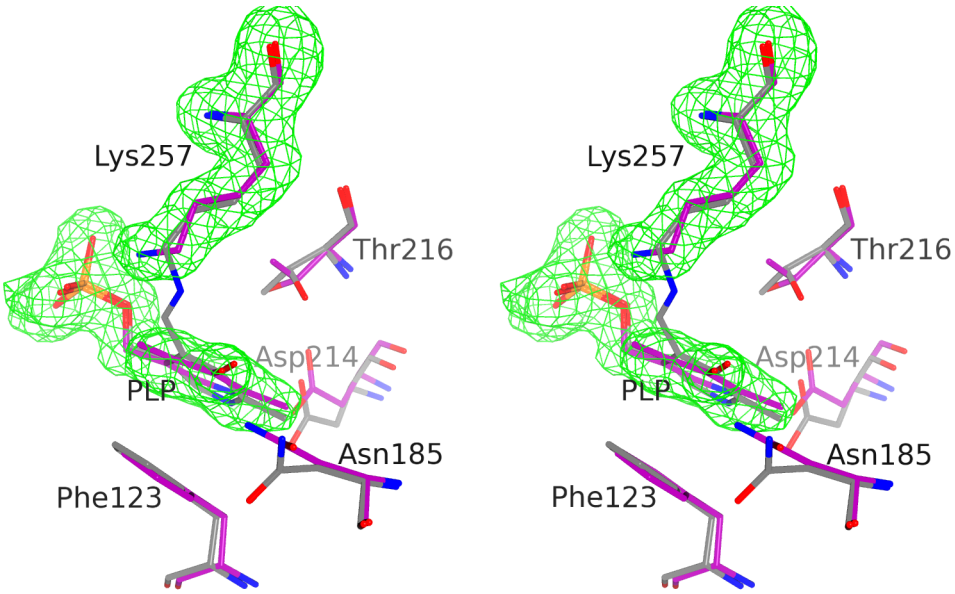

Figure 4.13. Radiation damage in active site B of TPL holoenzyme soaked with phenol (*purple*). The corresponding σ_A-weighted $|F_o| - |F_c|$ electron density omit map is colored *green*. The structure of the active site in holo-TPL (*grey*) is shown for comparison.

by analyzing the electron density maps. In addition, the electron density maps confirmed the radiation damage of the internal aldimine in both crystallographically independent active sites, which is manifested by a cleveage of the C4′–NZ bond in the PLP–Lys257 internal aldimine and the accompanied reorientation of the PLP ring (Fig. 4.13). Such radiation damage was previously observed for other PLP-dependent enzymes, even for relatively low doses of the incident X-irradiation and at temperatures as low as 100 K.[180] The high susceptibility of PLP–lysine internal aldimines to radiation damage is ascribed to a significant chemical strain on the internal aldimine bond that leads to a pronounced geometrical distortion of the PLP molecule. The strain in the internal aldimine is released by the cleavage of the aldimine bond. Active site A is also effected by the discrete disorder and is thus found in both closed and open conformations. A phosphate anion is bound in the second phosphate binding site (as found for the closed active site of the apo-TPL structure) which is formed only in the closed conformation of the disordered active site A.

4.4.2 Active sites of the holo-TPL soaked with ammonium pyruvate

Partial radiation damage of the internal aldimine molecule is observed in the ordered and open active site B of the holo-TPL soaked with ammonium pyruvate, so the PLP cofactor was modeled as being both bound (40 %) and not bound (60 %) to Lys257. The reported occupancies were refined in SHELX.[171] It is not completely clear from the corresponding electron density maps what is exactly present in the disordered active site of holo-TPL soaked with ammonium pyruvate. It is plausible that when the active site is closed (site

occupancy factor 54 %), a phosphate anion is bound in the second phosphate binding site (as in the holo-TPL soaked with phenol). The open conformation of the active site A (site occupancy factor 46 %) could be occupied by the α-aminoacrylate intermediate formed in the chemical reaction between the internal aldimine and ammonium pyruvate (Scheme 2.18).

4.5 Quinonoid intermediates of TPL formed with l-alanine and l-methionine

To prepare alanine and methionine quinonoid intermediates of TPL (Scheme 4.2), the

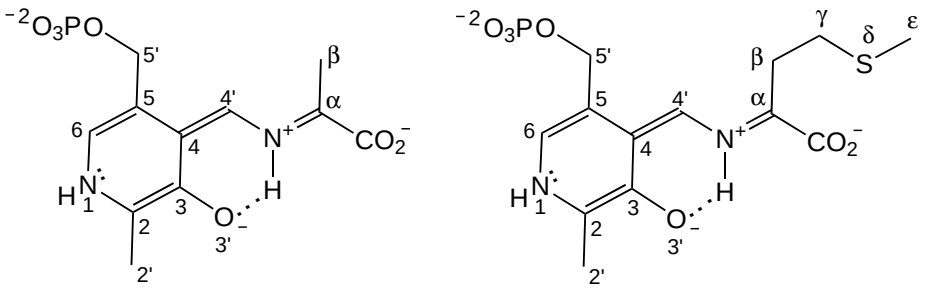

Scheme 4.2. Structural diagrams and the corresponding atom-numbering schemes of the quinonoids formed with alanine (*left*) and methionine (*right*).

competitive inhibitors of the enzyme, L-alanine ($K_i = 16\,\mathrm{mmol\,dm^{-3}}$) and L-methionine ($K_i = 0.73\,\mathrm{mmol\,dm^{-3}}$) were used.[50] The rates of the Cα hydron abstraction for the external aldimines of TPL with these amino acids are significantly higher than the rates of its return.[49] At the same time, the rates of the side half-transamination reaction for inhibitors of TPL are typically three orders of magnitude lower ($k_{cat} = 1.5 \cdot 10^{-3}\,\mathrm{s^{-1}}$ for L-alanine)[80] as compared to the rate of the Cα hydron abstraction ($k_f = 1.8\,\mathrm{s^{-1}}$ for L-alanine). As a result, when L-alanine and L-methionine are added to TPL, the quinonoid intermediates bound in the active sites are predominant and relatively stable species both in solution[50] and in the crystal.[156] These properties were used for trapping quinonoid intermediates in the crystalline form by relatively short soaking of the holoenzyme crystals in solutions containing the corresponding amino acids, followed by cryo-cooling in liquid nitrogen. Because of the significant difference in the absorption maxima of the holoenzyme and the quinonoid intermediate ($\approx$420 and $\approx$500 nm, respectively),[48,100,156,181] it was possible to monitor the formation of the quinonoid intermediate by a dramatic change in the color of crystals, which became dark yellow-red after 20–30 s of soaking. Longer soaking times (in excess of 5 minutes) led to significant deterioration of crystal quality. Structural data published here may explain why this happened: the observed dramatic conformation change upon substrate binding and formation of the quinonoid intermediate result in significant changes in intermolecular contacts within the crystal. Multiple amino

acid binding, Cα hydron abstraction and return events can take place during a longer soaking time, destabilizing crystal contacts. For the same reason and also because of the slow side transamination of L-alanine and L-methionine, it was not possible to prepare quinonoid complexes by co-crystallization.

The crystal structures of *C. freundii* TPL in the complex with L-alanine (TPL–Ala) and L-methionine (TPL–Met) were determined at 1.9 Å and 1.95 Å resolution, respectively. The electron density maps were very clear and allowed positioning of all protein residues in both structures.

4.5.1 Open and closed conformations in TPL–Ala and TPL–Met

As in the case of the holoenzyme, the asymmetric unit contains two protein subunits, which form the catalytic dimer. Unlike holo-TPL, where both active sites are found in the open conformation, in the quinonoid intermediates of both TPL–Ala and TPL–Met one subunit of the catalytic dimer (denoted by A) is found in the closed conformation while the other (B) remains in the open conformation. Positional adjustments of the small and large rigid regions, that accompany the closure of the active site during the quinonoid complex formation, result in formation of new interdomain contacts (in comparison with those present in the crystals of holoenzyme; *cf.* Tables 4.1 and 4.2). The observed main-chain conformations in both complexes are almost identical to those in the structure of apo-TPL (Fig. 4.5) with the Cα r.m.s. displacements of 0.16 Å for the closed and 0.24 Å for the open subunit of TPL–Ala (0.14 and 0.21 Å, respectively, in the TPL–Met structure). The most significant difference between structures of the apoenzyme and quinonoid complexes is in the main-chain conformation of the flexible loop covering the active site in the open subunit, residues 389–393, with the maximum Cα atom displacement of 1.5 Å for the TPL–Ala and 1.2 Å for the TPL–Met complexes.

Although the σ_A-weighted $2\,|F_o|-|F_c|$ electron density maps of the TPL–Met structure are very clear and unambiguously define positions of all protein residues, the average *B*-factor of the small rigid region and the flexible parts of subunit A (residues 14–44, 346–404 and 423–456) is 41.9 Å^2, significantly higher than the Wilson *B*-factor (27.1 Å^2) and the average *B*-factor of the large rigid region of the same subunit (28.2 Å^2). Moreover, there is some residual electron density near the residues of the small rigid region and the flexible parts of subunit A in the TPL–Met complex. This residual electron density appears to correspond to the open conformation of subunit A. Indeed, the highest unassigned peak at 0.31 e Å^{-3} (7.4 σ) level in the σ_A-weighted $|F_o| - |F_c|$ electron density maps, situated next to the CD2 atom of Tyr371(A), corresponds to the SD atom of Met28(A) in the open conformation (data not shown). Thus the small rigid region and the flexible parts in subunit A appear to be discretely disordered in the crystal of TPL–Met. Electron density maps suggest that the occupancy of the open conformation is very low, resulting

in separate unconnected peaks and preventing accurate modeling and refinement of this conformation. However, this minor (and not modeled) open conformation should be taken into account when interpreting the results of the structural analysis. Moreover, this disorder also affects one of the active sites of the TPL–Met complex, since it is composed of residues from both the large and the small domains of subunit A. In the TPL–Ala structure such disorder was not observed, but the side chains of Thr124(B), Thr216(B), Met288(B) and Phe449(B) in the open active site are found in two alternate conformations.

4.5.2 Structure of the alanine and methionine quinonoid intermediates

Previous spectroscopic studies showed that TPL forms a stable quinonoid complex in solution when incubated with L-alanine.[1,48,80,181] It was also suggested that a mixture of the external aldimine and the quinonoid intermediate is formed when L-methionine is added to TPL in a solution[50] or in crystals.[156] The main feature by which we can differentiate between the external aldimine and the quinonoid intermediates at the current resolution is the geometry around the Cα atom of the amino acid (covalently bound to the molecule of cofactor; Scheme 2.18). In the external aldimine the substrate Cα atom is sp^3 hybridized and has a tetrahedral geometry. Whereas in the quinonoid intermediate the Cα atom is sp^2 hybridized and has planar trigonal geometry (Scheme 4.2). Electron density maps clearly indicate presence of the alanine quinonoid intermediate in both active sites of the catalytic dimer (Fig. 4.14). In contrast, in the case of the TPL-Met complex, only the active site observed in the closed conformation (subunit A) is occupied by the quinonoid intermediate (Fig. 4.15). The active site of the other subunit (open conformation) contains the internal aldimine with the PLP molecule covalently bound to Lys257; its structure is essentially identical to that of the holo-TPL. As the external aldimine is not observed in either of the active sites, it is concluded that the 425 nm peak observed previously in absorption spectra of *C. freundii* TPL complexed with L-methionine in solution[50] and in the crystals[156] must be ascribed to the internal and not to the external aldimine.

The analysis of *B*-factors and difference electron density maps shows that the closed active site of TPL–Met is not fully occupied by the quinonoid intermediate. This analysis also suggests that a minor proportion of this site is occupied by the internal aldimine. Namely, the unassigned peak of $0.16\,\mathrm{e\,Å^{-3}}$ (3.8σ) in the σ_A-weighted $|F_o| - |F_c|$ electron density map[179] is situated between Lys257 Cε and PLP C4′, in the position where the Lys257 Nζ would be in the internal aldimine complex (Figs. 4.15 and 4.17). However, as in the case of the open conformation of subunit A, modeling of this intermediate was precluded due to its very low occupancy. The data suggest that the quinonoid is bound to subunit A only when the active site is in the closed conformation, while the internal aldimine (not modeled) occurs in the minor proportion of subunits that are in the open

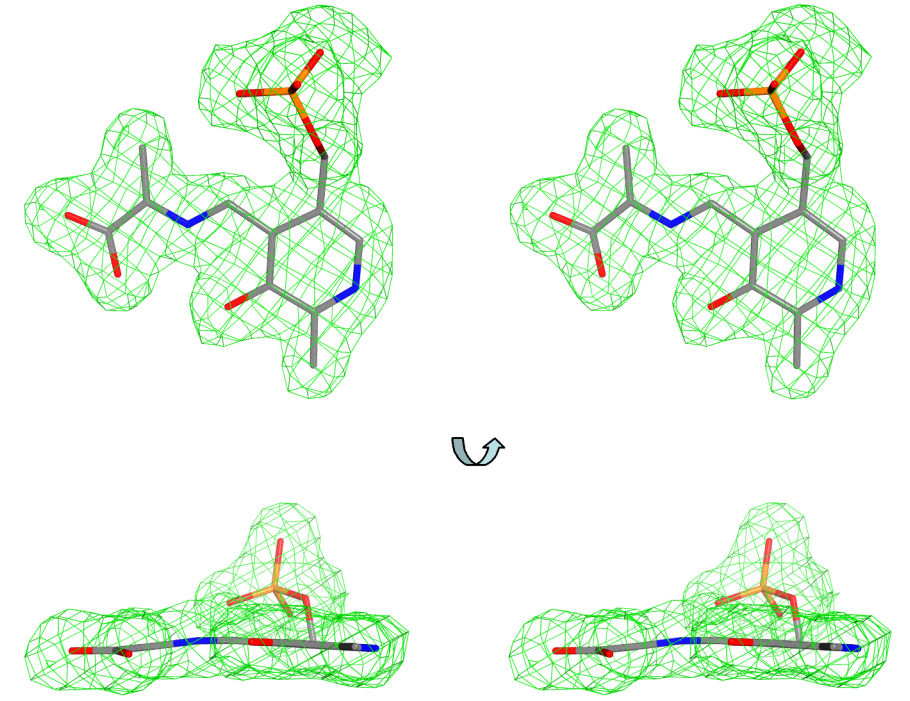

(*a*)

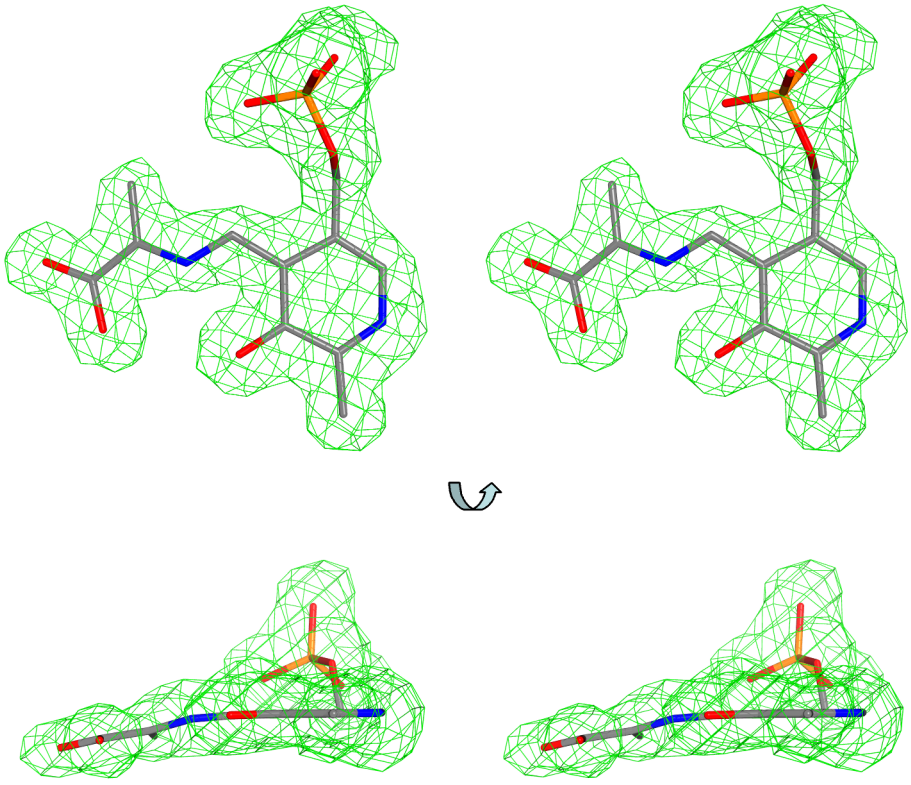

(*b*)

Figure 4.14. Alanine quinonoid intermediate in the closed (*a*) and open (*b*) active sites. Stereo views with structures of quinonoid superimposed with the corresponding σ_A-weighted $|F_o|-|F_c|$ electron density omit maps (*green*) contoured at the 3.0σ level.

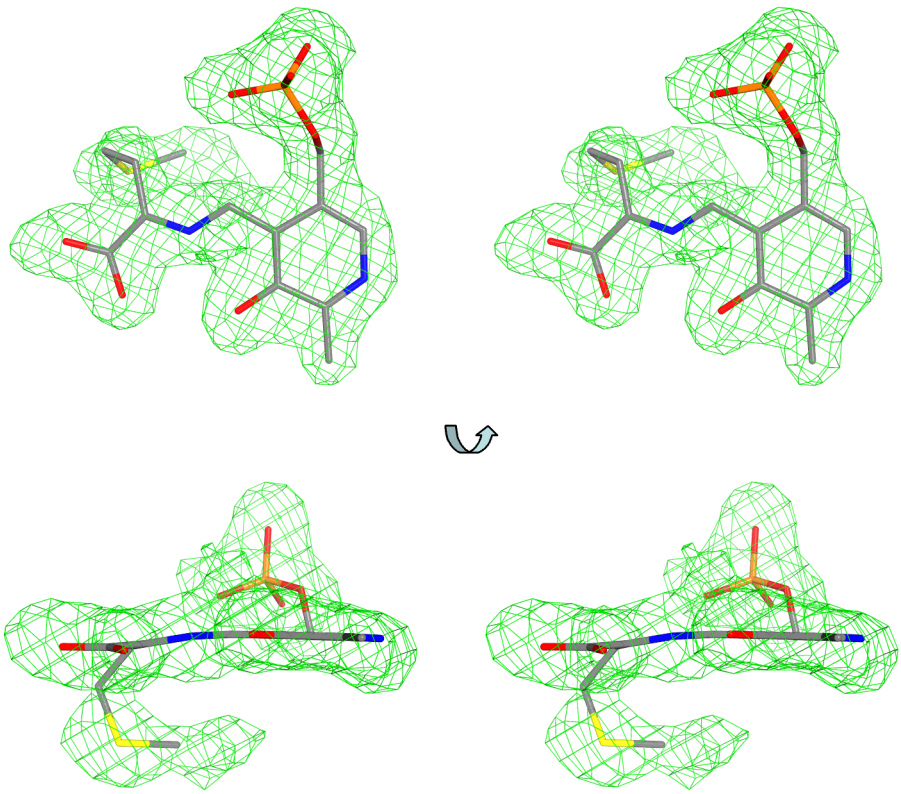

Figure 4.15. Methionine quinonoid intermediate in the closed active site. Stereo views with the quinonoid molecule superimposed with the corresponding σ_A-weighted $|F_o| - |F_c|$ electron density omit maps (*green*) contoured at the 3.0σ level.

conformation. This is further substantiated by the difference electron density observed next to the $-SCH_3$ moiety of the methionine quinonoid (Figs. 4.15 and 4.17), which could be ascribed to the conformation of Phe123 in a minor proportion of the internal aldimine.

The pyridoxal ring and the "alanine moiety", comprising atoms N, Cα, Cβ, and those of the carboxylic group, in the quinonoid molecules are almost coplanar (Figs. 4.14 and 4.15). The angle between planes of the pyridoxal ring and the "alanine moiety" (excluding oxygen atoms) is only 10° in the closed conformations of both TPL–Ala and TPL–Met complexes and 13° in the open active site of TPL–Ala complex. The carboxylate group is rotated with respect to the rest of the "alanine moiety" by 7° and 8° in the closed and open active sites of TPL–Ala, respectively. In TPL–Met this rotation amounts to 9°. Thus the interplanar angles are small and not significantly different in the different active sites. Such small angles between the planar moieties indicate that the electrons are highly delocalized along the system of conjugated double bonds in the quinonoid molecules.

4.5.3 Protein interactions with the quinonoid molecules formed with alanine and methionine

The ε-amino group of Lys257 is found on the *re* side of the quinonoid molecule at distances of 3.8 and 3.7 Å, respectively, from the Cα atom of the quinonoid in the closed and open

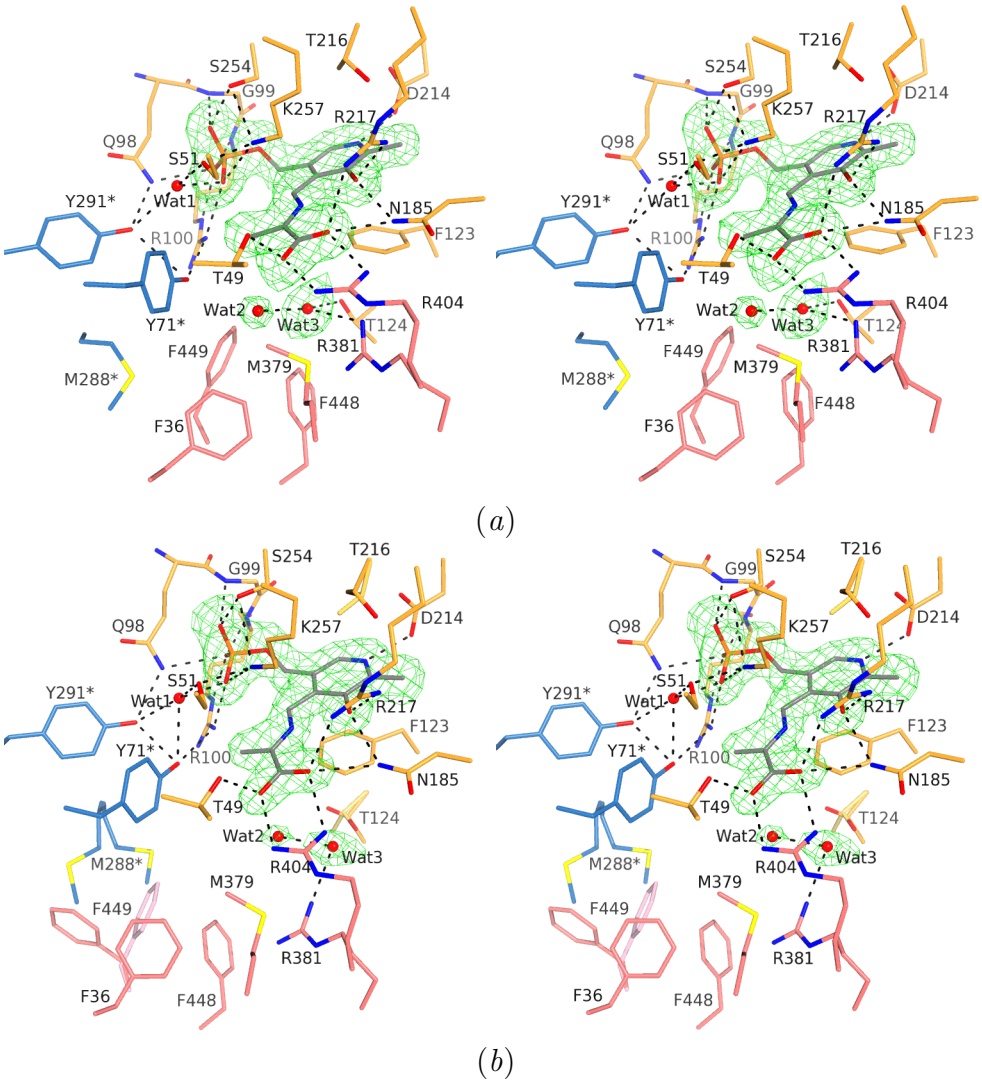

Figure 4.16. Enzyme interactions with the alanine quinonoid intermediate in the closed (*a*) and open (*b*) active sites. Stereo views with structures of quinonoid and two water molecules superimposed with the corresponding weighted $|F_o| - |F_c|$ electron density omit maps (*green*) contoured at the 3.0σ level. Hydrogen bonds are denoted by *dashed lines*. Carbon atoms of residues belonging to the large rigid region are shown in *orange*, those from the small rigid region are shown in *pink*, and the residues from the neighboring subunit are shown in *blue* and labeled with a *star*. The alternate conformations of Thr124, Thr216, Met288, and Phe449 in the open conformation are shown in corresponding *pale tones*.

active site conformations of TPL–Ala (Fig. 4.16). The distance between these two groups is very similar (3.7 Å) in the TPL–Met complex (Fig. 4.17). Thus the experimental data demonstrate that Lys257 is situated on the appropriate side of the bound substrate and, moreover, its ε-amino group is closest to the Cα atom of the quinonoid intermediate (and can come even closer by rotation around the Cδ–Cε bond). In TPL–Ala the closest entity to the Cα atom at the *si* side of the quinonoid is a water molecule (Wat2) found at a distance of 3.8 Å in the closed active site and 4.0 Å in the open one (Fig. 4.16). Wat2 is hydrogen-bonded to another water molecule (Wat3), which is situated at distances of 4.2 and 5.2 Å from the quinonoid Cα atom in the closed and open active sites, respectively.

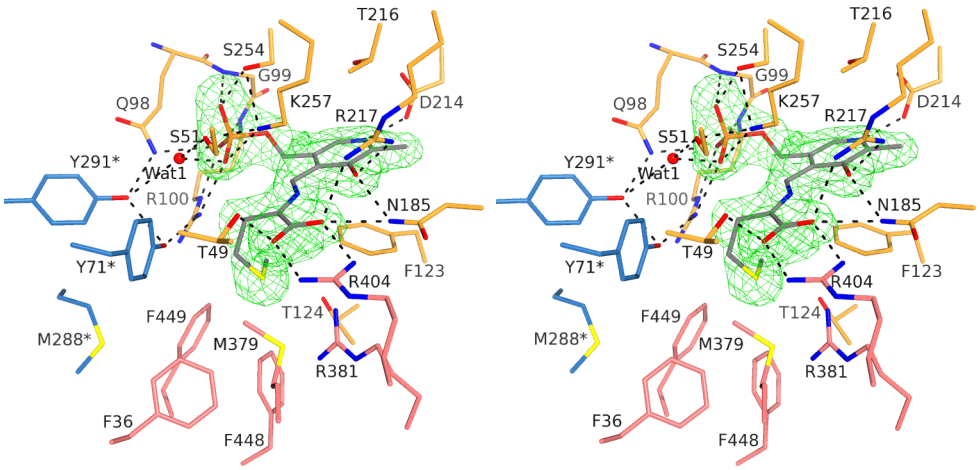

Figure 4.17. Enzyme interactions with the methionine quinonoid intermediate in the closed active site. Stereo view with the quinonoid molecule superimposed with the corresponding weighted $|F_o| - |F_c|$ electron density omit map (*green*) is contoured at the 3.0σ level. Carbon atoms of residues belonging to the large rigid region are shown in *orange*, those from the small rigid region are shown in *pink*, and the residues from the neighboring subunit are shown in *blue* and labeled with a *star*. Hydrogen bonds are denoted by *dashed lines*.

In the closed active site Wat3 is hydrogen-bonded with the Thr124 hydroxyl and with the Arg381 guanidinium group (Fig. 4.16*a*), but in the open active site the only protein residue to which Wat3 hydrogen-bonds is Arg381 (Fig. 4.16*b*). Wat2 is found farther from the Arg381 guanidinium group: at distances of 4.5 and 3.5 Å in the closed and the open active sites, respectively.

As expected, there are no water molecules at the *si* face of the quinonoid intermediate in TPL–Met. Instead, this space is occupied by the side chain of methionine which is situated in a relatively hydrophobic environment formed by the residues Phe36, Phe123, Phe448, Phe449, and Met379 (Fig. 4.17). The closest to its sulfur atom are the Cζ atom of Phe449 (at 3.7 Å) and the Nη1 atom of Arg381 (at 3.7 Å); interestingly Arg100, a residue which was proposed to be essential for the stabilization of the methionine quinonoid intermediate,[81] is found farther away with its closest atom (Nη2) positioned at a distance of 4.7 Å. The hydroxyl of Tyr71 from the adjacent subunit of the catalytic dimer is the closest protein group to the methionine Cγ positioned at a distance of 3.4 Å.

In all active sites occupied by the quinonoid intermediate, in both TPL–Ala and TPL–Met, the phenolic hydroxyl group of Tyr71 and the ε-amino group of Lys257 are connected by a network of hydrogen bonding interactions passing through the hydroxyl group of Tyr291, the water molecule Wat1, the amide group of Gln98, the phosphate group of PLP, the guanidinium group of Arg100 and the hydroxyl groups of Ser51 and Ser254 (Figs. 4.16 and 4.17). These interactions are critical for maintaining the conformation of Lys257 and Tyr71 side chains in the active site and define the potential route for the observed hydron transfer between the Cα and Cγ atoms of the substrate.[182]

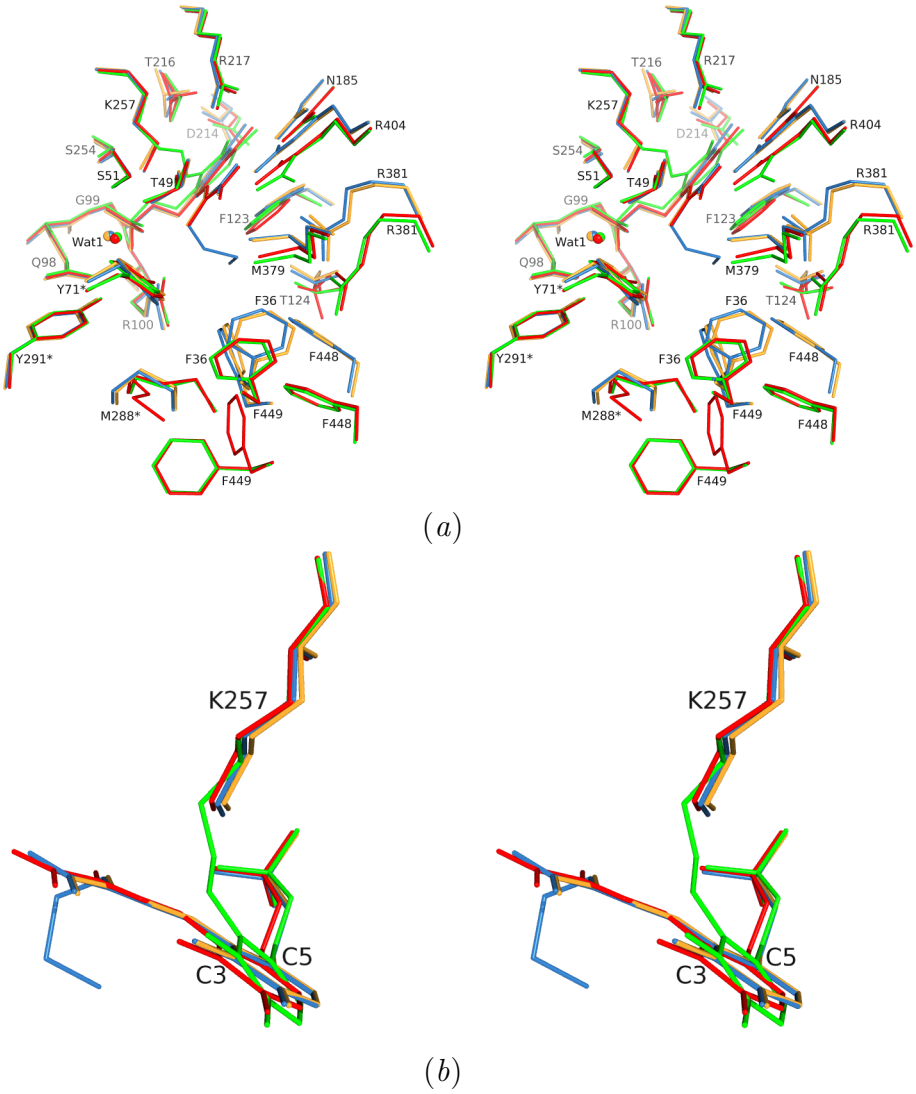

Figure 4.18. Comparisons of (*a*) the active sites and (*b*) the quinonoid intermediates with the internal aldimine. Stereo views with the following color scheme: TPL–Ala closed – *orange*; TPL–Ala open – *red*; TPL–Met closed – *blue*; TPL–Met open – *green*. The structures are superimposed using Cα atoms of the large rigid regions from each subunit.

4.5.4 Structural rearrangements in the active sites of alanine and methionine quinonoid complexes

All non-covalent interactions between the PLP and the active site residues observed for the internal aldimine are preserved in the quinonoid complexes. On the formation of the external aldimine the bond between Lys257 Nζ and PLP C4′ is cleaved, and a new aldimine bond between an amino acid and PLP is formed. During this transition the pyridoxal ring has to be reoriented, as predicted[183] and later confirmed by the X-ray analysis of the aspartate aminotransferase.[89] Indeed, while the PLP phosphate group in the quinonoid intermediates of TPL stays in essentially the same position as in the internal aldimine, the pyridoxal ring is rotated by 20° around an imaginary axis passing approximately through its C3 and C5 atoms (Fig. 4.18). As a result, the C4′ atom of PLP is moved from

Lys257 by ≈1.1 Å in comparison with its position in the internal aldimine. The ε-amino group of Lys257 in the quinonoid intermediates assumes a more relaxed, antiperiplanar conformation achieved by −98° rotation around the χ_4 torsion angle, resulting in its movement toward the PLP phosphate group and formation of hydrogen bonds with PLP phosphate and the side chain hydroxyls of Ser254 and Ser51. In addition to the salt bridge between the dehydronated hydroxyl of PLP (O3′) and the side chain of Arg217 observed in the internal aldimine, in the quinonoid intermediates the PLP O3′ atom makes a hydrogen bond with the side chain amide of Asn185 (Figs. 4.16 and 4.17).

The carboxylate group of each quinonoid intermediate forms several interactions with the active site residues, including a salt bridge with the guanidinium group of Arg404 and a hydrogen bond with the hydroxyl of Thr49 (Figs. 4.16 and 4.17). Similar interactions with Thr49 and Arg404 have been observed for the substrate analog 3-(4′-hydroxyphenyl)propanoate (HPPA) bound to *C. freundii* TPL[4] and also for a quasisubstrate *N*-(5′-phosphopyridoxyl)-L-tyrosine (PPT) in complex with the *E. herbicola* TPL.[5] Because the complex of TPL with HPPA resembles a Michaelis complex and the complex with PPT models the external aldimine, it appears that these interactions persist during the catalysis, from binding of the substrate to the formation of the quinonoid intermediate. The guanidinium group of Arg217 and the amide of Asn185 bridge one of the substrate carboxylate oxygen atoms with the O3′ atom of PLP through hydrogen-bonding and salt-bridge interactions (Figs. 4.16 and 4.17). Such bridging interactions are absent in the complex of TPL with HPPA where the substrate analog is farther away and is not covalently bound to PLP. In this complex the guanidinium group of Arg217 is hydrogen-bonded only to the O3′ atom of PLP, while no interactions of either O3′ or the carboxylate group with Asn185 were observed. In the complex with PPT, the side chain of Arg217 salt bridges the O3′ atom and the carboxylate group, but Asn185 forms a hydrogen bond only with the O3′ suggesting that the hydrogen bond with the substrate carboxylate group forms along with the quinonoid intermediate formation.

4.6 Complexes of F448H and Y71F TPL mutants with 3-fluoro-l-tyrosine

C. freundii F448H and Y71F TPL mutants lack the β-elimination activity with L-tyrosine or 3-fluoro-L-tyrosine as a substrate; instead, they accumulate stable quinonoid intermediates when incubated in the solution of either of these two amino acids.[15,52,156,184] This property was used to prepare the quinonoid complexes by soaking the crystals of the mutated holoenzymes with 3-fluoro-L-tyrosine (Scheme 4.3) followed by cryo-cooling in liquid nitrogen. 3-Fluoro-L-tyrosine was used for preparation of quinonoid intermediates because it is more than 5 times more soluble in the soaking solution than the physiological substrate L-tyrosine.[156] Nevertheless, the kinetic properties of 3-fluoro-L-tyrosine and

L-tyrosine were shown to be very similar.[15,49,52,184]

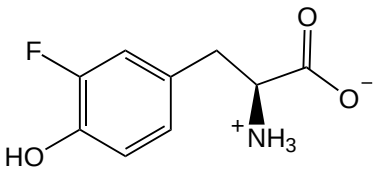

Scheme 4.3. Structural diagram of 3-fluoro-L-tyrosine.

4.6.1 Open active site of the Y71F TPL complex comprises the quinonoid molecule

The asymmetric unit of the quinonoid intermediate of *C. freundii* Y71F TPL formed with 3-fluoro-L-tyrosine is composed of the catalytic dimer with two corresponding active sites. One crystallographically independent subunit (B) is found in the open conformation. The corresponding open active site is occupied by the 3-fluoro-L-tyrosine quinonoid molecule (λ_{max} = 502 nm)[156] formed after the Cα-hydron abstraction from the external aldimine of 3-fluoro-L-tyrosine (Fig. 4.19; Scheme 4.4). The quinonoid geometry is characterized

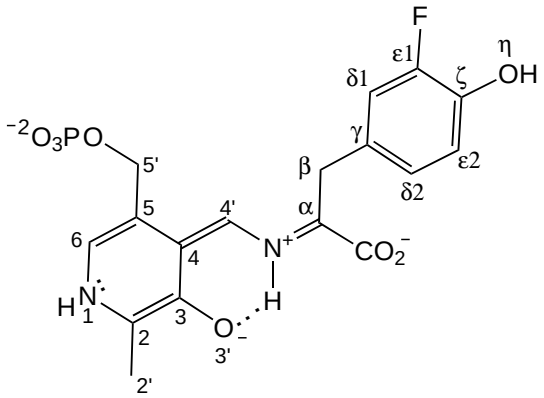

Scheme 4.4. Structural diagram and the corresponding atom-numbering scheme of the quinonoid intermediate formed with 3-fluoro-L-tyrosine.

by the sp^2-hybridized Cα atom in trigonal planar environment and the phenolic moiety rotated with respect to the Cα–Cβ bond (a torsion angle Cα–Cβ–Cγ–Cδ1) by 72°.

All hydrogen bonds and salt bridges between the ligand and the active-site residues observed for the quinonoid intermediates formed with L-alanine or L-methionine are also found in the open active site of 3-fluoro-L-tyrosine quinonoid (Fig. 4.20). Additionally, the 3-fluoro-L-tyrosine quinonoid hydroxyl group forms hydrogen bonds with two water molecules, while the fluoro group is hydrogen bonded to Arg381 NH1 and a water molecule. The substrate's hydroxyl group is positioned at 4.1 Å from the hydroxyl group of Thr124 and at 4.8 Å from the closest guanidino atom of Arg381. Distance between the ε-amino group of Lys257 and the Cα atom of the quinonoid molecule is 4.1 Å. The phenyl ring

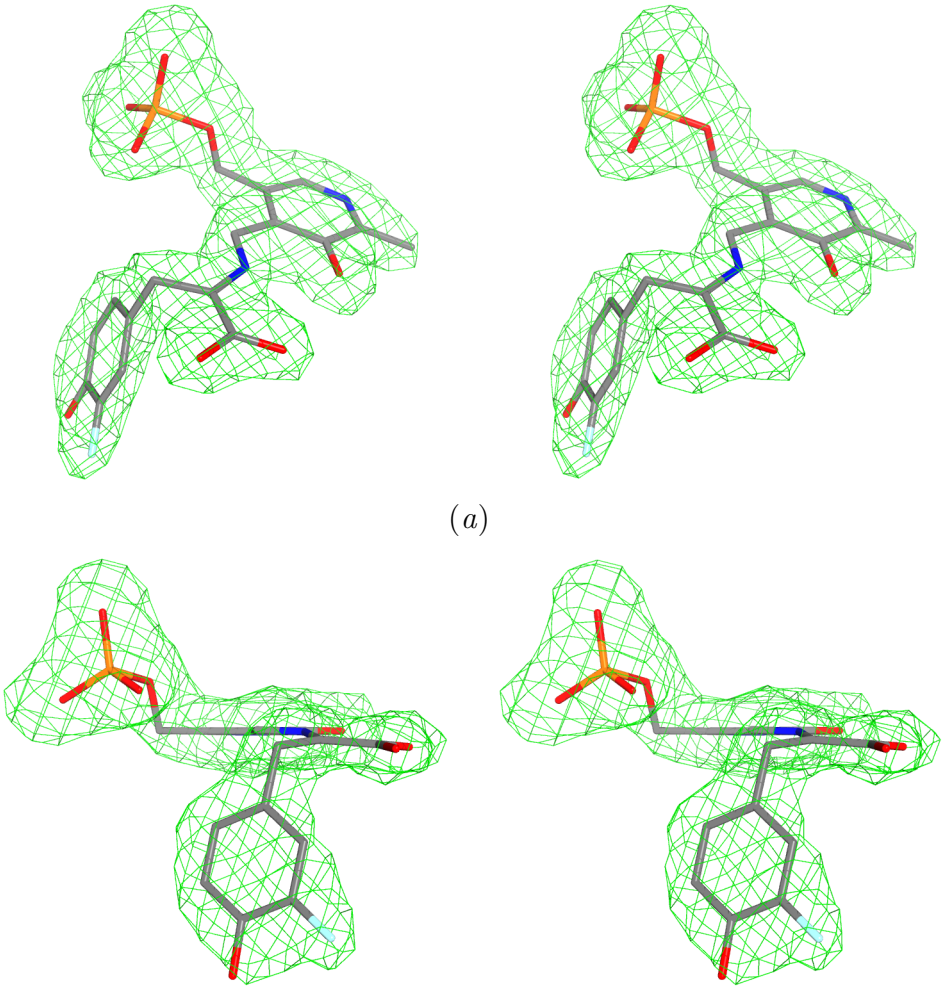

(*a*)

(*b*)

Figure 4.19. 3-Fluoro-tyrosine quinonoid molecule in the open active site of Y71F TPL. Stereo views with the quinonoid molecule superimposed with the corresponding σ_A-weighted $|F_o| - |F_c|$ electron density omit map (*green*) contoured at the 3.0σ level.

of Phe71, in comparison with that of Tyr71 in the wild-type holo-TPL, is shifted (by 1.5 Å for the CZ atoms of residue 71) towards the hydrophobic environment generated by residues Phe36, Leu48, Met288, Met379, Phe448, and Phe449. Since there is no strain on the quinonoid molecule induced by the active-site residues in the open conformation, this quinonoid geometry is referred to as the "relaxed" state.

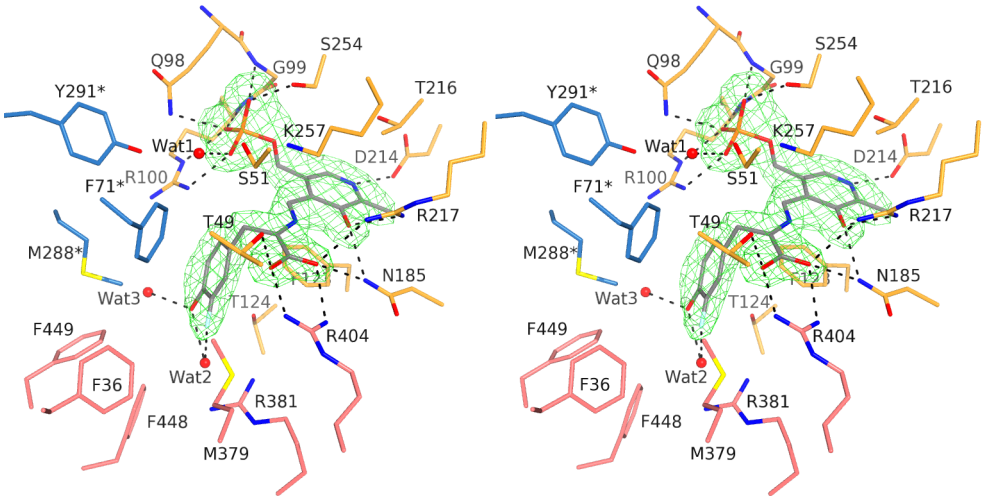

Figure 4.20. Enzyme interactions with the 3-fluoro-tyrosine quinonoid intermediate in the open active site. Stereo view with the quinonoid molecule superimposed with the corresponding σ_A-weighted $|F_o|-|F_c|$ electron density omit map (*green*) contoured at 3.0σ level. Carbon atoms of residues belonging to the large rigid region are shown in *orange*, those from the small region are shown in *pink*, and the residues from the neighboring subunit are shown in *blue* and labeled with a *star*. Hydrogen bonds are denoted by *dashed lines*.

4.6.2 Disordered active site of the Y71F TPL complex comprises either the quinonoid or the external aldimine molecule

The other protein subunit (A) of the Y71F TPL complex with 3-fluoro-L-tyrosine is found in the closed conformation. As in structures of the apoenzyme and the methionine quinonoid intermediate, the residual electron density suggests that the subunit A is discretely disordered in the analyzed crystal, with a minor portion of subunits A found in the open conformation. Due to the unconnected peaks in the electron density maps and the low occupancy, it was not possible to model the open conformation of subunit A.

The observed disorder also affects the corresponding active site (A): the electron density indicates that at least two different chemical species are bound in the active site A (Fig. 4.21). Minor proportion of the active sites A is occupied by the quinonoid molecules (modeled with the estimated site occupancy factor of 0.33) with the same geometry as found in the open active site B. The quinonoid molecule with such ("relaxed") geometry cannot exist in the closed active site: if it existed, there would be a significant steric clash between the phenol moiety and the side chains of Phe448 and Phe449 with distances between non-hydrogen atoms as short as 1.9 Å. Consequentially, the (major) closed conformation of the active site A is presumably occupied by the external aldimine molecule formed in the reaction of 3-fluoro-L-tyrosine and the internal aldimine. Spectroscopic studies confirmed the existence of the external aldimine intermediate ($\lambda_{max} = 400\,nm$) (along with the quinonoid intermediate) in the Y71F TPL crystals suspended in solution with a lower concentration of 3-fluoro-L-tyrosine (less than $20\,mmol\,dm^{-3}$).[156] The partial

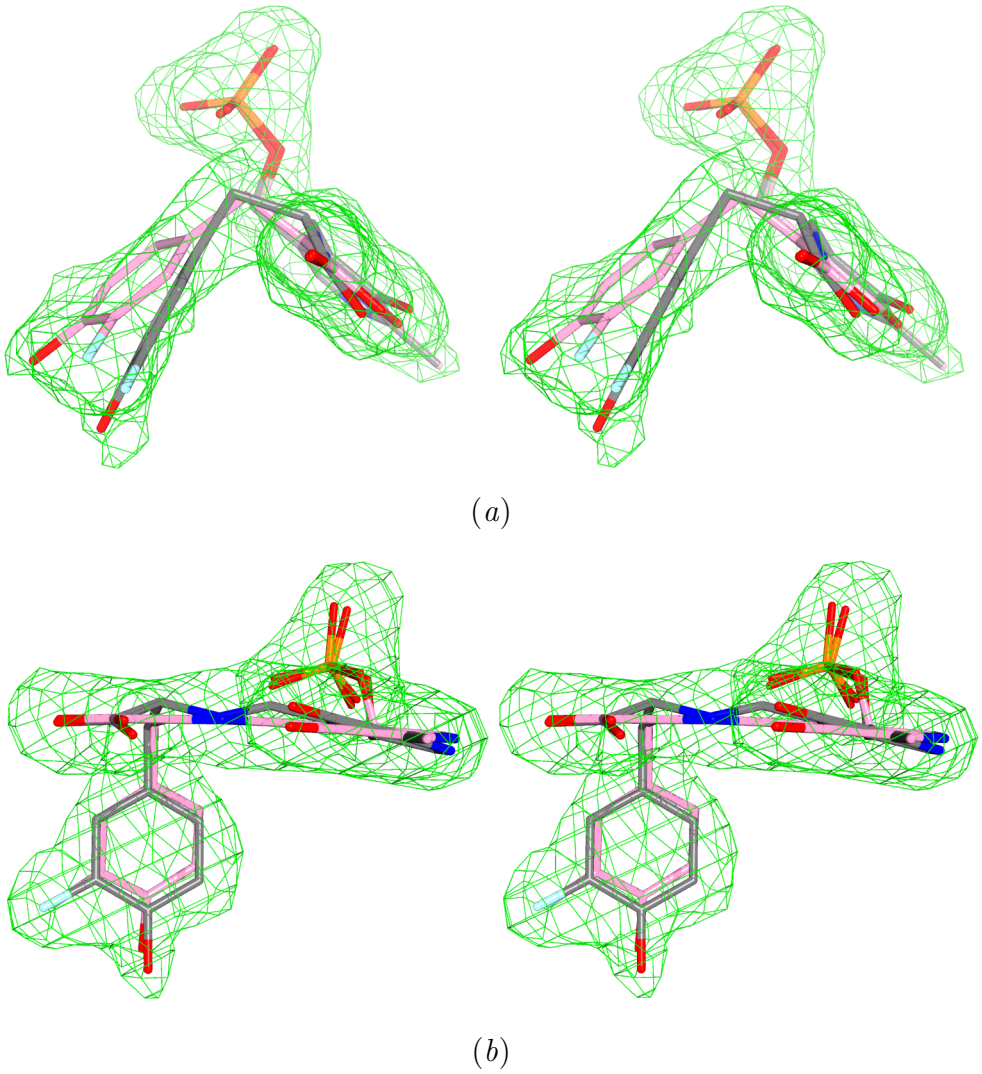

Figure 4.21. Ligands modeled in the disordered active site of Y71F TPL. Stereo views with the quinonoid (*pink*) and the external aldimine (*grey*) molecules superimposed with the corresponding σ_A-weighted $|F_o| - |F_c|$ electron density omit map (*green*) contoured at the 3.0σ level.

disorder in the active site A made the ligand modeling and characterization less straightforward. It is also possible that the third, unidentified chemical species also populates the disordered active site A, *e.g.* the quinonoid molecule with a conformation different to that in the open active site (*cf.* the structure of F448H TPL in complex with 3-fluoro-L-tyrosine).

As for the open active site, all hydrogen bonds and salt bridges found for the methionine and alanine quinonoids are also found in the closed active site occupied by the 3-fluoro-L-tyrosine external aldimine (Fig. 4.22). In addition, the substrate hydroxyl group forms hydrogen bonds with the hydroxyl group of Thr124 and the guanidine group of Arg381. As in the open active site, Arg381 is also hydrogen bonded to the ligand's fluoro group. The phenyl ring and the phenol group of the substrate in the closed active site are in the van der Waals contacts with the side chain of Phe448 (with the shortest distance of 2.8 Å), respectively. In both open and closed conformations, Arg381 is part of a triad

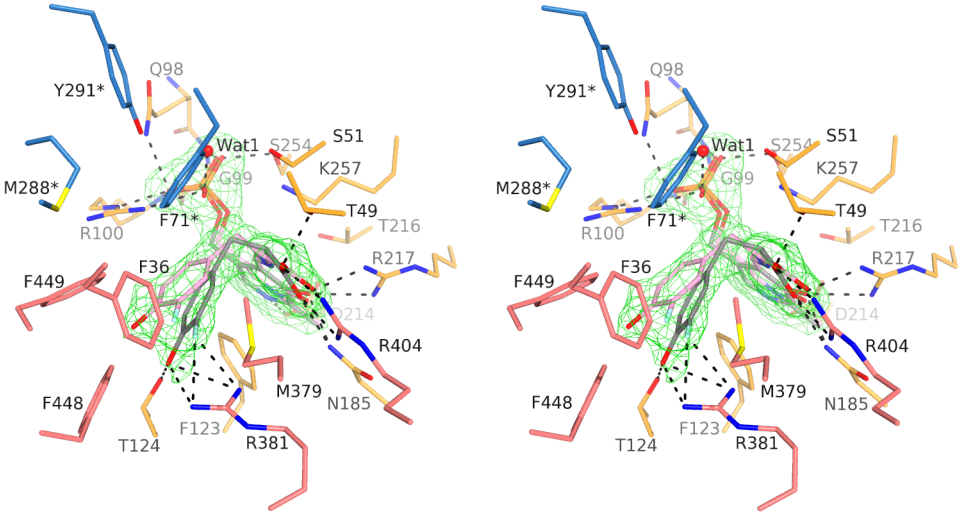

Figure 4.22. Enzyme interactions with the 3-fluoro-L-tyrosine external aldimine molecule in the disordered active site of Y71F TPL. Stereo view with the external aldimine (*grey*) and the quinonoid molecules (*pink*) superimposed with the corresponding σ_A-weighted $|F_o| - |F_c|$ electron density omit map (*green*) contoured at the 3.0σ level. Carbon atoms of residues belonging to the large rigid region are shown in *orange*, those from the small region are shown in *pink*, and the residues from the neighboring subunit are shown in *blue* and labeled with a *star*. Hydrogen bonds are denoted by *dashed lines*.

of hydrogen-bonded residues involving the guanidine of Arg381, the hydroxyl of Ser385 and carboxyl group of Glu380 (Fig. 4.23). ε-Amino group of Lys257 is at a distance of 3.5 Å from Cα atom of the external aldimine molecule in the closed conformation, and 3.8 Å from Cα atom of the quinonoid molecule in the open conformation.

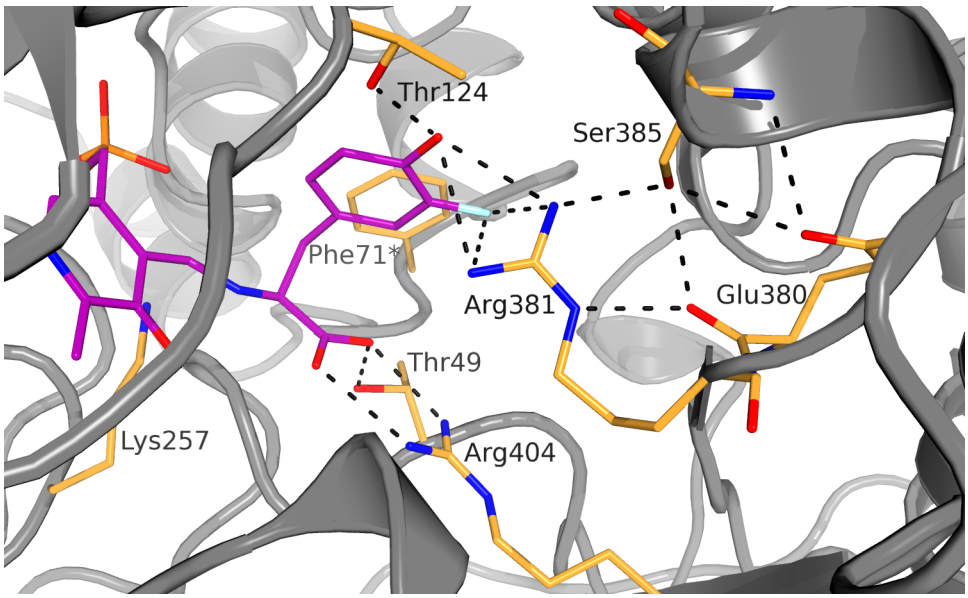

Figure 4.23. Arg381–Ser385–Glu380 triad is hydrogen-bonded with the external aldimine in the closed conformation of the Y71F TPL molecule. Hydrogen bonds are shown as *dashed lines*.

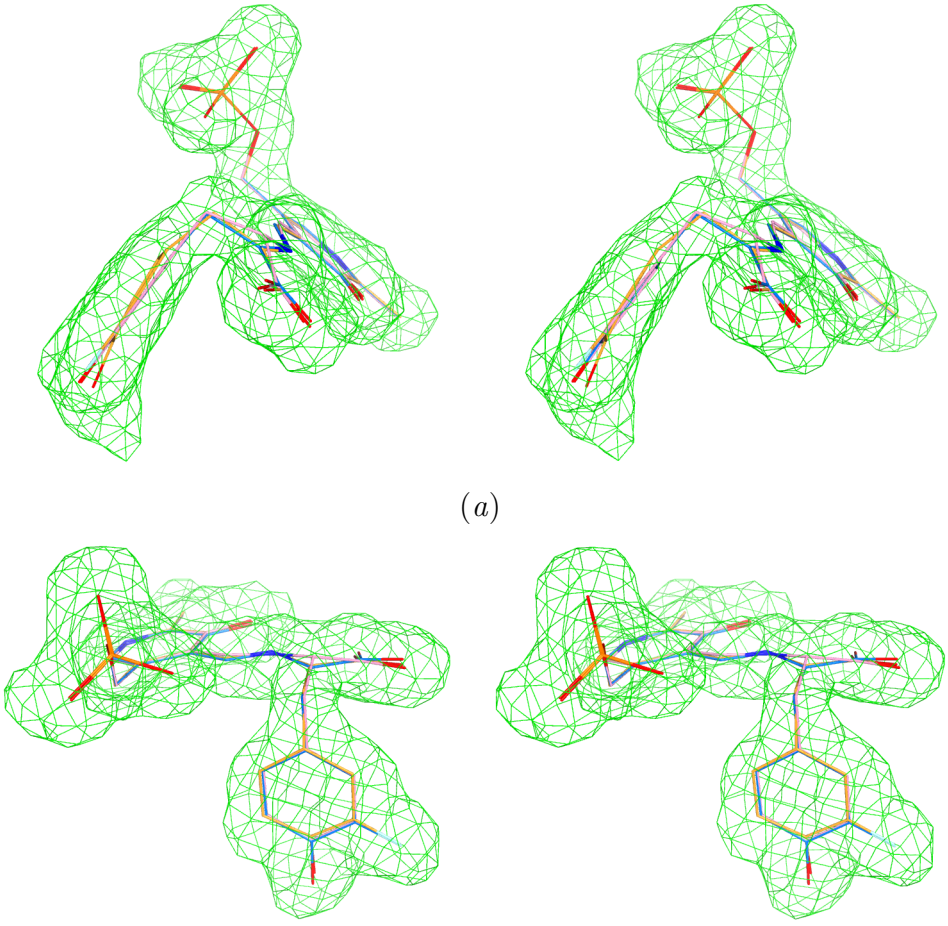

Figure 4.24. Ligands with different geometries can be fitted in the active sites of the F448H TPL complex with 3-fluoro-L-tyrosine. Stereo views of the external aldimine intermediate (*pink*), and the quinonoid intermediates refined with the standard (*blue*) and "relaxed" (*orange*) geometrical restraints. The σ_A-weighted $|F_o| - |F_c|$ electron density omit map (*green*) is contoured at 3.0σ level and corresponds to the active site B. The electron density maps in other active sites are very similar.

4.6.3 Complex of F448H TPL with 3-fluoro-l-tyrosine

The crystallographic asymmetric unit of *C. freundii* F448H TPL complexed with 3-fluoro-L-tyrosine consists of a whole TPL tetramer with four crystallographically independent active sites. All active sites are found in the closed conformation. The electron density maps of this 2.0 Å resolution structure are very clear and there is no sign of the whole-domain disorder. Also, the electron density corresponding to the ligands bound in all four active sites is well defined (Fig. 4.24), but its interpretation is ambiguous and the real identity of the ligands cannot be determined undoubtedly from the present crystallographic data. Moreover, the electron density could represent an equilibrium or steady-state mixture of two or more chemical species (different reaction intermediates) bound in the active site.

From the shape of the electron density, it is obvious that there is no bending in the

electron density which would correspond to a sp^3 hybridized Cγ atom, so the ligand is not the ketoquinonoid intermediate. It was shown by the rapid-scanning stopped-flow spectra that the F448H TPL accumulates the quinonoid intermediate ($\lambda_{max} = 515$ nm) when incubated with 3-fluoro-L-tyrosine.[15] Surprisingly, the quinonoid intermediate can be modeled in the F448H TPL active sites, but with the "tense" ("strained") geometry. If the standard geometrical restraints are used for the quinonoid molecule, its refined structural model has a very small tetrahedral Cα–Cβ–Cγ angle of only 90–96° (Fig. 4.24).* If more relaxed restraints on the quinonoid geometry are used in the refinement, the more realistic (although again "tense") Cα–Cβ–Cγ angle of 102° is obtained, but substrate's phenyl ring is slightly distorted in a boat-like ring conformation with the Cγ atom within the pyramidal geometry. An endocyclic angle between the mean planes Cγ–Cδ1–Cε1–Cζ and Cγ–Cδ2–Cε2–Cζ is ≈9°, Cγ is moved ≈0.1 Å from the plane defined by atoms Cβ, Cδ1, and Cδ2, and the maximal deviation of the hydroxylic O atom from the mean plane defined by the carbon atoms of the ring is 0.3 Å (Fig 4.24). At 2.0 Å resolution, these values are not significant and could be, to some extent, a consequence of the relaxed restraints used in the refinement. Nevertheless, the distortion of the benzene moiety (including bond length alternations and out-of-plane deformations) is a well known phenomenon found for the sterically constrained aromatic molecules (due to the bulky substituents or the crystal-packing interactions).[188–193] The quantum chemical calculations showed that transition from a planar conformation of benzene molecule to a non-planar structure with a value of the respective endocyclic angle at 15° results in an energy increase less than 1.5 kcal mol^{-1}.[190] Furthermore, the benzene molecule remains aromatic for distortions less than 0.3 Å[192] or, as showed by the other study, up to the respective endocyclic angle of 55°.[189] The interactions between the quinonoid molecule and the residues in the closed active site might compensate for the distortion of the phenyl ring and thus stabilize the quinonoid molecule in the "tense" geometry. It is important to note that the "tense" quinonoid molecule appears to be a species "prepared" for the attack of a hydron at Cγ atom and a consecutive formation of the ketoquinonoid form.

The available spectroscopic data suggest that some minor proportion of the external aldimine ($\lambda_{max} = 400$ nm) is also formed (together with the major quinonoid intermediate) when F448H TPL reacts with L-tyrosine or 3-fluoro-L-tyrosine.[15] Intermolecular contacts in the F448H TPL crystal could influence the equilibrium between the quinonoid and the external aldimine and drastically change the concentration ratio for these two species in F448H TPL. This could result in the external aldimine being the main intermediate in

*The search of the Cambridge Structural Database (CSD; Version 5.31, with February 2010 updates)[185] revealed 3 486 entries containing the C−CH_2−Ph non-cyclic structural fragment, not disordered and with *R*-factor less than 5 %. The mean value of the tetrahedral C−C−C angle was 113.84° with the sample s.u. of 2.26° (the minimal and maximal values were 96.50° and 131.93°, respectively). Only two entries which satisfy the above criteria have the C−CH_2−Ph angle smaller than 105°. Closer inspection of these two structures (CSD codes: REGGAM01[186] and RUYDOE)[187] revealed an error in the reported unit-cell parameters which accounts for the distorted geometrical parameters and the observed C−CH_2−Ph angle values of 101.0(7)° and 96.5(11)° for REGGAM01 and RUYDOE, respectively.

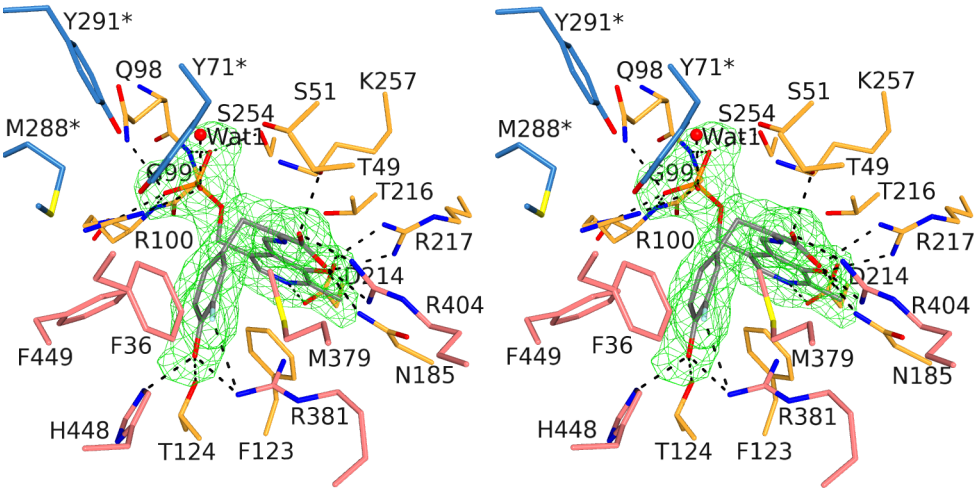

Figure 4.25. Enzyme interactions with the ligand molecule in the active site of F448H TPL. Stereo view with the quinonoid ligand refined using the "relaxed" geometrical restraints (*grey*) superimposed with the corresponding σ_A-weighted $|F_o|-|F_c|$ electron density omit map (*green*) contoured at the 3.0σ level. Carbon atoms of residues belonging to the large rigid region are shown in *orange*, those from the small region are shown in *pink*, and the residues from the neighboring subunit are shown in *blue* and labeled with a *star*. Hydrogen bonds are denoted by *dashed lines*.

the active site. Indeed, the external aldimine fits very well in the electron density map (Fig. 4.24), but only in somewhat strained geometry with the Cα–Cβ–Cγ angle of ≈ 103°.

In all three modeled geometries, the interactions between a ligand molecule and the active site protein residues are not significantly different (Fig. 4.25). All interactions observed for the external aldimine in the closed active site of Y71F TPL are also present in the active site of the F448H TPL complex. In addition, the substrate's phenolic group is not only hydrogen-bonded to the side chains of Arg381 and Thr124, but also to the imidazole ring of His448 (mutated Phe448). Distance between ε-amino group of Lys257 and Cα atom of the quinonoid molecule is in the range of 3.6–3.9 Å for crystallographically inependent active sites. The hydroxyl group of Tyr71 is at the distance of 3.9–4.0 Å from the Cγ atom of the substrate.

4.7 Calculated model of the ketoquinonoid intermediate

Modeling of the reaction intermediates in the active sites of apo-TPL shows that the ketoquinonoid structure fits best the active-site cleft in the closed conformation (Fig. 4.26). As expected, the phenolic group of the ketoquinonid forms hydrogen bonds with the side chains of Thr124 and Arg381. In addition, the van der Waals contact between the Phe448 phenyl ring and the bound substrate is possible only in the closed conformation. Other protein–ligand interactions are the same as those found for the structures with bound quinonoid intermediates.

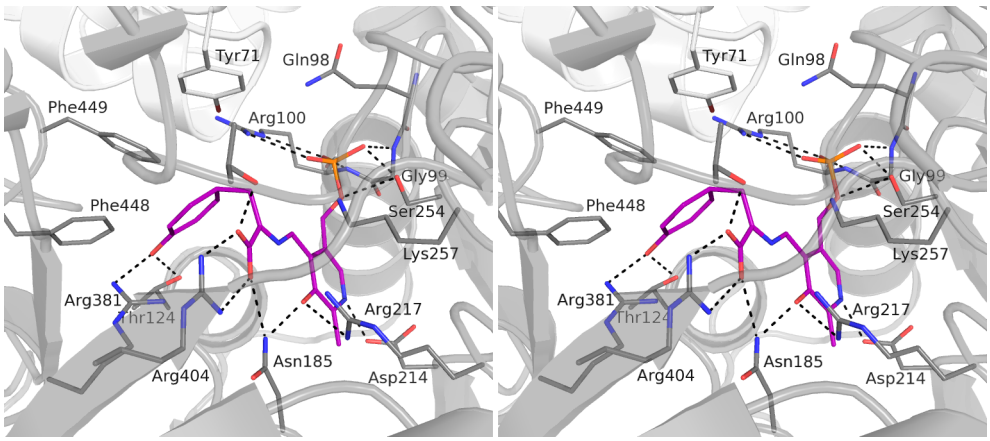

Figure 4.26. Model of the ketoquinonoid form bound in the closed conformation of the TPL active site (a stereo view). Hydrogen bonds (*dashed lines*) between the hydroxyl group of the ketoquinonoid form and both Thr124 and Arg381 side chains are possible only in the closed conformation, as well as van der Waals contacts between the Phe448 phenyl ring and the covalently bound substrate.

4.8 Alanine quinonoid intermediate of TPL in complex with pyridine *N*-oxide

As shown by previous spectroscopic studies[48,77,80,181] and also by the crystallographic studies described in this work, wild-type TPL forms the alanine quinonoid intermediate when incubated with L-alanine. Pyridine *N*-oxide (Scheme 4.5) binds selectively to the alanine quinonoid intermediate[48] thus enabling the preparation of the ternary complex by soaking the wild-type holo-TPL crystals with a mixture of L-alanine and pyridine *N*-oxide.

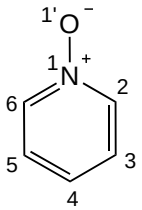

Scheme 4.5. Structural diagram of pyridine *N*-oxide with the corresponding atom-numbering scheme.

The asymmetric unit of the alanine quinonoid complex with pyridine *N*-oxide consists of the catalytic dimer with one subunit in the open and the other one in the closed conformation. The electron density is very clear, with no discrete disorder as found for the apoenzyme, the methionine quinonoid complex, and the Y71F TPL 3-fluoro-L-tyrosine quinonoid complex. However, there is a disorder of the ligands bound in the closed active site (Fig. 4.27). Namely, only a half of the closed active sites are occupied by the alanine quinonoid intermediate. The other half is occupied by the internal aldimine, a water molecule and a phosphate anion bound in the favorable phosphate binding site formed only in the closed conformation by the side chains of Arg404, Arg381, Arg217, Asn185

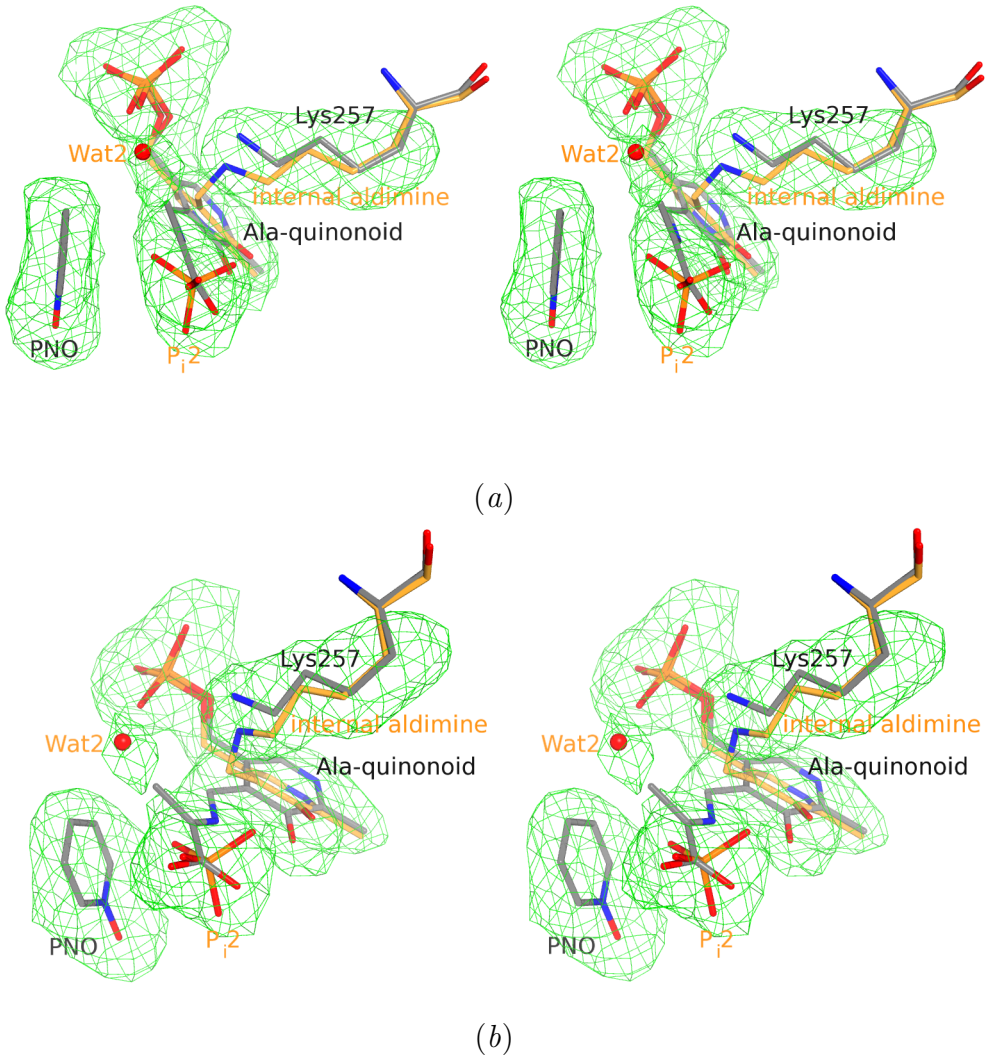

Figure 4.27. Ligands in the closed active site of the alanine quinonoid intermediate in complex with pyridine *N*-oxide (PNO). Stereo views with the ligand molecules superimposed with the corresponding σ_A-weighted $|F_o| - |F_c|$ electron density omit map (*green*) contoured at the 2.0σ level. The internal aldimine, alanine quinonoid intermediate (Ala-quinonoid), phosphate anion (P_i2) and water molecule Wat2 are modeled with 0.5 occupancy.

and Thr49 (the second phosphate binding site).

In the closed active site (Fig. 4.28), a molecule of pyridine *N*-oxide (Scheme 4.5) is bound in the pocket otherwise occupied by the phenyl ring of the 3-fluoro-L-tyrosine quinonoid in Y71F and H448F TPL complexes. The C4 atom of the pyridine *N*-oxide molecule (an equivalent of Cγ in L-tyrosine) is only 3.0 Å separated from the Cβ of the alanine quinonoid molecule and thus models a phenol molecule and the α-aminoacrylate intermediate just after the cleavage of the substrate's Cβ–Cγ bond. The plane of a pyridine *N*-oxide molecule and that of the "alanine" moiety of the quinonoid make an angle of only 26°, which is quite different from the equivalent angle in the "relaxed" quinonoid molecule (109°) in the Y71F mutant (Fig. 4.19). The oxygen atom of the pyridine *N*-oxide makes hydrogen bonds with the side chains of Thr124 and Arg381. The hydroxyl group of

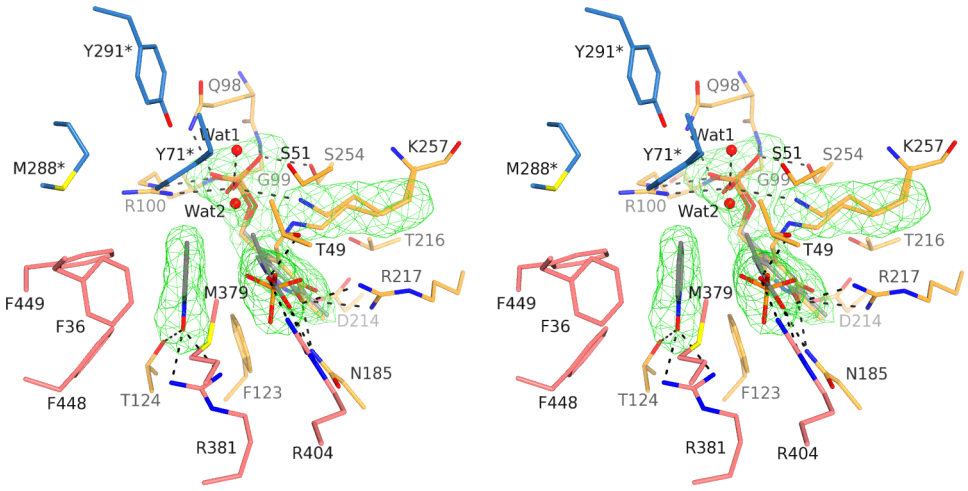

Figure 4.28. The closed active site of the alanine quinonoid intermediate in complex with pyridine *N*-oxide. Stereo view with the corresponding σ_A-weighted $|F_o| - |F_c|$ electron density omit map (*green*) contoured at 3.0σ. Carbon atoms of the residues belonging to the large rigid region are shown in *orange*, those from the small region are shown in *pink*, and the residues from the neighboring subunit are shown in *blue* and labeled with a *star*. Hydrogen bonds are denoted by *dashed lines*.

Tyr71 is at the distance of only 2.9 Å from the C4 atom of the pyridine *N*-oxide molecule.

There is no pyridine *N*-oxide molecule in the open active site. Instead, it is found near the entrance of the active-site cleft, next to Asp348(B) [Asp348(B) OD2 · · · pyridine *N*-oxide N 3.2 Å]. This pyridine *N*-oxide molecule is hydrogen-bonded to the water molecule which is fixed by hydrogen bonds made with the amide and carbonyl groups of Glu401(B), and the carboxyl group of Asp348(B). The pyridine *N*-oxide molecule located at this site is also surrounded by the hydrophobic side chains of Ala148(B), Val337(B) and Leu400(B). Another pyridine *N*-oxide molecule is situated next to the N-terminal arms. It is stacked between the indole rings of two Trp61 residues, each from different catalytic dimer, and hydrogen-bonded to the side chain of Ser12(A) and a water molecule which forms hydrogen bonds with the carbonyl group of Met65(B) and the side chain of Lys11(B) from the other catalytic dimer.

4.9 Summary of the results

Summary of the crystal structures of different forms of *C. freundii* TPL reported here is given in Table 4.4. The crystallographic asymmetric unit of the F448H TPL structure complexed with 3-fluoro-L-tyrosine (F448H TPL–F-Tyr) is a tetrameric protein molecule, whereas the asymmetric units of all other structures contain the catalytic dimer of TPL. Each protein subunit can possess either an open or a closed conformation. The closed conformation is formed by significant relative rotations of the two rigid protein regions. The loss of hydrogen bonds and salt bridges between different subunits in the open con-

Table 4.4. Summary of the crystal structures reported here

Structure	Subunits	Conformation	Ligands in the active site
holo-TPL	A, B	open	internal aldimine
D214A TPL	A, B	basically open, but with distortion	internal aldimine
apo-TPL	A	mainly closed, minor portion is open (not modeled)	1.5 PO_4^{3-} (2 PO_4^{3-} are bound only in closed active site)
	B	open	one PO_4^{3-}
TPL (phenol)	A	disordered: 52 % closed, 48 % open	radiation damaged internal aldimine, 0.52 PO_4^{3-}
	B	open	radiation damaged internal aldimine
TPL (AP)	A	disordered: 54 % closed, 46 % open	0.54 internal aldimine, 0.54 PO_4^{3-}, 0.46 α-aminoacrylate?
	B	open	radiation damaged internal aldimine
TPL–Ala	A	closed	alanine quinonoid
	B	open	alanine quinonoid
TPL–Met	A	mainly closed, minor portion is open (not modeled)	methionine quinonoid
	B	open	internal aldimine
Y71F TPL–F-Tyr	A	mainly closed, minor portion is open (not modeled)	0.67 3-fluoro-L-tyrosine external aldimine, 0.33 3-fluoro-tyrosine "relaxed" quinonoid
	B	open	3-fluoro-tyrosine "relaxed" quinonoid
F448H TPL–F-Tyr	A, B, C, D	closed	3-fluoro-L-tyrosine external aldimine or "tense" quinonoid?
TPL–Ala–PNO	A	closed	0.5 internal aldimine, 0.5 PO_4^{3-}, 0.5 alanine quinonoid, pyridine *N*-oxide
	B	open	internal aldimine

formation (Fig. 4.8) is compensated by the newly formed interactions between the small and large rigid regions in the closed subunit (Fig. 4.7). All TPL subunits in the structures of holo-TPL and D214A TPL are found in the open conformation. On the contrary, all protein subunits in the F448H TPL–F-Tyr structure have closed conformation. The discrete disorder of a protein subunit (always denoted by A) is observed in several structures, and in all such cases the closed conformation is dominant.

The phosphate group of the internal aldimine is hydrogen-bonded to residues Gln98, Gly99, Arg100 and Ser254 (Fig. 4.1). Additional salt-bridge interaction between the phosphate group and the hydronated side chain of Lys257 is formed in the external aldimine and the quinonoid intermediates (Figs. 4.16, 4.17, 4.20, 4.22, and 4.25). In the apo-TPL structure, a PO_4^{3-} anion is bound in the same site as the phosphate group of PLP. A second phosphate-binding site – composed of the side chains of Thr49, Asn185, Arg217, Lys257, Arg404, and Arg381 – is formed when the active site assumes the closed conformation (Fig. 4.9).

The O3′ atom of the internal aldimine in the wild-type protein is hydrogen-bonded to the side chain of Arg217, whereas the hydronated N1 atom of the pyridine ring makes hydrogen bonds with the side chain of Asp214 (Fig. 4.1). In addition to these interactions, the O3′ atom of the external aldimine and the quinonoid intermediates is hydrogen-bonded to the amide group of Asn185 (Figs. 4.16, 4.17, 4.20, 4.22, and 4.25). The O3′ atom of the internal aldimine in the D214A TPL structure makes interactions with the side chains of Thr216 and Asn185, whereas the pyridine N1 atom interacts with a water molecule (Wat2 in Fig. 4.4).

The carboxylate group of the reaction intermediates (the quinonoids and the external aldimine) forms hydrogen bonds with the side chains of Asp185, Arg217, Arg404, and Thr49 (Figs. 4.16, 4.17, 4.20, 4.22, and 4.25). In the structures of the TPL complexes with 3-fluoro-L-tyrosine, the hydrogen bonds between substrate's phenol group and the side chains of Thr124 and Arg381 are only observed in the closed conformation (Fig. 4.22). In addition, in the closed conformation there is a van der Waals contact between the side chain of Phe448 and the substrate's phenol ring. In the F448H TPL–F-Tyr structure, a hydrogen bond is formed between the imidazole ring of His448 and the substrate's phenol group (Fig. 4.25). It is also noted that the side chains of Thr124 and Arg381 make hydrogen bonding interactions with the oxygen atom of pyridine *N*-oxide in the TPL–Ala–PNO structure (Fig. 4.28).

5 Discussion

In the past, TPL has been the subject of intensive biochemical studies. Although valuable data have been deduced about the three-dimensional architecture of TPL and the structure of its active site, the relationship between molecular interactions in the active site and the chemical events associated with several intermediate steps of the reaction remained elusive. The aim of the research described in this thesis was to answer several questions about the mechanism of catalysis by TPL.

5.1 Structural role of monovalent cations

It was demonstrated that the cation-binding site and the active site are connected by hydrogen bonds via the ε-amino group of Lys256 (Fig. 4.2). These concatenated interactions of the cation-binding site with the active site residues demonstrate the critical role of Lys256 in the formation of the monovalent cation binding site, which is in agreement with previous biochemical observations,[194] and provide an insight into the influence of monovalent cations on the activity of TPL.[99,100,195] At cation concentrations lower than 100 mmol dm^{-3}, K^+, NH_4^+, and Rb^+ were shown to be the most effective activators, Cs^+ and Li^+ were significantly less effective, while the effect of Na^+ was negligible. Divalent cations (Mg^{2+}, Ca^{2+}, Ba^{2+}, and Sr^{2+}) did not activate TPL. Different alkaline and earth alkaline cations, because of their different radius to charge ratios, have considerably different coordinations, which explains their different binding affinities towards TPL. Differences in coordination of Li^+, K^+, Rb^+, and Cs^+ may cause differences in the cation-binding site conformation and, in turn, slight but key differences in the conformation of the active site.

In the previously determined structure of *C. freundii* TPL complexed with 3-(4′-hydroxyphenyl)propanoic acid, PLP, and Cs^+ ion (**2**; PDB code 2TPL),[4] only one of the two crystallographically independent active sites was occupied by the substrate analog. In the second site only PLP was bound, so this active site and the nearby cation-binding site (Cs^+) are comparable to those of the holoTPL structure in complex with K^+ described here. The coordination around Cs^+ is somewhat different from that of K^+ with distances between the metal cation and the coordinating protein atoms being longer by 0.2–0.4 Å. This results in slight changes in the conformation of Cs^+ coordinating residues and also in small changes in the active site conformation. In particular, the hydroxyl of the

catalytically critical Tyr71 is positioned 0.16 Å farther from the active site than in the K^+ structure. These small changes in the active site architecture presumably explain the significant reduction of TPL activity when K^+ is replaced by Cs^+ cation[100] and provide a ground for explaining the role of K^+ in the activation of TPL.

Historically, the important role of monovalent cations in stabilizing the quaternary structure of β-eliminating lyases was best illustrated by the example of *E. coli* Trpase.[196,197] In the absence of PLP and monovalent cations, *E. coli* Trpase reversibly dissociates into two nonactive dimers. As both PLP and the monovalent cation are bound at the subunit–subunit interface of the catalytic dimer, it is likely that the dissociation occurs along this interface. In the available structures of Trpase and TPL the two catalytic dimers are held together by intertwined N-terminal arms,[146] suggesting that the observed dissociation of the *E. coli* Trpase tetramer leads to noncatalytic dimers where the two subunits are bound through their N-terminal arms. Available data suggest that TPL does not undergo such dissociation in the absence of PLP and monovalent cations, but like in the case of Trpase, its activity is influenced by monovalent cations.

5.2 Differences between TPL apoenzyme structures determined at pH 6.0 and pH 8.0

While the optimum pH for the β-elimination of L-tyrosine is around 8.2, at pH 6.0 the enzyme is essentially inactive.[47] The differences in the activity of the enzyme at high and low pH were attributed to hydronation of two catalytic bases with average pK_a values of about 7.8.[105] The side chain of Arg381 was shown to be one of these two bases,[4] but the identity of the other catalytic base remained uncertain, although the previous structural study suggested it might be the amino group of Lys257.[4] In contrast to the new apoenzyme structure determined from the crystal grown with poly(ethylene glycol) 2000 monomethyl ether at pH 8.0, the previous structure was determined using a different crystal form, with crystals grown at pH 6.0 using ammonium sulfate as a precipitant.[83] In the previously determined structure (**1**, PDB code 1TPL; 2.3 Å resolution) several stretches of residues were not modeled due to poor electron density: residues 123–131, 384–398, and 442–447 in one subunit and residues 123–133, 384–398, and 442–445 in the crystallographically independent subunit.[3] Both noncrystallographically related subunits of **1** (which do not constitute the catalytic dimer) are very similar to each other and are basically in the open conformation. As major differences between the open and closed conformations of the TPL subunits have already been described in Subsection 4.3.2, the structure of **1** is only compared with the open conformation. These were found by the ESCET analysis[178] of the corresponding subunits of the apoenzyme structures determined previously and described here, using the standard parameters (see above) and lower and upper tolerance levels of $\epsilon_l = 5.0$ and $\epsilon_h = 10.0$. Except for the parts of the model **1** with

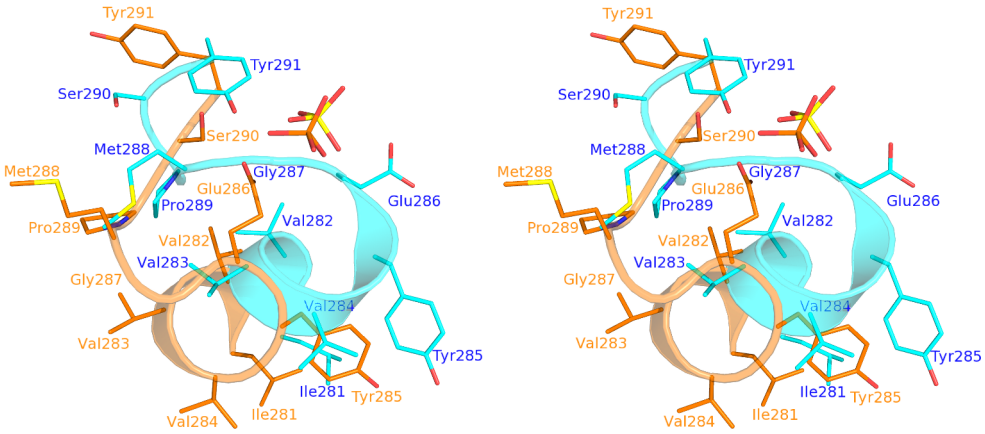

Figure 5.1. Structural comparison of residues 281–291 in the previously determined structure of the apoenzyme at low pH (1TPL; *orange*) and in the open conformation of apo-TPL (*cyan*). A sulfate ion in 1TPL is bound in the same site as the phosphate ion in the open active site of apo-TPL.

missing residues, ESCET found the difference between the two models in four polypeptide regions: 70–74, 187–188, 281–290, and 382–383. The most striking difference is in the tilt of helix α9,[3] where the Cα positions of C-terminal residues 281–285 differ by 1.0–4.7 Å, and in the following active site loop area, residues 286–290, which has a different conformation in the two structures (Fig. 5.1). Despite these major differences in both structures, the active sites remain open. It is reasonable to conclude that the observed different conformations in the previously determined structure of the apoenzyme are due to the difference in pH (6.0 as opposed to 8.0). In addition, some differences may account for different crystallization conditions (at pH 6.0 crystals were grown with 1 mol dm^{-3} $(NH_4)_2SO_4$ and kept in 1 mol dm^{-3} $MgSO_4$ during the data collection) and possibly also the radiation damage (at pH 6.0 the data were collected at room temperature).

5.3 Mechanism of β-elimination involves significant conformational change

Structures of the TPL complexes described here represent several snapshots of the β-elimination mechanism. Y71F TPL complexed with 3-fluoro-L-tyrosine models the external aldimine and quinonoid intermediates. F448H TPL complexed with 3-fluoro-L-tyrosine apparently mimicks the quinonoid intermediate in the "tense" conformation prepared for formation of the ketoquinonoid, while the alanine quinonoid in complex with pyridine *N*-oxide represents the α-aminoacrylate and phenol molecule immediately after cleavage of the Cβ–Cγ bond.

The experimental data show and clarify the structural and mechanistic roles of several residues (Scheme 5.1). In particular, the structures of TPL complexes show that Asn185

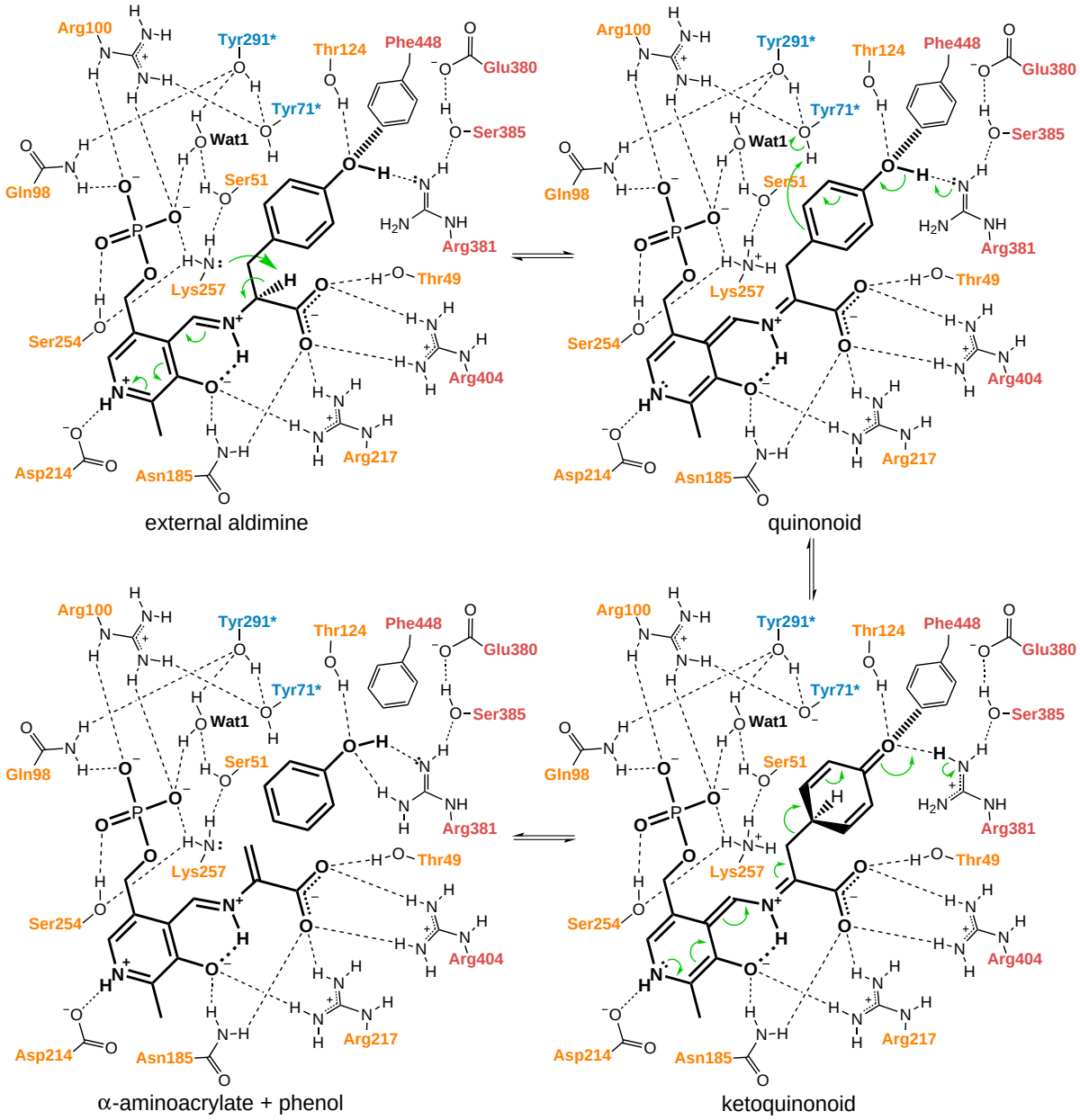

Scheme 5.1. Interactions in the closed active site during the β-elimination of L-tyrosine. Hydrogen bonds are shown as *dashed lines*. A short contact between the side chain of Phe448 and the substrate's phenolic group is denoted by a *hashed line*. Residues from the large domain are written in *orange*, those from the small domain are written in *pink*, and the residues from the neighboring subunit are written in *blue* and labeled with a *star*.

stabilizes the external aldimine and quinonoid intermediates by making hydrogen bonds bridging the O3′ atom of PLP with the carboxyl group of the substrate (Figs. 4.16, 4.17, 4.20, 4.22, and 4.25), in agreement with previous propositions based on mutagenesis and kinetic studies.[106] Lys257 is ideally positioned to be the base abstracting the Cα hydron with its ε-amino group being within a distance of 3.5 Å for the external aldimine in the closed active site of the Y71F mutant. Also, it is hydrogen-bonded to the negatively charged PLP phosphate group[198] and side chain hydroxyl groups of Ser51 and Ser254 (Scheme 5.1). These interactions facilitate the Cα hydron abstraction and position the

ε-amino group of Lys257 in an orientation suitable for this task. In agreement with structural observations, mutations of Ser254 to Ala and Cys significantly reduced the enzymatic activity.[199] In the structure of F448H TPL complexed with 3-fluoro-L-tyrosine the Tyr71 side chain hydroxyl is the closest group to the Cγ atom of the substrate (3.9–4.0 Å) and is thus in a suitable position for donating a hydron.[52] Furthermore, it is hydrogen-bonded to the positively charged side chain of Arg100 (Figs. 4.16, 4.17, and 4.25). This would facilitate the hydron donation by stabilizing the negatively charged phenolate (of Tyr71) formed in that process (Scheme 5.1). In addition to Tyr71, the side chain of the amino acid substrate is surrounded by Arg100, Phe123, Thr124, Met379, Arg381, Phe448, and Phe449 which form a tight pocket (Figs. 4.17, 4.22, and 4.25). It is postulated that these residues are important for determining the specificity toward the physiological substrate. A catalytic role has been previously established only for three of these residues: Arg381,[4] Thr124 and Phe448.[15] It was found that these three residues were important for the substrate specificity of TPL. Finally, it is noted that a hydrogen bonding network connecting the ε-amino group of Lys257 and the phenolic hydroxyl of Tyr71 may provide the route for the observed hydron transfer between the Cα and Cγ atoms of the substrate.[182] The observed 7–10 % efficiency of the transfer is consistent with the number of mediating hydrogen bonds connecting the two residues, indicating potential routes of hydron exchanges (Scheme 5.1).

The structures of TPL complexes described here suggest that the quinonoid intermediate with L-tyrosine in the "relaxed" geometry can be accommodated only if the active site is in the open conformation, due to unfavorable planar geometry at the Cγ atom. In the closed conformation the substrate phenol moiety may be accommodated only in the geometries corresponding to the external aldimine, the quinonoid intermediate in the "tense" geometry, and the ketoquinonoid which, in accordance with the generally accepted chemical mechanism of TPL catalysis, forms upon tautomerization of the phenol moiety into cyclohexadienone (Scheme 5.1). As found by the kinetic studies, the ketoquinonoid is probably not an intermediate, but a transition structure.[102–104] It is very indicative that the ketoquinonoid structure, as found by the molecular modeling, fits best the active site cleft in the closed conformation (Fig. 4.26). Interactions between the phenolic ring of the substrate and the active site residues of the small rigid region (Phe36, Phe448, Phe449, Met379, and Arg381) are only possible in the closed active site. In accordance, solvent-accessible areas of Thr124, Arg381, and Phe448 are most affected by the closure of the active site, and in the closed conformation these are decreased by 81, 58, and 31 Å^2. Thus, the transition to the closed conformation may be considered as a driving force for the tautomerization. Structural observations indicate that this process occurs through hydronation of the Cγ atom by Tyr71 assisted by the transfer of the phenolic hydron to Arg381. Since the guanidine group of Arg381 is hydrogen-bonded to Ser385 and Glu380 (Fig. 4.23), the carboxylate group of Glu380 could additionally activate the guanidine of Arg381 to act as the catalytic base (Scheme 5.1). The following β-elimination of phenol,

which is the rate-limiting stage of the whole enzymatic reaction,[103] should result from the breakdown of the stereoelectronically optimally oriented bond between the Cβ and Cγ atoms. Regeneration of aromaticity in the cyclic moiety implies the appearance of a negative charge on the oxygen atom, and the return of the hydron from Arg381. The hydrophobic conditions of the closed active site should result in the phenolate anion being about 4 orders of magnitude stronger base than the guanidine[200] thus favoring such a process.

The observed discrete disorder in several crystal structures indicates mobility of the flexible parts and the small rigid region of the TPL subunit. When the holoenzyme crystals, with all subunits in the open conformation, were soaked with the ligands, the closure of some subunits was observed despite each subunit being restrained by interactions in a crystalline state. Some of the interactions between subunits observed in the holoenzyme crystals are disrupted after the closure of one of the subunits (Table 4.2). To compensate for these broken interactions, new interactions are formed within the subunit in the closed conformation (Table 4.1). It is interesting to note that half of the broken hydrogen bonds and salt bridges are those within the same TPL tetramer (Fig. 4.8), and not between symmetrically related tetramers in the crystal. It is proposed that the same closure, as observed in crystalline state, also occurs in solution. The open conformation in solution can be stabilized by the interactions within the same tetramer. This might explain why TPL exists in the tetrameric form although the catalytic dimer is also active. Interestingly, no cooperativity between subunits was observed for TPL.[50,102,103,105,182] When TPL was encapsulated in wet nanoporous silica gel, the reduction of ligand-binding affinities and the modified steady-state distribution of the catalytic intermediates (with respect to solution) was observed.[201] These effects cannot be explained only by catalytic rates limited by substrate diffusion within gels of uncontrolled thickness. It seems that the dominant cause is the decrease of the rate of conformational changes that accompany the catalytic cycle. The conformational changes are partially constrained in the silica matrix, resulting in the modified reaction rates. Existence of the closed conformation in solution is also substantiated by the observed efficiency of the hydron transfer between the Cα and Cγ atoms of the substrate (7–10 %).[182] This transfer of a hydron takes place through the hydrogen-bonding network connecting the catalytically important Lys257 and Tyr71. If the active site remained open during the enzymatic reaction, the hydron could exchange with solvent, and the observed efficiency of its transfer between the Cα and Cγ atoms of the substrate would be significantly lower and not in accordance with the number of hydrogen bonds connecting Lys257 and Tyr71.

Movement of the small domain toward the large one has been observed for two out of eight crystallographically independent subunits of the external aldimine complex of *E. herbicola* TPL with PPT (**5**).[5] However, closure of the active site in these two subunits is not complete. In the reported structures of the quinonoid intermediates the Cζ atom of Phe448 is closer to the ligand by 1.9 Å with respect to its position in the TPL–PPT

complex.

Taken together, the structural observations indicate that the active site closure occurs after the formation of the Michaelis complex (Scheme 5.2). The partial closure (as observed in the TPL–PPT complex, **5**) might occur at the stage of the external aldimine formation (Scheme 2.18; Fig. 2.10), but the external aldimine can also be accomodated in the completely closed active site (Fig. 4.22). The quinonoid intermediate is found both in the open (Fig. 4.20) and closed (Figs. 4.22 and 4.25) active sites. So, the complete closure most probably occurs during or immediately after the formation of the external aldimine or quinonoid intermediate. Current data demonstrate that this closure protects the quinonoid molecule from the solvent and brings the catalytically important residues (Arg381, Thr124, and Phe448) into appropriate positions where they can interact with the quinonoid and the emerging transitional structure (Scheme 5.1). Thus the active site closure facilitates the following steps in the β-elimination mechanism, *i.e.* the ketoquinonoid formation and the subsequent elimination of phenol (Scheme 2.18), which most probably occurs in the closed active site as shown by the structure of the alanine quinonoid complexed with pyridine *N*-oxide (Fig. 4.27). It is suggested that after the Cβ–Cγ bond cleavage, the active site opens in order to release the products of the β-elimination reaction and to bind a new molecule of the substrate.

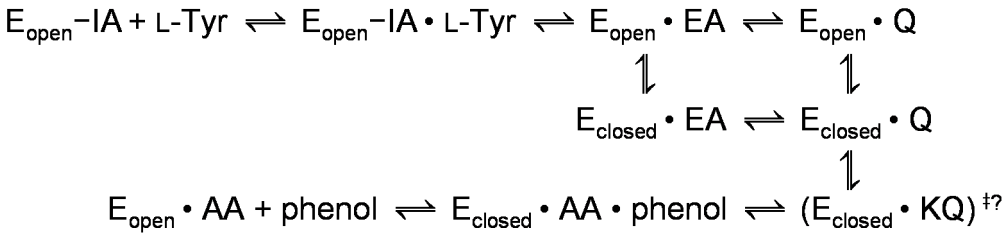

Scheme 5.2. The proposed mechanism for the β-elimination involves the closure of the active site. E_{open} and E_{closed} denote the open and closed conformation of the active site, respectively. Names of the reaction intermediates are abbreviated: IA – internal aldimine, EA – external aldimine, Q – quinonoid, KQ – ketoquinonoid, AA – α-aminoacrylate. The ketoquinonoid could be a transition structure instead of an intermediate.

In the structure of the F448H TPL mutant complexed with 3-fluoro-L-tyrosine, a hydrogen bond is formed between the substrate phenolic group and the side chain of His448. It is likely that this hydrogen bond stabilizes the closed conformation. Also, the presence of His instead of Phe in the pocket of the closed active site might perturb pK_a of the nearby Arg381, so it loses its capability as a general catalytic base. These observations explain why F448H TPL exhibits very low β-elimination activity with L-tyrosine, but retains significant activity with SOPC and *S*-alkyl-L-cysteines[15] – the substrates with good leaving groups which cannot form hydrogen bonds with His448 in the mutated enzyme.

The most closed conformation of apo-Trpase-I from *E. coli*[13] is basically the same as the closed conformation observed for TPL, whereas the wide-open conformation of apo-

Trpase-II from *E. coli*[14] corresponds to the open conformation of TPL. This denotes that the closure of the active site during the enzymatic reaction might be a common feature of both TPL and Trpase.

5.4 Mechanism of alanine racemization

As shown by the previous spectroscopic studies, incubation of *C. freundii* TPL with L- or D-alanine results in the formation of quinonoid complexes.[80,100] It was expected that the structure of *C. freundii* TPL–Ala may help to deduce the alanine racemization mechanism. Because the internal return of the α-hydron was observed in the conversion of L- to D-alanine catalyzed by TPL,[79] two possible mechanisms of the alanine racemization were suggested.[48] In the proposed single-base swinging door mechanism, the alanine quinonoid molecule would have to rotate by 180° in order to expose its other face to the fixed acid-base catalyst handling the hydron abstraction/donation. This is unlikely because the quinonoid molecule is tightly bound in both closed and open active sites of the TPL–Ala. The principal manner of the cofactor binding is the same in all known TPL structures, so drastic reorientation of the PLP plane looks quite improbable. According to the second, two-base mechanism of alanine racemization, two different acid-base catalysts participate in the reaction (Scheme 5.3). Structural data on the TPL–Ala complex support the second, two-base mechanism and indicate that the ε-amino group of Lys257 (Fig. 4.16) is the most probable base which abstracts the Cα hydron in the L-alanine external aldimine. For the D-alanine formation, the *si* face of the Cα atom in the quinonoid molecule has to be hydronated. The water molecules, denoted as Wat2 and Wat3 in Fig. 4.16, are in the most suitable position for this task and, furthermore, they could be activated by the guanidinium group of Arg381 through the hydrogen bond interactions. The observed internal return of the Cα hydron could be explained by a shuttle system between Lys257 and Wat2/Wat3 realized through a hydrogen bonding network in the closed active site. This network involves the PLP phosphate group, water molecule Wat1 and side chains of Ser51, Ser254, Asn98, Arg100, Tyr291, and Tyr71 (Fig. 4.16). It is suggested that a molecule of D-alanine binds in the active site in the same manner as a molecule of L-alanine, but this means that the α-hydrogen atom is oriented in the exactly opposite direction (Scheme 5.3). In the case of D-alanine, the roles of the catalytic base and acid in the racemization mechanism should be mutually interchanged with those proposed for D-alanine. These could explain a higher value of K_{m} and a lower value of k_{cat} observed for the racemization of D-alanine in comparison to those for L-alanine.[48]

A two-base mechanism of alanine racemization was also proposed for alanine racemase[202–204] where the ε-amino group of the PLP-binding lysine and the hydroxyl of Tyr situated on the opposite face of the substrate Cα act as acid/base catalysts. It should be noted, however, that in the framework of the suggested racemization mechanism the quinonoid intermediates formed with L- and D-alanine should be identical in every re-

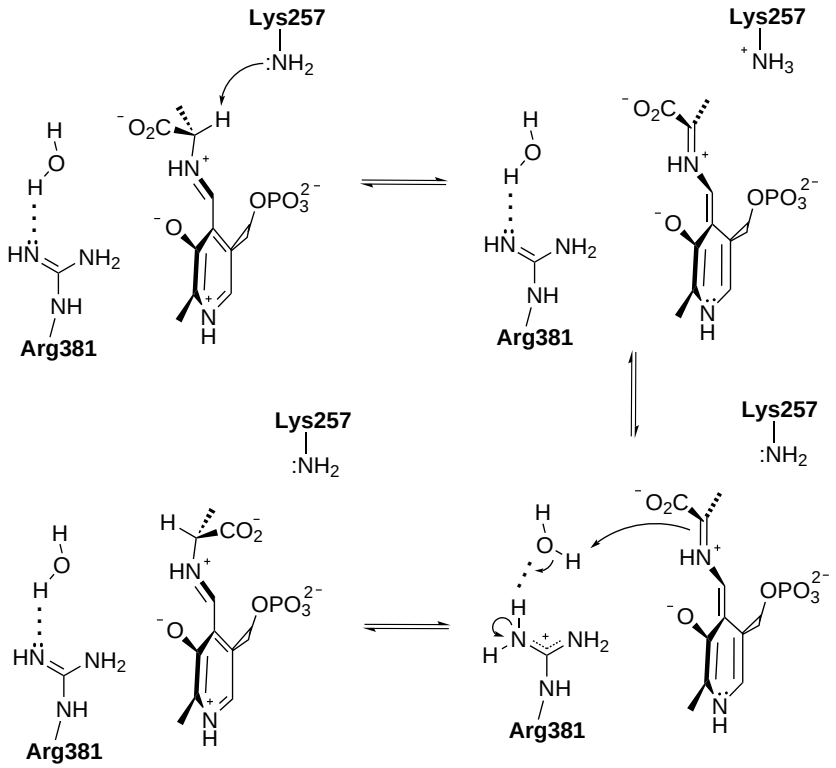

Scheme 5.3. Proposed mechanism of alanine racemization catalyzed by TPL.

spect except for the position of the hydron abstracted from the α-position of the bound enantiomer. Thus it is reasonable to expect the existence of only one quinonoid intermediate on the racemization reaction pathway. Meanwhile, as shown by the previous rapid kinetic studies of TPL interaction with L- and D-alanine, incubation of *C. freundii* TPL with L- or D-alanine results in the formation of two distinct quinonoid complexes. Interconversion of the two quinonoids, proceeding through formation of a third one, is the rate-limiting step of the racemization reaction.[48] It is likely that the observed slow rate of the interconversion is associated with the shuttle of the abstracted hydron between the catalytic bases. This process changes the charge distribution in the active site, and thus may be accompanied by considerable conformational adjustments. In this case, the chiral environment of the quinonoid formed with D-alanine could be somewhat different, and possibly even more favorable for the hydronation from the *si*-face than that observed in the complex with L-alanine.

5.5 Internal return and isotope exchange of the Cα hydron in TPL reactions

It was mentioned above that racemization of alanine, catalyzed by TPL, is characterized by the internal return of the Cα hydron.[79] Internal return of the Cα hydron to the leaving phenol group was also observed in the β-elimination reaction with the natural substrate, L-tyrosine.[182] The present structural data show that in both cases the internal return may

occur through the system of hydrogen bonds connecting the active site residues and water molecules which ensure hydron exchange. The observed extents of the internal return during alanine racemization (3.5 %) and β-elimination reaction (7–10 %) are consistent with the number of mediating hydrogen bonds connecting the Nζ of Lys257 with the water molecules Wat2 and Wat3 (alanine racemization) and with Tyr71 (β-elimination, Fig. 4.16). It is noted that in the closed conformation these residues and water molecules are isolated from the bulk solvent, while in the open conformation some of them are solvent accessible and thus prone to the hydrogen isotope exchange with the solvent. The rates of dehydronation-rehydronation processes (leading to the isotopic exchange) are higher than those for racemization or β-elimination reactions.[48,49] If the isotopic exchange occurred only in the open conformation, the extents of the internal return would be significantly lower than the observed ones.[79,182]

TPL also catalyzes the stereospecific isotope exchange of the Cα hydron of several L-amino acids, which occurs with the retention of the amino acid (*S*)-configuration. Kinetic data showed that the Cα hydrogen isotope exchange for L-phenylalanine proceeds via a quinonoid intermediate.[205] In contrast, in the case of L-methionine, an alternative mechanism of isotope exchange, not involving the quinonoid intermediate, must exist. This is because the quinonoid intermediate with L-methionine is a dead-end complex as indicated by the comparison of the reaction rates of the Cα hydron abstraction from the external aldimine and rehydronation of the quinonoid with the rate of the Cα hydrogen isotope exchange.[205] According to this alternative mechanism, the Cα hydrogen isotope exchange for L-methionine occurs by a concerted mechanism (Scheme 5.4) involving a six-membered transition state, which includes the ε-amino group of Lys257 and a water molecule (D_2O) hydrogen-bonded to it.[205] Analysis of the structure of the closed active site of TPL–Met shows that the active site does indeed contain a water molecule (Wat1 on Fig. 4.17), which could perform this task. Although this water molecule is not hydrogen-bonded to the ε-amino group of Lys257 in the structure of the quinonoid intermediate, such interaction may be favored in the external aldimine.

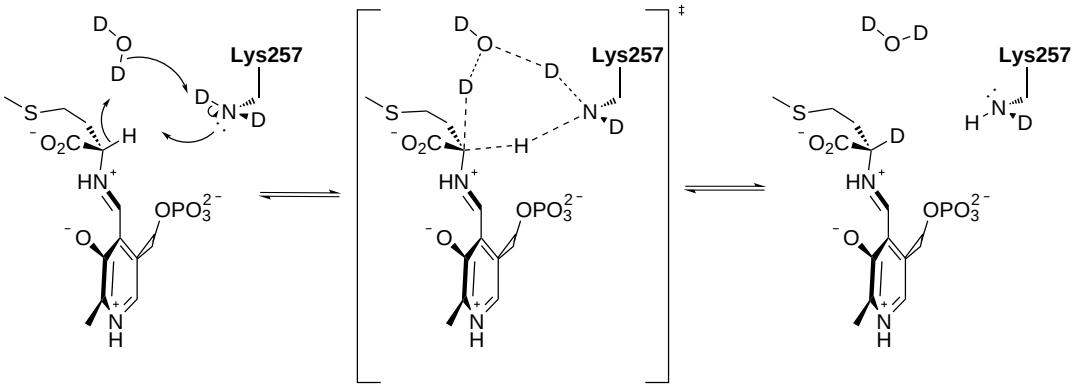

Scheme 5.4. Concerted mechanism of Cα hydrogen isotope exchange in the external aldimine of methionine.

5.6 Structural and functional consequences of the Asp214→Ala mutation

D214A and D214N TPL mutants from *C. freundii* were shown to be inactive for the β-elimination of L-tyrosine and 3-fluoro-L-tyrosine, but they decompose substrates with better leaving groups (such as SOPC, *S*-alkyl-L-cysteines, and β-chloro-L-alanine) at reduced rates (10- to 100-fold lower).[154] In addition, TPL affinity towards a cofactor PLP is reduced in the mutated enzymes by about four orders of magnitude. The structure of D214A TPL presented here indicates that the inability of residue 214 to form a hydrogen bond with the hydronated N1 nitrogen atom of the PLP pyridine ring causes significant structural reorganization in the active site of the mutated enzyme (Fig. 4.4). PLP molecule is reoriented and new hydrogen bonds are formed between the PLP O3′ atom and the side chains of Asn185 and Thr216, and between the PLP N1 atom and a nearby water molecule that is hydrogen bonded with the side chains of Glu103 and Thr126. The side chains of Asn185 and Glu103 are reoriented, while the helix α4′, including the catalitically important Thr124, is shifted by ≈1.2 Å from the active site cleft. Analysis of the hydrogen bonding network reveals that the PLP N1 atom is a hydrogen bond acceptor, *i.e.* the water molecule donates a hydrogen bond to the dehydronated pyridine nitrogen atom of PLP in the D214A mutant. This observation was also confirmed by the spectroscopic study[154] partially explaining the lack of catalytic activity in the mutant enzyme. Namely, the hydronated pyridine nitrogen atom of PLP should additionally stabilize a negative charge emerged upon Cα dehydronation. The stabilization of the formed carbanionic quinonoid intermediate by the hydronated (and positively charged) PLP N1 atom is possible through the system extended of conjugated π-electrons (Scheme 2.18). If the PLP N1 atom is dehydronated, the quinonoid intermediate cannot be stabilized by the described mechanism and Cα–H acidity of the external aldimine decreases. Another factor which contributes to the inactivity of D214A mutant towards L-tyrosine and 3-fluoro-L-tyrosine is considerable change in the active site conformation. The active site cleft is more closed than in the wild type, and the side chain of catalitically important residue Thr124 is moved by 1.0 Å from PLP. This prevents L-tyrosine molecule from forming a hydrogen bond with Thr124, so this residue cannot stabilize the ketoquinonoid structure and thus facilitate the Cβ–Cγ bond cleavage. The amino acids with good leaving groups are less affected by this conformational change.[154]

6 Conclusions

TPL protein subunit can exist in two different distinct conformations: open and closed. Since there is a transition between the open and closed conformation in the crystalline state of TPL, it is plausible that the same transition also occurs in solution at physiological conditions. The active site closes during the enzymatic reaction. The ketoquinonoid species, which appears to be a transition structure, fits best the active site in the closed conformation. Furthermore, the closure of the active site brings the catalytically important residues Arg381 and Thr124 into position in which they can form direct hydrogen bonds with the quinonoid intermediate thus facilitating a cleavage of the Cβ–Cγ bond in L-tyrosine derivatives and a consecutive abstraction of phenol (or its derivatives). Phe448 forms van der Waals contacts with the substrate's phenol ring and thus destabilizes the key quinonoid intermediate.

F448H TPL mutant shows a very low β-elimination activity towards L-tyrosine because the hydrogen bond formed between substrate's phenolic group and the imidazole ring of His448 stabilizes the closed conformation of the active site, so the active site cannot open to realease the reaction products at the end of the reaction. It is also possible that His448 significantly increases the pK_{a} value of the adjacent Arg381, so the guanidine group of Arg381 cannot act as a catalytic base.

Alanine racemization proceeds by a two-base mechanism involving Lys257 and a water molecule activated by Arg381.

The significant structural rearrangements in the active site of D214A TPL mutant result in the dehydronation of N1 atom of the PLP's pyridine ring switching off the β-elimination activity towards L-tyrosine and its derivatives.

References

1. H. Kumagai, H. Yamada, H. Matsui, H. Ohkishi, and K. Ogata, *J. Biol. Chem.* **245** (1970) 1773–1777.

2. H. Enei, H. Matsui, K. Yamashita, S. Okumura, and H. Yamada, *Agric. Biol. Chem.* **37** (1972) 1861–1868.

3. A. A. Antson, T. V. Demidkina, P. Gollnick, Z. Dauter, R. L. Von Tersch, J. Long, S. N. Berezhnoy, R. S. Phillips, E. H. Harutyunyan, and K. S. Wilson, *Biochemistry* **32** (1993) 4195–4206.

4. B. Sundararaju, A. A. Antson, R. S. Phillips, T. V. Demidkina, M. V. Barbolina, P. Gollnick, G. G. Dodson, and K. S. Wilson, *Biochemistry* **36** (1997) 6502–6510.

5. S. V. Pletnev, A. A. Antson, N. I. Sinitsyna, Z. Dauter, M. N. Isupov, E. N. Hurs, N. G. Faleev, K. S. Wilson, G. Dodson, T. V. Demidkina, and E. G. Arutyunyan, *Crystallogr. Rep.* **42** (1997) 809–819.

6. R. S. Phillips, T. V. Demidkina, and N. G. Faleev, *BBA – Proteins Proteomics* **1647** (2003) 167–172.

7. T. V. Demidkina, A. A. Antson, N. G. Faleev, R. S. Phillips, and L. N. Zakomirdina, *Mol. Biol.* **43** (2009) 269–283.

8. M. D. Toney, *Arch. Biochem. Biophys.* **433** (2005) 279–287.

9. D. M. E. Szebenyi, X. Liu, I. A. Kriksunov, P. J. Stover, and D. J. Thiel, *Biochemistry* **39** (2000) 13313–13323.

10. T. R. M. Barends, T. Domratcheva, V. Kulik, L. Blumenstein, D. Niks, M. F. Dunn, and I. Schlichting, *ChemBioChem* **9** (2008) 1024–1028.

11. A. C. Eliot and J. F. Kirsch, *Annu. Rev. Biochem.* **73** (2004) 383–415.

12. C. A. McPhalen, M. G. Vincent, D. Picot, J. N. Jansonius, A. M. Lesk, and C. Chothia, *J. Mol. Biol.* **227** (1992) 197–213.

13. S.-Y. Ku, P. Yip, and P. L. Howell, *Acta Crystallogr. Sect. D – Biol. Crystallogr.* **62** (2006) 814–823.

14. N. Tsesin, A. Kogan, G. Y. Gdalevsky, J.-P. Himanen, R. Cohen-Luria, A. H. Parola, Y. Goldgur, and O. Almog, *Acta Crystallogr. Sect. D – Biol. Crystallogr.* **63** (2007) 969–974.

15. T. V. Demidkina, M. V. Barbolina, N. G. Faleev, B. Sundararaju, P. D. Gollnick, and R. S. Phillips, *Biochem. J.* **363** (2002) 745–752.

16. S. Mooney, J.-E. Leuendorf, C. Hendrickson, and H. Hellmann, *Molecules* **14** (2009) 329–351.

17. A. Amadasi, M. Bertoldi, R. Contestabile, S. Bettati, B. Cellini, M. L. di Salvo, C. Borri-Voltattorni, F. Bossa, and A. Mozzarelli, *Curr. Med. Chem.* **14** (2007) 1291–1324.

18. M. T. Nakamura and T. Y. Nara, *Annu. Rev. Nutr.* **24** (2004) 345–376.

19. M. Gregoriou, M. E. Noble, K. A. Watson, E. F. Garman, T. M. Krulle, C. de la Fuente, G. W. Fleet, N. G. Oikonomakos, and L. N. Johnson, *Protein Sci.* **7** (1998) 915–927.

20. A. V. Cheltsov, W. C. Guida, and G. C. Ferreira, *J. Biol. Chem.* **278** (2003) 27945–27955.

21. W. H. Rottmann, G. F. Peter, P. W. Oeller, J. A. Keller, N. F. Shen, B. P. Nagy, L. P. Taylor, A. D. Campbell, and A. Theologis, *J. Mol. Biol.* **222** (1991) 937–961.

22. H. C. Dunathan, *Proc. Natl. Acad. Sci. U. S. A.* **55** (1966) 712–716.

23. P. A. Frey, *Annu. Rev. Biochem.* **70** (2001) 121–148.

24. N. B. Livanova, N. A. Chebotareva, T. B. Eronina, and B. I. Kurganov, *Biokhimiya* **67** (2002) 1089–1098.

25. G. Schneider, H. Käck, and Y. Lindqvist, *Structure* **8** (2000) R1–R6.

26. C. C. Hyde, S. A. Ahmed, E. A. Padlan, E. W. Miles, and D. R. Davies, *J. Biol. Chem.* **263** (1988) 17857–17871.

27. S. Rhee, K. D. Parris, S. A. Ahmed, E. W. Miles, and D. R. Davies, *Biochemistry* **35** (1996) 4211–4221.

28. J. P. Shaw, G. A. Petsko, and D. Ringe, *Biochemistry* **36** (1997) 1329–1342.

29. S. Sugio, G. A. Petsko, J. M. Manning, K. Soda, and D. Ringe, *Biochemistry* **34** (1995) 9661–9669.

30. Y. Kakihara and K. Ichihara, *Med. J. Osaka Univ.* **3** (1953) 497–507.

31. M. Uchida, Y. Takemoto, Y. Kakihara, and K. Ichihara, *Med. J. Osaka Univ.* **3** (1953) 509–519.

32. H. Yoshimatsu, *Med. J. Osaka Univ.* **9** (1957) 727–731.

33. N. Brot, Z. Smit, and H. Weissbach, *Arch. Biochem. Biophys.* **112** (1965) 1–6.

34. S. S. Duffey, J. R. Aldrich, and M. S. Blum, *Comp. Biochem. Physiol.* **56B** (1977) 101–102.

35. S. Duffey and M. Blum, *Insect Biochem.* **7** (1977) 57–65.

36. R. D. Fleischmann, M. D. Adams, O. White, R. A. Clayton, E. F. Kirkness, A. R. Kerlavage, C. J. Bult, J. F. Tomb, B. A. Dougherty, J. M. Merrick, K. McKenney, G. Sutton, W. FitzHugh, C. Fields, J. D. Gocayne, J. Scott, R. Shirley, L. I. Liu, A. Glodek, J. M. Kelley, J. F. Weidman, C. A. Phillips, T. Spriggs, E. Hedblom, M. D. Cotton, T. R. Utterback, M. C. Hanna, D. T. Nguyen, D. M. Saudek, R. C. Brandon, L. D. Fine, J. L. Frichman, J. L. Fuhrmann, N. S. M. Geoghagen, C. L. Gnehm, L. A. McDonald, K. V. Small, C. M. Fraser, H. O. Smith, and J. C. Venter, *Science* **269** (1995) 496–512.

37. Y. Kurusu, M. Fukushima, K. Kohama, M. Kobayashi, M. Terasawa, H. Kumagai, and H. Yukawa, *Biotechnol. Lett.* **13** (1991) 769–772.

38. S. Iwamori, S. Yoshino, K.-I. Ishiwata, and N. Makiguchi, *J. Ferment. Bioeng.* **72** (1991) 147–151.

39. H. Suzuki, K. Nishihara, N. Usui, H. Matsui, and H. Kumagai, *J. Ferment. Bioeng.* **75** (1993) 145–148.

40. F. Foor, N. Morin, and K. A. Bostian, *Appl. Environ. Microbiol.* **59** (1993) 3070–3075.

41. T. Hirahara, S. Horinouchi, and T. Beppu, *Appl. Microbiol. Biotechnol.* **39** (1993) 341–346.

42. S. F. Altschul, W. Gish, W. Miller, E. W. Myers, and D. J. Lipman, *J. Mol. Biol.* **215** (1990) 403–410.

43. T. Nagasawa, T. Ishii, and H. Yamada, *FEMS Microbiol. Lett.* **30** (1985) 269–272.

44. H. Enei, K. Yamashita, S. Okumura, and H. Yamada, *Agric. Biol. Chem.* **37** (1973) 485–492.

45. H. Q. Smith and R. L. Somerville, *J. Bacteriol.* **179** (1997) 5914–5921.

46. T. Katayama, H. Suzuki, K. Yamamoto, and H. Kumagai, *Biosci. Biotechnol. Biochem.* **63** (1999) 1823–1827.

47. H. Kumagai, H. Yamada, H. Matsui, H. Ohkishi, and K. Ogata, *J. Biol. Chem.* **245** (1970) 1767–1772.

48. H. Chen and R. S. Phillips, *Biochemistry* **32** (1993) 11591–11599.

49. H. Chen, P. Gollnick, and R. S. Phillips, *Eur. J. Biochem.* **229** (1995) 540–549.

50. N. G. Faleev, S. B. Ruvinov, T. V. Demidkina, I. V. Myagkikh, M. Y. Gololobov, V. I. Bakhmutov, and V. M. Belikov, *Eur. J. Biochem.* **177** (1988) 395–401.

51. H. Yamada and H. Kumagai, *Adv. Appl. Microbiol.* **19** (1975) 249–288.

52. H. Y. Chen, T. V. Demidkina, and R. S. Phillips, *Biochemistry* **34** (1995) 12276–12283.

53. R. S. Phillips, *Arch. Biochem. Biophys.* **256** (1987) 302–310.

54. N. Faleev, N. Martinkova, M. Sadovnikova, M. Saporovskaya, and V. Belikov, *Enzyme Microb. Technol.* **1** (1979) 269–272.

55. T. Nagasawa, T. Utagawa, J. Goto, C. Kim, Y. Tani, H. Kumagai, and H. Yamada, *Eur. J. Biochem.* **117** (1981) 33–40.

56. N. G. Faleev, Y. N. Zhukov, E. N. Khurs, O. I. Gogoleva, M. V. Barbolina, N. P. Bazhulina, V. M. Belikov, T. V. Demidkina, and R. M. Khomutov, *Eur. J. Biochem.* **267** (2000) 6897–6902.

57. H. Enei, H. Nakazawa, H. Matsui, S. Okumura, and H. Yamada, *FEBS Lett.* **21** (1972) 39–41.

58. H. Yamada, H. Kumagai, N. Kashima, H. Torii, H. Enei, and S. Okumura, *Biochem. Biophys. Res. Commun.* **46** (1972) 370–374.

59. S.-G. Lee, H.-S. Ro, S.-P. Hong, E.-H. Kim, and M.-H. Sung, *J. Microbiol. Biotechnol.* **6** (1996) 98–102.

60. E. B. Watkins and R. S. Phillips, *Bioorg. Med. Chem. Lett.* **11** (2001) 2099–2100.

61. Y. Monden, F. Hamano-Takaku, N. Shindo-Okada, and S. Nishimura, in: H. Maruta (Ed.), *Anticancer Molecules: Structure, Function, and Design*, New York Acad Sciences, New York, *Annals of the New York Academy of Sciences*, Vol. 886 (1999) pp. 109–121.

62. K. Yamano and H. Shirahama, *Tetrahedron* **48** (1992) 1457–1464.

63. E. B. Watkins and R. S. Phillips, *Biochemistry* **40** (2001) 14862–14868.

64. R. L. Von Tersch, E. Secundo, R. S. Phillips, and M. G. Newton, in: I. Ojima, J. R. McCarthy, and J. T. Welch (Eds.), *Biomedical frontiers of fluorine chemistry*, ACS Symposium Series, American Chemical Society, Washington, DC, Vol. 639 (1996) pp. 95–104.

65. D. Hebel, D. C. Furlano, R. S. Phillips, S. Koushik, C. R. Creveling, and K. L. Kirk, *Bioorg. Med. Chem. Lett.* **2** (1992) 41–44.

66. S. Kaneko, K. Ishiwata, K. Hatano, H. Omura, K. Ito, and M. Senda, *Appl. Radiat. Isot.* **50** (1999) 1025–1032.

67. P. Bjurling, P. Malmborg, and B. Langström, *J. Labelled Compd. Radiopharm.* **30** (1991) 399–400.

68. R. Torstenson, J. Tedroff, P. Hartvig, K.-J. Fasth, and B. Langström, *J. Cereb. Blood Flow Metab.* **19** (1999) 1142–1149.

69. K. Kim and P. A. Cole, *Bioorg. Med. Chem. Lett.* **9** (1999) 1205–1208.

70. E. Nicolás, K. C. Russell, J. Knollenberg, and V. J. Hruby, *J. Org. Chem.* **58** (1993) 7565–7571.

71. H. Kumagai, H. Matsui, H. Ohgishi, K. Ogata, H. Yamada, T. Ueno, and H. Fukami, *Biochem. Biophys. Res. Commun.* **34** (1969) 266–270.

72. H. Enei, H. Matsui, H. Nakazawa, S. Okumura, and H. Yamada, *Agric. Biol. Chem.* **37** (1973) 493–499.

73. T. Ueno, H. Fukami, H. Ohkishi, H. Kumagai, and H. Yamada, *BBA – Enzymology* **206** (1970) 476–479.

74. P. Rapp, H. Kumagai, H. Yamada, T. Ueno, and H. Fukami, *Biochem. Biophys. Res. Commun.* **64** (1975) 241–247.

75. R. S. Phillips, K. Ravichandran, and R. L. Von Tersch, *Enzyme Microb. Technol.* **11** (1989) 80–83.

76. R. S. Phillips, J. G. Fletcher, R. L. V. Tersch, and K. L. Kirk, *Arch. Biochem. Biophys.* **276** (1990) 65–69.

77. H. Kumagai, N. Kashima, and H. Yamada, *Biochem. Biophys. Res. Commun.* **39** (1970) 796–801.

78. H. Kumagai, T. Utagawa, and H. Yamada, *J. Biol. Chem.* **250** (1975) 1661–1667.

79. M. M. Palcic, S. J. Shen, E. Schleicher, H. Kumagai, S. Sawada, H. Yamada, and H. G. Floss, *Z. Naturforsch.* **42C** (1987) 307–318.

80. T. V. Demidkina, I. V. Myagkikh, and A. V. Azhayev, *Eur. J. Biochem.* **170** (1987) 311–316.

81. B. Mouratou, P. Kasper, H. Gehring, and P. Christen, *J. Biol. Chem.* **274** (1999) 1320–1325.

82. H. Yamada, H. Kumagai, H. Matsui, H. Ohkihhi, and K. Ogata, *Biochem. Biophys. Res. Commun.* **33** (1968) 10–14.

83. T. Demidkina, I. Myagkikh, A. Antson, and E. Harutyunyan, *FEBS Lett.* **232** (1988) 381–382.

84. M. B. Sherman, A. A. Antson, E. V. Orlova, O. N. Zograf, and T. V. Demidkina, *Dokl. Akad. Nauk USSR* **312** (1990) 1256–1258.

85. A. A. Antson, B. V. Strokopytov, G. N. Murshudov, M. N. Isupov, E. H. Harutyunyan, T. V. Demidkina, D. G. Vassylyev, Z. Dauter, H. Terry, and K. S. Wilson, *FEBS Lett.* **302** (1992) 256–260.

86. B. Mikami, Y. Yamamoto, T. Katayama, H. Suzuki, and H. Kumagai, The Structure of Tyrosine Phenol-lyase from *Erwinia herbicola* (2000), PDB code: 1C7G, DOI: http://dx.doi.org/10.2210/pdb1c7g/pdb.

87. V. K. Kazakov, I. I. Tarusina, I. V. Myagkikh, and T. V. Demidkina, *Biokhimiya* **52** (1987) 1319–1323.

88. A. A. Antson, G. G. Dodson, K. S. Wilson, S. V. Pletnev, E. G. Harutyunyan, and T. V. Demidkina, in: G. Marino, G. Sannia, and F. Bossa (Eds.), *Biochemistry of Vitamin B6 and PQQ*, Birkhäuser Verlag, Basel (1994) pp. 187–191.

89. J. F. Kirsch, G. Eichele, G. C. Ford, M. G. Vincent, J. N. Jansonius, H. Gehring, and P. Christen, *J. Mol. Biol.* **174** (1984) 497–525.

90. J. N. Jansonius, *Curr. Opin. Struct. Biol.* **8** (1998) 759–769.

91. H. Käck, J. Sandmark, K. Gibson, G. Schneider, and Y. Lindqvist, *J. Mol. Biol.* **291** (1999) 857–876.

92. W. Kabsch and C. Sander, *Biopolymers* **22** (1983) 2577–2637.

93. P. Gouet, X. Robert, and E. Courcelle, *Nucleic Acids Res.* **31** (2003) 3320–3323.

94. C. A. Orengo, A. D. Michie, S. Jones, D. T. Jones, M. B. Swindells, and J. M. Thornton, *Structure* **5** (1997) 1093–1108.

95. A. L. Cuff, I. Sillitoe, T. Lewis, O. C. Redfern, R. Garratt, J. Thornton, and C. A. Orengo, *Nucleic Acids Res.* **37** (2009) D310–D314.

96. J. S. Richardson, *Nature* **268** (1977) 495–500.

97. V. V. Borisov, S. N. Borisova, N. I. Sosfenov, and B. K. Vainshtein, *Nature* **284** (1980) 189–190.

98. G. C. Ford, G. Eichele, and J. N. Jansonius, *Proc. Natl. Acad. Sci. U. S. A.* **77** (1980) 2559–2563.

99. T. Toraya, T. Nihira, and S. Fukui, *Eur. J. Biochem.* **69** (1976) 411–419.

100. T. V. Demidkina and I. V. Myagkikh, *Biochimie* **71** (1989) 565–571.

101. N. P. Bazhulina, Y. V. Morozov, A. I. Papisova, and T. V. Demidkina, *Eur. J. Biochem.* **267** (2000) 1830–1836.

102. B. S. Axelsson, P. Bjurling, O. Matsson, and B. Langström, *J. Am. Chem. Soc.* **114** (1992) 1502–1503.

103. N. G. Faleev, S. N. Spirina, T. V. Demidkina, and R. S. Phillips, *J. Chem. Soc., Perkin Trans. 2* **1996** (1996) 2001–2004.

104. R. S. Phillips, H. Y. Chen, and N. G. Faleev, *Biochemistry* **45** (2006) 9575–9583.

105. D. M. Kiick and R. S. Phillips, *Biochemistry* **27** (1988) 7333–7338.

106. M. V. Barbolina, R. S. Phillips, P. D. Gollnick, N. G. Faleev, and T. V. Demidkina, *Protein Eng.* **13** (2000) 207–215.

107. T. Lütke-Eversloh, C. N. S. Santos, and G. Stephanopoulos, *Appl. Microbiol. Biotechnol.* **77** (2007) 751–762.

108. T. Koyanagi, T. Katayama, H. Suzuki, H. Nakazawa, K. Yokozeki, and H. Kumagai, *J. Biotechnol.* **115** (2005) 303–306.

109. B. Seisser, R. Zinkl, K. Gruber, F. Kaufmann, A. Hafner, and W. Kroutil, *Adv. Synth. Catal.* **352** (2010) 731–736.

110. H. Enei, H. Nakazawa, S. Okumura, and H. Yamada, *Agric. Biol. Chem.* **37** (1973) 725–735.

111. I. V. Tysyachnaya, V. I. Yakovleva, M. B. Kupletskaya, and I. V. Berezin, *Biokhimiya* **44** (1979) 1739–1744.

112. K. I. Voivodov, I. V. Tysyachnaya, L. S. Gubnitskii, V. I. Yakovleva, and I. V. Berezin, *Appl. Biochem. Microbiol.* **21** (1985) 127–131.

113. G. Para, P. Lucciardi, and J. Baratti, *Appl. Microbiol. Biotechnol.* **21** (1985) 273–279.

114. G. Para and J. Baratti, *Appl. Microbiol. Biotechnol.* **28** (1988) 222–228.

115. I. Lloyd-George and T. M. S. Chang, *Biotechnol. Bioeng.* **48** (1995) 706–714.

116. S. Fukui, S.-i. Ikeda, M. Fujimura, H. Yamada, and H. Kumagai, *Eur. J. Biochem.* **51** (1975) 155–164.

117. S. Fukui, S. Ikeda, M. Fujimura, H. Yamada, and H. Kumagai, *Eur. J. Appl. Microbiol.* **1** (1975) 25–39.

118. T. K. Lee and H.-y. Hsiao, *Enzyme Microb. Technol.* **8** (1986) 523–526.

119. H.-S. Park, J.-Y. Lee, and H.-S. Kim, *Biotechnol. Bioeng.* **58** (1998) 339–343.

120. D. Y. Kim, E. Rha, S.-L. Choi, J. J. Song, S.-P. Hong, M.-H. Sung, and S.-G. Lee, *J. Microbiol. Biotechnol.* **17** (2007) 116–122.

121. J. H. Kim, J. J. Song, B. G. Kim, M. H. Sung, and S. C. Lee, *J. Microbiol. Biotechnol.* **14** (2004) 153–157.

122. S.-G. Lee, S.-P. Hong, D. Y. Kim, J. J. Song, H.-S. Ro, and M.-H. Sung, *FEBS J.* **273** (2006) 5564–5573.

123. E. Rha, S. Kim, S.-L. Choi, S.-P. Hong, M.-H. Sung, J. J. Song, and S.-G. Lee, *FEBS J.* **276** (2009) 6187–6194.

124. S.-G. Lee, S.-P. Hong, and M.-H. Sung, *Enzyme Microb. Technol.* **19** (1996) 374 – 377.

125. S.-G. Lee, S.-P. Hong, and M.-H. Sung, *Enzyme Microb. Technol.* **25** (1999) 298–302.

126. N. J. P. Wierckx, H. Ballerstedt, J. A. M. de Bont, and J. Wery, *Appl. Environ. Microbiol.* **71** (2005) 8221–8227.

127. G. G. Meadows, J. DiGiovanni, L. Minor, and G. W. Elmer, *Cancer Res.* **36** (1976) 167–171.

128. G. G. Meadows and G. W. Elmer, *Res. Commun. Chem. Pathol. Pharmacol.* **19** (1978) 513–527.

129. H. F. Pierson and G. G. Meadows, *Biochim. Biophys. Acta – Gen. Subj.* **676** (1981) 177–186.

130. W. A. Wood, I. C. Gunsalus, and W. W. Umbreit, *J. Biol. Chem.* **170** (1947) 313–321.

131. T. Watanabe and E. E. Snell, *Proc. Natl. Acad. Sci. U. S. A.* **69** (1972) 1086–1090.

132. W. A. Newton, Y. Morino, and E. E. Snell, *J. Biol. Chem.* **240** (1965) 1211–1218.

133. H. Yoshida, T. Utagawa, H. Kumagai, and H. Yamada, *Agric. Biol. Chem.* **38** (1974) 2065–2072.

134. E. E. Snell, in: M. Alton (Ed.), *Adv. Enzymol. Relat. Areas Mol. Biol.*, Vol. 42 (1975) pp. 287–333.

135. T. Watanabe and E. E. Snell, *J. Biochem.* **82** (1977) 733–745.

136. C. H. Suelter, J. Wang, and E. E. Snell, *Anal. Biochem.* **76** (1976) 221–232.

137. A. Shimada, H. Shishido, and I. Nakamura, *Amino Acids* **11** (1996) 83–89.

138. A. Shimada, H. Kogure, H. Shishido, and I. Nakamura, *Amino Acids* **12** (1997) 379–383.

139. A. Shimada, H. Ozaki, T. Saito, and F. Noriko, *Int. J. Mol. Sci.* **10** (2009) 2578–2590.

140. D. Blankenhorn, J. Phillips, and J. L. Slonczewski, *J. Bacteriol.* **181** (1999) 2209–2216.

141. D. Wang, X. Ding, and P. N. Rather, *J. Bacteriol.* **183** (2001) 4210–4216.

142. P. Di Martino, R. Fursy, L. Bret, B. Sundararaju, and R. S. Phillips, *Can. J. Microbiol.* **49** (2003) 443–449.

143. R. S. Mueller, D. McDougald, D. Cusumano, N. Sodhi, S. Kjelleberg, F. Azam, and D. H. Bartlett, *J. Bacteriol.* **189** (2007) 5348–5360.

144. E. L. Chant and D. K. Summers, *Mol. Microbiol.* **63** (2007) 35–43.

145. R. Scherzer, G. Y. Gdalevsky, Y. Goldgur, R. Cohen-Luria, S. Bittner, and A. H. Parola, *J. Enzym. Inhib. Med. Chem.* **24** (2009) 350–355.

146. M. N. Isupov, A. A. Antson, E. J. Dodson, G. G. Dodson, I. S. Dementieva, L. N. Zakomirdina, K. S. Wilson, Z. Dauter, A. A. Lebedev, and E. H. Harutyunyan, *J. Mol. Biol.* **276** (1998) 603–623.

147. A. Kogan, G. Y. Gdalevsky, R. Cohen-Luria, Y. Goldgur, R. S. Phillips, A. H. Parola, and O. Almog, *BMC Struct. Biol.* **9** (2009) 65.

148. A. G. Murzin, S. E. Brenner, T. Hubbard, and C. Chothia, *J. Mol. Biol.* **247** (1995) 536–540.

149. T. V. Demidkina, L. N. Zakomirdina, V. V. Kulikova, I. S. Dementieva, N. G. Faleev, L. Ronda, A. Mozzarelli, P. D. Gollnick, and R. S. Phillips, *Biochemistry* **42** (2003) 11161–11169.

150. D. M. Kiick and R. S. Phillips, *Biochemistry* **27** (1988) 7339–7344.

151. V. V. Kulikova, L. N. Zakomirdina, I. S. Dementieva, R. S. Phillips, P. D. Gollnick, T. V. Demidkina, and N. G. Faleev, *BBA – Proteins Proteomics* **1764** (2006) 750–757.

152. R. S. Phillips, N. Johnson, and A. V. Kamath, *Biochemistry* **41** (2002) 4012–4019.

153. R. S. Phillips, B. Sundararaju, and N. G. Faleev, *J. Am. Chem. Soc.* **122** (2000) 1008–1014.

154. T. Demidkina, N. Faleev, A. Papisova, N. Bazhulina, V. Kulikova, P. Gollnick, and R. Phillips, *BBA – Proteins Proteomics* **1764** (2006) 1268–1276.

155. A. M. Brzozowski and S. P. Tolley, *Acta Crystallogr. Sect. D – Biol. Crystallogr.* **50** (1994) 466–468.

156. R. S. Phillips, T. V. Demidkina, L. N. Zakomirdina, S. Bruno, L. Ronda, and A. Mozzarelli, *J. Biol. Chem.* **277** (2002) 21592–21597.

157. Z. Otwinowski and W. Minor, *Methods Enzymol.* **276** (1997) 307–326.

158. Collaborative Computational Project, Number 4, *Acta Crystallogr. Sect. D – Biol. Crystallogr.* **50** (1994) 760–763.

159. J. Navaza, *Acta Crystallogr. Sect. A* **50** (1994) 157–163.

160. A. J. McCoy, R. W. Grosse-Kunstleve, P. D. Adams, M. D. Winn, L. C. Storoni, and R. J. Read, *J. Appl. Crystallogr.* **40** (2007) 658–674.

161. P. Emsley and K. Cowtan, *Acta Crystallogr. Sect. D – Biol. Crystallogr.* **60** (2004) 2126–2132.

162. A. Perrakis, R. Morris, and V. S. Lamzin, *Nat. Struct. Biol.* **6** (1999) 458–463.

163. G. N. Murshudov, A. A. Vagin, and E. J. Dodson, *Acta Crystallogr. Sect. D – Biol. Crystallogr.* **53** (1997) 240–255.

164. M. D. Winn, M. N. Isupov, and G. N. Murshudov, *Acta Crystallogr. Sect. D – Biol. Crystallogr.* **57** (2001) 122–133.

165. R. A. Laskowski, M. W. MacArthur, D. S. Moss, and J. M. Thornton, *J. Appl. Crystallogr.* **26** (1993) 283–291.

166. I. W. Davis, A. Leaver-Fay, V. B. Chen, J. N. Block, G. J. Kapral, X. Wang, L. W. Murray, I. Arendall, W. Bryan, J. Snoeyink, J. S. Richardson, and D. C. Richardson, *Nucleic Acids Res.* **35** (2007) W375–383.

167. D. Cruickshank, *Acta Crystallogr. Sect. D – Biol. Crystallogr.* **55** (1999) 583–601.

168. B. W. Matthews, *J. Mol. Biol.* **33** (1968) 491–497.

169. C. Ramakrishnan and G. N. Ramachandran, *Biophys. J.* **5** (1965) 909–933.

170. J. Hašek, *Z. Kristallogr. Suppl.* **23** (2006) 613–618.

171. G. Sheldrick, *Acta Crystallogr. Sect. A* **64** (2008) 112–122.

172. G. Kleywegt, *Acta Crystallogr. Sect. D – Biol. Crystallogr.* **52** (1996) 842–857.

173. S. Hayward and H. J. C. Berendsen, *Proteins* **30** (1998) 144–154.

174. E. Krissinel and K. Henrick, *J. Mol. Biol.* **372** (2007) 774–797.

175. G. Jones, P. Willett, R. C. Glen, A. R. Leach, and R. Taylor, *J. Mol. Biol.* **267** (1997) 727–748.

176. M. L. Verdonk, J. C. Cole, M. J. Hartshorn, C. W. Murray, and R. D. Taylor, *Proteins: Structure, Function, and Genetics* **52** (2003) 609–623.

177. W. L. DeLano, The PyMOL Molecular Graphics System, DeLano Scientific, Palo Alto, CA, USA (http://www.pymol.org) (2002).

178. T. Schneider, *Acta Crystallogr. Sect. D – Biol. Crystallogr.* **58** (2002) 195–208.

179. R. Read, *Acta Crystallogr. Sect. A* **42** (1986) 140–149.

180. A. P. Dubnovitsky, R. B. G. Ravelli, A. N. Popov, and A. C. Papageorgiou, *Protein Sci.* **14** (2005) 1498–1507.

181. T. Muro, H. Nakatani, K. Hiromi, H. Kumagai, and H. Yamada, *J. Biochem.* **84** (1978) 633–640.

182. N. G. Faleev, A. E. Lyubarev, N. S. Martinkova, and V. M. Belikov, *Enzyme Microb. Technol.* **5** (1983) 219–224.

183. V. I. Ivanov and M. Y. Karpeisky, *Adv. Enzymol. Relat. Areas Mol. Biol.* **32** (1969) 21–53.

184. R. S. Phillips, R. L. Von Tersch, and F. Secundo, *Eur. J. Biochem.* **244** (1997) 658–663.

185. F. Allen, *Acta Crystallogr. Sect. B – Struct. Sci.* **58** (2002) 380–388.

186. H. Elhamzaoui, B. Jousseaume, T. Toupance, and H. Allouchi, *Organometallics* **26** (2007) 3908–3917.

187. Z. Xu, D. B. Mitzi, C. D. Dimitrakopoulos, and K. R. Maxcy, *Inorg. Chem.* **42** (2003) 2031–2039.

188. H. Wynberg, W. C. Nieuwpoort, and H. T. Jonkman, *Tetrahedron Lett.* **14** (1973) 4623–4628.

189. F. Dijkstra and J. H. Van Lenthe, *Int. J. Quantum Chem.* **74** (1999) 213–221.

190. O. V. Shishkin, K. Y. Pichugin, L. Gorb, and J. Leszczynski, *J. Mol. Struct.* **616** (2002) 159–166.

191. Y. Endo, C. Songkram, K. Ohta, P. Kaszynski, and K. Yamaguchi, *Tetrahedron Lett.* **46** (2005) 699–702.

192. A. Datta and S. K. Pati, *Chem. Phys. Lett.* **433** (2006) 67–70.

193. F. Feixas, E. Matito, J. Poater, and M. Sola, *J. Phys. Chem. A* **111** (2007) 4513–4521.

194. R. S. Phillips, H. Y. Chen, D. Shim, S. Lima, K. Tavakoli, and B. Sundararaju, *Biochemistry* **43** (2004) 14412–14419.

195. B. Sundararaju, H. Chen, S. Shilcutt, and R. S. Phillips, *Biochemistry* **39** (2000) 8546–8555.

196. C. H. Suelter and E. E. Snell, *J. Biol. Chem.* **252** (1977) 1852–1857.

197. T. Erez, G. Y. Gdalevsky, Y. M. Torchinsky, R. S. Phillips, and A. H. Parola, *BBA – Protein Struct. Mol. Enzymol.* **1384** (1998) 365–372.

198. K. D. Schnackerz, J. Keller, R. S. Phillips, and M. D. Toney, *BBA – Proteins Proteomics* **1764** (2006) 230–238.

199. A. I. Papisova, N. P. Bazhulina, N. G. Faleev, and T. V. Demidkina, *Dokl. Biochem. Biophys.* **391** (2003) 225–228.

200. N. G. Faleev, in: V. N. Uversky (Ed.), *Protein structures. Kaleidoscope of structural properties and structures*, Research Signpost, Kerala, India (2003) pp. 3–86.

201. B. Pioselli, S. Bettati, T. V. Demidkina, L. N. Zakomirdina, R. S. Phillips, and A. Mozzarelli, *Protein Sci.* **13** (2004) 913–924.

202. C. G. F. Stamper, A. A. Morollo, and D. Ringe, *Biochemistry* **37** (1998) 10438–10445.

203. S. Sun and M. D. Toney, *Biochemistry* **38** (1999) 4058–4065.

204. A. Watanabe, T. Yoshimura, B. Mikami, and N. Esaki, *J. Biochem.* **126** (1999) 781–786.

205. N. G. Faleev, T. V. Demidkina, M. A. Tsvetikova, R. S. Phillips, and I. A. Yamskov, *Eur. J. Biochem.* **271** (2004) 4565–4571.

List of Abbreviations

L-DOPA 3,4-dihydroxyphenyl-L-alanine

AA α-aminoacrylate

AMP adenosine monophosphate

AP ammonium pyruvate

AspAT aspartate aminotransferase

CATH Class, Architecture, Topology, Homologous Superfamily (the CATH database is a hierarchical domain classification of protein structures in the Protein Data Bank)

CCD charge-coupled device

CSD Cambridge Structural Database

DPI diffraction-component precision index

DTT dithiotreitol

EA external aldimine

EC Enzyme Commission

EMBL European Molecular Biology Laboratory

ESRF European Synchrotron Radiation Facility

F448H TPL–F-Tyr F448H tyrosine phenol-lyase complexed with 3-fluoro-L-tyrosine

HEPES 2-[4-(2-hydroxyethyl)piperazin-1-yl]ethanesulfonic acid

IA internal aldimine

IUPAC International Union of Pure and Applied Chemistry

KQ ketoquinonoid

MME monomethyl ether

p. part

PDB Protein Data Bank

PEG poly(ethylene glycol)

PL pyridoxal

PLP pyridoxal 5′-phosphate

PM pyridoxamine

PMP pyridoxamine 5′-phosphate

PN pyridoxine

PNP pyridoxine 5′-phosphate

PPT *N*-(5′-phosphopyridoxyl)-L-tyrosine

Q quinonoid

r. r. rigid region(s)

r.m.s. root mean square

s.u. standard uncertainty

SAS solvent accessible surface

SCOP Structural Classification of Proteins

SOPC *S*-(*o*-nitrophenyl)-L-cysteine

TLS Translation Libration Screw-motion

TPL tyrosine phenol-lyase

TPL (AP) holo-TPL soaked in the ammonium pyruvate solution

TPL (phenol) holo-TPL soaked in the phenol solution

TPL–Ala tyrosine phenol-lyase complexed with L-alanine

TPL–Ala–PNO tyrosine phenol-lyase complexed with L-alanine and pyridine *N*-oxide

TPL–Met tyrosine phenol-lyase complexed with L-methionine

Trpase tryptophan indole-lyase

Y71F TPL–F-Tyr Y71F tyrosine phenol-lyase complexed with 3-fluoro-L-tyrosine

List of Tables

List of Schemes

List of Figures

Curriculum Vitae

Name:	Dalibor Milić
Date of birth:	February 8, 1981
Place of birth:	Zagreb, Croatia

Academic Degree:

2003	Diploma Degree in Chemistry, Faculty of Science, University of Zagreb, Croatia Diploma Thesis: "Y71F tyrosine phenol-lyase from *Citrobacter freundii* complexed with 3-fluoro-L-tyrosine" (original in Croatian; *supervisor*: Prof. Dubravka Matković-Čalogović)

Education:

2004 – present	Dr. Sc. student in Chemistry, Faculty of Science, University of Zagreb, Croatia (*supervisors*: Prof. Dubravka Matković-Čalogović and Dr. Alfred A. Antson)
1999 – 2003	Undergraduate student in Chemistry, Faculty of Science, University of Zagreb, Croatia
1995 – 1999	High school (*V. gimnazija*, Zagreb, Croatia)
1987 – 1995	Elementary school (Zagreb, Croatia)

Employment History:

2008 – present	Research/Teaching Assistant, Laboratory of General and Inorganic Chemistry, Department of Chemistry, Faculty of Science, University of Zagreb, Croatia
[2007 – 2008	8 months spent in the civilian service (as an alternative for the compulsory military service)]
2004 – 2007	Research/Teaching Assistant, Laboratory of General and Inorganic Chemistry, Department of Chemistry, Faculty of Science, University of Zagreb, Croatia

Achievements/Awards:

2003	Honor awarded by the Council of the Faculty of Science, University of Zagreb, for extraordinary study achievements
2001 – 2003	Fellowship awarded by the City of Zagreb
2001	University of Zagreb Rector's Award for student research entitled "Selected Schiff Bases and Their Complexes with Zinc(II) Chloride: Preparation and Characterization" (original in Croatian; *supervisor*: Prof. Zora Popović)
1999	Second Place in the Croatian National Chemistry Contest for high-school students
1998 – 1999	Fellowship awarded by the City of Zagreb
1998	First Place in the Croatian National Chemistry Contest for high-school students

Additional Training:

2004 – 2008	each year spent 1–4 weeks in the York Structural Biology Laboratory, University of York, UK (Dr. Antson's group)
2005	International School of Crystallography, 37th Course, a Nato ASI and a EuroSummerSchool: Evolving Methods for Macromolecular Crystallography, Erice, Italy, May 12–22, 2005
2004	EMBO workshop "3D Structure Databases – Uses for Biological Problem Solving", Cambridge, UK, September 19–24, 2004
2003	8th International Summer School on Biophysics "Supramolecular Structure and Function", Rovinj, Croatia, September 14–26, 2003

Experience in Formal Teaching:

Teaching Assistant for undergraduate courses (Faculty of Science, University of Zagreb):

- Laboratory Exercises in General and Inorganic Chemistry (*for students in Biology, Ecology, Physics, Geology and Geography*),
- Bioinorganic Chemistry (*seminar for students in Chemistry and Molecular Biology*),
- Laboratory Exercises in General Chemistry (*for students in Chemistry*),
- Methods in Chemistry Teaching (*seminar for students in Chemistry, Biology and Chemistry, Physics and Chemistry*),
- Laboratory Exercises in General Chemistry 1 (*for students in Chemistry*),
- Laboratory Exercises in General Chemistry 2 (*for students in Chemistry*),
- General and Inorganic Chemistry (*seminar for students in Physics, Geophysics, Physics and Polytechnics, Physics and Informatics*),
- General Chemistry (*seminar for students in Chemistry*),
- Laboratory Exercises in Inorganic Chemistry (*Single Crystal X-ray Diffraction Method Tutorial for students in Chemistry*),
- General Chemistry (*laboratory exercises for students in Environmental Science*),
- Advanced Laboratory Exercises in Inorganic Chemistry (*Single Crystal X-ray Structural Analysis Tutorial for students in Chemistry*),
- Introduction to Inorganic Chemistry (*laboratory exercises for students in Environmental Science*).

Trained and directed 11 undergraduate students during their research for diploma thesis.

Membership in Professional Affiliations:

Croatian Chemical Society (from 2001)
Croatian Crystallographic Association (from 2005)
American Chemical Society (from 2007)

Scientific Publications:

19. S. Jamali, Z. Mazloomi, S. M. Nabavizadeh, D. Milić, R. Kia, and M. Rashidi, Cyclometalated Cluster Complex with a Butterfly-Shaped Pt_2Ag_2 Core, *Inorg. Chem.* **49** (2010) 2721–2726.

18. V. Mirkhani, R. Kia, D. Milić, A. Rostami Vartooni, and D. Matković-Čalogović, Synthesis, spectroscopic studies and crystal structures of $Re(I)(CO)_3(NN)Cl$ complexes with *N*,*N*′-bis(substituted benzylidene)ethane-1,2-diamine Schiff base ligands, *Transition Met. Chem.* **35** (2010) 81–87.

17. D. Milić, M. Alešković, D. Matković-Čalogović, and K. Mlinarić-Majerski, (1-Adamantyl)methyl esters: whole-molecule disorder in the crystal structure of (1-adamantyl)methyl-1-adamantanecarboxylate, *Croat. Chem. Acta* **82** (2009) 833–839.

16. M. Rubčić, D. Milić, G. Horvat, I. Đilović, N. Galić, V. Tomišić, and M. Cindrić, Vanadium-Induced Formation of Thiadiazole and Thiazoline Compounds. Mononuclear and Dinuclear Oxovanadium(V) Complexes with Open-Chain and Cyclized Thiosemicarbazone Ligands, *Dalton Trans.* (2009) 9914–9923.

15. J. Bauer, D. Milić, and M. Modrić, Three quinolone compounds featuring $O \cdots I$ halogen bonding, *Acta Crystallogr. Sect. C – Cryst. Struct. Commun.* **65** (2009) o512–o516.

14. D. Milić, Ž. Soldin, G. Giester, Z. Popović, and D. Matković-Čalogović, Crystal Structure of the First Polymeric Tetramercurated Methane Derivative of Hofmann's Base, *Croat. Chem. Acta* **82** (2009) 337−344.

13. V. Vrdoljak, D. Milić, M. Cindrić, D. Matković-Čalogović, J. Pisk, M. Marković, and P. Novak, Synthesis, Structure and Characterization of Dinuclear Pentacoordinate Molybdenum(V) Complexes with Thiosemicarbazone Ligands, *Z. Anorg. Allg. Chem.* **635** (2009) 1242−1248.

12. D. Milić, V. Vrdoljak, D. Matković-Čalogović, and M. Cindrić, Synthesis and structure of *cis*-dioxo(3-methoxysalicylaldehyde 4-methylthiosemicarbazonato-*N*,*O*,*S*)(γ-picoline-*N*)molybdenum(VI), *J. Chem. Crystallogr.* **39** (2009) 553−557.

11. V. Mirkhani, R. Kia, A. Rostami Vartooni, and D. Milić, Tricarbonylrhenium(I) complexes with *N*,*N*′-bis(2- and 4-nitrobenzaldehyde)-1,2-diiminoethane Schiff base ligands: synthesis, spectroscopic and crystal structure studies, *Transition Met. Chem.* **34** (2009) 225−230.

10. I. Čorić, D. Milić, D. Matković-Čalogović, and L. Tomašković, Synthesis and crystal structures of two isomeric nitro-α-resorcylic acids, *Struct. Chem.* **20** (2009) 73−80.

9. D. Milić, Z. Džolić, M. Cametti, B. Prugovečki, and M. Žinić, Supramolecular architectures of simple aminoanthraquinones: Revised structure of 1-aminoanthraquinone, *J. Mol. Struct.* **920** (2009) 178−182.

8. M. Rubčić, D. Milić, B. Kamenar, and M. Cindrić, Synthesis and Structure of (4-methyl-pyridine-*N*-oxide)oxo-(salicylaldehyde 4-phenylthiosemicarbazonato)vanadium(IV), *Acta Chim. Slov.* **55** (2008) 810−814.

7. D. Milić, T. V. Demidkina, N. G. Faleev, D. Matković-Čalogović, and A. A. Antson, Insights into the catalytic mechanism of tyrosine phenol-lyase from X-ray structures of quinonoid intermediates, *J. Biol. Chem.* **283** (2008) 29206−29214.

6. V. Vrdoljak, D. Milić, M. Cindrić, D. Matković-Čalogović, and D. Cinčić, Synthesis of novel molybdenum(V) complexes: Structural characterization of two thiosemicarbazonato complexes $[MoOCl_2\{C_6H_4(O)CH{:}NNHC{:}SNHC_6H_5\}]$ and $[MoOCl_2\{C_{10}H_6(O)CH{:}NNHC{:}SNHC_6H_5\}] \cdot CH_3CN$, and two oxohalomolybdates $NH_4[MoOCl_4(CH_3CN)]$ and $[C_5H_5NH]_2[MoOCl_5] \cdot CH_2Cl_2$, *Polyhedron* **26** (2007) 3363−3372.

5. M. Jurić, P. Planinić, N. Brničević, D. Milić, D. Matković-Čalogović, D. Pajić, and K. Zadro, New Heterometallic (Cu^{II} and Cr^{III}) Complexes − First Crystal Structure of an Oxalate-Bridged Ferromagnetically Coupled $[Cu^{II}Cr^{III}Cu^{II}]$ System, *Eur. J. Inorg. Chem.* (2006) 2701−2710.

4. D. Milić, D. Matković-Čalogović, T. V. Demidkina, V. V. Kulikova, N. I. Sinitzina, and A. A. Antson, Structures of Apo- and Holo-Tyrosine Phenol-lyase Reveal a Catalytically Critical Closed Conformation and Suggest a Mechanism for Activation by K^+ Ions, *Biochemistry* **45** (2006) 7544−7552.

3. M. Eckert-Maksić, D. Margetić, S. Kirin, D. Milić, and D. Matković-Čalogović, Synthesis of Fused Norbornenes containing two 7-Metallonorbornene Units Assisted by High Pressure, *Eur. J. Org. Chem.* (2005) 4612−4620.

2. V. Vrdoljak, M. Cindrić, D. Milić, D. Matković-Čalogović, P. Novak, and B. Kamenar, Synthesis of five new molybdenum(VI) thiosemicarbazonato complexes. Crystal structures of salicylaldehyde and 3-methoxy-salicylaldehyde 4-methylthiosemicarbazones and their molybdenum(VI) complexes, *Polyhedron* **24** (2005) 1717−1726.

1. D. Milić, M. Renić, and D. Matković-Čalogović, Caesium chloride 2-(*N*-morpholinio)ethanesulfonate, *Acta Crystallogr. E – Struct. Rep. Online* **61** (2005) m757–m758.

Invited Talks:

2. D. Milić, T. V. Demidkina, D. Matković-Čalogović, and A. A. Antson, *Structural Studies of the Enzymatic Mechanism of* Citrobacter freundii *Tyrosine Phenol-lyase*, Second International Interdisciplinary Conference on Vitamins, Coenzymes, and Biofactors, Athens, Georgia, USA, October 26−31, 2008. Abstr. 15.

1. D. Milić, *Crystallization of biological macromolecules*, CEEPUS program H-76, Faculty of Medicine, University of Pécs, Pécs, Hungary, June 20, 2005.

Other Oral Presentations at Scientific Meetings:

4. D. Milić, E. Oppici, B. Cellini, and D. Matković-Čalogović, *Structure of the orthorhombic crystal form of human alanine:glyoxylate aminotransferase*, Eighteenth Croatian-Slovenian Crystallographic Meeting, Varaždin, Croatia, June 17−21, 2009, Abstr. 29.

3. D. Milić, D. Matković-Čalogović, T. V. Demidkina, and A. A. Antson, *Discrete disorder of a whole protein domain in the crystals of tyrosine phenol-lyase*, Sixteenth Croatian-Slovenian Crystallographic Meeting, Petrčane, Croatia, June 13–17, 2007, Abstr. 58.

2. D. Milić, V. Bubaš, and D. Matković-Čalogović, *Crystallization and preliminary X-ray crystallographic analysis of human serum apotransferrin*, Fifteenth Slovenian-Croatian Crystallographic Meeting, Jezersko, Slovenia, June 15—18, 2006, Abstr. 21.

1. D. Milić, D. Matković-Čalogović, T. V. Demidkina, and A. A. Antson, *Structural aspects of tyrosine phenol-lyase catalytic activity*, Fourteenth Croatian-Slovenian Crystallographic Meeting, Vrsar, Croatia, June 15—17, 2005, Abstr. 20.

Poster Presentations at Scientific Meetings:

5. D. Milić, D. Matković-Čalogović, T. V. Demidkina, and A. A. Antson, *Structural Details in the β-elimination Mechanism of Tyrosine Phenol-lyase*, 24th European Crystallographic Meeting, Marrakech, Morocco, 22–27 August 2007, *Acta Crystallogr. Sect. A* **63** (2007) s122.

4. D. Milić, D. Matković-Čalogović, T. V. Demidkina, and A. A. Antson, *Structural Study Reveals the Role of Phenylalanine-448 in* Citrobacter freundii *Tyrosine Phenol-lyase*, XX Croatian Meeting of Chemists and Chemical Engineers, Zagreb, Croatia, February 26 – March 1, 2007, Abstr. 101.

3. D. Milić, V. Vrdoljak, M. Cindrić, and D. Matković-Čalogović, *Structural Characterisation of Two Molybdenum(V) Thiosemicarbazonato Complexes and Mo-containing Intermediates Derived from $X_2[MoCl_5]$ ($X = NH_4$ or PyH)*, 23rd European Crystallographic Meeting, Leuven, Belgium, 6—11 August 2006, *Acta Crystallogr. Sect. A* **62** (2006) s284.

2. D. Milić, D. Matković-Čalogović, T. V. Demidkina, and A. A. Antson, *Towards the elucidation of structural events during the catalysis by tyrosine phenol-lyase: crystal structures of different enzyme forms and their complexes with substrate analogues*, International School of Crystallography, 37th Course, a Nato ASI and a EuroSummerSchool: Evolving Methods for Macromolecular Crystallography, Erice, Italy, May 12—22, 2005, Abstr. 216.

1. D. Milić, D. Matković-Čalogović, T. V. Demidkina, and A. A. Antson, *The Structure of Y71F Tyrosine Phenol-lyase from* Citrobacter freundii *Complexed with 3-Fluoro-L-tyrosine*, 2nd Central European Conference "Chemistry towards Biology", Seggau, Austria, September 25—28, 2004, Abstr. 55—56.

Co-authored Contributions, but not the Presenting Author:

15. A. Jurković, D. Milić, and D. Matković-Čalogović, *Crystallization of the chloro derivative of bovine insulin*, 8$^{\text{th}}$ Meeting of Young Chemical Engineers, Zagreb, Croatia, February 18–19, 2010, Abstr. 95. (*poster presentation*)

14. D. Matković-Čalogović, D. Milić, I. Đilović, and B. Prugovečki, *Crystallography in bioanalysis*, CEEPUS International Symposium and Summer School on Bioanalysis, Blagoevgrad, Bulgaria, September 6–12, 2009. (*plenary lecture*)

13. A. Rostami Vartooni, V. Mirkhani, R. Kia, S. Tangestaninejad, M. Moghadam, I. Mohammadpoor-Baltork, D. Milić, *New Re(I) tricarbonyl-diimine complexes with* N,N′*-bis(2- and 4-nitrobenzaldehyde)-1,2-diiminoethane Schiff base ligands: Synthesis, spectroscopic and the crystal structure studies*, 11th Iranian Inorganic Chemistry Conference, Isfahan, Iran, May 13–14, 2009. (*oral presentation*)

12. D. Milić, D. Matković-Čalogović, M. Alešković, and K. Mlinarić-Majerski, *Whole-molecule disorder in the crystal structure of (1-adamantyl)methyl-1-adamantane-carboxylate*, XX Croatian Meeting of Chemists and Chemical Engineers, Trogir, Croatia, April 19—22, 2009, Abstr. 90. (*poster presentation*)

11. M. Jurić, P. Planinić, D. Žilić, D. Milić, and D. Pajić, *A Heterometallic $Cu^{II}Zn^{II}$ System with Three Types of mutually Analogous Dinuclear Entities (CuCu, CuZn, ZnZn)*, 38th International Conference on Coordination Chemistry, Jerusalem, Israel, July 20—25, 2008, Abstr. 328. (*poster presentation*)

10. P. Planinić, M. Jurić, N. Brničević, D. Milić, and D. Pajić, *The Oxalate-Bridged Antiferromagnetically Coupled $Cu^{II}Cu^{II}$ and $Ni^{II}Ni^{II}$ Systems*, 38th International Conference on Coordination Chemistry, Jerusalem, Israel, July 20—25, 2008, Abstr. 327. (*poster presentation*)

9. M. Jurić, P. Planinić, N. Brničević, D. Milić, and D. Matković-Čalogović, *Heterodimetallic Oxalate-Bridged $Cu^{II}Zn^{II}$ System*, XX Croatian Meeting of Chemists and Chemical Engineers, Zagreb, Croatia, February 26 – March 1, 2007, Abstr. 115. (*poster presentation*)

8. D. Margetić, M. Eckert-Maksić, Y. Murata, K. Komatsu, D. Milić, D. Matković-Čalogović, B. Prugovečki, and I. Đilović, *Experimental and Computational Investigation of Double Bond Pyramidalization in 7-sila and 7-germanorbornenes*, XX Croatian Meeting of Chemists and Chemical Engineers, Zagreb, Croatia, February 26 – March 1, 2007, Abstr. 161. (*poster presentation*)

7. P. Planinić, M. Jurić, N. Brničević, D. Milić, D. Matković-Čalogović, and D. Pajić, *A New Polynuclear Nickel(II) System with Bridging Oxalate Groups*, XX Croatian Meeting of Chemists and Chemical Engineers, Zagreb, Croatia, February 26 – March 1, 2007, Abstr. 313. (*poster presentation*)

6. M. Rubčić, M. Cindrić, D. Milić, and M. Tuksar, *Reactions of β-Diketonato Complexes of Vanadium(IV) with O,N,S-donors*, XX Croatian Meeting of Chemists and Chemical Engineers, Zagreb, Croatia, February 26 – March 1, 2007, Abstr. 83. (*poster presentation*)

5. M. Jurić, P. Planinić, N. Brničević, D. Milić, and D. Pajić, *First Crystal Structure of Oxalate-Bridged [Cu(II)Cr(III)Cu(II)] System*, 1st European Chemistry Congress, Budapest, Hungary, August 27—31, 2006, Abstr. 362. (*poster presentation*)

4. D. Milić, I. Đilović, D. Matković-Čalogović, B. Prugovečki, M. Eckert-Maksić, and D. Margetić, *Crystal structures of two polycyclic compounds containing 7-metalonorbornene (silicon and germanium) units*, Fourteenth Croatian-Slovenian Crystallographic Meeting, Vrsar, Croatia, June 15—17, 2005, 42. (*oral presentation*)

3. V. Vrdoljak, M. Cindrić, D. Milić, D. Matković-Čalogović, P. Novak, and B. Kamenar, *Molybdenum(VI) Complex Compounds with ONS-Thiosemicarbazone Ligands*, XIX Croatian Meeting of Chemists and Chemical Engineers, Opatija, Croatia, April 24—27, 2005, Abstr. 50. (*poster presentation*)

2. G. Pavlović, Z. Popović, V. Roje, D. Matković-Čalogović, and D. Milić, *Crystal and molecular structures of* N-*(3-methoxyphenyl)-2-hydroxy-1-naphthaldimine and bis(bromo-*N*-benzyl-2-oxo-1-naphtylideneamine)zinc(II)*, Tenth Croatian-Slovenian Crystallographic Meeting, Lovran, Croatia, June 21—24, 2001, Abstr. 18. (*oral presentation*)

1. Z. Popović, V. Roje, G. Pavlović, D. Matković-Čalogović, K. Užarević, D. Milić, and I. Đilović, N-*hydroxyphenyl Structural Isomers of 5-metoxysalicylaldimine and Their Compounds with Zinc(II) and Mercury(II)*, XVII Croatian Meeting of Chemists and Chemical Engineers, Osijek, Croatia, June 10−13, 2001, Abstr. 16. (*poster presentation*)